NASA Contractor Report 3644

An Analysis of Aerodynamic Requirements for Coordinated Bank-to-Turn Autopilots

A. Arrow

NOVEMBER 1982

NASA Contractor Report 3644

An Analysis of Aerodynamic Requirements for Coordinated Bank-to-Turn Autopilots

A. Arrow
The Johns Hopkins University
Laurel, Maryland

Prepared for
Langley Research Center

National Aeronautics
and Space Administration

**Scientific and Technical
Information Branch**

1982

TABLE OF CONTENTS

List of Figures

List of Tables

1 Summary

The objective of this report is to determine desirable aerodynamic properties for bank-to-turn (BTT) control by considering both aerodynamic and autopilot design goals and concerns. Toward this end, two planar airframes were compared having the potential for improved BTT control but having different aerodynamic properties. The comparison was made with advanced level autopilots (i.e., having sufficient high frequency attenuation and relative stability) using both linear and nonlinear 3-D aerodynamic models to obtain realistic missile body angular rates and control surface incidence.

Critical cross-coupling effects are identified and desirable aerodynamics are recommended for improved coordinated BTT (CBTT) performance. In addition, recommendations are made for autopilot control law analysis and design techniques for improving CBTT performance.

2 Introduction

Although it has long been understood that bank-to-turn (BTT) controlled missiles offer increased maneuverability and drag reduction over conventional cruciform, roll stabilized, skid-to-turn (STT) controlled missiles, limitations in technology [1] have delayed the development of BTT control systems. Major technology advances during the past decade, however, have re-opened the issue of BTT control for missiles. The availability of advanced on-board and laboratory digital computers make bank-to-turn control feasible in spite of the added complexity of the control laws of the autopilot. In addition, certain types of ramjet engines [2], which are candidate propulsion systems for modern mission requirements of long range and high altitude [3], have presented a need for a missile control technique for maintaining effective air inlet flow and have given further impetus to investigation of BTT control.

Many missile programs [3] were initiated during the past decade to improve their capability via BTT control. The results have advanced the understanding of the different missile subsystems. In the autopilot area, many types of autopilots have been found which force the missile to roll or bank so that the steering maneuver occurs with the airframe oriented in a specified or preferred direction with respect to the incoming airstream. This entire class of autopilots may be referred to as Preferred Orientation Control (POC) autopilots. Each autopilot has different architecture, results in different missile motion for the same guidance command, and has different design concerns.

The choice of autopilot depends on guidance/airframe/propulsion system requirements. Cruciform missiles with axisymmetric bodies, for example, have POC autopilots which are steered using pitch and yaw channels like STT except that the roll channel is commanded so that the missile Rolls During the Turn (RDT). If missile roll and yaw motion are coordinated for RDT control to minimize sideslip, the POC autopilot is referred to as Coordinated Roll During Turn (CRDT). Missiles with either one or two planes of symmetry use a POC autopilot which forces the missile to Bank in order To Turn (BTT) like an aircraft and if the motion is coordinated it is referred to as CBTT.

In the guidance area, radome aberration errors for radio frequency guidance are of major concern [3] and are currently being investigated. The interaction between BTT control and antenna stabilization and sensor orientation are additional concerns to be addressed. However, simplified guidance studies [4] which neglect radome effects and assume coordinated missile motion, have shown that CBTT can provide acceptable performance with roll rates that are not excessive for autopilot control. These studies were made for a medium range area defense mission and a long range suppression mission and considered both high lift (planar) and moderate lift (cruciform) configurations.

To take full advantage of CBTT control, planar airframes have been designed to increase lifting capability in one direction without the weight and drag penalty associated with orthogonal lifting surfaces [5]. These airframes have aerodynamic properties which have the potential to enhance CBTT control.

The objective of this investigation is to determine what type of aerodynamic properties are desirable for an efficient CBTT autopilot (i.e., small control surface effort, small sideslip, high relative stability for a required acceleration response in the desired maneuver plane). To reach this objective, two planar airframes were selected which have potential for CBTT control and have sufficiently different aerodynamic properties. Their performance with CBTT control was studied at M = 3.95 for an engagement at 60000 ft altitude.

3 Symbols

BTT — Bank-to-Turn

CBTT — coordinated Bank-to-Turn, minimum sideslip, positive α, $\phi_e \leq 180$ deg

CRDT — coordinated Roll-During-Turn

C_ℓ — rolling moment coefficient

C_{ℓ_β} — slope of curve of rolling moment coefficient, C_ℓ vs β

$C_{\ell_{\delta_R}}$ — change in C_ℓ per degree roll control incidence, δ_R

$C_{\ell_{\delta_Y}}$ — change in C_ℓ per degree yaw control incidence, δ_Y

C_m — pitching moment coefficient

C_{m_α} — slope of curve of pitching moment coefficient C_m vs α

$C_{m_{\delta_P}}$ — change in C_m per degree pitch control incidence, δ_P

C_N — normal force coefficient

C_{N_α} slope of curve of normal force coefficient C_N vs α

$C_{N_{\delta_P}}$ change in C_N per degree pitch control incidence, δ_P

C_n yawing moment coefficient

C_{n_β} slope of curve of yawing moment coefficient, C_n vs β

$C_{n_{\delta_Y}}$ change in C_n per degree yaw control incidence, δ_Y

$C_{n_{\delta_R}}$ change in C_n per degree roll control incidence, δ_R

C_Y side force coefficient

C_{Y_β} slope of curve of side force coefficient C_Y vs β

$C_{Y_{\delta_Y}}$ change in C_Y per degree yaw control incidence, δ_Y

$C_{Y_{\delta_R}}$ change in C_Y per degree roll control incidence, δ_R

d_1 inertial cross-coupling into yaw channel, $-pq(I_{yy}-I_{xx})/I_{zz} \cong -pq$

d_2 kinematic cross-coupling into yaw channel, αp

d_3 inertial cross-coupling into pitch channel, $-rp(I_{xx}-I_{zz})/I_{yy} \cong rp$

d_4 kinematic cross-coupling into pitch channel, $-\beta p$

d reference length for coefficients = 2 ft.

I_{yy} moment of inertia about $\bar{y}_B$ axis

I_{zz} moment of inertia about $\bar{z}_B$ axis

I_{xx} moment of inertia about $\bar{x}_B$ axis

K_A autopilot pitch acceleration error gain

K_{YP} CBTT autopilot coordination branch gain

LBTT limited Bank-to-Turn, may or may not be coordinated, positive and negative α, $\phi_e \leq 90$ or 45 degrees

p roll rate about $\bar{x}_B$

$\dot{p}$ roll acceleration about $\bar{x}_B$

P_e constant or equilibrium roll angular rate

POC	preferred orientation control
$\bar{q}$	dynamic pressure
q	pitch rate about $\bar{y}_B$
$\dot{q}$	pitch angular acceleration about $\bar{y}_B$
Q_e	constant or equilibrium pitch angular rate
r	yaw angular rate about $\bar{z}_B$
r_c	yaw angular rate command (coordination command)
$\dot{r}$	yaw angular acceleration about $\bar{z}_B$
RDT	Roll-During-Turn
S	reference area for coefficients = π ft^2
STT	Skid-to-Turn, roll attitude stabilized
u	velocity component in $\bar{x}_B$ direction

v velocity component in $\bar{y}_B$ direction, assumed to be constant

V constant missile flight path velocity

$\bar{V}$ missile velocity vector

w velocity component in $\bar{z}_B$ direction

$\bar{x}_B$ body-fixed roll axis, along axis of symmetry, positive forward

$\bar{y}_B$ body-fixed pitch axis, positive starboard

$\bar{y}_v$ vehicle axis in local horizontal direction, approximated as inertial axis

$\bar{z}_B$ body-fixed yaw axis, forms right handed orthogonal system with $\bar{x}_B$ and $\bar{y}_B$

$\bar{z}_v$ vehicle axis in downward direction along local gravity vector, approximated as inertial axis

η_z achieved normal acceleration in $\bar{z}_B$ direction

η_{z_c} commanded normal acceleration in $\bar{z}_B$ direction

η_y achieved normal acceleration in $\bar{y}_B$ direction

η_Z achieved normal acceleration in $\bar{z}_v$ direction

η_Y achieved normal acceleration in $\bar{y}_v$ direction

η_c normal acceleration command from guidance computer in $\bar{z}_v$ direction plus anti-gravity bias command

η_{Z_c} normal acceleration guidance command in $\bar{z}_v$ direction

η_{Y_c} normal acceleration guidance command in $\bar{y}_v$ direction

ϕ_c roll attitude command from guidance computer, zero degrees in $-\bar{z}_v$ direction and 90 degrees in $\bar{y}_v$ direction

ϕ roll attitude, zero degrees in $-\bar{z}_v$ direction and 90 degrees in $\bar{y}_v$ direction

ϕ_e roll attitude error, $\phi_c - \phi$

θ Elevation Euler Angle, second rotation, $\int(q \cos\phi - r \sin\phi)\, dt$

ψ Azimuth Euler Angle, first rotation about $\bar{y}_v$, $\int(q \sin\phi + r \cos\phi)\, dt$

δ_P pitch control incidence (positive tail incidence produces negative pitching moment)*

δ_{P_c} commanded pitch control incidence, δ_P

δ_Y yaw control incidence (positive tail incidence produces negative yawing moments)*

δ_{Y_c} commanded yaw control incidence, δ_Y

δ_R roll control incidence (positive tail incidence produces positive rolling moment)

δ_{R_c} commanded roll control incidence, δ_R

α_e constant or equilibrium angle-of-attack

α angle-of-attack

$\dot{\alpha}$ angle-of-attack rate

* Note that the sign convention used herein for δ_p and δ_Y, but not δ_R, are different from those of Ref. 1.

α_T total angle-of-attack, $\tan^{-1}((v^2 + w^2)^{1/2}/u)$

$\bar{\alpha}$ modified form of estimated angle-of-attack for autopilot coordination command

β angle of sideslip

$\dot{\beta}$ sideslip angular rate

4 Comparison of Airframe Configurations

The two airframe configurations studied in this investigation were taken from Ref. 5 and are shown in Figures 4.1 and 4.2. Although the configuration shown in Fig. 4.1 has a body of circular cross section and the configuration shown in Fig. 4.2 has a body with a 3:1 elliptical cross section, both configurations have the same cross-sectional area distribution. The configurations are both tail-controlled using four identical control surfaces which are located flush with the body base with a ± 30 degrees dihedral. In the case of the elliptical body, the hinge line was skewed such that a 10 degree control deflection measured at the body-tail juncture had a resultant 7.04 degree surface deflection. Thus the aerodynamic control effectiveness in terms of deflection measured at the body-tail juncture is lower for the elliptical configuration than for the circular configuration although nearly the same in terms of resultant surface deflection. The total span of the mono-wings is the same for each configuration which results in larger wing area for the circular body configuration.

Missile configurations were sized to provide realistic mass properties needed for this study. The details are given in Appendix A. The required aerodynamic data were taken from Ref. 5 and are presented in Appendix B as used in the simulation for this study.

Section 4.1 contains a brief comparison of in-channel dynamic characteristics which are covered in more detail in Appendices D through F. Section 4.2 develops and compares the measures of cross-coupling influence.

4.1 In-Channel Characteristics

4.1.1 Pitch Channel

The normal force generated by the elliptical configuration of Figure 4.2 is 20 to 30 percent higher than that generated by the circular configuration of Figure 4.1 for the same angle-of-attack. Thus for the same acceleration command, the elliptical will operate at a smaller angle of attack. The circular airframe is stable for all angles-of-attack. The elliptical is slightly unstable at low angles-of-attack and slightly stable at the higher angles-of-attack. For the elliptical airframe, the combination of a nearly neutrally stable airframe aided by a larger C_{N_α} results in reduced control effort which is desired in autopilot design. The more neutrally stable airframe and larger C_{N_α} offsets the reduced control effectiveness of the elliptical airframe. In addition, since a smaller control incidence is required for a given acceleration command, lower angles-of-attack for the elliptical configuration also result in lower body angular rates needed to achieve the same response time.

4.1.2 Yaw Channel

The circular is unstable in yaw at all angles-of-attack whereas the elliptical is stable. Since the magnitude of instability of the circular configuration is less than the magnitude of stability of the elliptical configuration (especially at higher angles-of-attack), and the control effectiveness, $C_{n_{\delta_Y}}$, of the circular configuration is larger, it requires less tail incidence δ_Y to minimize sideslip β. On the other hand, the stability of the elliptical configuration should aid the airframe in minimizing sideslip although it may require a larger control incidence in responding to coordinating commands.

4.1.3 Roll Channel

Compared with the circular configuration, the elliptical configuration is more stable in roll (i.e., larger negative C_{ℓ_β}), has a roll inertia approximately 2.75 times that of the circular and has approximately 30 percent less roll control effectiveness, $C_{\ell_{\delta_R}}$. Hence it is expected that the elliptical airframe would require much larger roll control surface incidence for the same roll commands to the roll channel.

4.2 Measures of Cross-Coupling Influence

Measures of cross-coupling (i.e., aerodynamic, kinematic and inertial) influence on POC autopilot stability and performance are developed in this section. The measures, which are functions of missile parameters, show how to minimize the effects of undesirable cross-coupling or to enhance the effects of desirable coupling. Measures are calculated for the elliptical and circular configurations and compared to determine whether the coupling of one airframe will have relatively more or less influence than the other. The remainder of this report will determine the significance of the specific measures for the two airframes (i.e., whether the CBTT autopilot control law can remain simple with only the coordinating command or will require additional complexity). Figure 4.3 shows a block diagram of simplified yaw aerodynamics (i.e., only the direct effects of yawing moment on sideslip are included). Inertial cross-coupling is denoted as d_1 and kinematic cross-coupling is denoted as d_2. The equations which are represented by the block diagram in Fig. 4.3 are,

$$\dot{\beta} = d_2 - r \tag{4-1}$$

$$\dot{r} = d_1 + \frac{57.3\bar{q}Sd}{I_{zz}} \left(C_{n_{\delta_R}} \delta_R + C_{n_{\delta_Y}} \delta_Y + C_{n_\beta} \beta\right) \tag{4-2}$$

Removing C_{n_β} from the parentheses in (4-2)results in,

$$\dot{r} = d_1 + \frac{57.3\bar{q}Sd}{I_{zz}} C_{n_\beta} \left(\frac{C_{n_{\delta_R}}}{C_{n_\beta}} \delta_R + \frac{C_{n_{\delta_Y}}}{C_{n_\beta}} \delta_Y + \beta\right) . \qquad (4\text{-}3)$$

Taking the time derivative of (4-1), solving for $\dot{r}$ and substituting it into (4-3) to eliminate $\dot{r}$ results in (4-4).

$$\ddot{\beta} = \dot{d}_2 - d_1 - \frac{57.3\bar{q}Sd}{I_{zz}} C_{n_\beta} \left(\frac{C_{n_{\delta_R}}}{C_{n_\beta}} \delta_R + \frac{C_{n_{\delta_Y}}}{C_{n_\beta}} \delta_Y + \beta\right) \qquad (4\text{-}4)$$

Rewriting (4-4) results in (4-5).

$$\ddot{\beta} = -K_3 \left(\frac{d_1 - \dot{d}_2}{K_3} + K_1\delta_Y + K_2\delta_R + \beta\right) \qquad (4\text{-}5)$$

where $$K_1 = \frac{C_{n_{\delta_Y}}}{C_{n_\beta}} , \quad K_2 = \frac{C_{n_{\delta_R}}}{C_{n_\beta}} , \quad K_3 = \frac{57.3\bar{q}Sd}{I_{zz}} C_{n_\beta} .$$

Taking the Laplace transform of (4-5) and solving for β results in (4-6) or the block diagram in Fig. 4.4.

$$\beta = \frac{-1}{\frac{s^2}{K_3} + 1} \left(\frac{d_1 - sd_2}{K_3} + K_1\delta_Y + K_2\delta_R\right) \qquad (4\text{-}6)$$

Applying the measures K_1, K_2, and $1/K_3$ to any missile airframe, the effect of changing missile parameters on cross-coupling can be determined. Increasing the magnitude of C_{n_β} for either a stable or unstable airframe will decrease the magnitudes of K_1, K_2, and $1/K_3$. Decreasing K_1 by increasing the magnitude of C_{n_β} will decrease the influence of δ_Y on sideslip while increasing the influence of the missile's inherent stability. Decreasing K_2 reduces the effect of the yawing moment due to δ_r. Decreasing $1/K_3$ in turn reduces the influence of d_1 and d_2 (i.e., the inertal and kinematic couplings). It appears that if C_{n_β} were sufficiently large and stable, yaw control surfaces may not be necessary as the stable airframe may minimize the effects of aerodynamic, inertial and kinematic cross coupling on sideslip. Decreasing the ratio of $I_{zz}/(\bar{q}sd)$ will also decrease $1/K_3$ which will in-turn reduce the influence of d_1 and d_2 and increase synthetic control effectiveness (i.e., moment per control surface incidence). Increasing control effectiveness $C_{n_{\delta_Y}}$, increases K_1 and decreases K_2/K_1 which in turn reduces the influence of roll tail incidence δ_R relative to yaw tail incidence δ_Y.

The table in Fig. 4.4 shows the magnitudes of K_1, K_2/K_1, and $1/K_3$ for two angles-of-attack of the circular and elliptical airframes. The magnitudes of K_2/K_1 show that both airframes have nearly the same attenuation for aerodynamic cross-coupling $C_{n_{\delta_R}}$. Large angles-of-attack indicate a substantial reduction (i.e., approximately 6 dB) in attenuation. The large magnitude of K_1 at $\alpha = 20$ degrees, shows that as a result of its nearly neutral stability in yaw at high angles-of-attack the circular airframe sideslip β can be controlled by small yaw incidence δ_Y. However this also results in a loss of attenuation for kinematic and inertial cross-coupling due to an increase in $1/K_3$. At lower angles-of-attack, the magnitudes of K_1 and $1/K_3$ are approximately the same for both airframes.

Roll acceleration is shown in (4-7).

$$\dot{p} = \frac{\bar{q}Sd}{I_{xx}} \left(C_{\ell_{\delta_R}} \delta_R + C_{\ell_{\delta_Y}} \delta_Y + C_{\ell_\beta} \beta\right) \tag{4-7}$$

Removing $C_{\ell_{\delta_R}}$ from the parentheses results in (4-8) and the block diagram in Fig. 4.5.

$$\dot{p} = K_6(\delta_R + K_4\delta_Y + K_5 \beta) \tag{4-8}$$

where $$K_6 = \frac{\bar{q}Sd}{I_{xx}} C_{\ell_{\delta_R}}, \qquad K_5 = \frac{C_{\ell_\beta}}{C_{\ell_{\delta_R}}}, \qquad K_4 = \frac{C_{\ell_{\delta_Y}}}{C_{\ell_{\delta_R}}}.$$

Increasing roll control effectiveness, $C_{\ell_{\delta_R}}$, of any missile airframe will reduce the influence of aerodynamic cross-coupling from sideslip and yaw tail incidence by decreasing K_4 and K_5 while increasing K_6.

The table in Fig. 4.5 show the magnitudes of measures K_4, K_5, and K_6 for the elliptical and circular airframes. The attenuation of aerodynamic cross-coupling due to yaw tail incidence, K_4, is approximately the same for both airframes and is substantially reduced at high angles-of-attack (i.e., approximately 5 dB). The K_5 gains for the elliptical and low K_5 attenuation for the circular may not result in additional autopilot complexity because C_{ℓ_β} is negative for both airframes. Any sideslip during a gee maneuver would be counteracted by a stabilizing rolling moment tending to reduce the sideslip which in turn would reduce the demand on the roll control surfaces. The influence of C_{ℓ_β} on CBTT performance during changes in maneuver direction is to be determined in this report. The gains for K_6 reflect primarily the lower roll moment of inertia of the circular airframe and its

slightly greater control effectiveness which result in providing stronger roll control for the circular airframe than for the elliptical.

Pitch angular acceleration and rate of angle-of-attack are shown in (4-9) and (4-10), where only direct effects of pitching moment on angle-of-attack are included.

$$\dot{q} = d_3 + \frac{57.3\bar{q}Sd}{I_{yy}} (C_{m_{\delta_p}} \delta_p + C_{m_\alpha} \alpha) \tag{4-9}$$

$$\dot{\alpha} = q - d_4 \tag{4-10}$$

where d_3 = kinematic cross-coupling = $-p\beta$

d_4 = inertia cross-coupling = rp.

Removing C_{m_α} from the parenthesis in (4-9) and combining with (4-10) to eliminate $\dot{q}$ results in (4-11).

$$\ddot{\alpha} = d_3 - \dot{d}_4 + K_8(K_7\delta_p + \alpha) \tag{4-11}$$

where $$K_8 = \frac{57.3\bar{q}Sd}{I_{xx}} C_{m_\alpha}, \quad K_7 = \frac{C_{m_{\delta_p}}}{C_{m_\alpha}}.$$

Taking the Laplace transform of (4-11) and solving for α, results in (4-12) and the block diagram in Fig. 4.6.

$$\alpha = \frac{-1}{\frac{-s^2}{K_8} + 1} \left(\frac{d_3 - sd_4}{K_8} + K_7\delta_p\right) \tag{4-12}$$

Increasing the magnitude of C_{m_α} will decrease both K_7 and $1/K_8$. Although the effects on angle-of-attack due to inertial cross-coupling d_3 and kinematic cross-coupling d_4 will be reduced via the increase in C_{m_α}, so will the influence of δ_p. Since good pitch synthetic control effectiveness (i.e., large moment per control surface incidence) is required for maneuvering using CBTT, reduction in $1/K_8$ by decreasing the ratio $I_{yy}/(\bar{q}sdC_{m_\alpha})$ can be offset by increasing control effectiveness $C_{m_{\delta_p}}$ and by obtaining more lift per angle-of-attack by increasing C_{N_α}.

The table in Fig. 4.6 shows the values of K_7 and $1/K_8$ for the circular and elliptical airframes. The values of K_7 show that the elliptical airframe has more control influence on pitching moment due to a more neutrally stable airframe. However, values of $1/K_8$ show that more neutral stability has resulted in a loss of attenuation of kinematic and inertial cross-coupling.

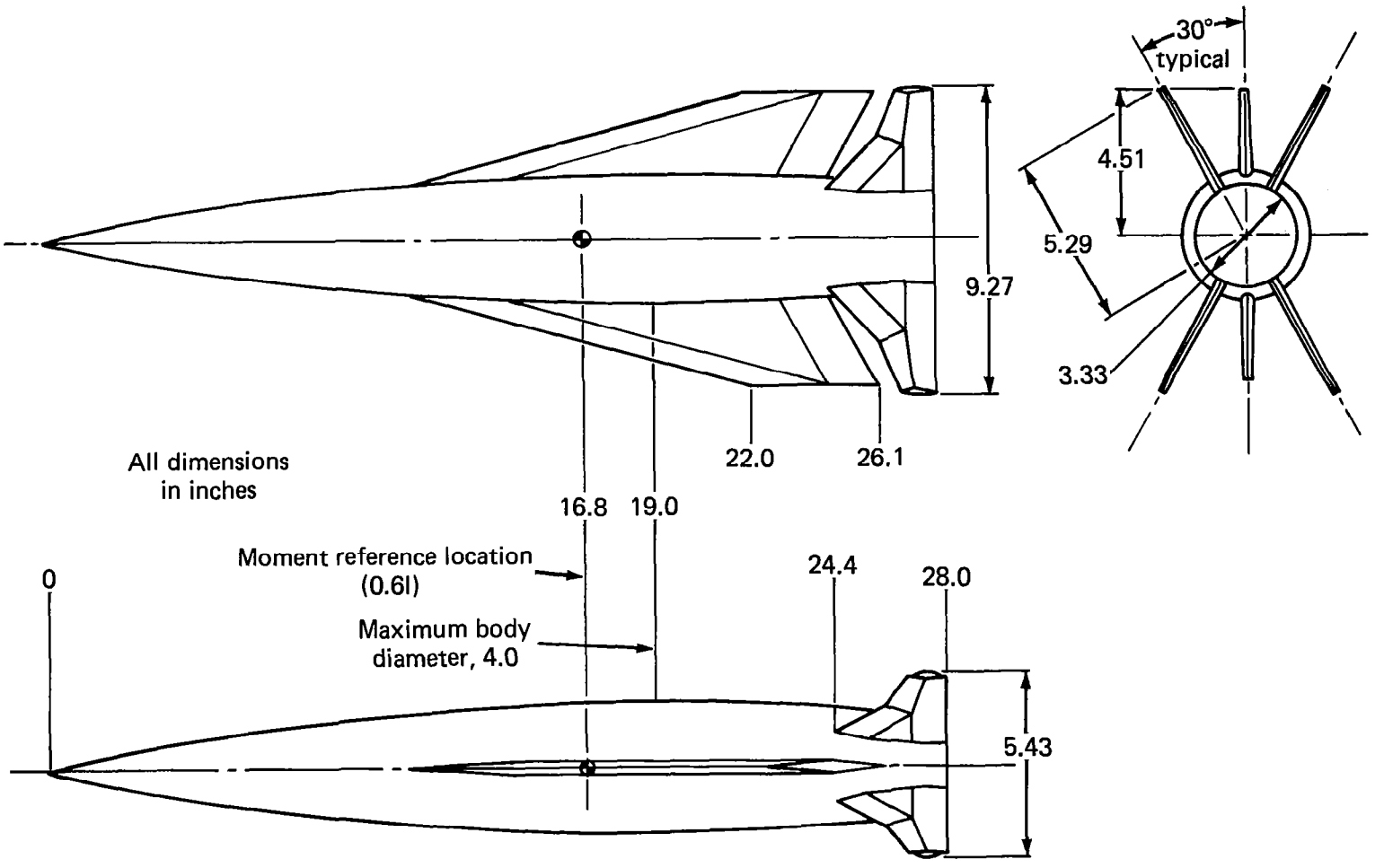

Fig. 4.1 Model of circular configuration — 1/6 scale.

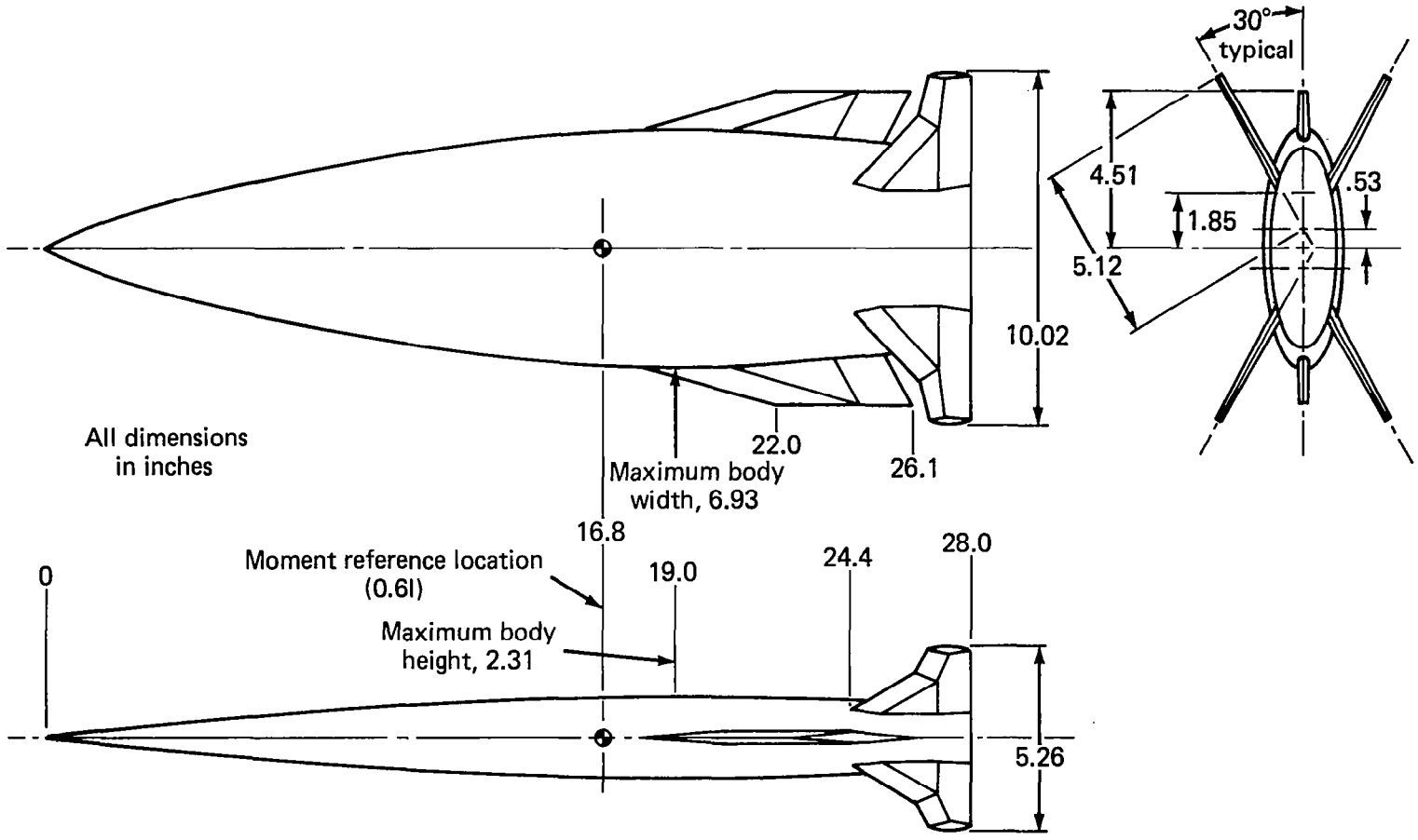

Fig. 4.2 Model of elliptical configuration — 1/6 scale.

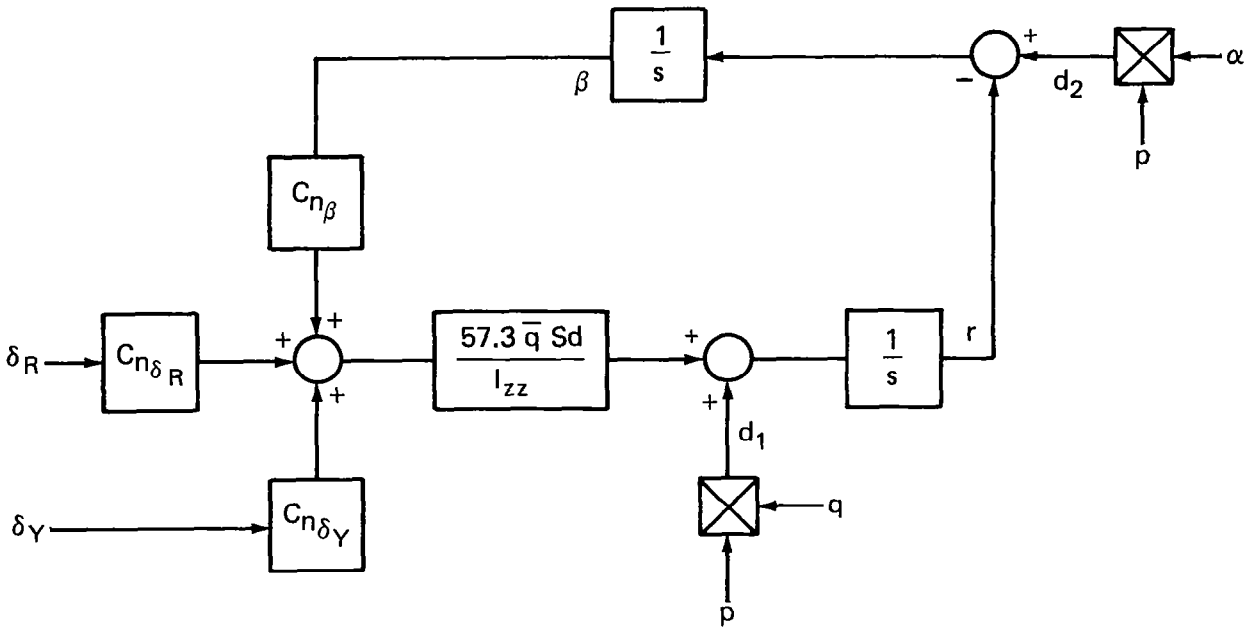

Fig. 4.3 Simplified yaw aerodynamics.

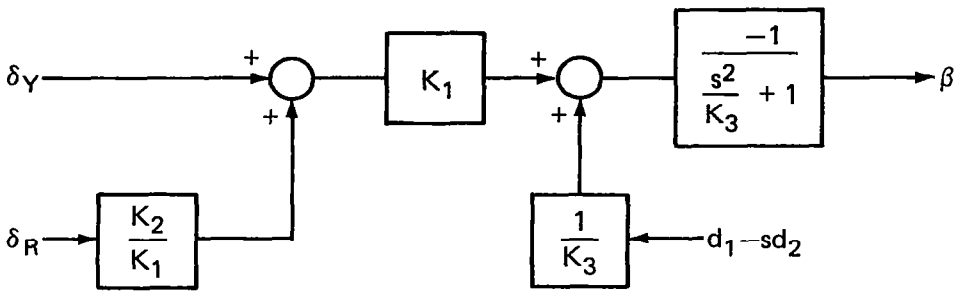

Airframe	Angle of attack (deg)	$\frac{K_2}{K_1} = \frac{C_{n\delta_R}}{C_{n\delta_Y}}$	$K_1 = \frac{C_{n\delta_Y}}{C_{n\beta}}$	$\frac{1}{K_3} = \frac{I_{zz}}{57.3\bar{q}Sd\,C_{n\beta}}$
Elliptical (Stable in yaw)	10	−0.359 (−8.9dB)	−1.63 (4.2dB)	0.0598 (−24.5dB)
	20	−0.711 (−3dB)	−1.41 (3dB)	0.0449 (−27dB)
Circular (Unstable in yaw)	10	−0.339 (−9.4dB)	2.79 (8.9dB)	−0.0718 (−22.9dB)
	20	−0.71 (−3dB)	20.7 (26.3dB)	−0.455 (−6.9dB)

Fig. 4.4 Influence of cross-coupling in yaw channel.

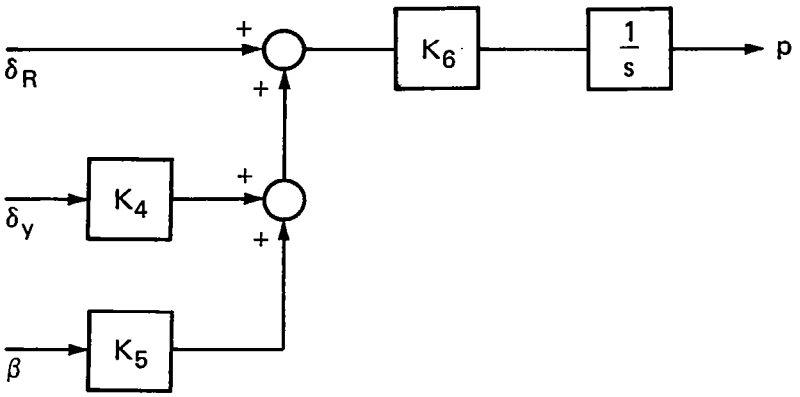

Airframe	Angle of attack (deg)	$K_4 = \frac{C_{l_{\delta_Y}}}{C_{l_{\delta_R}}}$	$K_5 = \frac{C_{l_\beta}}{C_{l_{\delta_R}}}$	$K_6 = \frac{57.3\bar{q}\,Sd\,C_{l_{\delta_R}}}{I_{xx}}$
Elliptical	10	−0.435 (−7.2dB)	−1.17 (1.39dB)	124.2 (41.9dB)
	20	−0.793 (−2dB)	−1.38 (2.8dB)	156.6 (43.9dB)
Circular	10	−0.457 (−6.8dB)	−0.257 (−11.8dB)	519.9 (54.3dB)
	20	−0.864 (−1.3dB)	−0.455 (−6.9dB)	653.6 (56.3dB)

Fig. 4.5 Influence of cross-coupling in roll channel.

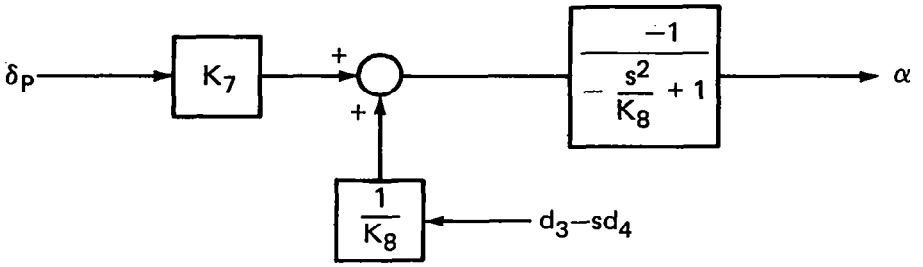

Airframe	Angle of attack (deg)	$K_7 = \frac{C_{m_{\delta_P}}}{C_{m_\alpha}}$	$\frac{1}{K_8} = \frac{I_{yy}}{57.3\bar{q}SdC_{m_\alpha}}$
Elliptical Unstable, α=10 Stable, α=20	10	−4.00 (12dB)	0.0967 (−20.3dB)
	20	6.00 (15.6dB)	−0.106 (−19.5dB)
Circular (Stable)	10	1.46 (3.3dB)	−0.0208 (−33.6dB)
	20	0.975 (−0.2dB)	−0.0115 (−38.8dB)

Fig. 4.6 Influence of cross coupling in pitch channel.

5 Dynamic Simulations

The objective of this section is to produce models of the missile airframe dynamics which have a level of complexity sufficient to determine the critical areas of concern regarding the stability and response of CBTT control for the circular and elliptical airframes. Section 5.1 presents the nonlinear 3-D model used for response studies and for verification of the linear model presented in Section 5.2. The linear model is necessary for autopilot design and analysis prior to the use of the nonlinear model. This procedure reduces computer cost and increases the understanding of critical system features.

5.1 Nonlinear Airframe Model

For the configurations under consideration, the following five assumptions have been found to be consistent with the above mentioned objective when used for the design of skid-to-turn (i.e., roll stabilized) missile autopilots and were also used in this study:

1. Fixed Flight Conditions, i.e., constant or time independent altitude, total velocity V, axial velocity u (Figure 5.1) and mass properties (weight, moment of inertia and center of gravity).

2. Rigid Missile With Geometric and Mass Symmetry in both $\bar{x}_B$-$\bar{y}_B$ and $\bar{x}_B$-$\bar{z}_B$ planes shown in Figure 5.1 (i.e., product of inertia $J_{xy} = J_{xz} = J_{yz} = 0$). Future studies should include the complexity that an airframe with single-plane of symmetry (about the $\bar{x}_B$-$\bar{z}_B$ plane) such that the product of inertia $J_{xz} \neq 0$.

3. Missile Roll Inertia I_{xx} Much Smaller Than Missile Pitch and Yaw Inertias, With Pitch and Yaw Inertias Nearly Equal

This assumption influences the inertial cross-coupling in the pitch and yaw channels. Using the nomenclature and body-fixed axes in

Figure 5.1 and applying Newton's laws of motion, the moments about the missile axes are,

$$\begin{aligned} M_x &= \dot{p}I_{xx} + qr(I_{zz}-I_{yy}) \\ M_y &= \dot{q}I_{yy} + pr(I_{xx}-I_{zz}) \\ M_z &= \dot{r}I_{zz} + pq(I_{yy}-I_{xx}) \end{aligned} \tag{5-1}$$

where M_x, M_y, and M_z are the components of the summation of external moments about the missile axes and I_{xx}, I_{yy}, I_{zz} are the missile moments of inertia.

For most tactical missiles the length is an order of magnitude larger than the diameter and as a result the roll inertia I_{xx} is considerably smaller than either the pitch inertia I_{yy} or the yaw inertia I_{zz}. Hence any appreciable missile roll rate p will result in inertial coupling between channels which can be important in bank-to-turn control.

Solving (5-1) for the angular accelerations and applying assumption 3 results in,

$$\begin{aligned} \dot{p} &= \frac{M_x}{I_{xx}} \\ \dot{q} &= \frac{M_y}{I_{yy}} + pr \\ \dot{r} &= \frac{M_z}{I_{zz}} - pq \end{aligned} \tag{5-2}$$

A good autopilot design should be insensitive to the small changes in inertial coupling which might arise from the use of the actual inertia values. However, because this report shows that inertial coupling is important in bank-to-turn, they should be added for completeness in actual missile design.

4. Autopilot Instruments (Accelerometers and Rate Gyros) Located at the Missile Center of Gravity (cg). Future studies must account for the location of the sensors with respect to the center of gravity which is required to assess high frequency autopilot stability. Until a detailed missile design is undertaken, however, such a refinement is neglected except that attention is paid to providing high frequency attenuation in the choice of autopilot parameters.

5. Small Angle Approximation , i.e., angle-of-attack α and sideslip angle $\beta \leq 20$ degrees, where $\alpha = \tan^{-1}(w/u)$ and $\beta = \tan^{-1}(v/u)$. This assumption allows small angle approximations $\alpha \cong w/u$ and $\beta \cong v/u$.

Block diagrams of the resulting missile nonlinear equations of motion are shown in Figures 5.2 and 5.3. Functions $C_N(\alpha,\delta_P)$ and $C_m(\alpha,\delta_P)$ in Figure 5.2 are nonlinear functions shown in Appendix B that vary with α and δ_P . All aerodynamic roll and yaw stability and control derivatives shown in Figure 5.3 are nonlinear functions which vary with α and are provided in Appendix B. The pitch channel is coupled to the lateral channel via missile roll rate. Part of the coupling is inertial (i.e., pr and -qp) and the other part is kinematic (i.e., $p\beta$ and αp). Both will be shown to be important for bank-to-turn control. In addition, the roll and yaw channels are aerodynamically coupled via C_{ℓ_β}, $C_{\ell_{\delta_Y}}$ and $C_{n_{\delta_R}}$

5.2 Linear Airframe Model

A linearized aerodynamic model was developed for stability studies in the frequency domain. The method used is an extension of the linearization technique used for skid-to-turn (STT) aerodynamic models. The following three assumptions were made:

1. Plane $\bar{x}_B - \bar{z}_B$ of Figure 1 is the maneuver plane.

2. Missile is trimmed in pitch (i.e., $M_y = 0$, at fixed values of α, q, and δ_p).

Rather than use the assumption that missile roll rate (p) is approximately zero as is done for the roll rate stabilized STT control, the following assumption was made for BTT:

3. Missile roll rate is constant.

The resulting model is shown in block diagram form in Figures 5.4 and 5.5. Aerodynamic stability derivatives are provided in Appendix C. Pitch and lateral channels are coupled via constant missile roll rate P_e. The same inertial, kinematic and aerodynamic cross couplings mentioned above for the nonlinear model are also in the linear model.

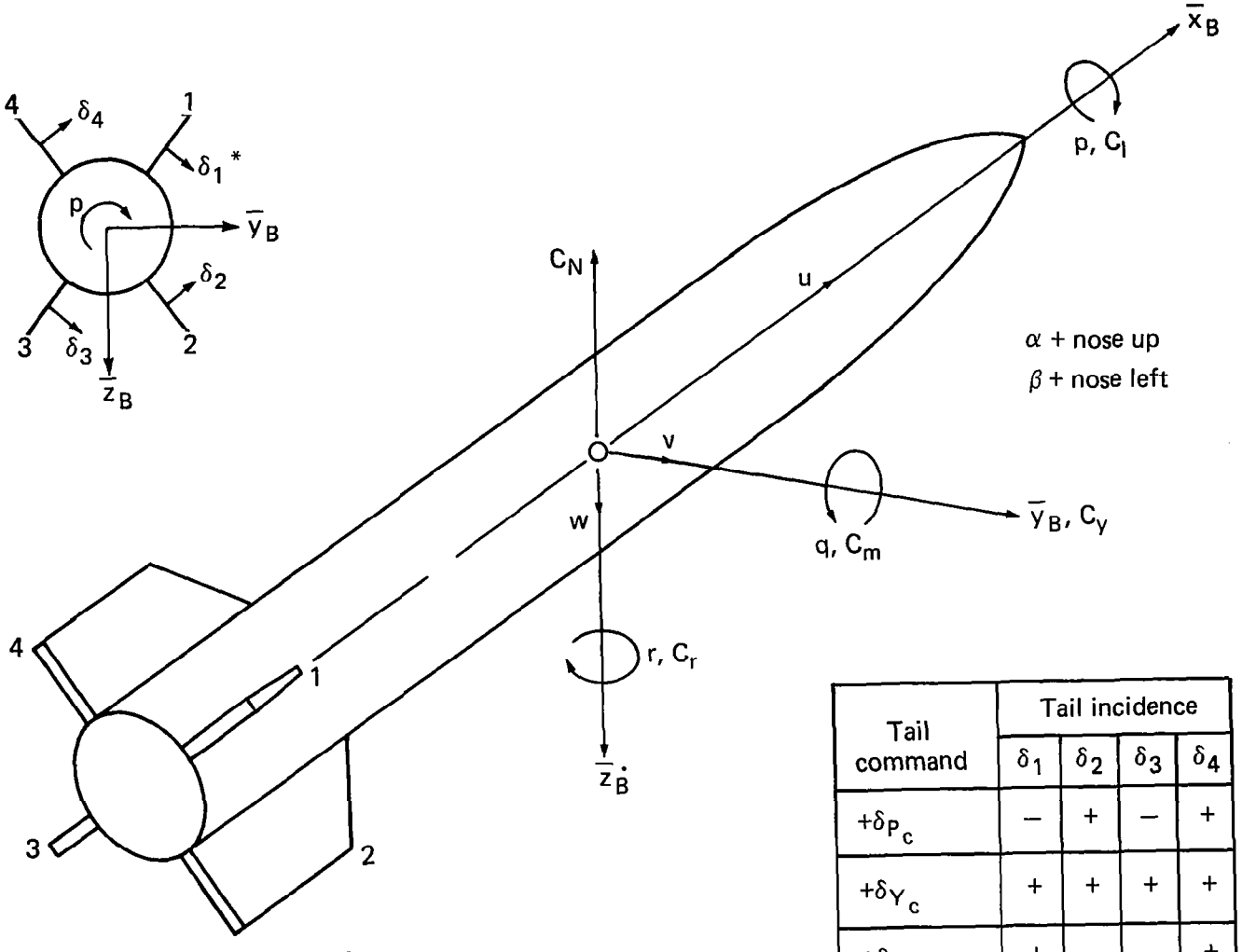

*Arrow indicates direction of positive leading edge deflection

Tail command	Tail incidence			
	δ_1	δ_2	δ_3	δ_4
$+\delta_{P_c}$	−	+	−	+
$+\delta_{Y_c}$	+	+	+	+
$+\delta_{R_c}$	+	−	−	+

Fig. 5.1 Aerodynamic sign convention.

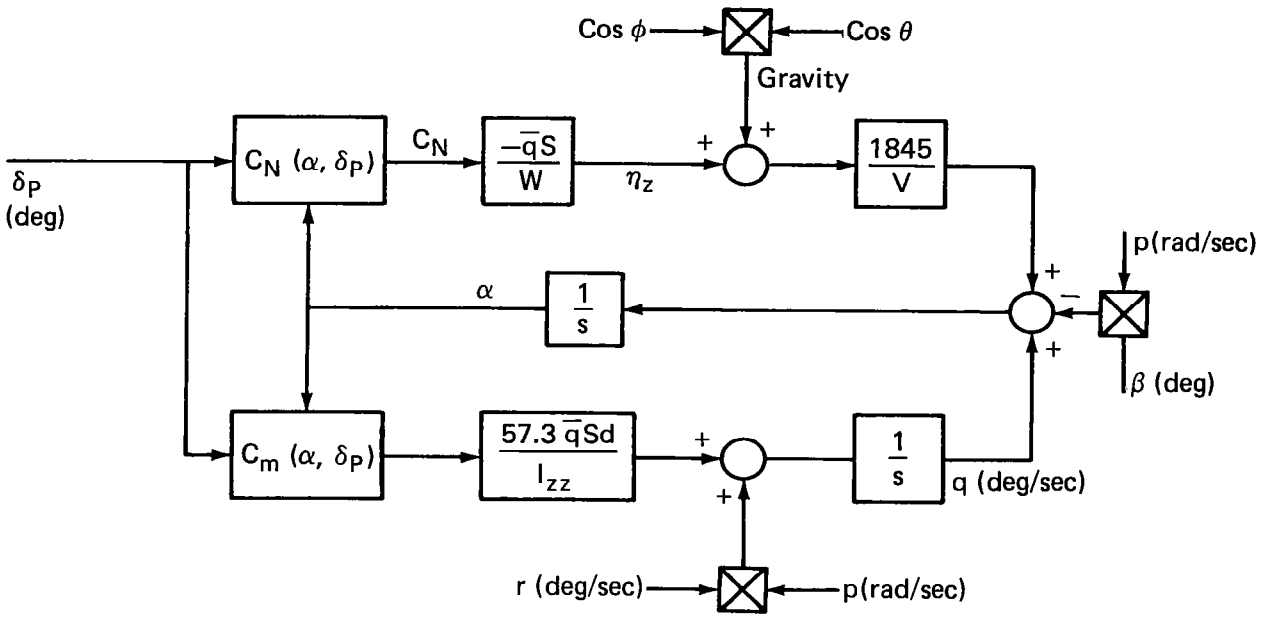

Fig. 5.2 Nonlinear pitch channel dynamic model.

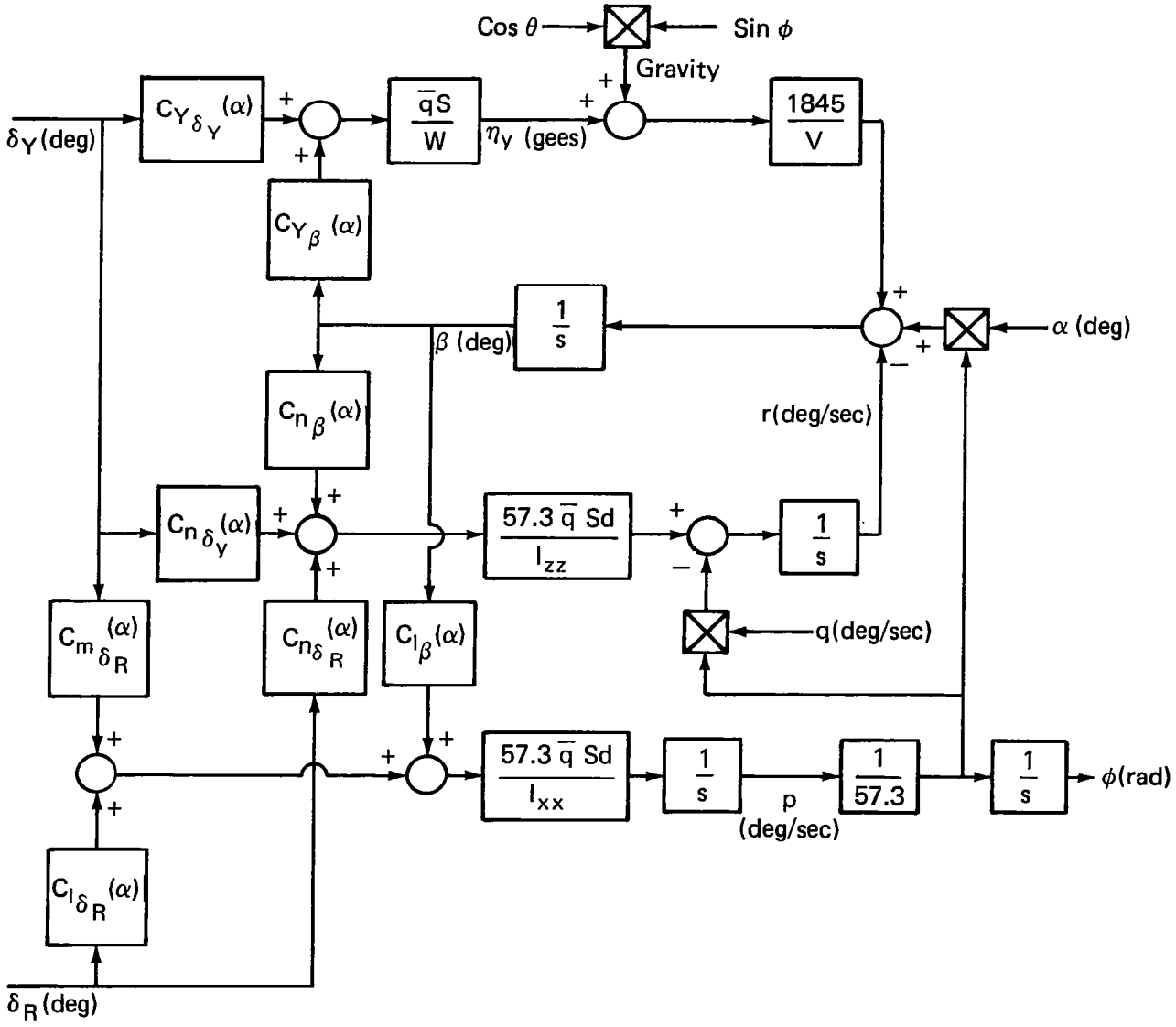

Fig. 5.3 Nonlinear lateral (roll/yaw) channel dynamics model.

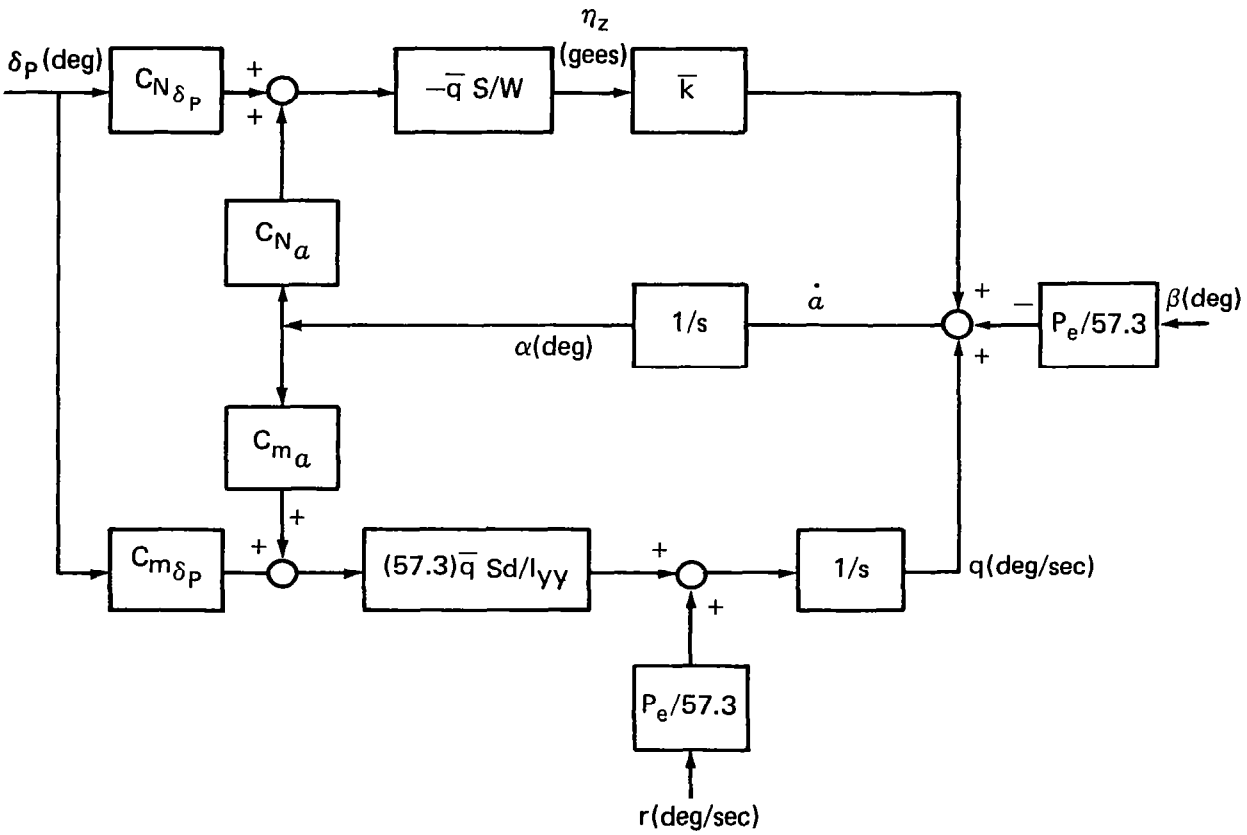

Note: 1. P_e = constant roll rate (deg/sec).

2. η_z,α,β,q, r are perturbation of missile from trim.

Fig. 5.4 Linear pitch channel dynamic model.

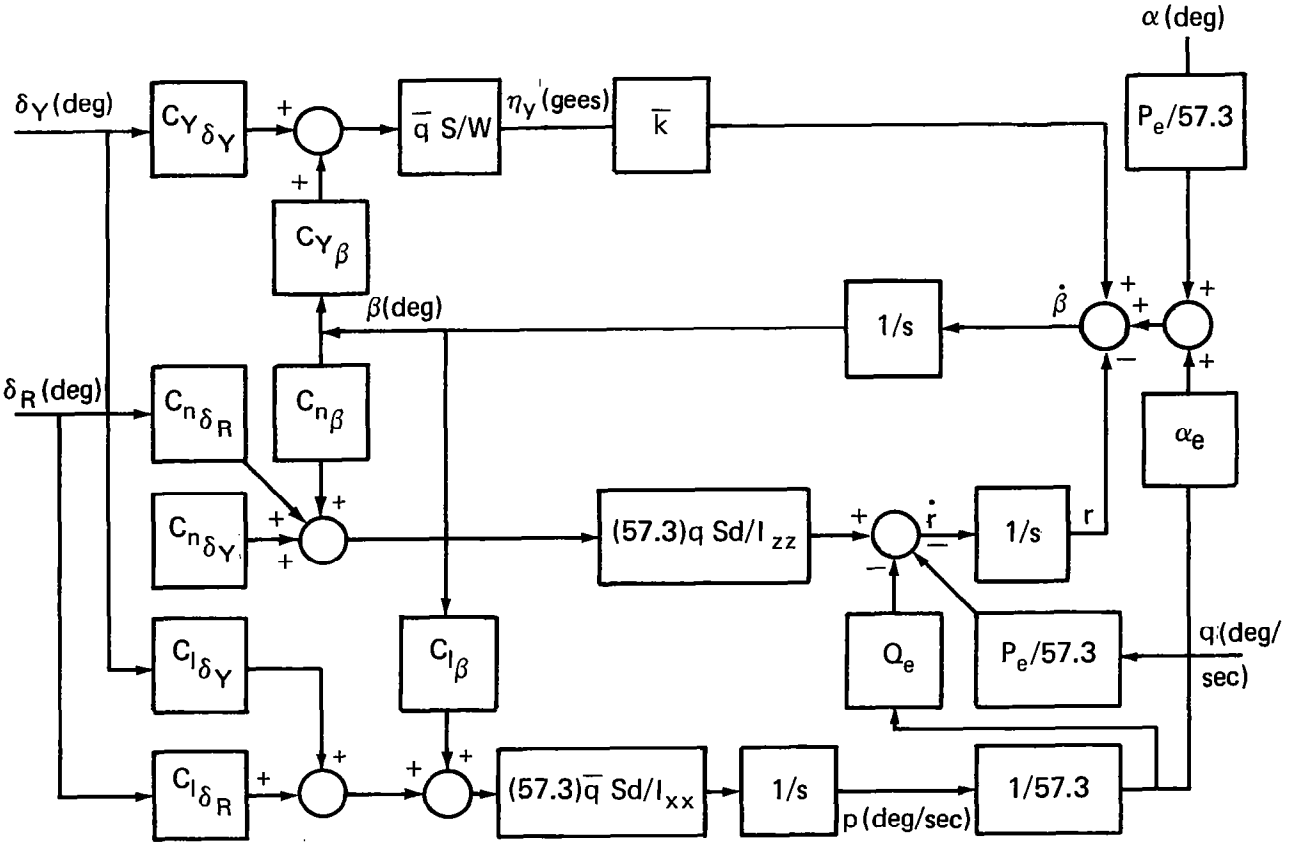

Note: 1. P_e = constant roll rate (deg/sec).
2. α_e = constant angle of attack (deg).
3. Q_e = constant pitch rate (deg/sec)

Fig. 5.5 Linear lateral (roll-yaw) channel dynamic model.

6 Bank-to-Turn Autopilot

In order to isolate and identify the critical areas of concern for the Bank-To-Turn (BTT) control of the circular and elliptical airframes, the scope of the investigation was confined. Section 6.1 introduces the BTT autopilot and selects one of its steering policies which is applicable to both rocket and ramjet propulsion systems. Section 6.2 is an introduction to the autopilot design approach and requirements which are discussed in detail throughout the report.

6.1 Introduction and Steering Policies

Bank-To-Turn (BTT) control, which may be used to enhance the performance of cruciform airframes, is also compatible with an airframe that has either one or two preferred maneuver directions. Figure 6.1 shows a block diagram of a BTT autopilot. Inertial acceleration commands are applied in polar coordinates (i.e., magnitude of the command (η_c) applied to the pitch autopilot and the direction (ϕ_c) is applied to the roll autopilot). The yaw autopilot is slaved to the roll autopilot to minimize sideslip angle by coordinating the missile yaw and roll motion. Achieved maneuver plane or inertial acceleration in rectangular coordinates (i.e., η_Z and η_Y) is determined by resolving achieved body-fixed accelerations (i.e., η_z and η_y) through missile roll angle (ϕ) (i.e., Euler angles θ and ψ are assumed to be sufficiently small).

Table 6.1 shows the steering policy control features used in BTT [4]. One policy is referred to as Coordinated Bank-To-Turn (CBTT) or BTT-180. The other policy is referred to as Limited Bank-To-Turn (LBTT) or BTT-90. The policies differ in the command logic used by the guidance computer. For LBTT the missile moves its preferred maneuver plane to the desired maneuver plane through the smallest roll attitude excursion. In addition, maneuvers in one plane will require no change in missile roll attitude. For

CBTT, the missile uses polar control for maximum maneuverability. Because it is desired that the missile avoid negative angles-of-attack, the missile is forced to roll about its velocity vector when the desired maneuver direction is in the negative angle-of-attack direction.

Coordinated motion or zero sideslip angle is achieved by directing the body fixed pitch axis of the missile at the missile velocity vector so that there is no component of missile velocity along the body fixed yaw axis of the missile. The top of Figure 6.2 shows the attitude of the missile body with respect to its velocity vector $\bar{V}$. When commanding an upward maneuver (i.e., $\phi = 0$), the missile body moves upward with its pitch axis directed at the velocity vector until it reaches the desired maneuver level or angle-of-attack. No roll motion is required to maintain coordination for this maneuver. For maneuvers in the $\phi = 45$ or 90 degree directions, LBTT and CBTT will result in the same missile motion. However when the desired maneuver direction can force the missile to develop negative angles-of-attack, the missile motion is different for LBTT and CBTT as shown for the 180 and 135 degree commands in Figure 6.2. Because CBTT is forced to maintain positive angles-of-attack, the missile must roll about the velocity vector while the yaw channel directs the pitch axis towards the velocity vector for minimum sideslip. LBTT requires considerably less roll motion.

The choice of steering policy depends on whether the airframe has one or two preferred maneuver directions which are in-turn dictated by guidance, airframe, propulsion system or flight conditions. The circular and elliptical airframes of this report are planar configurations which are symmetric about their wing planes and therefore have two preferred maneuver directions which are normal to the plane of their wings. Since the more strigent demands on BTT are experienced in the case of a single preferred maneuver direction, however, it was decided to carry out the study as though the configurations had only a single preferred maneuver direction.

For a missile having one preferred maneuver direction, CBTT or LBTT control is used depending on flight condition. For high altitude, low dynamic pressure conditions sideslip angles are expected to be larger due to higher required angles-of-attack. Large sideslip angles and/or negative angles-of-attack may cause loss of inlet air flow and therefore the missile motion of CBTT control (i.e., minimization of sideslip angles and positive angles-of-attack constraint) is desired for efficient operation of some ramjet designs. Medium or low altitude, high dynamic pressure conditions will result in lower angles-of-attack and small sideslip angles. Therefore, LBTT may be used to take advantage of smaller missile roll attitude excursions that are required compared to CBTT and therefore the speed of response in the desired maneuver plane is faster. In addition, smaller missile roll attitude excursions result in lower maximum missile roll rates which will be shown to reduce kinematic and inertial coupling problems.

A missile having two preferred maneuver directions has a choice between CBTT and LBTT at high altitude conditions. Therefore, the steering policy chosen is dictated by which one will provide the fastest speed of response in the desired maneuver direction.

This report will consider the control and aerodynamic requirements of the CBTT steering policy. LBTT may be a subject for future studies.

6.2 Design Approach and General Requirements

A fixed flight condition (i.e., constant altitude, Mach number and missile weight and inertias) was selected for these preliminary performance studies of circular and elliptical airframes. Fixed flight conditions are typically used in preliminary autopilot designs to identify and cure critical areas of concern. When autopilot requirements are satisfied at fixed flight

conditions, areas of concern introduced by time varying flight conditions are then addressed. The selected flight condition, at 60K ft altitude and Mach 3.95, provides a sufficiently low dynamic pressure so that missile maneuvers will result in large enough angles-of-attack to exercise sideslip control. Follow-on studies should study even lower dynamic pressures which will further increase angles-of-attack and exercise sideslip control further and also higher dynamic pressures and more rapid speeds of response which would increase missile angular rates and in turn kinematic and inertial coupling problems. This will be expanded upon in Sections 8 through 10.

The effect of gravity was included in the nonlinear 3-D performance studies. In addition, a series of acceleration commands was applied to reveal the critical problem areas which may be present for CBTT control. In particular, the first "climb" command was applied to cause the missile to increase angle-of-attack without a corresponding roll maneuver (i.e., pull an upward maneuver from a trimmed cruise attitude). The second "dive" command forced the missile to roll about its velocity vector while at an angle-of-attack which could result in sideslip control and kinematic and inertial coupling problems.

The first phase of the design approach for the CBTT autopilot was to design each channel independently with all coupling between channels removed. This reduced the problem to the well-established linear and nonlinear design techniques of roll stabilized, skid-to-turn missile autopilots. Sufficient high frequency attenuation was added for actuator and missile elastic mode frequencies so that the resulting missile body angular rates and control surface motion would represent a practical missile design. A relationship was established among the relative speeds of response of the uncoupled channels in order to meet CBTT requirements. The acceleration response of the pitch channel must be the same as the required response in the desired maneuver plane to satisfy a "climb" maneuver when the roll and yaw channels are not required. The roll channel must have an attitude response which is at least as fast as the pitch channel so that the missile may be rolled around the

velocity vector sufficiently fast to achieve the required maneuver plane response. To coordinate missile motion or minimize sideslip, the response of the yaw channel must be faster than the roll channel to which it is slaved. Details of the requirements for the uncoupled channels are provided in Appendices D through F.

The second phase in the design approach for the CBTT autopilot is addressed in Section 7.0. A linear design and analysis technique was used to predict and adjust when necessary the stability of the coupled autopilot and the quality of sideslip control. In addition, the influence of cross-coupling (i.e., aerodynamic, kinematic and inertial) was isolated in order to reveal ideal airframe characteristics for CBTT. The combination of linear analysis in Section 7 and nonlinear 3-D analysis in Sections 8 through 10 identifies the limitations of CBTT control of the circular and elliptical airframes investigated and the importance of the various aerodynamic parameters in establishing satisfactory CBTT control.

STEERING POLICY	PITCH CHANNEL	YAW CHANNEL	ROLL CHANNEL
LBTT BTT-90	Develop commanded acceleration. Equal positive and negative angle-of-attack capability.	Coordinate with roll channel to minimize sideslip.	Roll airframe to direct lift vector. Maximum roll attitude error of 90 degrees.
CBTT BTT-180	Develop commanded acceleration. Positive angle-of-attack capability only.	Coordinate with roll channel to minimize sideslip.	Roll airframe to direct lift vector. Maximum roll attitude error of 180 degrees.

TABLE 6.1 Steering Policy Control Features

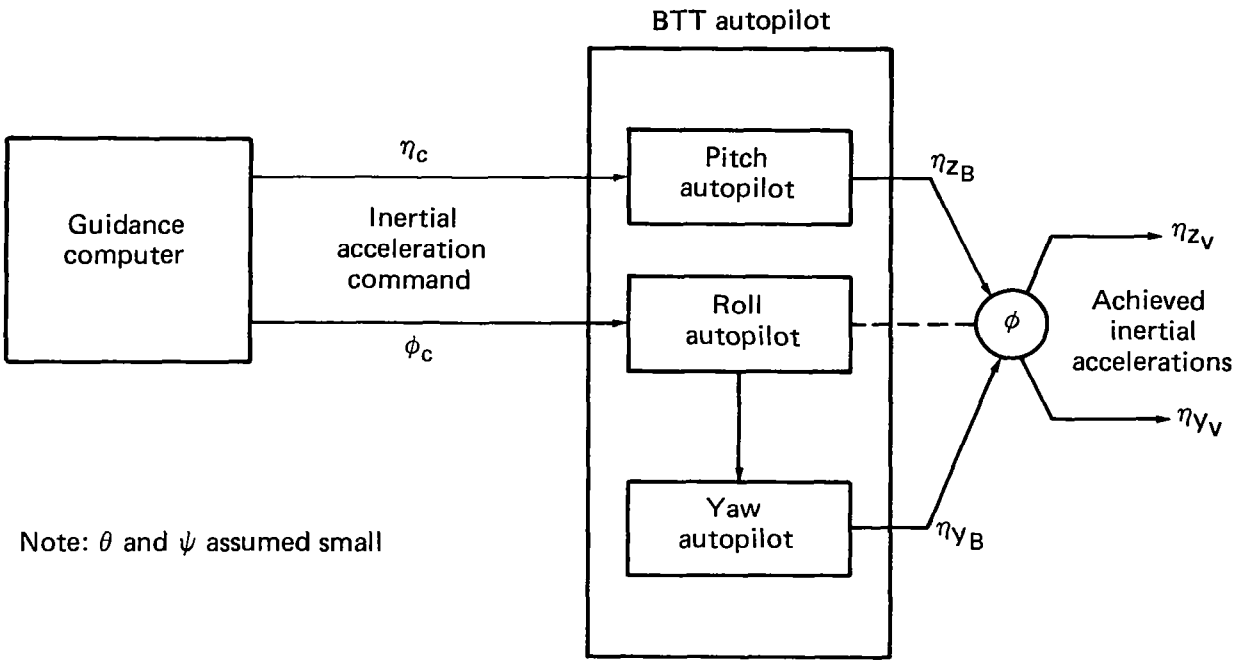

Fig. 6.1 BTT autopilot.

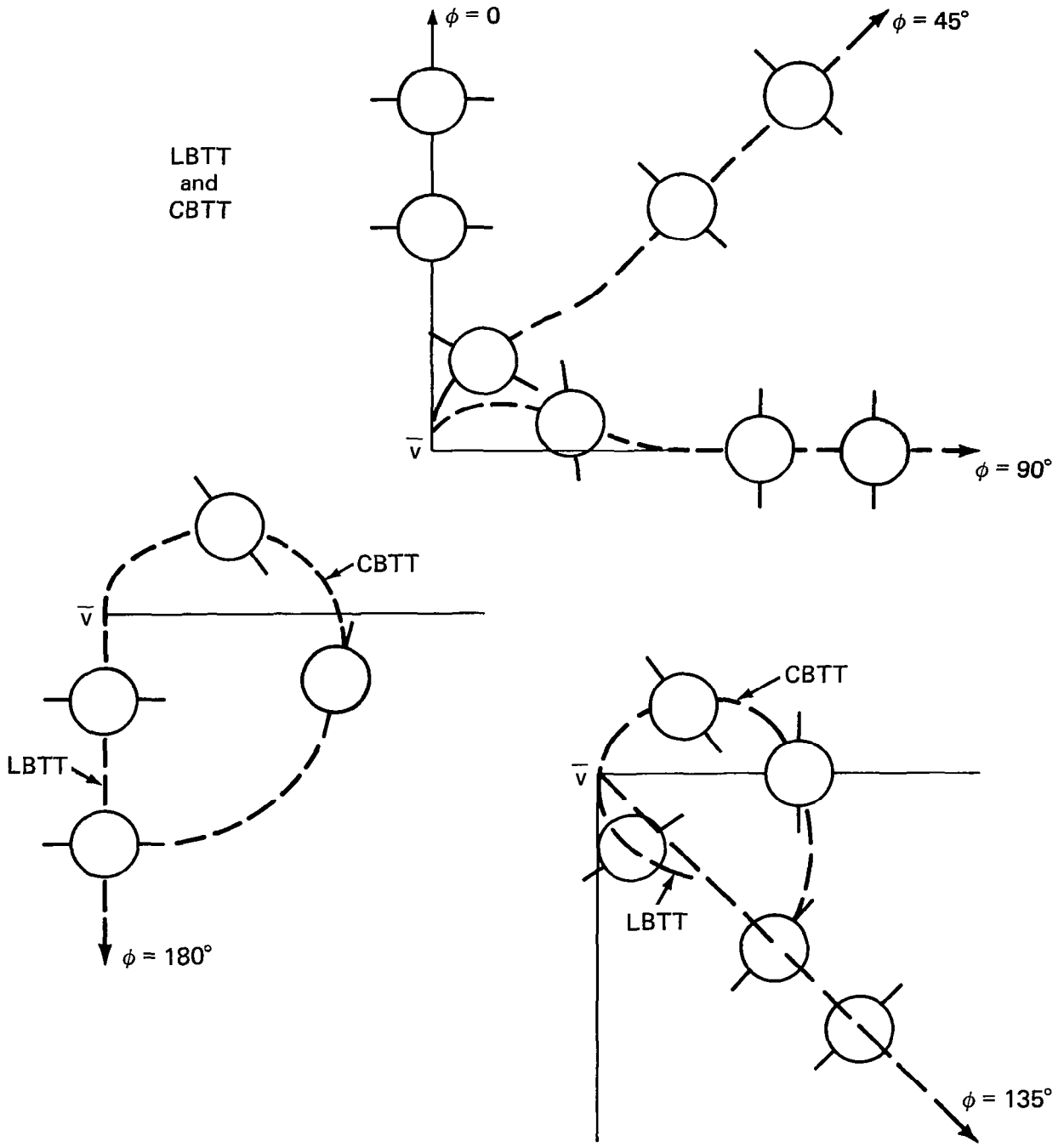

Fig. 6.2 *Coordinated missile motion for coordinated bank-to-turn (CBTT) and limited bank-to-turn (LBTT) control policies.*

7 LINEAR DESIGN AND ANALYSIS OF CBTT AUTOPILOT

The linear design and analysis technique began with uncoupled autopilot channels (i.e., aerodynamic, kinematic and control law cross-coupling between pitch, yaw and roll channels were removed). Using the experience gained in skid-to-turn missile autopilot design, pitch, yaw and roll autopilots were designed for the circular and elliptical airframes as described in detail in Appendices D, E, and F. The uncoupled autopilot design technique was classical, using a combination of Frequency Response and Root Locus techniques, to achieve practical bandwidths (i.e., sufficient high frequency attenuation) and in-turn provide the range of required missile body angular rates and control motions. In addition, the resulting design minimized the influence of aerodynamic variations on desired response. Finally, and most important, the design approach has been proven by many skid-to-turn missile programs to produce desired results. The application of the uncoupled autopilot channels to the CBTT autopilot is accomplished by an appropriate choice of the relative time constants of the uncoupled autopilot channels. To achieve the desired maneuver plane acceleration response for the CBTT autopilot, both pitch and roll uncoupled autopilots were designed to have the desired maneuver plane speed of response. The yaw channel, which follows the roll channel motion to produce desired coordination (or minimization of sideslip angles), was designed to have a more rapid response than the roll channel. In particular, the goal for maneuver plane acceleration response was a 0.5 second time constant for the flight condition of interest (i.e., 60 Kft altitude, Mach 3.95). The uncoupled autopilot designs in Appendices D through F resulted in the following time constants,

	Circular	Elliptical
PITCH ACCELERATION	0.5	0.5
ROLL ANGLE	0.55	0.55
YAW ACCELERATION	0.39	0.36

Although the roll time constants are not equal to the goal of 0.5 seconds and the yaw time constants are not to equal 0.4 seconds, they were considered close enough to the goal to be acceptable for this analysis.

In the next phase of the linear design technique the autopilot channels are coupled using the aerodynamic model of Section 5. For both airframes, CBTT control laws are devised to add control coupling for coordinated missile motion (Section 7.1). A measure of sideslip control is obtained by applying a roll angle command to the linearized CBTT autopilot (Section 7.2). The relative stability of the autopilot branches and means for improving stability are discussed in Section 7.3. An examination of the autopilot sensitivity to aerodynamic cross-coupling is made in Section 7.4. Conclusions from the linear analysis are presented in Section 7.5.

7.1 CBTT CONTROL LAWS

The control laws which were used by the CBTT autopilots of the circular and elliptical airframes are shown in Figures 7.1 and 7.2. The pitch control laws shown in Figure 7.1 are the same as determined in the uncoupled pitch channel study of Appendix D. The autopilot cross-coupling branch, shown in bold lines in Figure 7.2, has been added to provide coordinated motion between roll and yaw channels as discussed in Section 6. The coordinating command, r_c, is a yaw angular rate command which is equal to $-p\bar{\alpha}$ when gain K_{YP} is unity. Missile roll rate, p, is measured with a rate gyro. However, $\bar{\alpha}$ is estimated angle-of-attack which for the purpose of this study is exactly equal to α. For the linear dynamics model in Fig. 5.5, the coordinating command r_c is equal to $-p\alpha_e$ where α_e is the trim or equilibrium angle-of-attack. The choice of the coordinating gain K_{YP}, and the change in the lead of the roll actuator command branch compensation from the uncoupled roll autopilot design value of 110 rad/sec to 60 rad/sec, are discussed in Section 7.3.

7.2 TIME DOMAIN ANALYSIS OF THE LATERAL CHANNELS

7.2.1 CBTT Autopilots of Circular and Elliptical Airframes

Linear time domain analysis of the CBTT autopilots, which used the linear aerodynamic model shown in Section 5, assumed that the missile is initially in the desired maneuver plane and trimmed at ten degrees angles-of-attack (i.e., the equilibrium or trim angle-of-attack α_e in the model of Fig. 5.5 equals 10 degrees and the equilibrium roll rate P_e in the models of Figures 5.4 and 5.5 equals zero). The lateral dynamics model, uncoupled from the pitch dynamics as a result of $P_e = 0$, is typically used for skid-to-turn controlled missiles to determine relative stability at different trim angles-of-attack. When $P_e = 0$, Q_e (i.e., equilibrium pitch rate) has been found to have negligible influence in the lateral model compared to α_e and was therefore set equal to zero. To determine sideslip control of the CBTT autopilots for small changes in maneuver direction, the roll autopilot is now commanded with a small roll angle command to force the sideslip to be perturbed from its zero trim value. Since the model is linear, and therefore the magnitude of the sideslip is directly proportional to the magnitude of the input command, a one radian roll angle command was used for convenience. It has been found that if the resulting maximum sideslip angle is less than 1 degree, the maximum sideslip angle obtained from the nonlinear 3-D simulation is well within 5 degrees. The technique is also useful for comparing the relative quality of sideslip control of different control laws or airframes.

Figures 7.3 and 7.4 show that the sideslip control of the linearized CBTT autopilot for the elliptical airframe is considerably better than the CBTT autopilot of the circular airframe. The coupled

autopilots had roll angle responses which were essentially the same as the uncoupled roll channel response differing slightly in overshoot.

When the coordinating branch gain K_{YP} was set to zero in the CBTT autopilot of the circular airframe, the maximum sideslip angle increased to 2.8 degrees. Therefore, for the circular airframe, the coordinating branch is not very effective in helping the yaw autopilot to reduce sideslip angle. If K_{YP} is increased to unity, as it is for the CBTT autopilot of the elliptical airframe, the maximum sideslip remains below one degree for 3 seconds but the autopilot is unstable. Before attempting to modify the control law of the CBTT autopilot of the circular airframe to improve sideslip control, the linear analysis will first be verified by the nonlinear analysis of section 9.

Removal of the aerodynamic cross-coupling, (i.e., C_{ℓ_β}, $C_{\ell_{\delta_Y}}$, $C_{n_{\delta_R}}$) had no effect on the sideslip angle. This showed that the aerodynamic cross-coupling plays an indirect role in determining the quality of sideslip control. The aerodynamic cross-coupling limits the quality of sideslip control by determining the relative stability of the coordination branch or the magnitude of the coordination gain K_{YP}. The magnitude of sideslip angle is dependent on the nulling effects of two parallel paths shown in Figure 7.5. The contribution of yaw acceleration η_y to the maximum β is negligible and therefore neglected. β is formed mainly by the subtraction of the kinematic paths of $\alpha_e p$ (shown in aerodynamic model of Section 5) and the yaw angular rate r. The coordination is obtained in the CBTT control law by commanding the yaw autopilot with a yaw angular rate command r_c (Figure 7.2) of $K_{YP}\ \alpha_e p$ which forces r to be equal to $\alpha_e p$ and therefore nulling $\dot{\beta}$ as shown in Figure 7.5. The nulling process will be accomplished more efficiently if $K_{YP} = 1.0$. The reason the sideslip is not nulled completely is that η_y is not zero and r cannot equal r_c over all frequencies.

7.2.2 Slower Response CBTT Autopilot for Circular Airframe

Slowing the roll angle response will in-turn slow down the desired maneuver plane acceleration response. A slower roll channel should make the job of coordinating missile motion easier for the yaw channel. To determine the effect on sideslip control, the roll angle response of the circular airframe was slowed to a time constant of 0.93 seconds by reducing the roll angle error gain from 2.2 to 1.1. Maximum sideslip angle reduced from 2.3 to 1.38 degrees (i.e., a factor of 0.6). Since a desired maneuver plane acceleration time constant for the flight condition of interest is 0.5 seconds, the roll channel would not be slowed down to improve sideslip control unless nonlinear 3-D analysis showed that the desired maneuver plane acceleration time constant of 0.5 seconds cannot be obtained. On the other hand if the mission of the missile does not require a 0.5 sec time constant, improved sideslip control can be achieved by going to a slower roll channel.

7.3 AUTOPILOT STABILITY

7.3.1 CBTT Autopilots of Circular and Elliptical Airframes

The linearized CBTT autopilot of the circular airframe was unstable when the uncoupled channel control laws determined in Appendices D through F were used with a coordinating branch gain K_{YP} (Figure 7.2) of unity. The autopilot was stabilized by decreasing K_{YP} to 0.458. However, the roll actuator command branch had only a 19 degree phase margin which was increased to the required magnitude of 30 degrees by decreasing the lead of the actuator command compensation from 110 rad/sec. to 60 rad/sec. while still maintaining required high frequency attenuation of at least 15 dB at 100 rad/sec.

Although the 60 rad/sec actuator lead was retained for the elliptical control law, the stability was considerably better for the CBTT autopilot of the elliptical airframe. Due to the improved stability, K_{YP} could be set at unity which resulted in a substantial decrease in the magnitude of sideslip angle as is shown in Section 7.2. The reason for the improvement in stability of the elliptical airframe compared to the circular airframe is discussed in Section 10.

A comparison of the relative stability of autopilot branches for the two airframes subject to small roll perturbations is shown in Tables 7.1 and 7.2 when the missiles are in the desired maneuver plane at ten degrees angles-of-attack. The effect of constant pitch rate Q_e on lateral dynamics has been neglected by setting Q_e to zero. Since the pitch channel is uncoupled from the lateral channel when $P_e = 0$, the stability margins for the pitch channel will be the same as shown in Appendix D. It is important to note that the comparison between autopilots is being made with $K_{YP} = 1.0$ for the elliptical and $K_{YP} = 0.458$ for the circular. Table 7.2 shows that the coordination branch of the elliptical autopilot still has 4.6 dB more stable gain margin than the circular

The uncoupled autopilots, see Appendices D, E, and F, must have sufficient relative stability at small angles-of-attack to maintain required stability margins when angles-of-attack are increased and/or effects of cross-coupling due to CBTT control are added. Comparison of the relative stability and frequency responses of the CBTT autopilot branches with the corresponding uncoupled autopilot branches will indicate which are more sensitive to the dynamic changes. The sensitive branches may then be used to isolate the critical type of cross-coupling, by removing each cross-coupling and observing whether the response differs from that of the uncoupled version. Once the critical cross-coupling is known, a method of compensating for it can be determined if the effect of the coupling is

or becomes too severe with increased angle-of-attack or a change in flight condition.

The critical autopilot branch in the roll channel is actuator command. Comparing the margins of the roll channels in the CBTT autopilots shown in Table 7.1 for α = 10 deg with the uncoupled version in Tables F.2 (i.e., α = 0) and F.3 (i.e., α = 20 deg), the actuator commands of both circular and elliptical airframes have acquired decreasing gain margins (denoted by the negative signs) in the CBTT autopilots. A decreasing gain margin is the number of dB that a gain must be decreased to cause instability. An increasing gain margin, denoted by a positive sign, is the number of dB a gain must be increased to cause instability. The significance of the negative gain margins in the actuator command branches is that it may be important to prevent large commands from limiting. Limiting will decrease the gain of the fundamental frequency in the branch, reducing the decreasing gain margin, and can result in nonlinear stability problems. The roll actuator command branch margins and high frequency attenuation are satisfactory for both airframes for the CBTT autopilots (i.e., gain margins $\geq$ 6 dB, phase margins $\geq$ 30 degrees with a goal of 12 dB and 50 deg; high frequency attenuation $\geq$ 15 dB at 100 rad/sec). However, the roll actuator command branch of the CBTT autopilots is the most sensitive to cross-coupling. A comparison of the corresponding frequency responses of Figures 7.6 and 7.7 with the uncoupled version in Figure F.6 shows that the response of the circular airframe has been modified considerably. A peak in gain occurs at 2.9 rad/sec and a large loss in gain and phase occurs below 1 rad/sec. Approximately 5 dB of high frequency attenuation at 100 rad/sec was also lost in the CBTT of the circular. The large change in actuator command frequency response for the circular airframe implies considerable change in roll tail motion for the CBTT autopilot. The roll actuator command response (Figure 7.7) for the elliptical airframe on the other hand had an increase in gain over the

frequencies calculated except for a 5 dB loss in high frequency gain like the circular compared to the uncoupled system. Phase shift has increased a small amount for frequencies below 5 rad/sec. The response of the elliptical is a lot closer to the uncoupled roll channel than the circular and therefore so should the time response of roll tail incidence. Both the elliptical and circular roll actuator command branches have increasing gain margins above 100 rad/sec which is the highest frequency calculated. These margins, which will therefore be dependent on high frequency elastic mode autopilot filters, must be greater than the attenuation at 100 rad/sec at a frequency above 100 rad/sec.

Comparing Table 7.1 and F.2 shows that the attenuation at 100 rad/sec for the roll rate error branch of both airframes decreased 4.2 dB, compared to the uncoupled roll autopilot at $\alpha = 0$, but are still satisfactory. Phase margin has increased for the elliptical and decreased for the circular but both margins are large. The effect of the coupling on the frequency response of the roll rate error branch has been considerably reduced for the circular airframe compared to the effect the coupling had on the roll actuator command branch. The circular has a loss in low frequency gain and phase below 1 rad/sec. The gain for the elliptical is close to the uncoupled version except at frequencies above 10 rad/sec where a loss of attenuation and a decrease in phase occurs.

The roll angle error branch has large margins for both airframes. The effect of the coupling is even less than it was for the roll rate error branch. The gain margins have lost a few dB. The phase margin of the elliptical has increased whereas the margin for the circular has decreased. The changes in the frequency responses were minor compared to the uncoupled version.

Frequency responses for the coordination branch are shown in Figures 7.8 and 7.9. The circular has considerable loss in low frequency gain which apparently influences the quality of coordination. Although stability margins of both airframes are satisfactory, it would be desirable to increase K_{YP} of the circular coordination branch 6.8 dB to unity for improved sideslip control, however, this would leave the circular with unsatisfactory relative stability.

A comparison of Tables 7.2 and E.2 show that the yaw actuator command branch of the circular CBTT autopilot has a 0.8 dB loss in the decreasing gain margin and a 9.1 degree loss in phase margin compared to the uncoupled version. The elliptical has lost the decreasing gain margin of the uncoupled version and has lost 9 degrees of phase margin. A comparison of frequency response for the circular in Figures 7.10 and E.10 shows an increase in gain below 10 rad/sec and an increase in attenuation above 20 rad/sec. The phase shift is close to the uncoupled system except for a sudden increase at 40 rad/sec. Comparing the frequency response for the elliptical in Figures 7.11 and E.12 shows that the elliptical yaw actuator command branch has lost gain below 10 rad/sec and increases attenuation above 20 rad/sec. Phase shift is the same until a sudden increase at 30 rad/sec. The circular airframe is unstable airframe in yaw and the elliptical is stable in yaw. As shown in Appendix E, the stable airframe requires additional yaw control surface effort compared to the unstable airframe. The change in low frequency gains of the coupled actuator branches will increase the difference in control effort between the two airframes. The coupling effect into the roll actuator was much greater than the effect on the yaw actuator.

The yaw acceleration feedback branch of the circular lost 2.2 dB and the phase margin 4.2 degrees compared to the uncoupled version as shown in Tables 7.2 and E.2. Attenuation at 100 rad/sec is the

same. The elliptical has lost 1.5 dB and has approximately the same phase margin. Changes in the frequency responses from the uncoupled version were minor.

7.3.2 Effects of Removing Aerodynamic Cross-Coupling

In order to study the effects of aerodynamic cross-coupling on autopilot performance, the terms describing the aerodynamic cross-coupling were removed for the circular airframe case. The roll channel frequency responses changed to that of the uncoupled version except above 50 rps where there was a slight loss in attenuation of the actuator and rate error branches. The yaw actuator had an increase in gain below 10 rad/sec. Otherwise the yaw channel margins were the same as the uncoupled version.

Aerodynamic cross-coupling has therefore produced the large variations in frequency responses shown in Section 7.3.1 (Figure 7.6) and the decrease in autopilot stability. The coordinating autopilot command without aerodynamic cross-coupling only influences the magnitude of sideslip angle.

7.3.3 Effect of Slowing Roll Angle Response

Slowing the roll angle response of the circular CBTT autopilot by reducing the roll angle error gain from 2.2 to 1.1 has been shown in Section 7.2 to reduce the maximum sideslip angle. The only stability margins to be affected by the change are in the roll channel. The roll angle error branch gain margin increases 6 dB by the change in the error branch gain. Roll rate error phase margin decreases 1.1 degrees and its high frequency attenuation remains the same. The decreasing gain margin in the roll actuator command branch increases 5.3 dB while its phase margin and high frequency attenuation remain the same.

7.3.4 Autopilot Stability vs. Constant Roll Rate

The relative stability determined in Sections 7.3.1 through 7.3.3 was for a missile at constant angle-of-attack in the desired maneuver plane with small roll rate perturbations. To study the stability of a CBTT autopilot when it is changing desired maneuver directions, the linear aerodynamic model shown in Section 5 is used. It couples the pitch and lateral aerodynamics via a constant missile roll rate. The missile is at a constant angle-of-attack and the roll channel of the CBTT autopilot is commanded with a ramp function of roll angle which rolls the missile about its velocity vector with a constant missile roll rate.

A constant missile roll rate of 300 deg/sec (i.e., P_e = 5.24 rad/sec which is the maximum expected roll rate for the conditions studied) and a constant pitch rate of 1.29 deg/sec (i.e., Q_e = 0.0225 rad/sec which was the approximate trim rate for α = 10 degrees was used for the stability study. The resulting autopilot stability margins are shown in Table 7.3 for the circular airframe. The constant roll rate has not had a large effect on the stability margins. The stability is still satisfactory and the major changes are in frequency responses. Although the roll actuator command margins remained essentially the same, the sharp peak in gain shown in Figure 7.6 for P_e = 0 is gone and the phase shift has become more like the uncoupled version but with a larger phase shift at low frequencies. The constant roll rate caused a reduction in gain and phase shift below 10 rad/sec for the yaw actuator command branch. The sharp peak in gain of the uncoupled pitch actuator command branch in Figure D.9 is gone. The gain has increased below 10 rad/sec and phase shift variations are less. The deep notch in gain of the co-ordination branch (Fig. 7.8) is gone and phase shift has increased below 10 rad/sec. The uncoupled pitch acceleration feedback

(Fig. D.8) has considerable loss in gain and decrease in phase shift below 10 rad/sec. The same change results for yaw acceleration feedback as for pitch acceleration feedback.

The results for constant roll rate show that autopilot stability is not greatly affected but that the kinematic and inertial coupling between pitch and yaw channels will oppose changes in pitch acceleration due to loss in gain at low frequencies in pitch acceleration feedback. The loss in gain at low frequencies for the yaw actuator and acceleration should also affect sideslip control which has been shown to be influenced by frequency below 5 rad/sec in the coordination branch frequency response.

7.4 AERODYNAMIC CROSS-COUPLING SENSITIVITY

Section 7.3 has shown that the CBTT autopilot of the circular airframe has less stability than the CBTT autopilot of the elliptical. This results in larger sideslip due to a lower coordination command branch gain. The reduction in stability is due to aerodynamic cross-coupling. The sensitivity of aerodynamic cross-coupling for the CBTT autopilot of the circular airframe is shown in Table 7.4. The gain margins listed show how much each cross-coupling stability derivative must be increased in magnitude to cause instability. A decrease in margin denotes an increase in the sensitivity of the cross-coupling derivative.

To assure autopilot stability, the sensitivity of the autopilot is considered satisfactory if the gain margins on the aerodynamic parameters $C_{\ell_{\delta_Y}}$, $C_{\ell_{\delta_R}}$, and C_{ℓ_β} are $\geq$ 3 dB for any given flight condition. The sensitivity, which increased for $C_{\ell_{\delta_Y}}$ with constant missile roll rate, is satisfactory for roll perturbations and constant roll rate at 10 degrees angle-of-attack.

7.5 CONCLUSIONS

Linear CBTT autopilot studies have revealed the following:

1. CBTT autopilot of circular airframe (Figures 7.1, 7.2) required a coordinating gain K_{YP} much less than the desired value of unity and a change in roll actuator compensation of the uncoupled autopilot (Fig. F.2) to achieve the desired relative stability (Table 7.1, 7.2) at 10 degrees angle-of-attack with roll perturbations. The relative stability is not greatly effected by missile roll rate (Section 7.3.4, Table 7.3).

2. The desired relative stability of the CBTT autopilot for the elliptical airframe (Tables 7.1, 7.2) is achieved with the desired coordinating gain of unity and no change in the uncoupled autopilot (Figures 7.1 and 7.2). Therefore, the relative stability of the CBTT autopilot of the elliptical airframe is not influenced as much by the coupling as is the CBTT autopilot of the circular airframe.

3. Sideslip control by the CBTT autopilot for the elliptical airframe is considerably better than by the CBTT autopilot of the circular airframe (Figures 7.3 and 7.4).

4. Sideslip amplitude is not changed by aerodynamic cross-coupling for a particular coordination gain K_{YP} at 10 degrees angle-of-attack (Section 7.2.1).

5. Sideslip magnitude is minimized by setting K_{YP} to unity (Section 7.2.1) and the minimum magnitude is determined by the uncoupled yaw channel.

6. Cross-coupling aerodynamics determines autopilot stability which in-turn may prevent setting K_{YP} to its desired value of unity to minimize sideslip angle (Section 7.3.2, 7.2.1).

7. The sensitivity of the CBTT autopilot of the circular airframe to aerodynamic cross-coupling coefficients is satisfactory for the roll perturbutions and constant missile roll rate (Section 7.4, Table 7.4) at 10 degrees angle-of-attack.

8. As a result of the linear analysis in Section 7, it is expected that the nonlinear 3-D dynamic analysis would show that the CBTT autopilots of the circular and elliptical autopilots should have satisfactory sideslip control and performance (i.e., for maneuvers up to 10 degrees angles-of-attack at the flight condition of interest). Maneuvers requiring larger angles-of-attack may require additional linear stability and response studies and possibly autopilot modification.

The above conclusions are verified in 3-D nonlinear time domain simulation studies.

Airframe (2)	Branch	*Gain Margin (dB)	(rad/sec)	Phase Margin (deg)	(rad/sec)	Attenuation at 100 rps (dB)
Circular	Roll Actuator Command	-28.8 >15.6	4.34 >100.	30.9	31.51	15.6
Elliptical		-30.9 >15.5	2.58 >100.	36.9	31.48	15.5
Circular	Roll Rate Error	>23.	>100.	76.9	23.14	23.
Elliptical		>23.	>100.	101.1	14.66	23.
Circular	Roll Angle Error	24.1	12.73	65.7	2.053	77.6
Elliptical		23.1	11.69	64.3	2.094	77.6

Note: 1) negative gain margin indicates how much the gain can be decreased before autopilot is unstable.
2) K_{YP} = 1 elliptical, K_{YP} = 0.458 circular

TABLE 7.1 A Comparison of Linear CBTT Roll Channel Stability Margins, α_e = 10 deg, P_e = 0, Q_e = 0

Airframe (2)	Branch	(1) Gain Margin (dB)	(rad/sec)	Phase Margin (deg)	(rad/sec)	Attenuation at 100 rps (dB)
Circular	Yaw Actuator Command	-9.6	5.71	41.7	15.78	24.3
Elliptical		>24.5	>100.	40.	14.2	24.5
Circular	Yaw Accel-eration Feedback	8.2	9.89	53.5	3.47	34.6
Elliptical		6.3	10.5	54.6	3.02	29.2
Circular	Coordination	8.4	26.85	---	---	19.9
Elliptical		15.69 13.	4.07 24.82	---	---	24.2

Note: 1) negative gain margin indicates how much the gain can be decreased before autopilot is unstable.
2) K_{YP} = 1 elliptical, K_{YP} = 0.458 circular.

TABLE 7.2 Comparison of Linear CBTT Yaw Channel and Coordination Branch Stability Margins, α_e = 10 deg , P_e = 0, Q_e = 0

Branch	Gain Margin (dB)	(rad/sec)	Phase Margin (deg)	(rad/sec)
Roll Actuator Command	-27.8	3.17	31.2	31.49
Yaw Actuator Command	-7.0	6.43	46.8	15.23
Pitch Actuator Command	---	---	70.8	24.31
Coordination	8.6	26.92	---	---
Pitch Acceleration Feedback	12.7	13.4	134.3	0.159
Yaw Acceleration Feedback	6.9	9.51	134.5	0.1496

TABLE 7.3 Linear CBTT Autopilot Stability Margins, Circular Airframe, α_e = 10 deg, , P_e = 5.2356 rad/sec, Q_e = 0.022483 rad/sec.

Aerodynamic Cross-Coupling Stability and Control Derivatives	P_e = 0 Gain (dB)	Margin (rad/sec)	P_e = 300 deg/sec Gain (dB)	Margin (rad/sec)
$C_{n_{\delta_R}}$	16.2 13.1	2.78 6.27	12.	6.11
C_{ℓ_β}	>52.	>100.	>52.	>100.
$C_{\ell_{\delta_Y}}$	10.9	7.74	8.4	7.3

TABLE 7.4 Sensitivity of Aerodynamic Cross-Coupling vs Missile Roll Rate for Circular Airframe

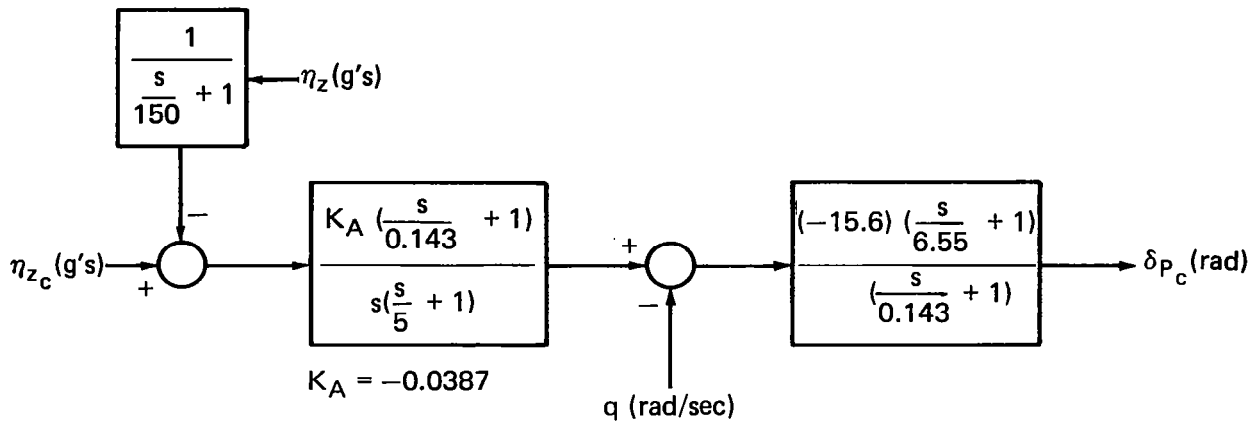

Circular airframe

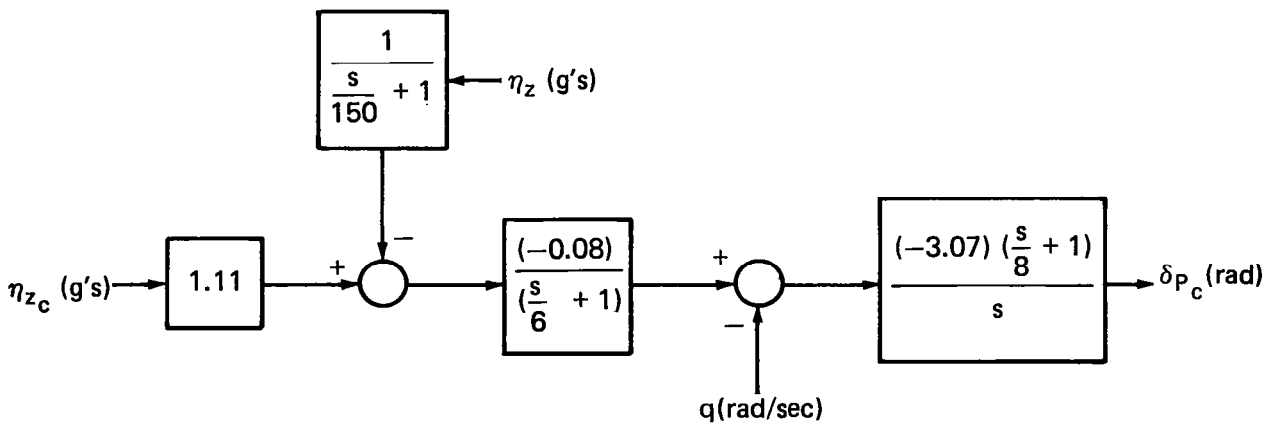

Elliptical airframe

Fig. 7.1 Pitch control laws.

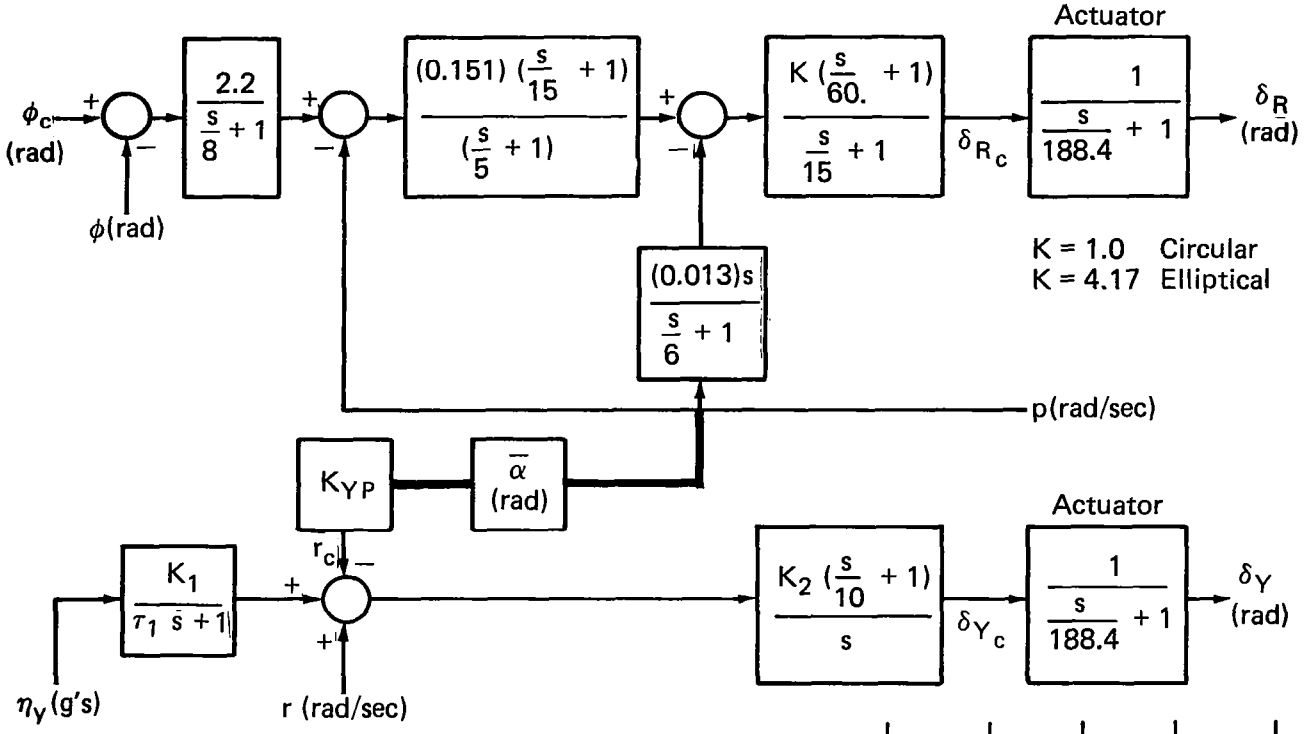

	K_1	τ_1	K_2	K_{YP}
Circular	0.32	0.2	4.85	0.458
Elliptical	0.839	0.25	6.08	1.0

Fig. 7.2 CBTT lateral control laws.

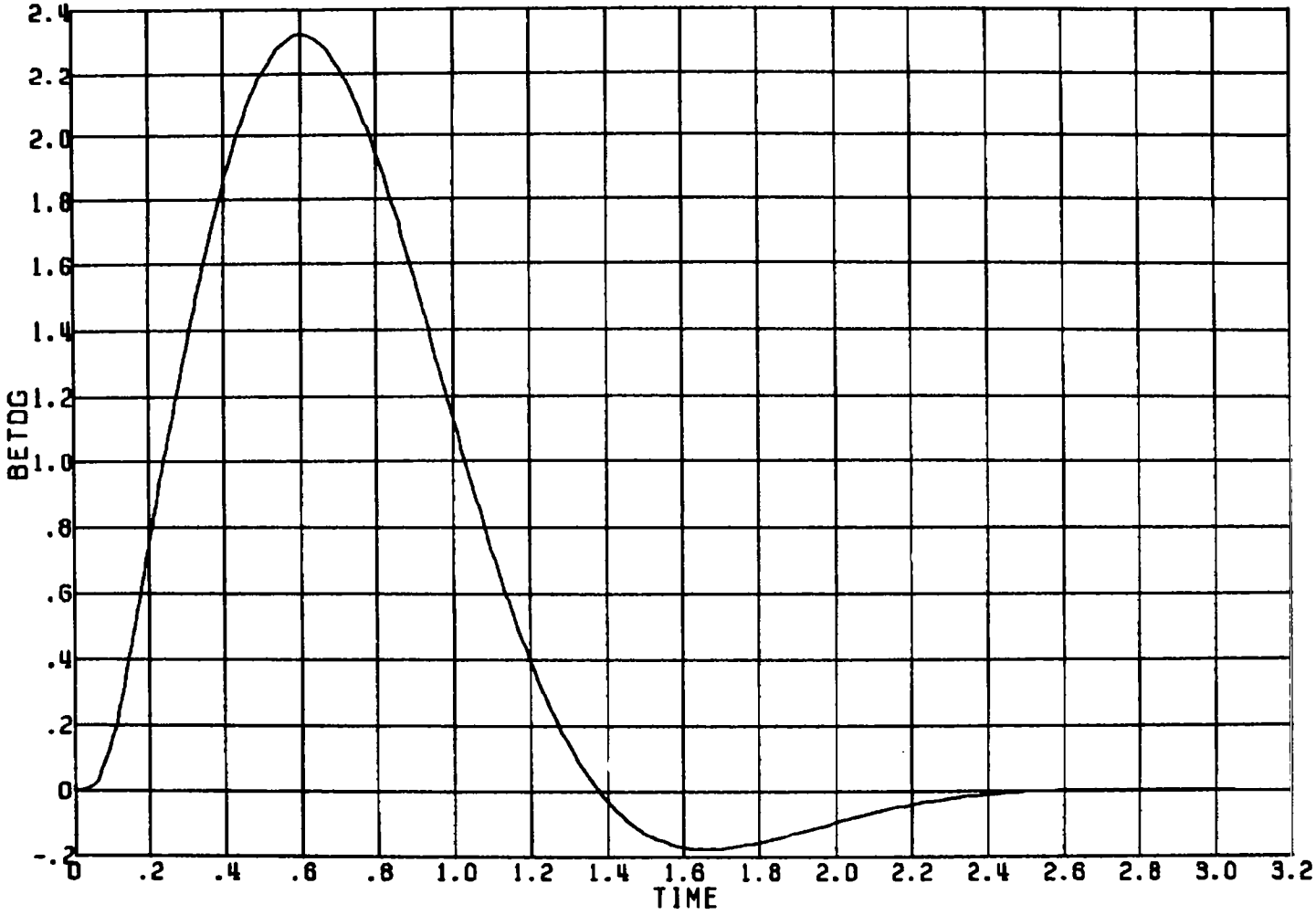

Figure 7.3 SIDESLIP ANGLE (DEG) VS. TIME (SEC); ONE RADIAN ROLL COMMAND; LINEAR CBTT AUTOPILOT, CIRCULAR AIRFRAME (α_e = 10 deg, $P_e = Q_e = 0$)

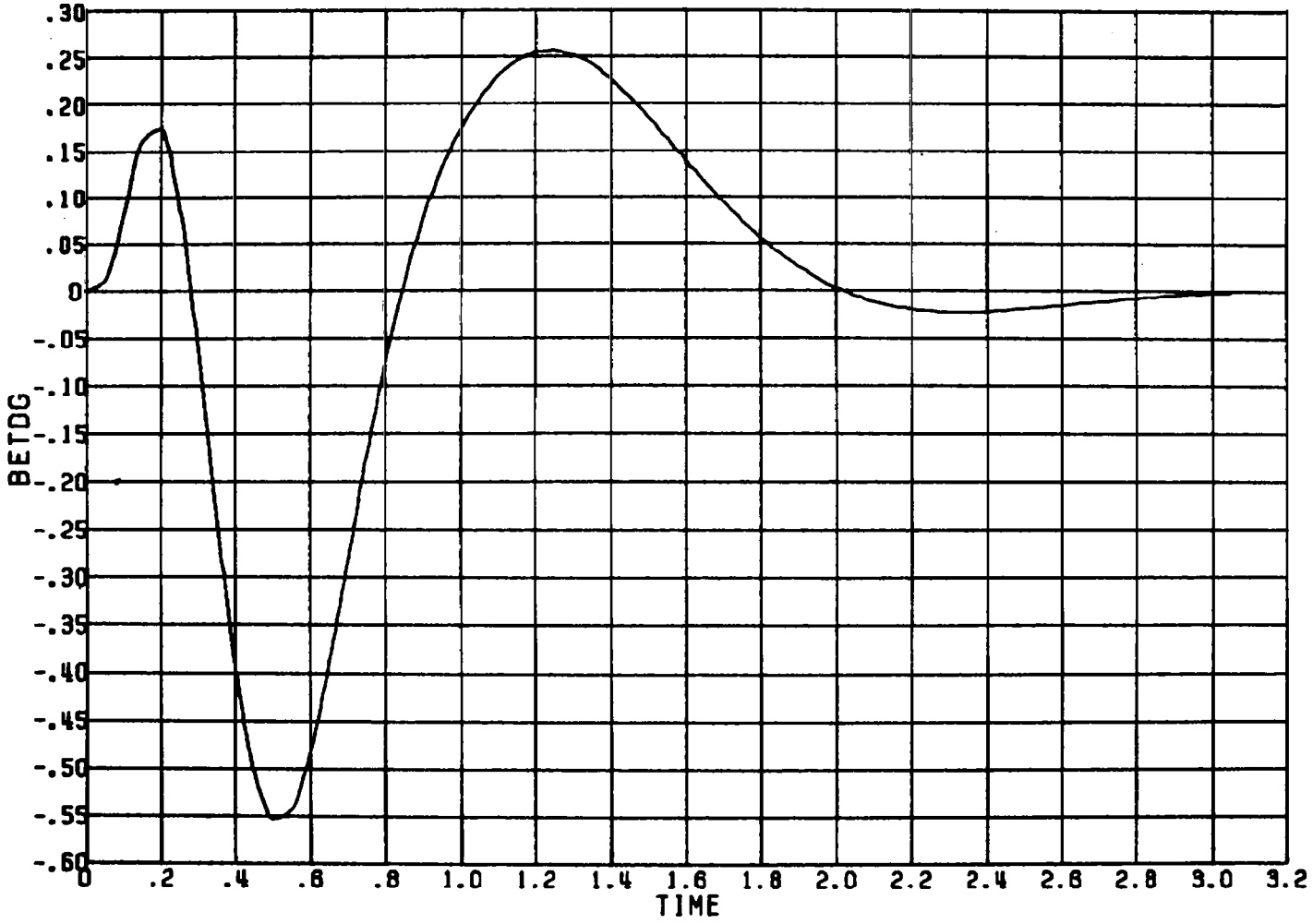

Figure 7.4 SIDESLIP ANGLE (DEG) VS. TIME (SEC); ONE RADIAN ROLL COMMAND; LINEAR CBTT AUTOPILOT, ELLIPTICAL AIRFRAME (α_e = 10 deg, $P_e = Q_e = 0$)

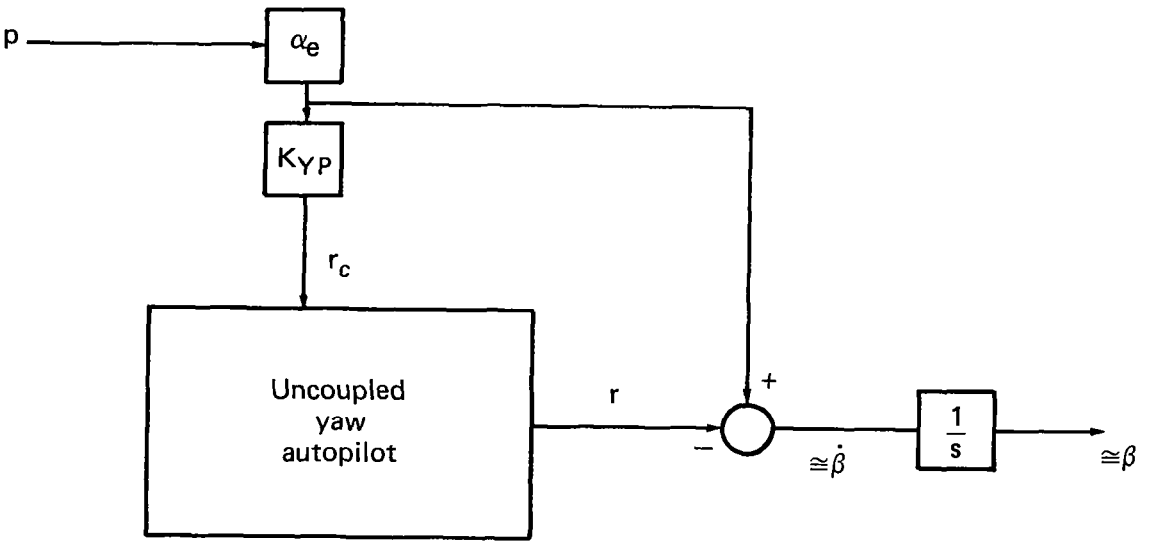

Fig. 7.5 Major contributors to quality of sideslip control of CBTT autopilot.

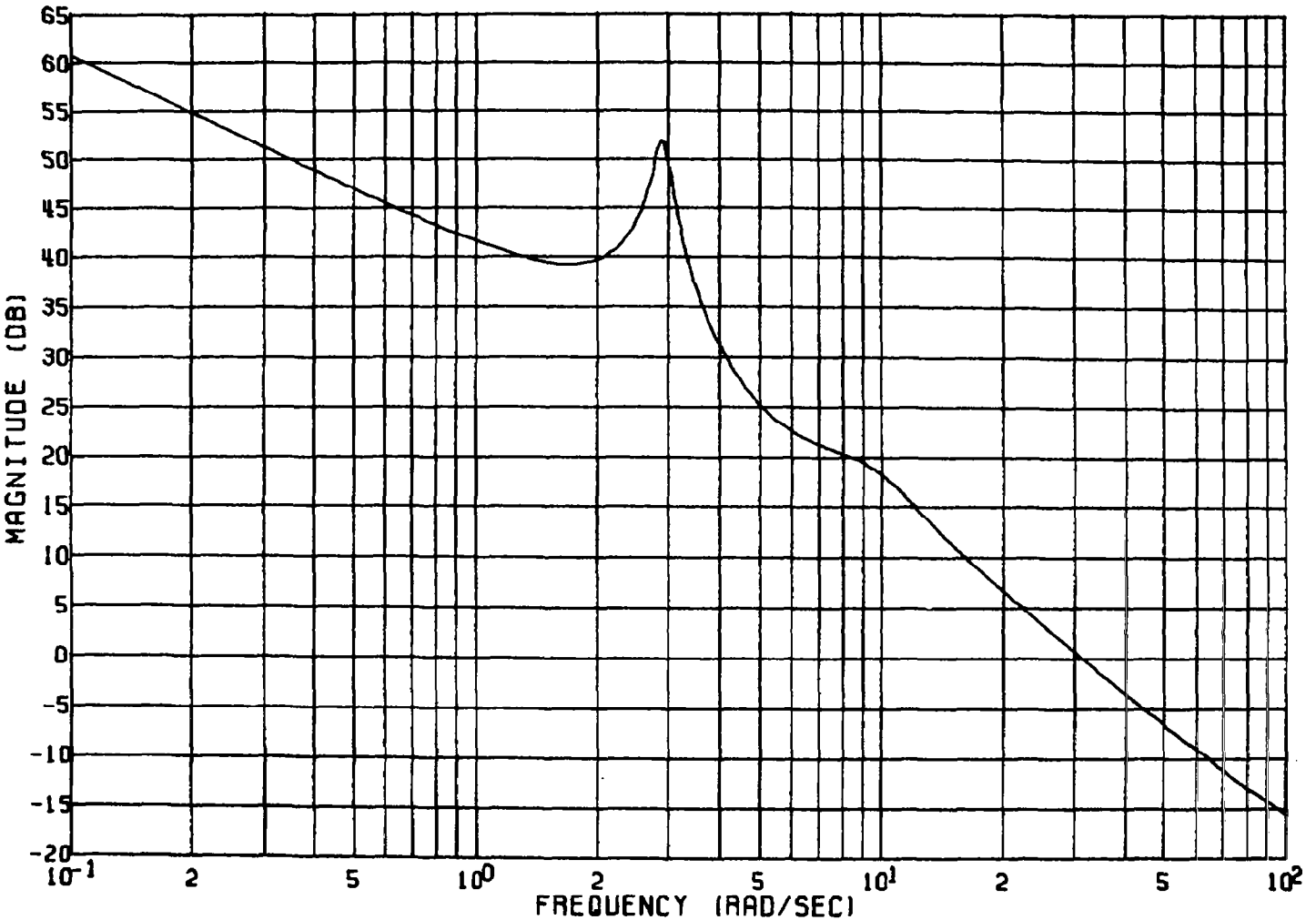

Figure 7.6(a) ROLL ACTUATOR COMMAND; LINEAR CBTT AUTOPILOT, CIRCULAR AIRFRAME (α_e = 10 deg, P_e = Q_e = 0) GAIN VS. FREQUENCY

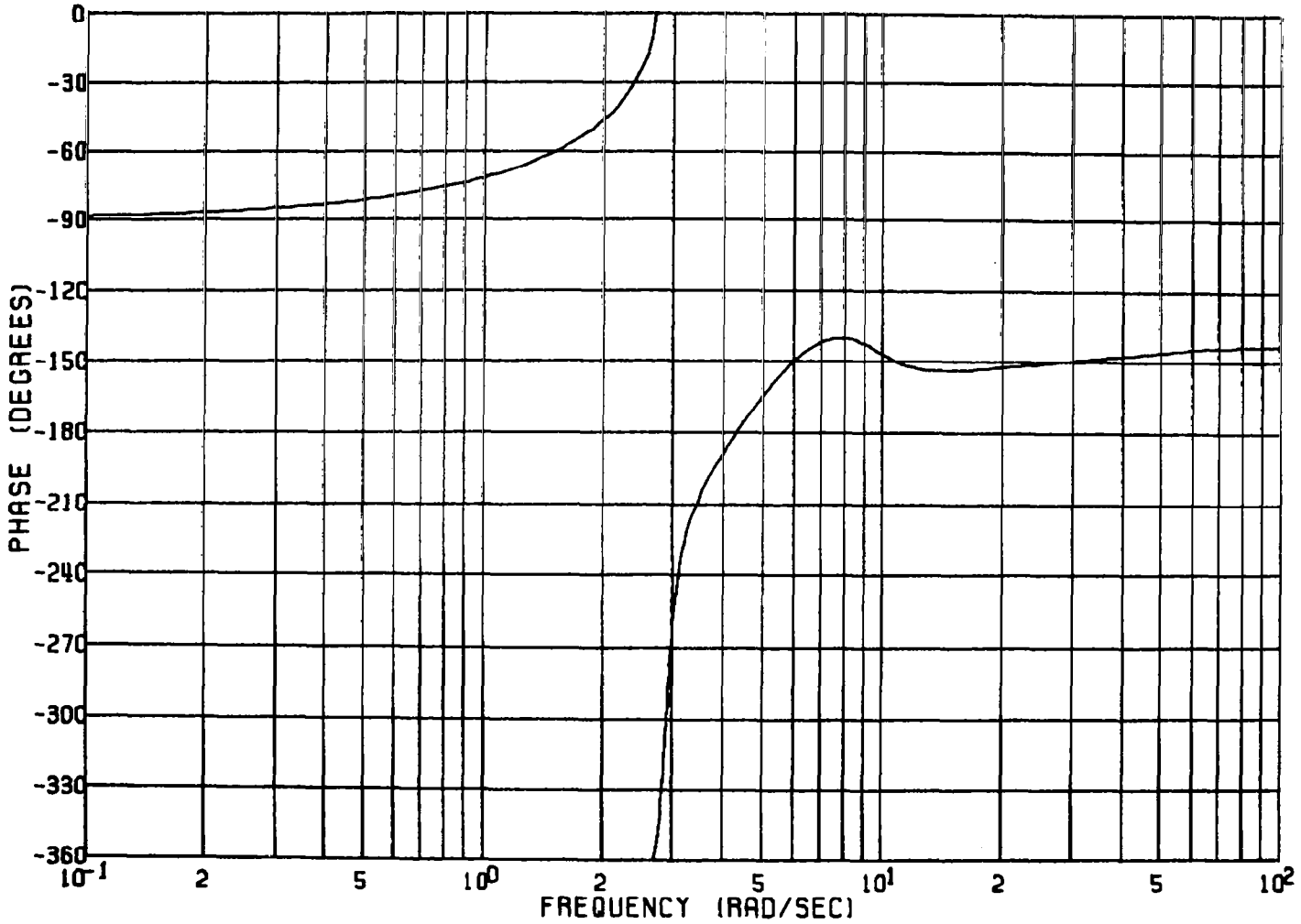

Figure 7.6(b) ROLL ACTUATOR COMMAND; LINEAR CBTT AUTOPILOT, CIRCULAR AIRFRAME (α_e = 10 deg, $P_e = Q_e = 0$) PHASE VS. FREQUENCY

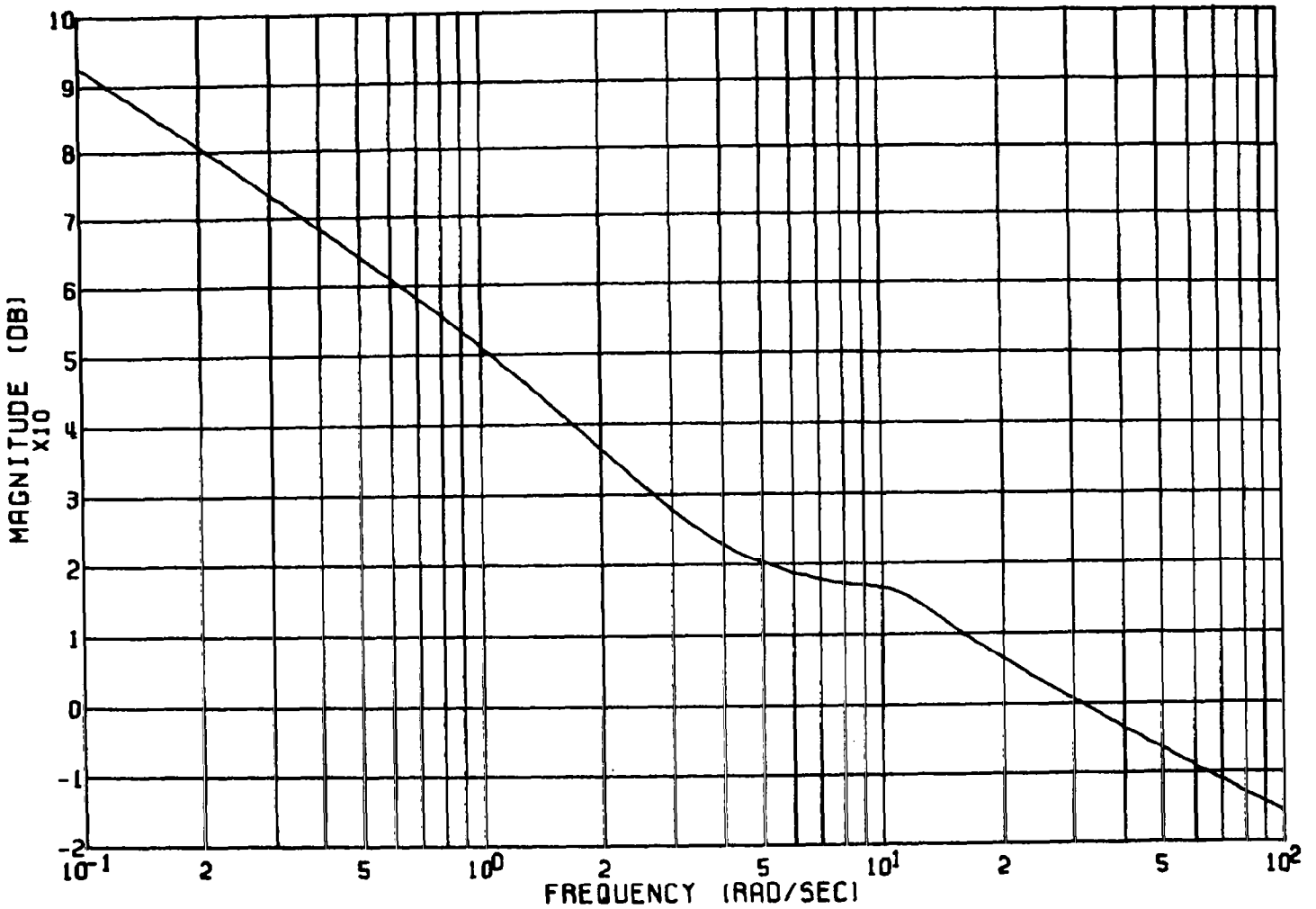

Figure 7.7(a) ROLL ACTUATOR COMMAND; LINEAR CBTT AUTOPILOT, ELLIPTICAL AIRFRAME (α_e = 10 deg, $P_e = Q_e = 0$) GAIN VS. FREQUENCY

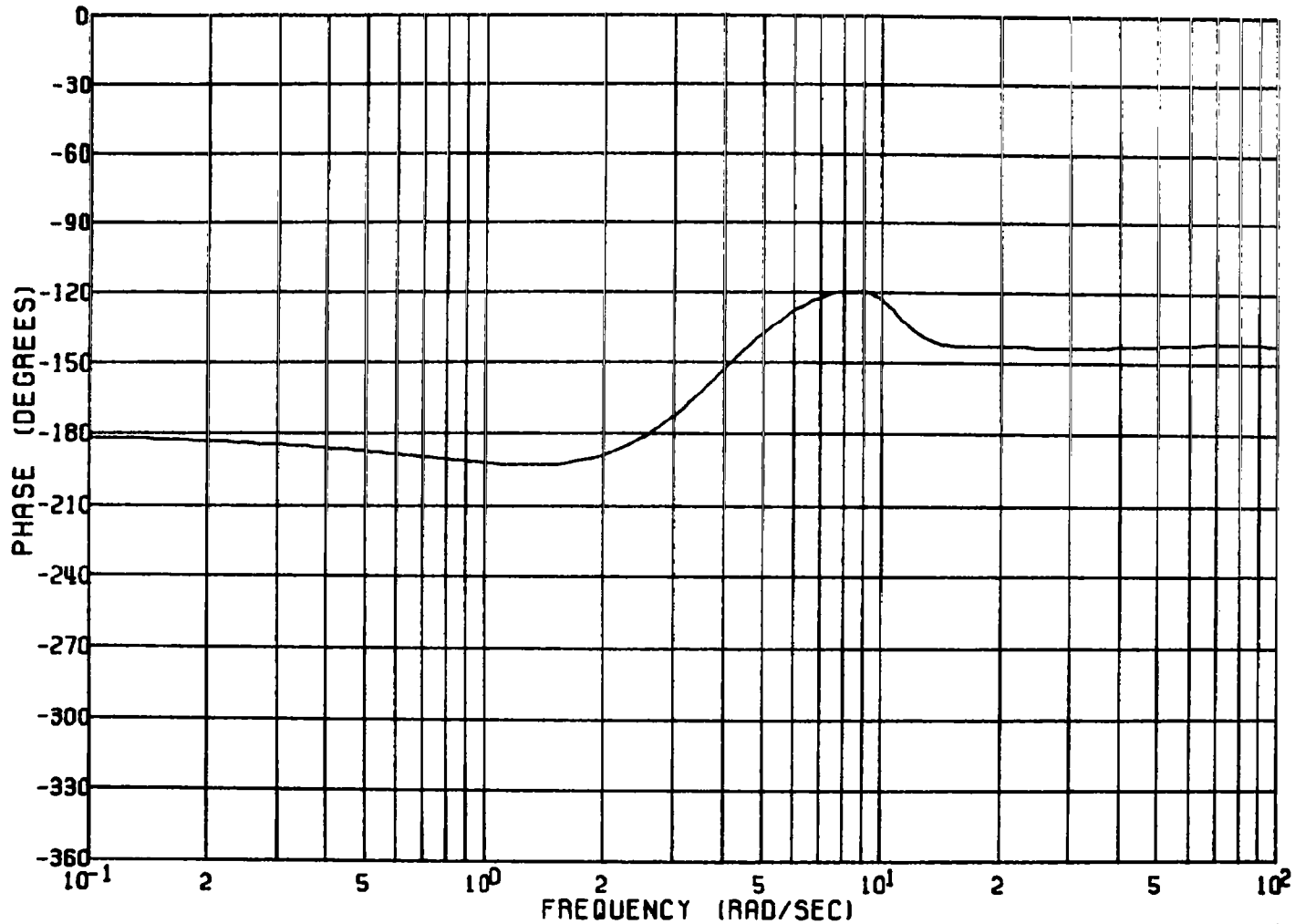

Figure 7.7(b) ROLL ACTUATOR COMMAND; LINEAR CBTT AUTOPILOT, ELLIPTICAL AIRFRAME (α_e = 10 deg, P_e = Q_e = 0) PHASE VS. FREQUENCY

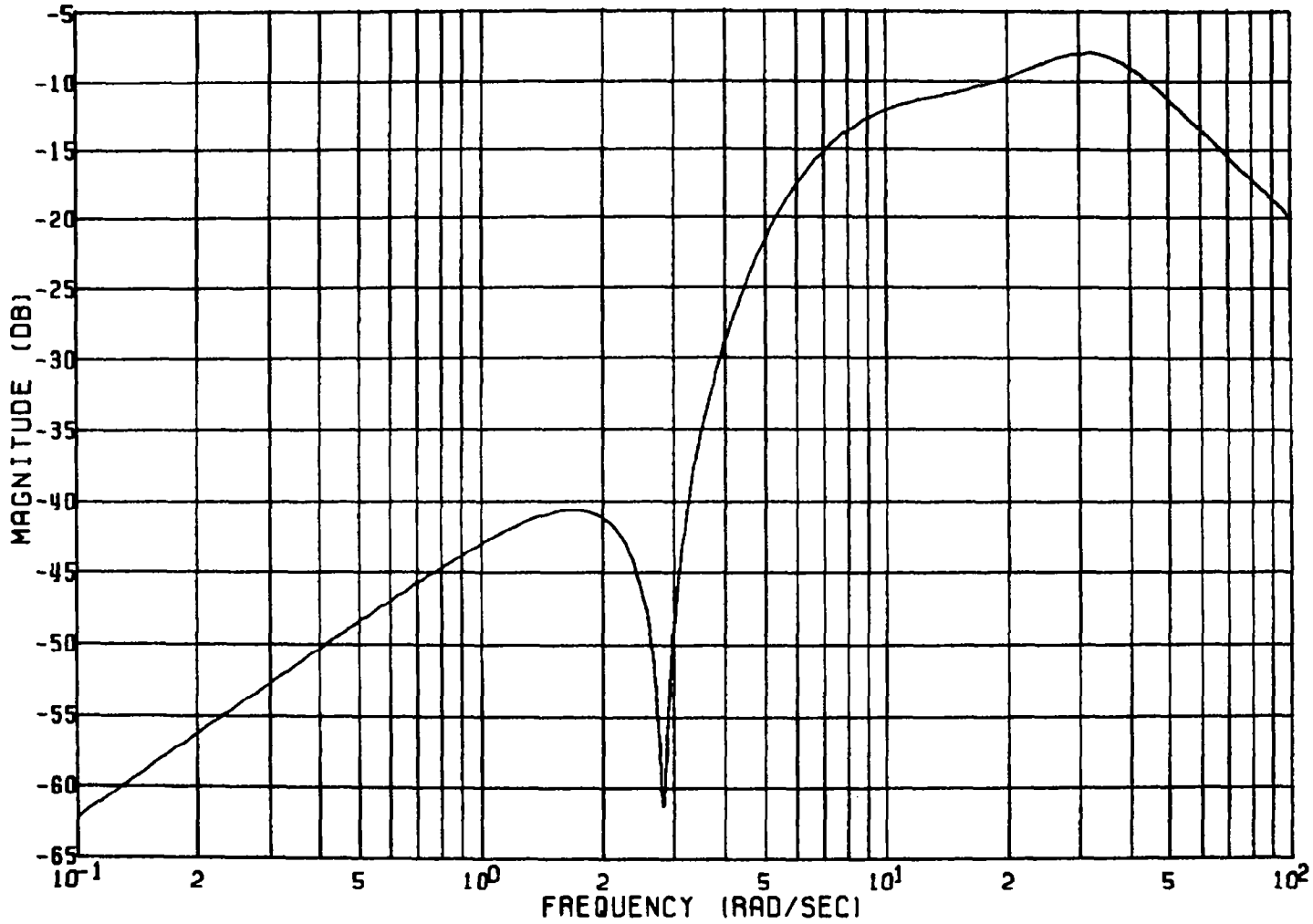

Figure 7.8(a) COORDINATION BRANCH; LINEAR CBTT AUTOPILOT, CIRCULAR AIRFRAME (α_e = 10 deg, $P_e = Q_e = 0$) GAIN VS. FREQUENCY

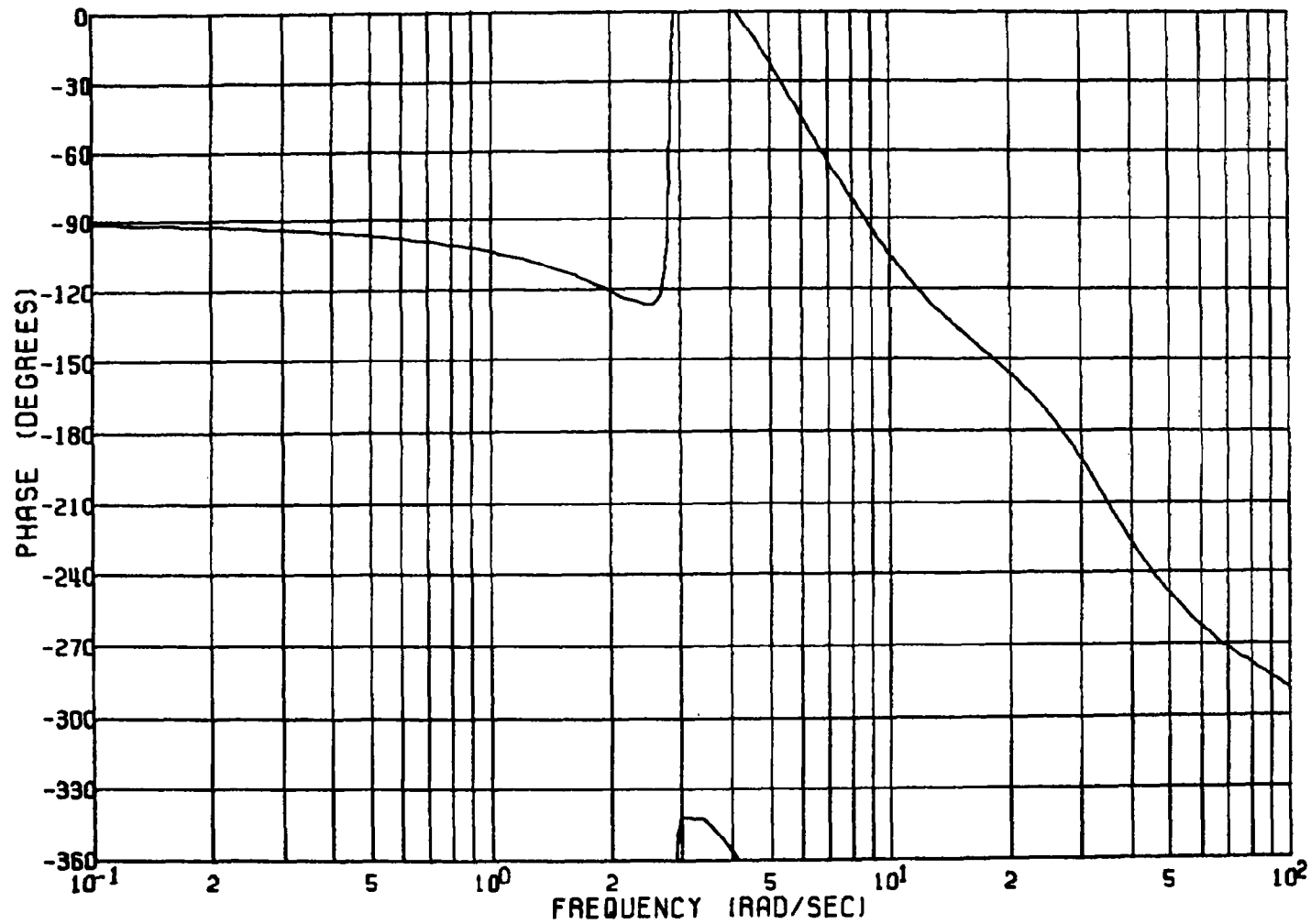

Figure 7.8(b) COORDINATION BRANCH; LINEAR CBTT AUTOPILOT, CIRCULAR AIRFRAME (α_e = 10 deg, $P_e = Q_e = 0$) PHASE VS. FREQUENCY

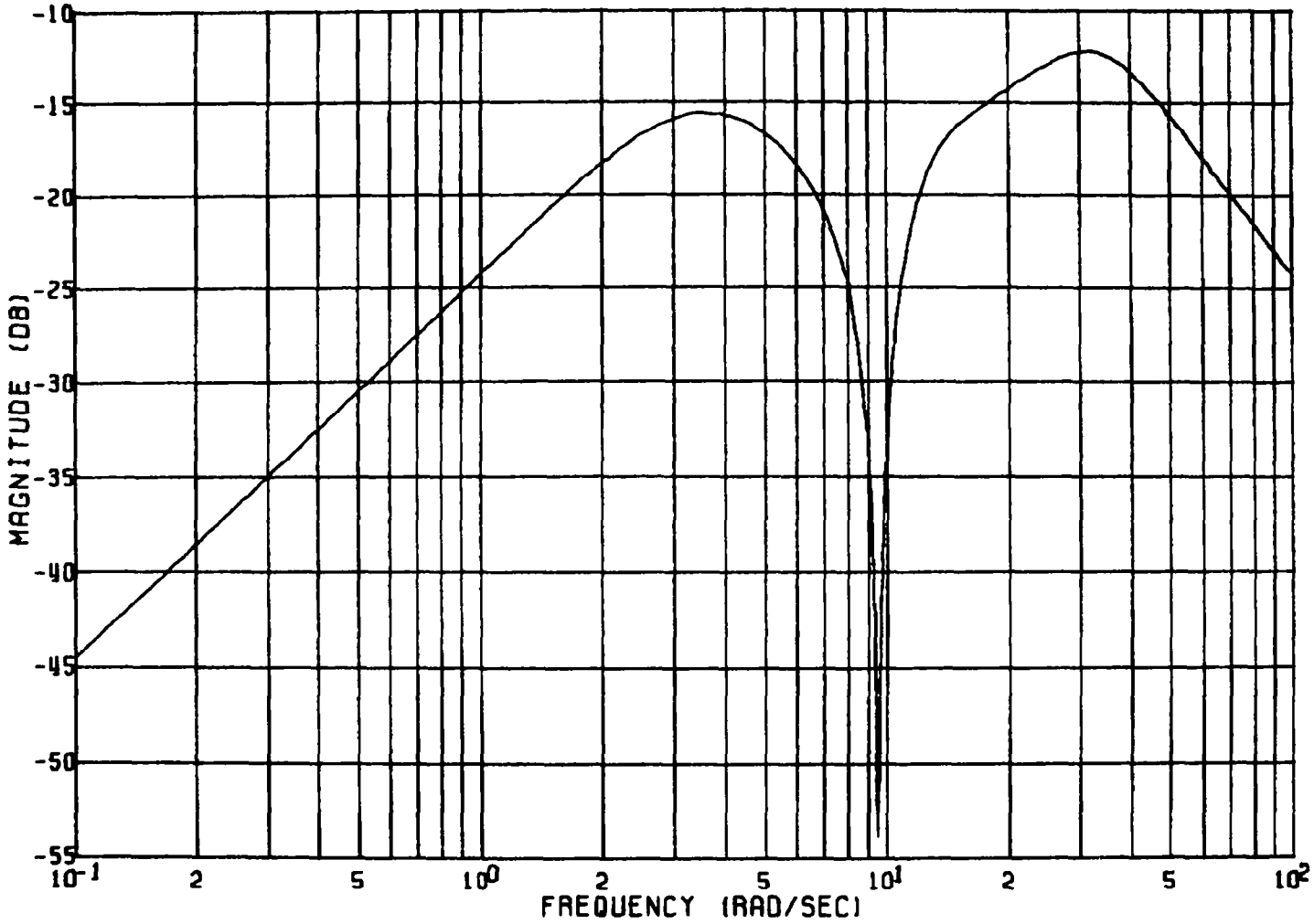

Figure 7.9(a) COORDINATION BRANCH; LINEAR CBTT AUTOPILOT, ELLIPTICAL AIRFRAME (α_e = 10 deg, $P_e = Q_e = 0$) GAIN VS. FREQUENCY

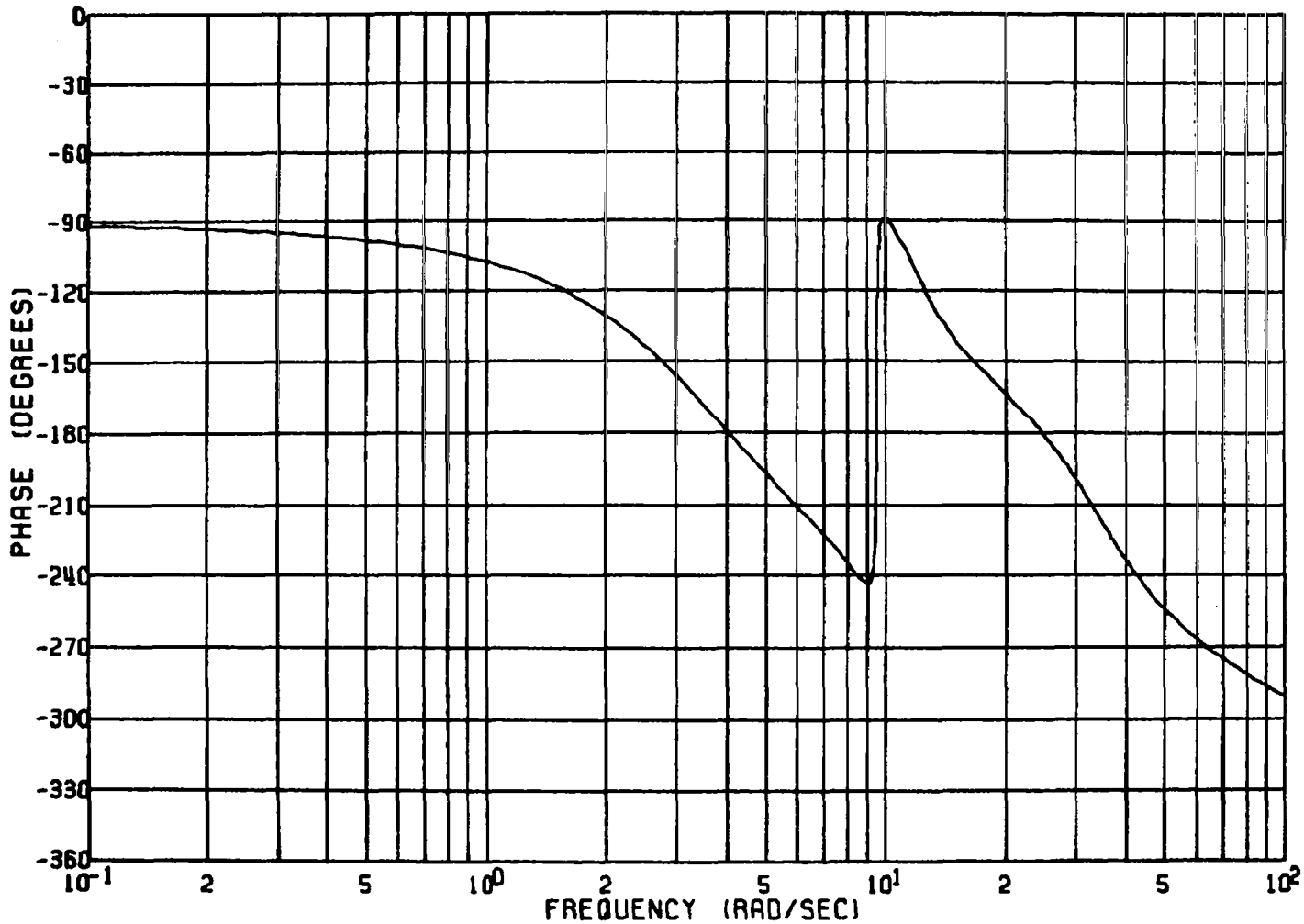

Figure 7.9(b) COORDINATION BRANCH; LINEAR CBTT AUTOPILOT, ELLIPTICAL AIRFRAME (α_e = 10 deg, $P_e = Q_e = 0$) PHASE VS. FREQUENCY

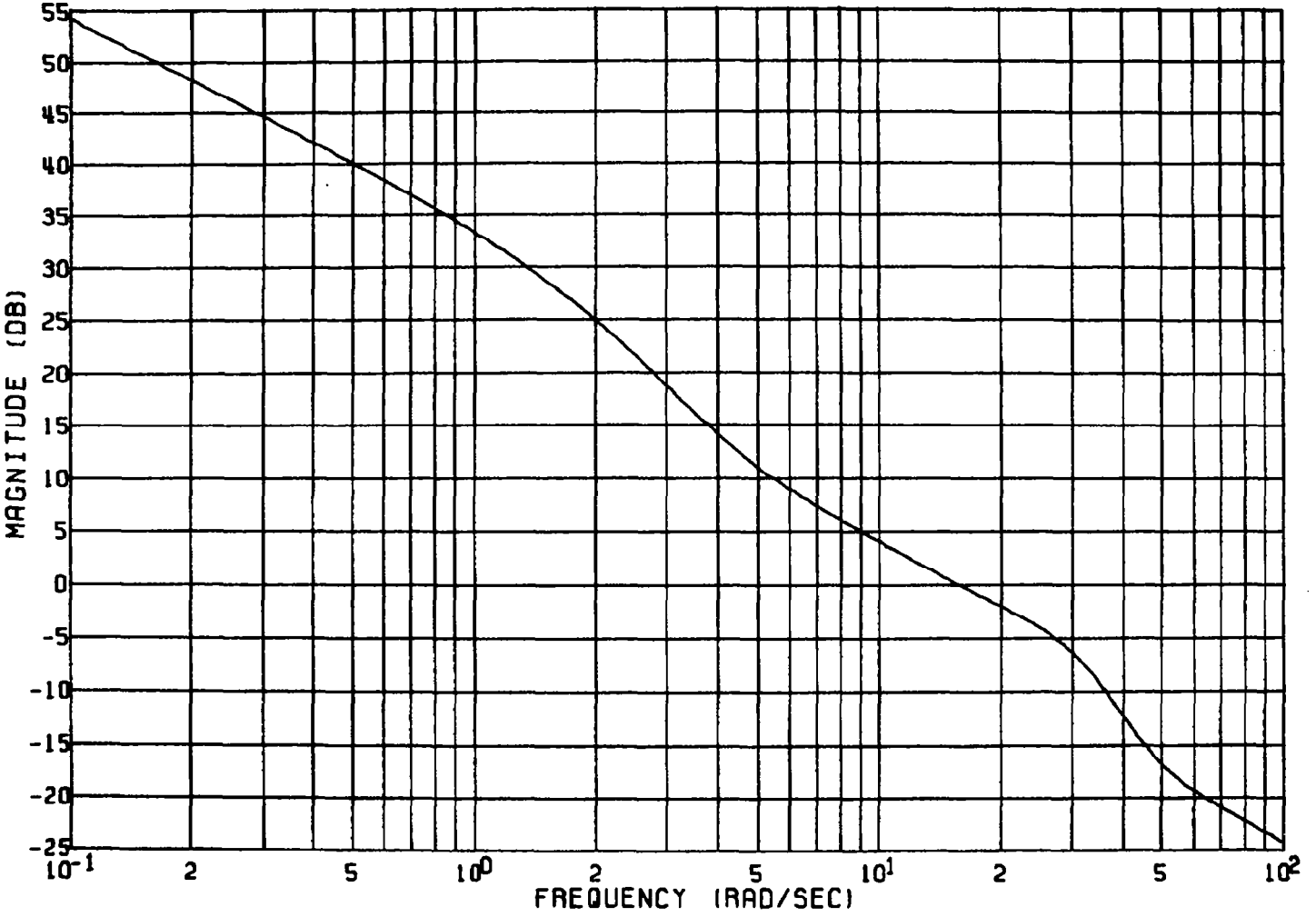

Figure 7.10(a) YAW ACTUATOR COMMAND; LINEAR CBTT AUTOPILOT, CIRCULAR AIRFRAME (α_e = 10 deg, P_e = Q_e = 0) GAIN VS. FREQUENCY

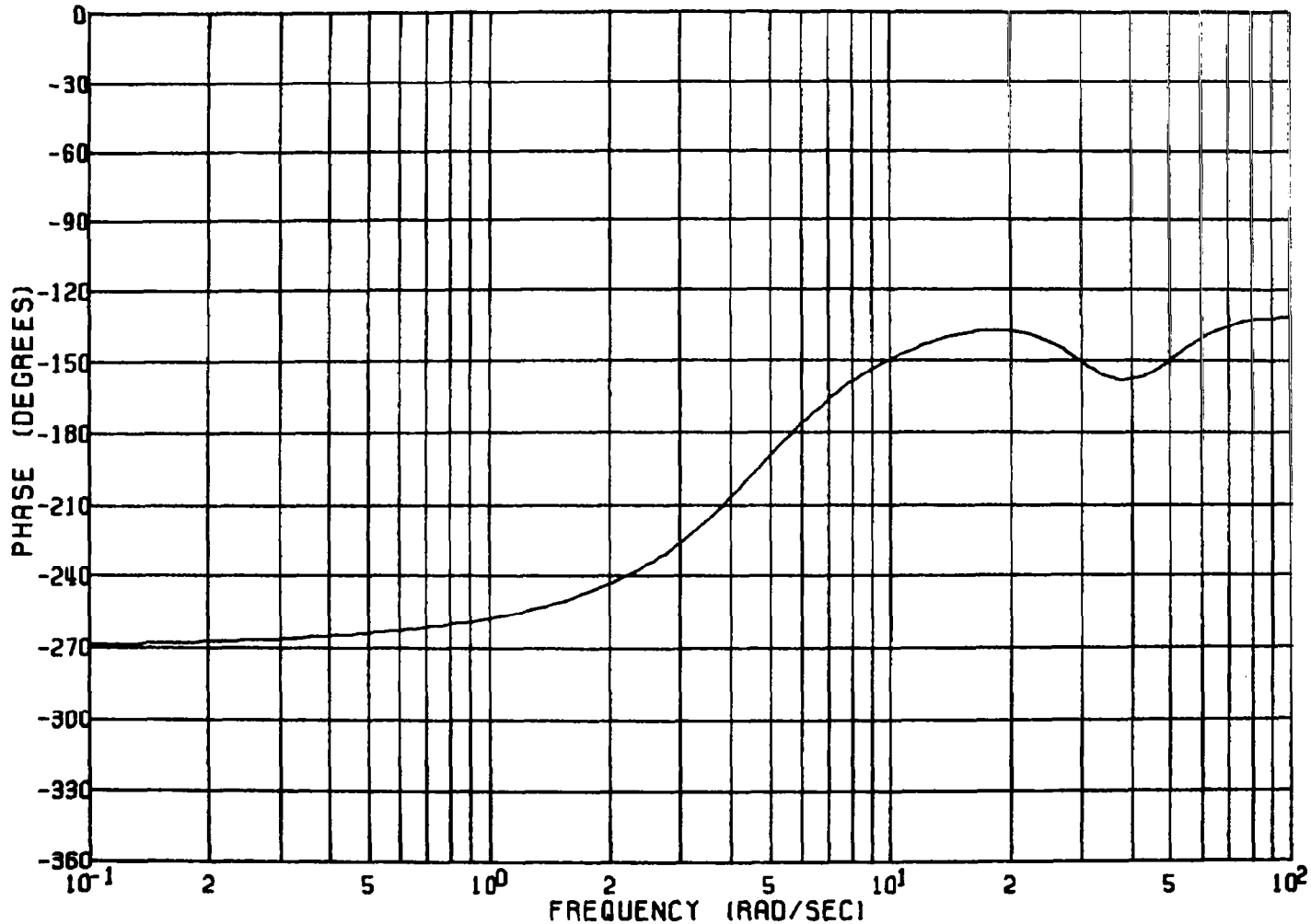

Figure 7.10(b) YAW ACTUATOR COMMAND; LINEAR CBTT AUTOPILOT, CIRCULAR AIRFRAME (α_e = 10 deg, $P_e = Q_e = 0$) PHASE VS. FREQUENCY

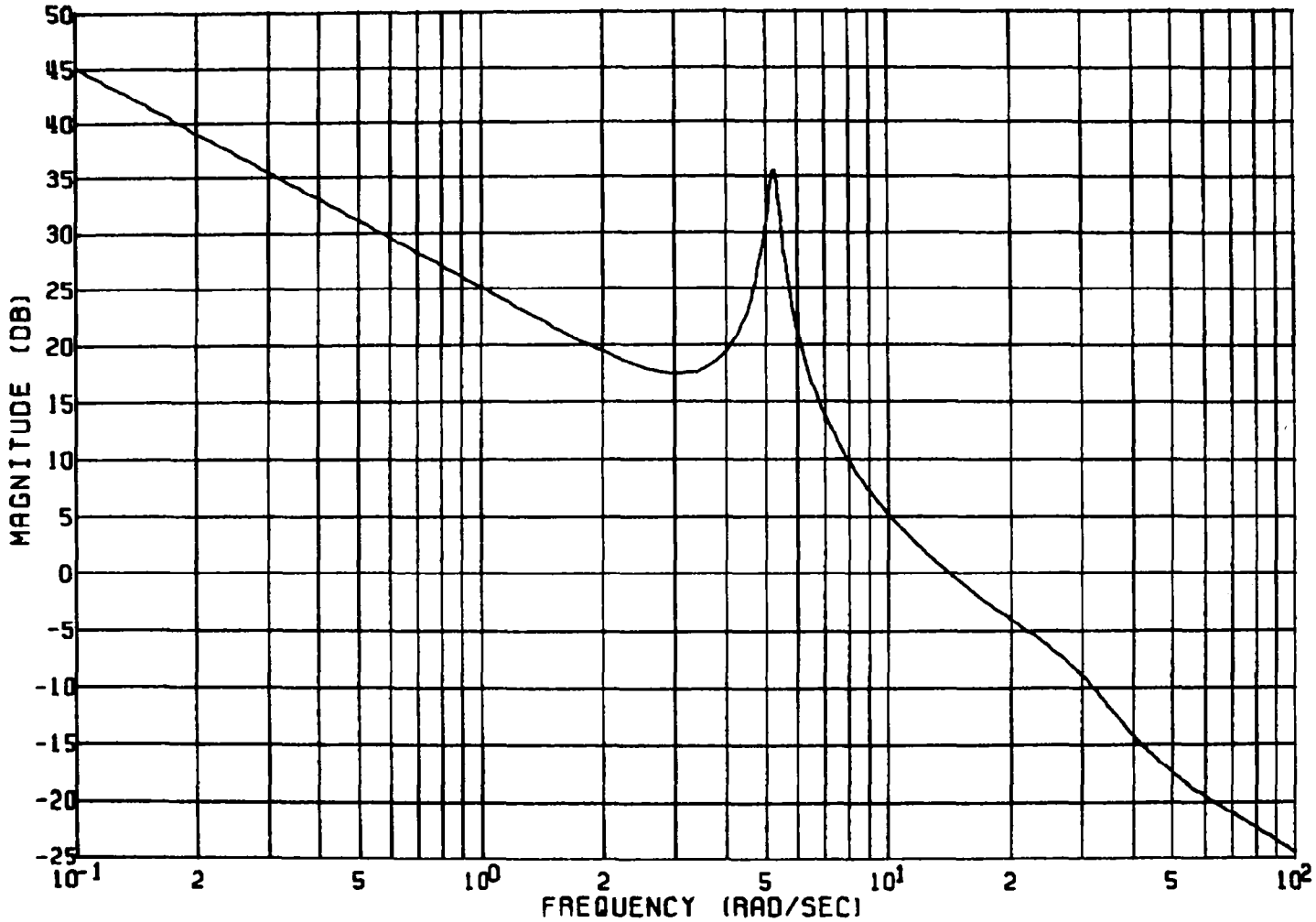

Figure 7.11(a) YAW ACTUATOR COMMAND; LINEAR CBTT AUTOPILOT, ELLIPTICAL AIRFRAME (α_e = 10 deg, P_e = Q_e = 0) GAIN VS. FREQUENCY

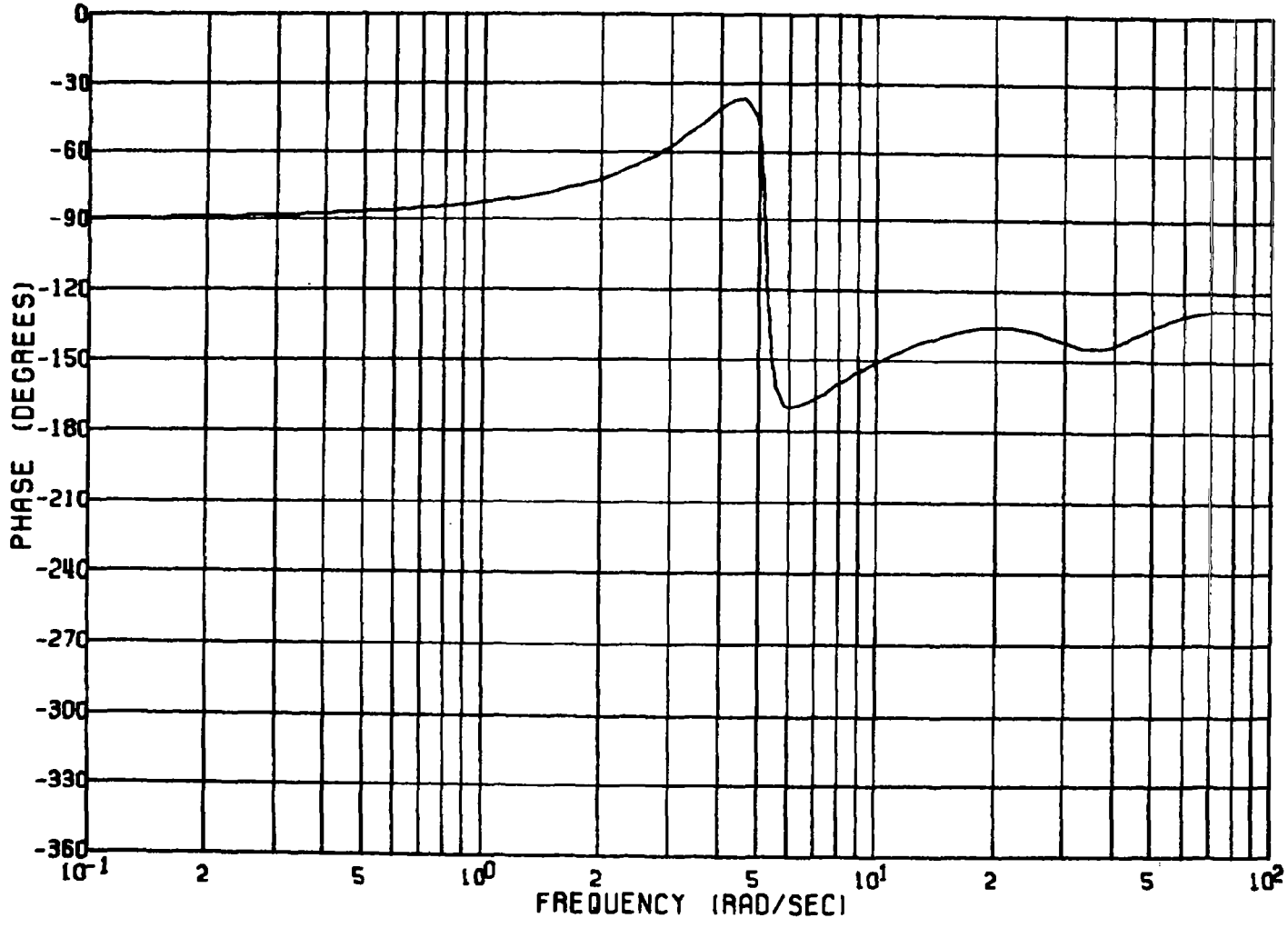

Figure 7.11(b) YAW ACTUATOR COMMAND; LINEAR CBTT AUTOPILOT, ELLIPTICAL AIRFRAME (α_e = 10 deg, $P_e = Q_e = 0$) PHASE VS. FREQUENCY

8 NONLINEAR ANALYSIS OF CBTT AUTOPILOT FOR ELLIPTICAL AIRFRAME

The three dimensional nonlinear aerodynamic model used for the following analysis was presented in Section 5.0. Nonlinear aerodynamics and mass parameter values are presented in Appendices A and B. The same flight condition used for linear analysis in Section 7 is used for the following nonlinear analysis (i.e., 60 Kft altitude, Mach 3.95). Control laws described in Section 8.1 are the same used for the linear studies except for a minor modification to the coordinating branch dependence on angle-of-attack and also the inclusion of anti-gravity bias. Sections 8.2 and 8.3 show the results for commanding the CBTT autopilot of the elliptical airframe and determine the desired aerodynamic model to enhance CBTT performance. Section 8.4 states the conclusions of the nonlinear analysis.

8.1 CONTROL LAW

The control laws used for the following nonlinear 3-D studies were the same those used for the linear studies in Section 7.0 (i.e., Figures 7.1 and 7.2) except for the gain $\bar{\alpha}$ shown in the bold line of the coordination branch in Figure 7.2. The new gain $\bar{\alpha}$ is held constant at one degree magnitude for angles-of-attack less than one degree positive and greater than negative 5 degrees. For angles-of-attack greater than one degree positive, the gain $\bar{\alpha}$ is equal to the angle-of-attack. This maintains coordination for very small angles-of-attack.

Gravity effects were not included in the linear studies of Section 7 and Appendices D, E, and F because it was assumed to have a negligible influence on autopilot stability and response for perturbations about a missile trim condition. However, gravity effects were included in the following nonlinear studies where the missile body-fixed yaw axis will be subjected to the full force of gravity and may therefore have a significant influence on sideslip.

Gravity effects were minimized using anti-gravity bias commands. However, when anti-gravity bias was inserted in fixed-body coordinates (i.e., $-\cos\theta \cos\phi$ for the pitch anti-gravity bias command in gees, and $-\cos\theta \sin\phi$ for the yaw anti-gravity bias command in gees) the results were not as good as when the anti-gravity bias was inserted in inertial coordinates. An anti-gravity body-fixed yaw acceleration command increases sideslip. When the anti-gravity acceleration command is in inertial coordinates, the command is resolved into a body-fixed pitch acceleration command and a roll angle command. Thus, gravity effects are compensated for by pitch and roll motions of the missile which have less influence on sideslip than yaw motion. In inertial rectangular coordinates,

η_c = acceleration command in inertial $\bar{z}_v$ direction = $\eta_{Z_c} - \cos\theta$

where η_{Z_c} = guidance command (gees)

$-\cos\theta$ = anti-gravity bias command (gees)

acceleration command in the inertial $\bar{y}_v$ direction = η_{Y_c}

where η_{Y_c} = guidance command (gees)

There is no gravity effect in y direction.

Therefore, the polar commands to the autopilot are,

$$\eta_{z_c} = -((\eta_{Z_c} - \cos\theta)^2 + \eta_{Y_c}{}^2)^{1/2}$$

$$\phi_c = \tan^{-1}\left(\frac{\eta_{Y_c}}{-\eta_{Z_c}}\right)$$

Since the pitch control law of the elliptical airframe does not have an integration in the acceleration error path, and requires a gain in series with the acceleration command shown in Figure 7.1, it was necessary to modify the anti-gravity command as follows to assure an anti-gravity bias of just one gee.

$$\text{elliptical airframe inertial acceleration command} = \eta_{Z_c} - (0.913)\cos\theta$$

8.2 CBTT PERFORMANCE

The commands 2 gees (0^o, 180^o) denote an inertial guidance command of 2 gees which is first applied in the 0^o or upward direction at 2 seconds. Since both the missile roll angle and roll angle command are at zero degrees, there is no roll motion and the missile turns upward as a skid-to-turn controlled missile. At 5 seconds, a second 2 gees inertial guidance command is applied in the downward or 180^o direction. The missile is commanded to roll through 180 degrees while moving in a coordinated manner in yaw and roll to minimize sideslip angle and prevent or minimize negative angles-of-attack.

Figure 8.1 shows the achieved maneuver plane acceleration η_Z and the acceleration in the plane perpendicular to the maneuver plane η_Y which is referred to as cross-plane acceleration. It is assumed that the desired achieved maneuver plane acceleration response should satisfy the same requirements imposed on the uncoupled pitch channel in Appendix D (i.e., $\leq$ 0.5 sec time constant with $\leq$ 10 percent overshoot). No requirements for cross-plane acceleration will be imposed for the following autopilot studies but should be determined in guidance studies. The responses of achieved maneuver and cross-plane accelerations during the first 2 seconds are due to initial conditions, gravity and anti-gravity bias effects. The initial conditions were added to minimize the transients which result when anti-

gravity bias commands the autopilot for constant altitude missile flight. This was done to study the autopilot response without adding the complexities of gravity and anti-gravity bias transients. In practice, the missile would have been flying long enough for the gravity transients to have subsided. The transients may be minimized by running the simulation until transients subside. However, computer time may be decreased by inserting appropriate initial conditions. The initial conditions were:

α = angles-of-attack = 2.41 degrees

δ_p = pitch tail angle = 0.658 degrees

θ = pitch Euler angle = 3.65 degrees

output of pitch acceleration feedback lag = -1.0 gees

pitch control law acceleration error lag
prior to dc gain = -0.0105

δ_{p_c} = pitch actuator command = 0.658 degrees.

Due to the minus 2 gees guidance command applied at 2 seconds and the minus one gee anti-gravity bias command, the achieved maneuver plane acceleration seeks a level of minus 3 gees. The maneuver plane acceleration response for the 2 second guidance command satisfies requirements with a 0.46 second time constant and negligible overshoot. At 5 seconds, the second guidance command causes the maneuver plane acceleration to seek a level of plus one gee due to the sum of a plus 2 gees guidance command and a minus one gee anti-gravity bias command. The resulting maneuver plane response does not satisfy requirements. The time constant of 0.42 seconds satisfies the requirements but the overshoot of 12.5 percent at 5.65 seconds and the 10.3 percent under-

shoot at 6.05 seconds exceeds requirements. Although the transients do not exceed the requirements by a large amount, the results were obtained with an uncoupled pitch autopilot designed with small overshoot. Small overshoot is difficult to obtain practically due to an autopilot control law which is not optimum for all flight conditions. When the pitch control law in Figure 7.1 was modified to have a response in maneuver plane acceleration in the uncoupled pitch channel with the same time constant but with ten percent overshoot, the CBTT control law resulted in larger transients in maneuver plane acceleration.

The reason for an overshoot limit in the maneuver plane acceleration for low gee autopilot commands is that structural limitations of the missile will be avoided for large acceleration commands. Whether the maneuver plane acceleration transients for CBTT increase with acceleration level (which is determined in Section 8.5) will establish overshoot limits for the low gee commands. Also, the effect of requirements for overshoots and undershoots due to step function commands applied in autopilot design studies must be assessed in guidance level studies. Section 8.4 identifies the cause of the transients and discusses methods for reducing them to within conservative limits.

The achieved maneuver plane acceleration η_Z (Figure 8.1) is calculated from the body-fixed accelerations η_z, and η_y (Figure 8.2), and the roll angle ϕ as follows:

$$\eta_Z = \eta_z \cos\phi + \eta_y \sin\phi \qquad 8.1$$

During the first command, achieved body-fixed yaw acceleration (η_y) and missile roll angle are equal to zero because the roll channel is not commanded. Therefore, achieved maneuver plane acceleration is equal to the body-fixed acceleration η_z. During the second command, the missile roll angle shown in Figure 8.6 has the same roll angle response as the uncoupled roll autopilot in Appendix F. When the achieved maneuver plane is at the acceleration level which determines its 63 percent time constant (i.e., -.48

gees), the body-fixed acceleration has hardly changed its level (i.e., -2.72 gees) due to a transient. However, the achieved maneuver plane acceleration is at the time constant level due to the missile roll angle which has reached 76.7 degrees. The product $\eta_z \cos\phi = -0.625$ is reduced to the time constant level of -.48 gees by the positive achieved yaw acceleration of 0.145 gees. Hence, by the missile rolling around its velocity vector the maneuver plane acceleration is able to change rapidly in the desired direction even though the body-fixed pitch acceleration is changing slowly. However, the slowness of the pitch channel causes the overshoot in the maneuver acceleration when the missile roll angle reaches 135 degrees and η_z is still at -1.9 gees. The undershoot in the achieved maneuver acceleration is caused by the overshoot in body-fixed pitch acceleration when the missile roll angle has reached 183.4 degrees. The reason for the slowing transient in the body-fixed pitch acceleration at 5.3 seconds and the 10.5 percent overshoot at 6.1 seconds is explained in Section 8.4.

Angle-of-attack (Figure 8.3) remains positive and shows evidence of the above mentioned slow-down transient at 5.3 seconds. Sideslip angle (Figure 8.4) satisfies requirements reaching a maximum of only 1.6 degrees. The contribution of achieved yaw acceleration and gravity to sideslip rate is negligible. The main contribution to sideslip rate and in turn sideslip angle is from the kinematic coupling term αp which is minimized by the achieved missile yaw rate r. It is the autopilot coordination command (i.e., yaw rate command) which forces -r to be approximately equal to αp . The peaks in sideslip angle are due to the ability of the coordination branch to follow rapid changes of missile roll rate and angle-of-attack.

The peak yaw angular rate r (Figure 8.5) is a factor of 3.4 times larger than the pitch angular rate q in order to maintain coordinated missile motion. Roll angular rate reaches a maximum of 281.8 deg/sec. None of the angular rates are considered excessive for the conditions studied.

Maximum roll tail incidence δ_R (Figure 8.7) is 14 degrees at 5.1 seconds. This angle should not cause the tails to exceed any physical limits because the maximum pitch and yaw tail incidences are less than one half the maximum roll tail incidence. However, large roll tail incidence may be a concern for lower dynamic pressure conditions. The large yaw tail incidence δ_Y which is almost as large as the pitch tail incidence δ_p results from the missile stability in yaw as shown in Appendix E.

A method for displaying missile motion which provides both sideslip and angle-of-attack information is shown in Figure 8.8. Missile motion is shown with respect to the velocity vector due to the second command of 2 gee (0^o, 180^o). The plane of the figure is normal to the velocity vector which is located at the origin. The direction of the solid arrows represent the missile body orientation with respect to the velocity vector where the direction of the arrow is the preferred maneuver direction. The tail of the arrow represents the missile center line angular orientation with respect to the velocity vector which can be expressed by angle-of-attack α and sideslip angle β . α_T (total angle-of-attack) is the radial distance of the tail of the arrow with respect to the origin. β is the straight line distance from the origin to the closest approach of the line extension of the arrow. α is the straight line distance from the origin along a line perpendicular to the line representing β and intersecting the origin.

The missile starts at 5 seconds, as shown by the arrow at the top of Figure 8.8, with zero roll angle. To maneuver in the downward direction, the missile is shown to roll through 180 degrees about the velocity vector while maintaining small sideslip angles (i.e., tail of arrow points at the origin or velocity vector for zero sideslip angle). The angle-of-attack changes as a result of anti-gravity bias. The maximum sideslip angle is shown to occur at 6.05 seconds.

8.3 CBTT PERFORMANCE WITH NO LATERAL AERODYNAMIC CROSS-COUPLING

Linear studies in Section 7.0 have shown that the aerodynamic cross-coupling does not have a direct effect on minimizing sideslip angles. The aerodynamic cross-coupling influences the stability of the autopilot which determines whether the coordination gain K_{YP} can be set at unity and sideslip angles can be minimized. To check this result, the aerodynamic cross-coupling $C_{\ell_{\delta_Y}}$, C_{ℓ_β}, and $C_{n_{\delta_R}}$ was removed and responses were obtained from the results due to the same commands as applied in Section 8.2.

Comparing Figure 8.9 with Figure 8.1 shows that removal of the aerodynamic cross-coupling has increased the overshoot of the achieved maneuver plane acceleration response at 5.65 seconds from 12.5 to 19.8 percent. The undershoot at 6.1 seconds has decreased from 10.3 to 8.4 percent. The overshoot in the body-fixed pitch acceleration at 6.1 seconds (Figures 8.10 and 8.2) decreased from 10.5 to 8.8 percent.

Figure 8.11 shows that the transient at 5.3 seconds in angle-of-attack has become more severe than in Figure 8.3 but the minimum value at 6.14 seconds has increased slightly. Sideslip angle has increased in magnitude.

Table 8.1 summarizes the performance shown in Figures 8.9, 8.11, and 8.12 and compares it to the results which included aerodynamic coupling which was analyzed in Section 8.2. There has been no change in time constants for the achieved maneuver plane acceleration as a result of both guidance commands. The largest sideslip angle occurs at 6.1 seconds and the change is small.

Missile body pitch and yaw angular rates (Figure 8.13) have the same shape as in Figure 8.5 and only slightly different magnitudes as summarized in Table 8.2. Roll angle and rate had negligible changes as noted in Table

8.2. The change in control surface incidence (Figure 8.14) changes primarily in yaw. With maximum δ_Y increasing from -5 to -7.5 degrees.

In conclusion, the major influence of the aerodynamic cross-coupling in the elliptical airframe response has been to decrease the overshoot in the achieved maneuver plane acceleration resulting from the second guidance command. The other effects on missile variables were small but in a direction which improves performance (e.g., decreased missile body angular rates, less control surface motion, less sideslip variations). The results of linear studies have been verified (i.e., maximum sideslip magnitude is not directly influenced by aerodynamic cross-coupling). However, the nonlinear studies show that the aerodynamic cross-coupling of the elliptical airframe decreases the overshoot of the maneuver plane acceleration response which may be possibly further lessened by increasing the appropriate aerodynamic cross-coupling via a change in the airframe or by autopilot cross-coupling.

8.4 CBTT PERFORMANCE WITH IDEAL AIRFRAME DYNAMICS

The purpose of the following simplifications to the airframe dynamics model is to isolate the critical cross-coupling paths which have caused the transients in the maneuver plane acceleration responses of Sections 8.2 and 8.3. The dynamic model without the coupling paths will be referred to as ideal dynamics. Although ideal dynamics are not physically attainable, it is a useful goal for both autopilot and airframe designers.

The same guidance commands are applied to the CBTT autopilot of the elliptical airframe as in Sections 8.2 and 8.3 (i.e., 2 gees (0^o, 180^o)) but with the lateral aerodynamic cross-coupling removed as in Section 8.3. In addition, the kinematic cross-coupling of $-\beta p$ into $\dot{\alpha}$ and inertial cross-coupling of pr into $\dot{q}$ were removed. Therefore, the only cross-couplings which exist in the airframe dynamic model are the kinematic coupling of

αp into $\dot{\beta}$ and the inertial coupling of $-qp$ into $\dot{r}$. There is also the autopilot cross-coupling of the coordinating command from the roll to yaw channel.

Figures 8.15 through 8.20 show that all of the transients found in Sections 8.2 and 8.3 have been removed. Tables 8.1 and 8.2 also show these results. Figure 8.21 shows the critical feedback paths which couple the pitch and yaw channels via missile roll rate. These inertial and kinematic couplings cause transients in CBTT performance. The coupling influences both $\dot{\alpha}$ and $\dot{\beta}$ and becomes more severe with higher roll rates which imply faster responding pitch and yaw channels. Section 8.3 showed that lateral aerodynamic cross-coupling reduced the transients due to the kinematic and inertial cross-coupling. This effect is evidently due primarily to the aerodynamic stability in roll (negative C_{ℓ_β}) which helps to minimize $\dot{\beta}$. The coupling, as shown in Figure 8.21, is minimized by minimizing either $\dot{\alpha}$ or $\dot{\beta}$. The combination of the aerodynamic and inertial characteristics of the elliptical airframe and the autopilot coordination technique is already doing a very good job in minimizing sideslip angles. However, the coordination technique may be improved further by a more rapidly responding yaw channel or by adding an anticipation or lead to the roll command. An even simpler technique would be to reduce maximum roll rate with a slower responding uncoupled roll channel since achieved maneuver plane acceleration time constants are smaller than required. Further reduction in the transients may be accomplished in the control law by minimizing the effects of the gyroscopic coupling into the pitch channel (i.e., $-\beta p$ and $rp \tilde{=} \alpha p^2$ on $\dot{\alpha}$). This is addressed in Section 10.

Figure 8.22 and 8.23 show the achieved maneuver plane acceleration when lateral aerodynamic cross-coupling is removed and either pr is inserted into $\dot{q}$ (Figure 8.22) or βp is inserted into $\dot{\alpha}$ (Figure 8.23). This was done to determine whether one of the coupling inputs to the pitch dynamics was negligible. Both types of coupling inputs are shown to be important. The pr input to $\dot{q}$ causes a 12.3 percent undershoot. The βp input to $\dot{\alpha}$ causes a 13.5

percent overshoot. If the uncoupled pitch channel autopilot were not designed for minimum overshoot, the transients could be worse. Hence, the effects of both coupling inputs need to minimized.

8.5 INERTIAL AND KINEMATIC CROSS-COUPLING EFFECTS AT LARGE ACCELERATION LEVELS

To determine whether the transient effects due to inertial and kinematic cross-coupling are changed at large achieved maneuver plane acceleration levels guidance commands of 8 gees (0^o, 180^o) were applied to the CBTT autopilot of the elliptical airframe with the lateral aerodynamic cross-coupling removed.

Figure 8.24 shows that for the second guidance command the overshoot is 8.9 percent and the undershoot in 4.7 percent which now satisfies requirements. Adding lateral aerodynamic cross-coupling which aids in reducing sideslip while minimizing the effect of destabilizing aerodynamic cross-coupling should improve the results further. The transients in the body-fixed pitch acceleration, shown in Figure 8.25, were reduced by the missile roll angle which was already at 145 degrees at the peak of the overshoot. The transients due to inertial and kinematic cross-coupling have increased the body-fixed pitch acceleration beyond the minus 9 gees level. If replacing the lateral cross-coupling aerodynamics does not reduce this transient problems may result. One problem is maintaining required relative stability of the autopilot at higher acceleration levels where cross-coupling lateral aerodynamics may have greater effects on autopilot stability. Another problem may be at high dynamic pressures which have higher level guidance commands that may have to be reduced to avoid structural limitations. Although angles-of-attack are lower at higher dynamic pressures, angular rates are higher as a result of faster speeds of response and inertial and kinematic cross-coupling effects may be severe.

Inertial and kinematic cross-coupling effects cause the sideslip angle (Figure 8.27) to increase to a maximum of 4.8 degrees. Also the coupling transient increases the angle-of-attack (Figure 8.26) beyond 20 degrees which can result in the same problems mentioned above for body-fixed pitch acceleration. Table 8.1 summarizes the performance results.

Figure 8.28 and Table 8.2 show that to maintain coordination the maximum yaw rate is higher because of the larger angles-of-attack but is well within rate gyro capabilities. Higher dynamic pressure conditions and faster speeds of response will increase roll rate (Figure 8.29) but required angles-of-attack are lower and therefore maximum yaw rates may still not be excessive.

Figure 8.30 shows that maximum yaw control surface incidences are now 21 degrees. If the control surfaces angles are reaching mechanical limitations, the same cure can be used as suggested for reducing the inertial and kinematic cross-coupling transients. Maximum roll rate may be reduced so that the yaw channel does not have to work as hard. As mentioned earlier, the time constants to maneuver plane acceleration are now lower than required so that both roll and pitch channels may be slowed down.

8.6 CONCLUSION

1. The result of the nonlinear 3-D performance study verify the linear study of Section 7, namely, that maximum sideslip angle is determined by the autopilot coordination command (Section 8.3, Table 8.1, Figures 8.4, 8.12).

2. The maneuver plane response, which is the combined result of body-fixed pitch and yaw accelerations and roll angle, may have a response which is not evident from the responses of its component parts (Figures 8.1, 8.2, and 8.6).

3. Transients, which may have to be reduced, are caused by inertial and kinematic coupling between pitch and yaw dynamics through missile roll rate (Section 8.4, Figure 8.21). Transients cause excessive over shoots and undershoots in achieved maneuver plane acceleration as the missile rolls through 180 degrees (Figure 8.1). The transients may be reduced by the following methods.

a) Decreasing maximum missile roll rate (Section 8.4, Figure 8.21). This is the simplest method and has many other benefits (Section 7.2.2 and 7.3.3). Achieved maneuver plane acceleration time constants for the commands studied are now smaller than required and can therefore be increased if desired via slowing the uncoupled roll and pitch autopilots. However, the performance of other commanded directions (i.e., 0^{o}, 180^{o}) may become slower than required.

b) Improving the autopilot coordination technique to minimize sideslip rate (Figure 8.21, Section 8.4).

c) Changing the airframe physically or synthetically by the autopilot control law to increase the effects of stabilizing lateral aerodynamic coupling (negative C_{ℓ_β}) (Section 8.3, Figures 8.1 and 8.9).

The transients due to inertial and kinematic cross-coupling may become more severe at other flight conditions and may limit faster speeds of response of maneuver plane acceleration.

4. The CBTT autopilot of the elliptical airframe has achieved less than the required 0.5 second speed of response for maneuver plane acceleration. At 60 Kft altitude Mach 3.95, the time constant for a 2 gee climb command is 0.46 seconds. A 4 gee dive command from the 2 gee climb command (which required a 180 degree roll) has a time

constant of 0.42 seconds. The maneuver plane time response for the dive is faster than the climb command because in the former case the missile rolls around its velocity vector (Table 8.1)

5. Acceptable sideslip, missile body angular rates and control surface rates and incidences were obtained for the commands which were applied (i.e., 2 gees climb then 2 gee dive) and the flight condition studied (60 Kft, Mach 3.95).

COMMAND	Cross-Coupling	τ_1	τ_2	α_{min}		α_{max}		β_{min}		β_{max}	
		(sec)	(sec)	(deg)	(sec)	(deg)	(sec)	(deg)	(sec)	(deg)	(sec)
2 (0°,180°)	All	0.46	0.42	1.4	6.09	6.9	3.11	-0.9	5.5	1.6	6.03
2 (0°,180°)	No Aero	0.46	0.42	1.6	6.14	6.9	3.11	-1.45	5.5	1.83	6.06
2 (0°,180°)	Ideal	0.46	0.39	2.4	6.46	6.9	3.11	-1.52	5.45	1.17	5.91
8 (180°,0°)	No Aero	0.45	0.47	2.4	0.0025	21.7	5.55	-4.8	5.5	4.6	6.07

τ_1 = 63 percent time constant of achieved maneuver plane acceleration due to first command.

τ_2 = 63 percent time constant constant of achieved maneuver plane acceleration due to second command.

TABLE 8.1 CBTT Performance Summary of Elliptical Airframe

Command	Cross-Coupling	q_{min}		q_{max}		p_{min}		p_{max}		r_{min}		r_{max}	
		deg/sec	sec	deg/sec	sec	deg/sec	sec	deg/sec	sec	deg/sec	sec	deg/sec	sec
2 (0°,180°)	All	-10.6	5.66	9.3	2.34	-14.	6.6	281.8	5.39	-2.3	5.88	34.7	5.33
2 (0°,180°)	No Aero	-11.7	5.68	9.3	2.34	-14.4	6.6	282.	5.39	-3.71	5.89	39.1	5.32
2 (0°,180°)	Ideal	-7.3	5.33	9.3	2.34	-14.4	6.6	282.	5.39	-.23	6.98	37.6	5.3
8 (0°,180°)	No Aero	-21.3	5.67	36.9	2.33	-13.9	6.6	280.2	5.39	-2.3	6.88	119.3	5.37

TABLE 8.2 Range of CBTT Missile Body Angular Rates of Elliptical Airframe

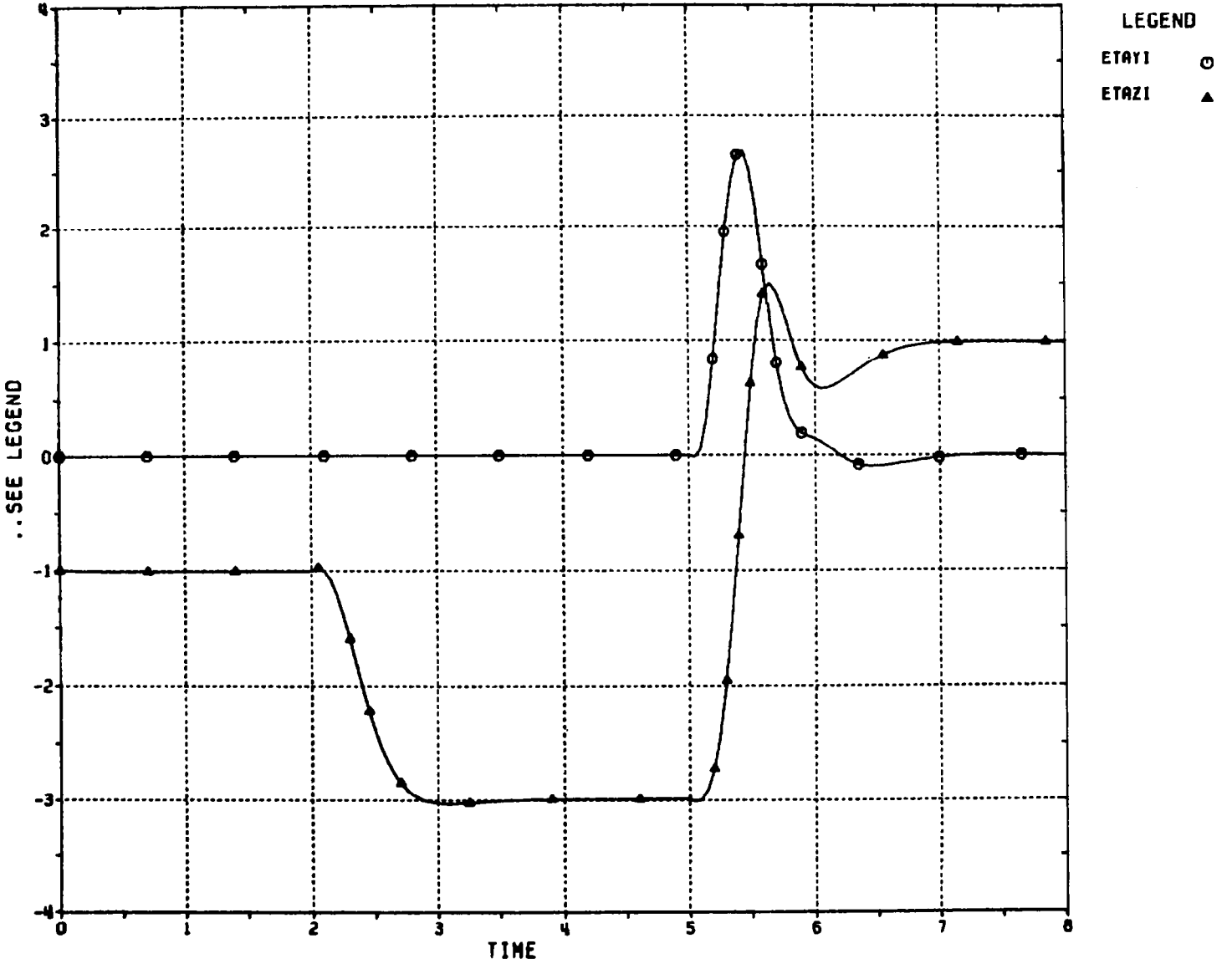

Figure 8.1 ACHIEVED INERTIAL ACCELERATIONS VS. TIME (SEC);
CBTT OF ELLIPTICAL AIRFRAME: 2 GEES (0^{o}, 180^{o})
ETAYI = CROSS-PLANE (GEES), ETAZI = MANEUVER PLANE (GEES)

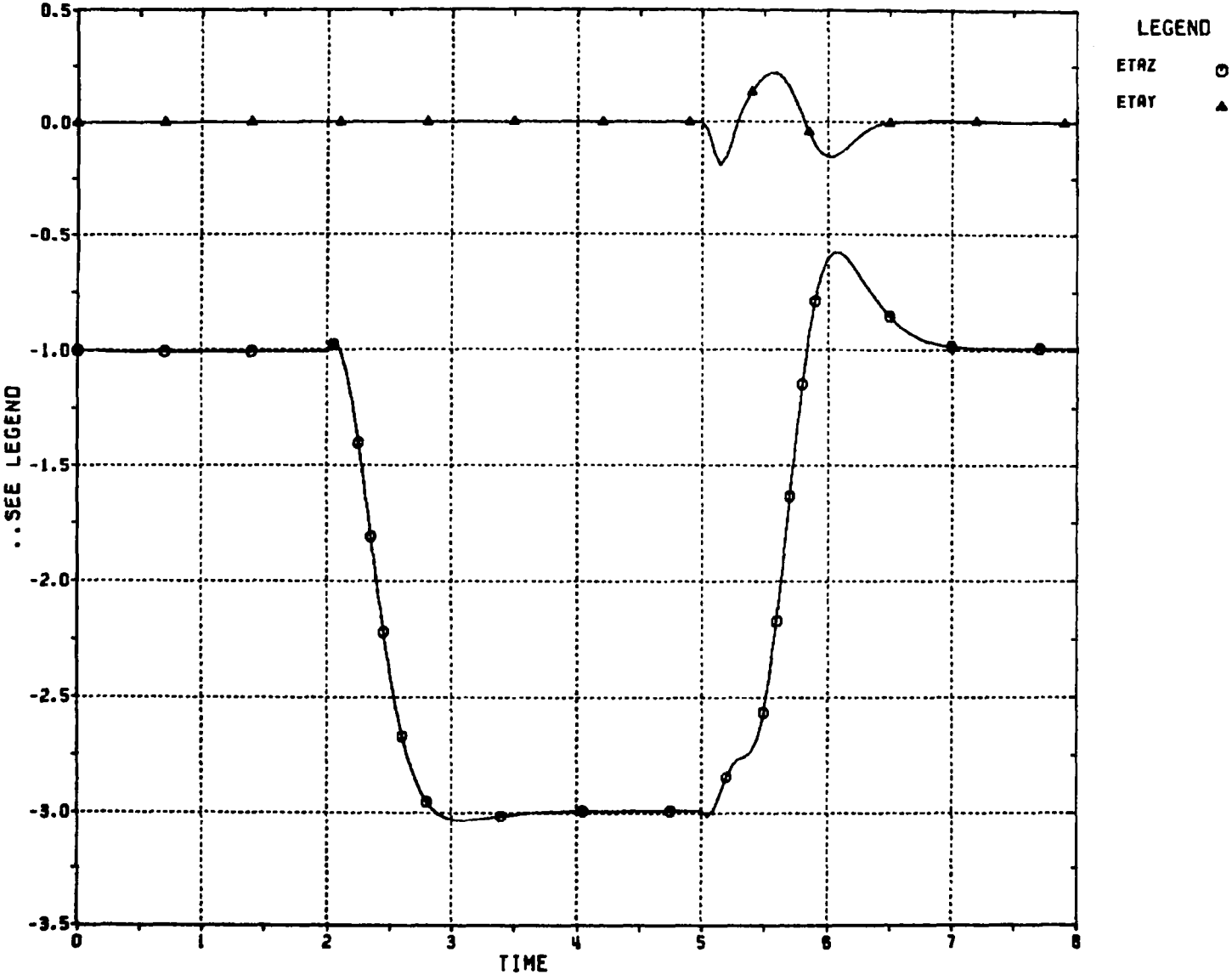

Figure 8.2 ACHIEVED BODY-FIXED ACCELERATIONS VS. TIME (SEC)
CBTT OF ELLIPTICAL AIRFRAME; 2 GEES (0^{o}, 180^{o})
ETAY = YAW (GEES), ETAZ = PITCH (GEES)

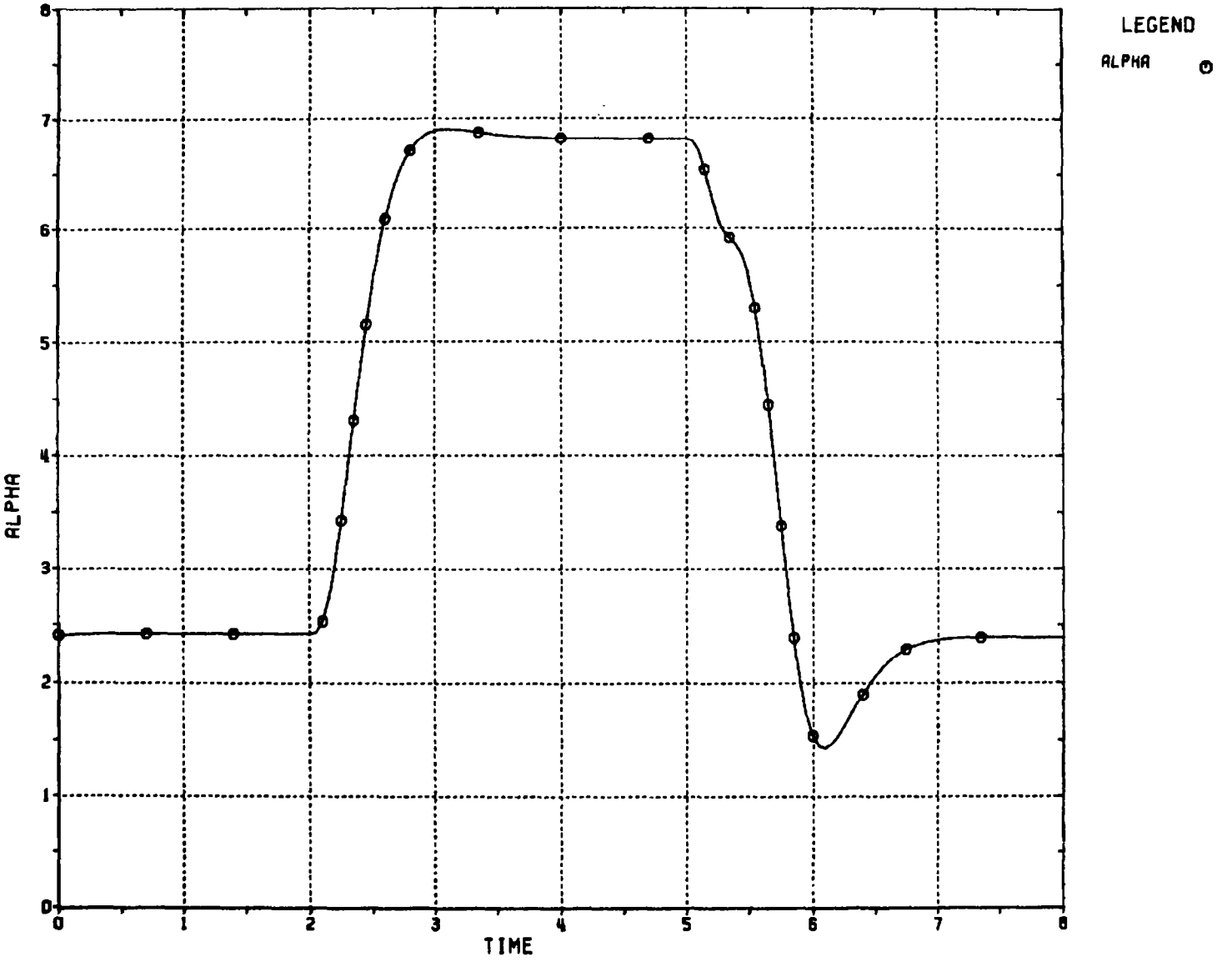

Figure 8.3 ANGLE OF ATTACK (DEG) VS. TIME (SEC); CBTT OF ELLIPTICAL AIRFRAME; 2 GEES (0^{o}, 180^{o})

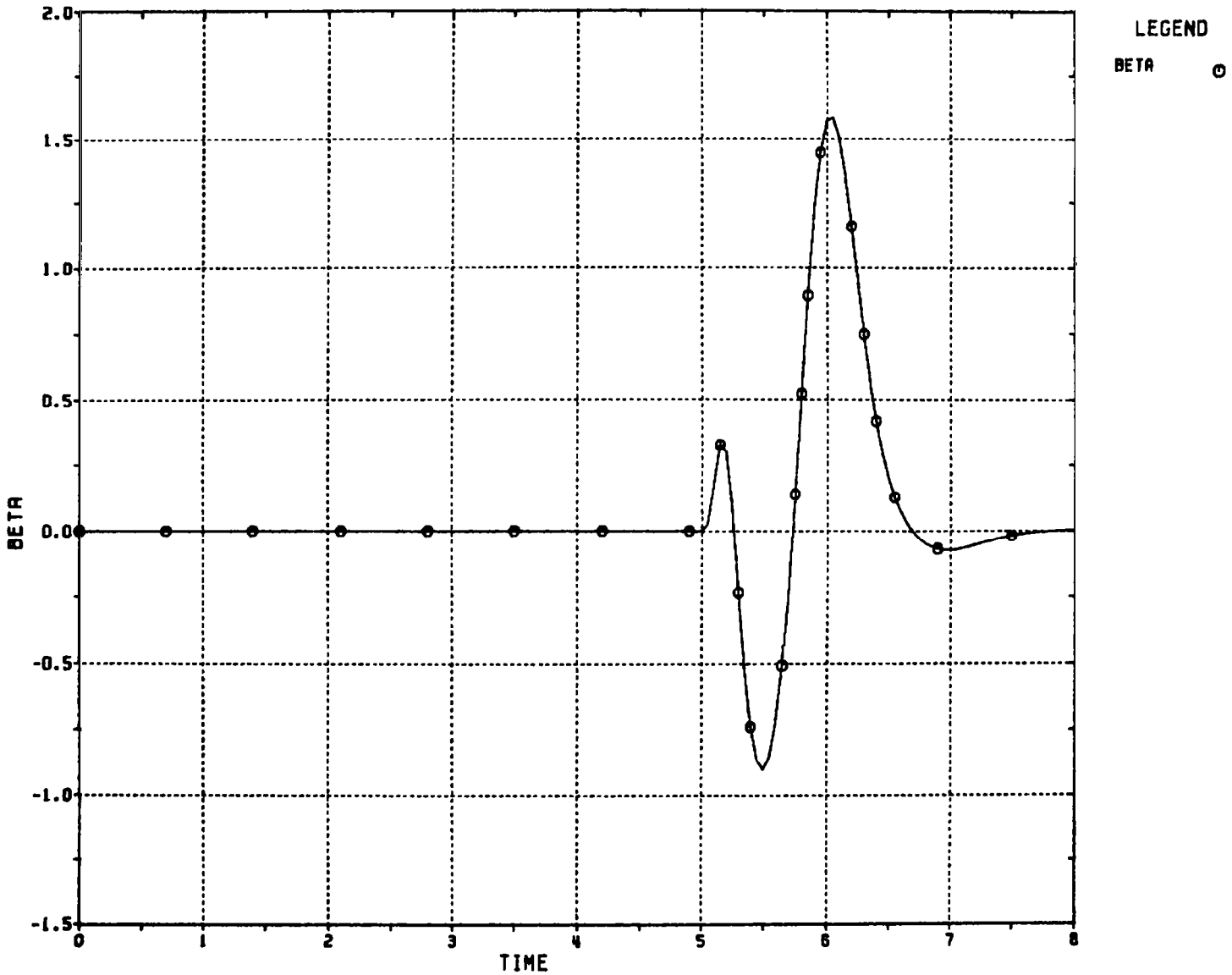

Figure 8.4 SIDESLIP ANGLE (DEG) VS. TIME (SEC); CBTT OF ELLIPTICAL AIRFRAME; 2 GEES (0^{o}, 180^{o})

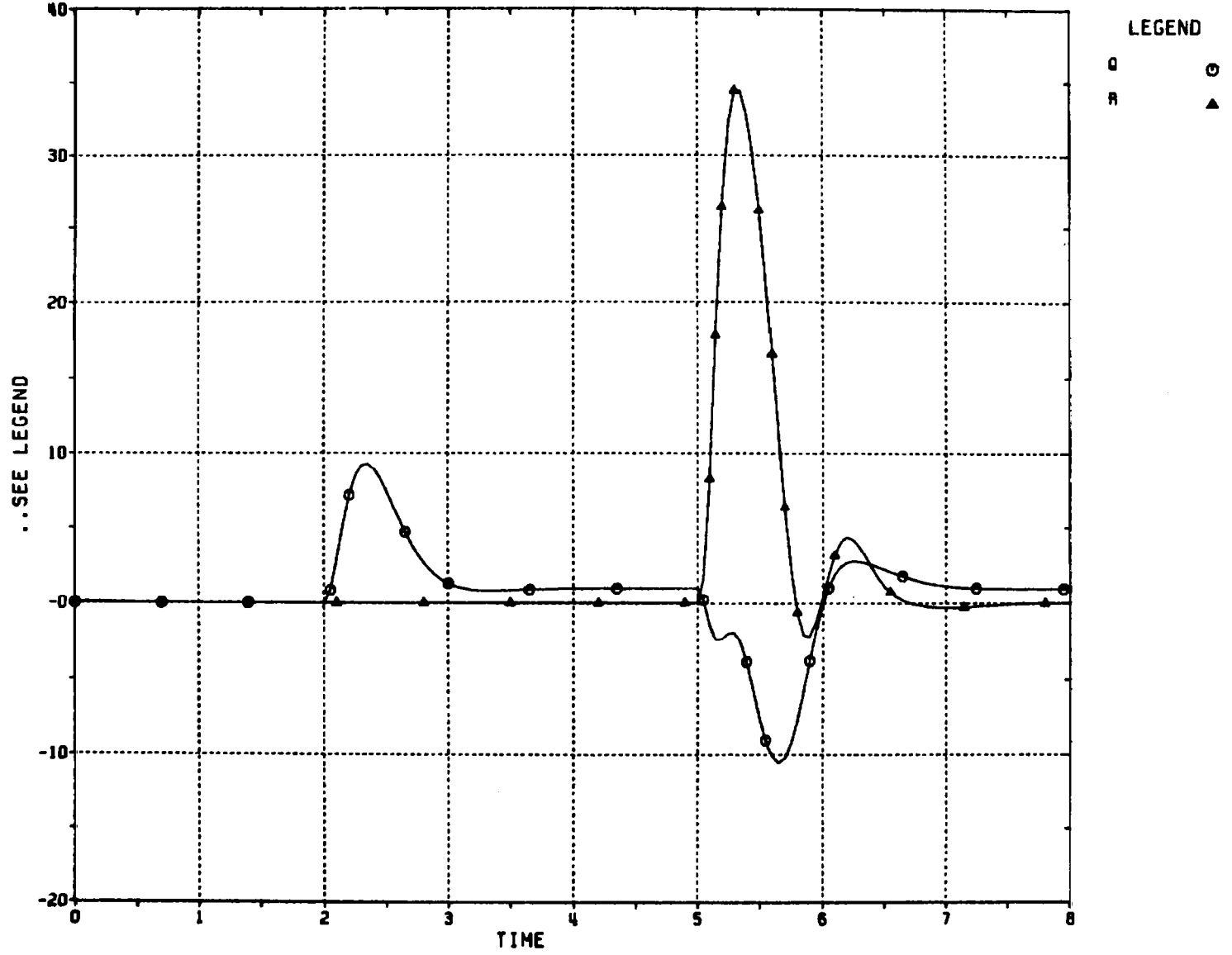

Figure 8.5 BODY ANGULAR RATES VS. TIME (SEC);
CBTT OF ELLIPTICAL AIRFRAME; 2 GEES (0^{o}, 180^{o})
Q = PITCH (DEG/SEC), R= YAW (DEG/SEC)

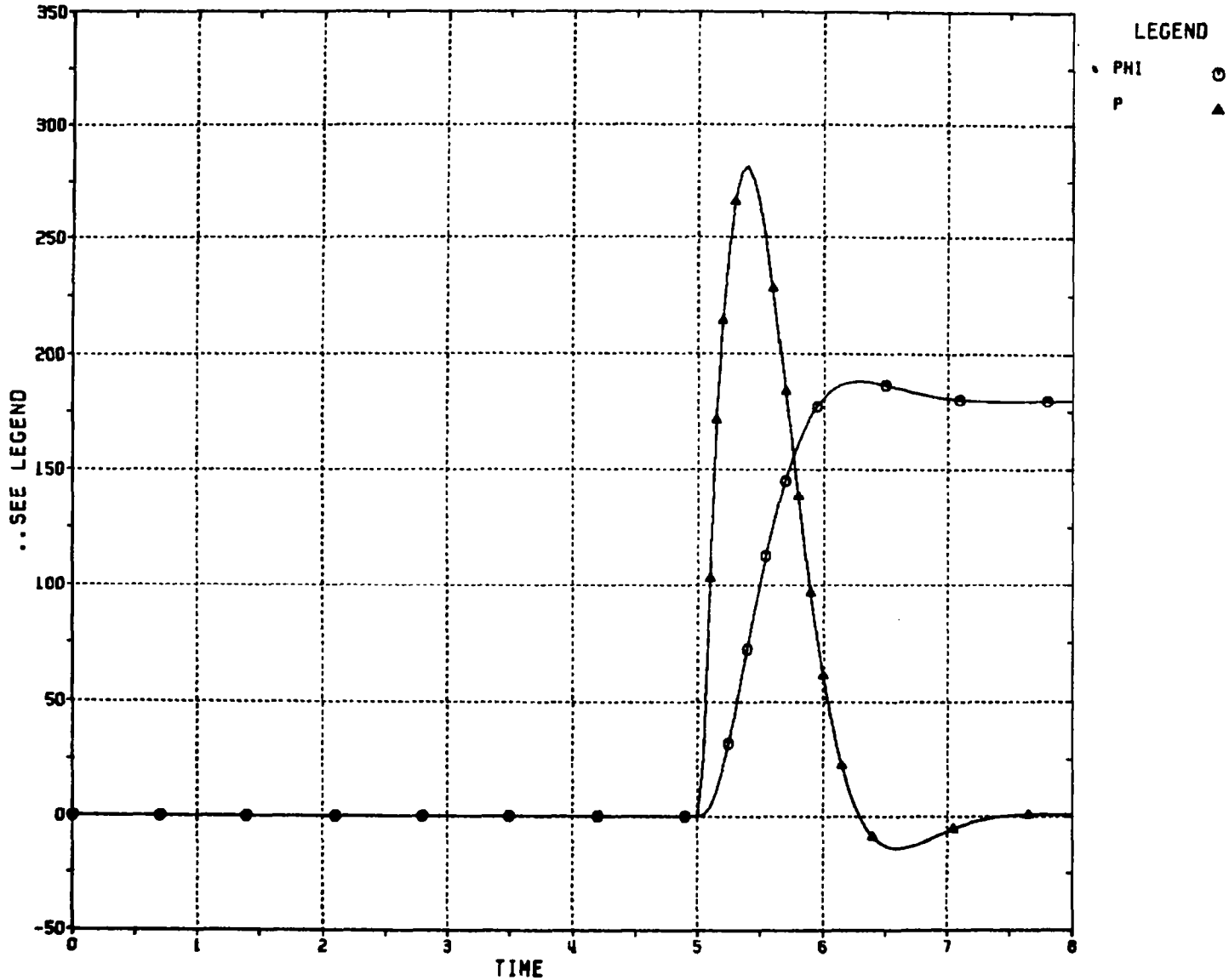

Figure 8.6 ROLL ANGLE AND ANGULAR RATE VS. TIME (SEC);
CBTT OF ELLIPTICAL AIRFRAME; 2 GEES (0^{o}, 180^{o})
PHI = ROLL ANGLE (DEG), P = ROLL ANGULAR RATE (DEG/SEC)

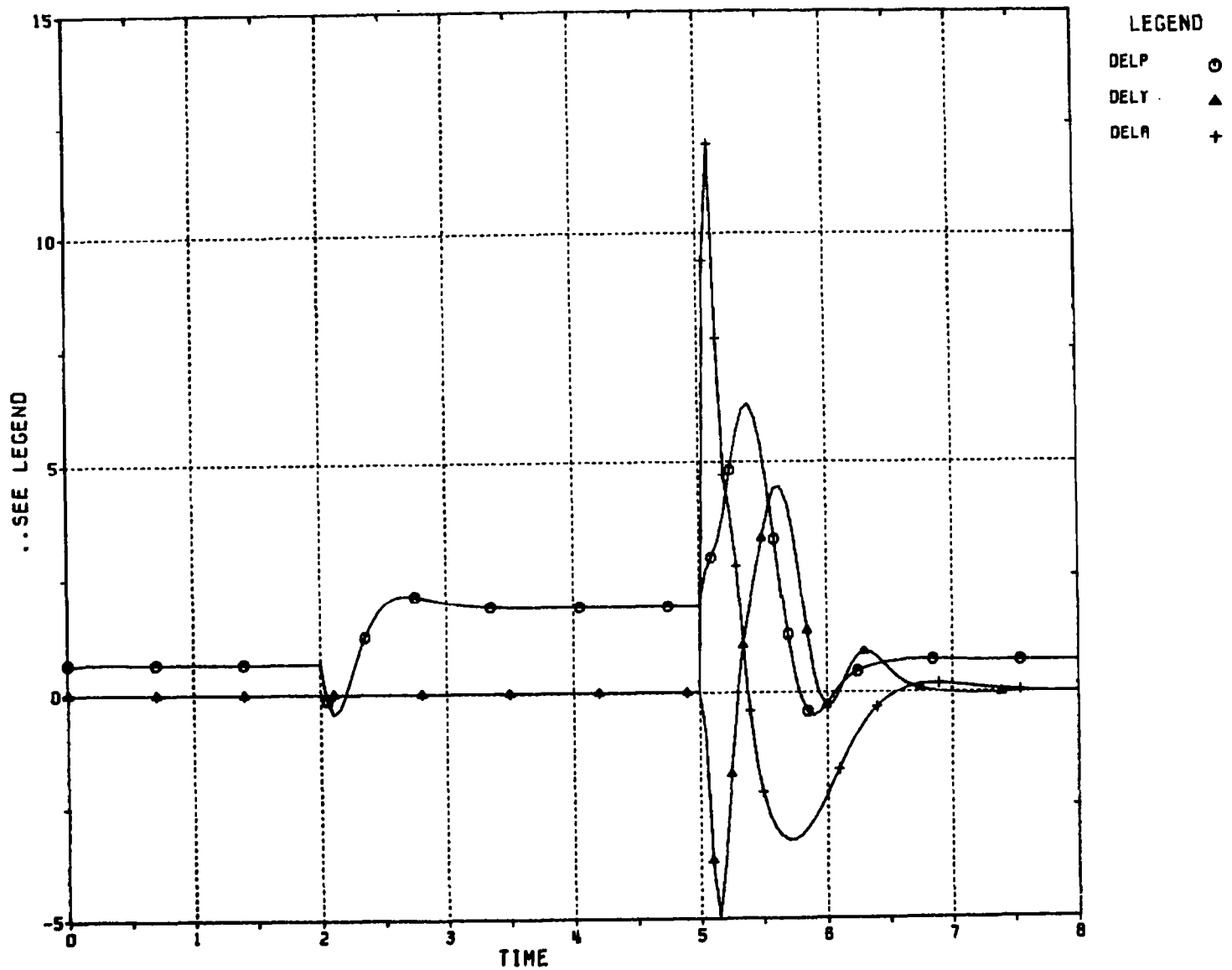

Figure 8.7 TAIL INCIDENCES VS. TIME (SEC); CBTT OF ELLIPTICAL AIRFRAME; 2 GEES (0^{o}, 180^{o}); DELP = PITCH (DEG), DELY = YAW (DEG), DELR = ROLL (DEG)

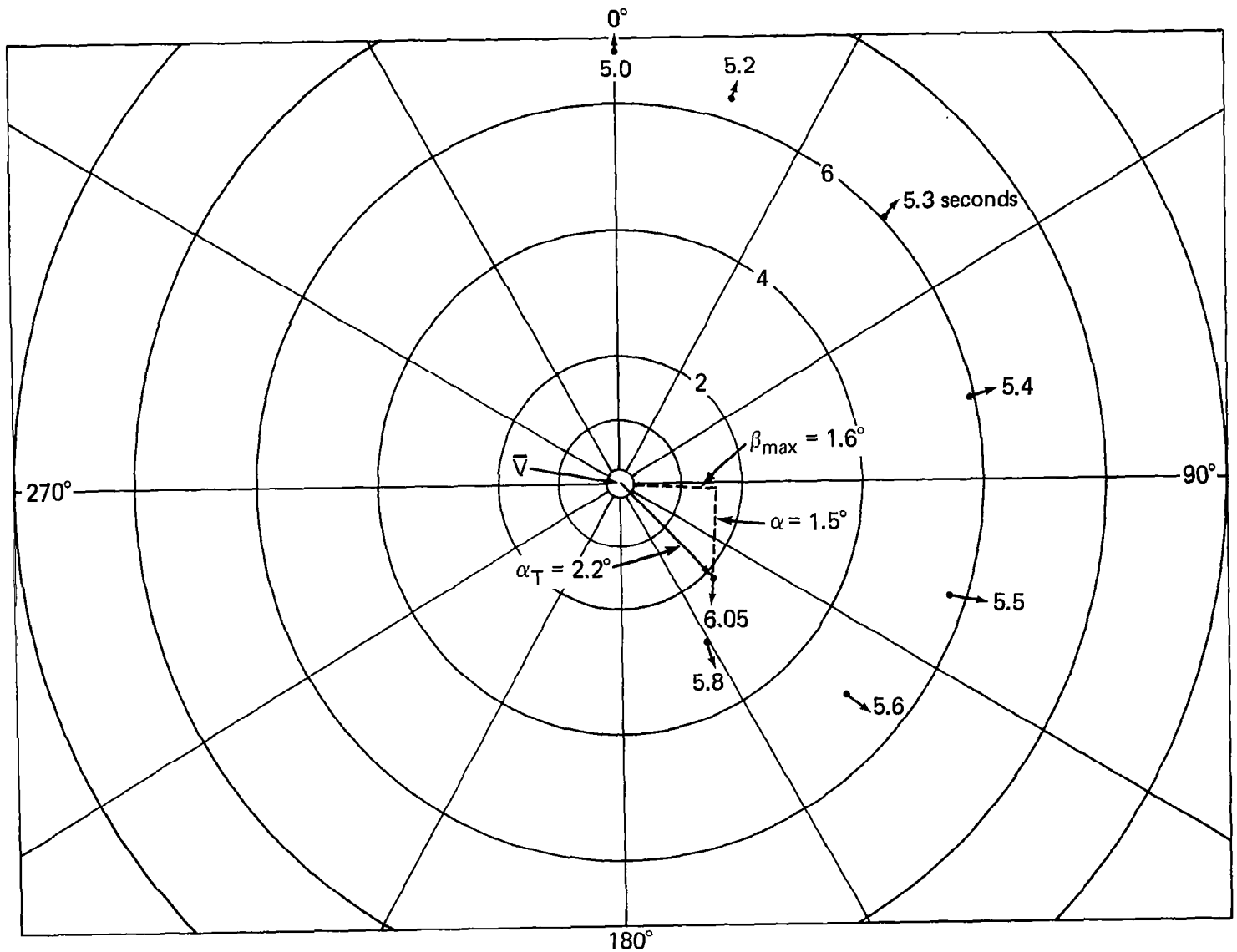

Fig. 8.8 Orientation of missile body with respect to velocity vector, CBTT of elliptical airframe, 2 gees (0°, 180°).

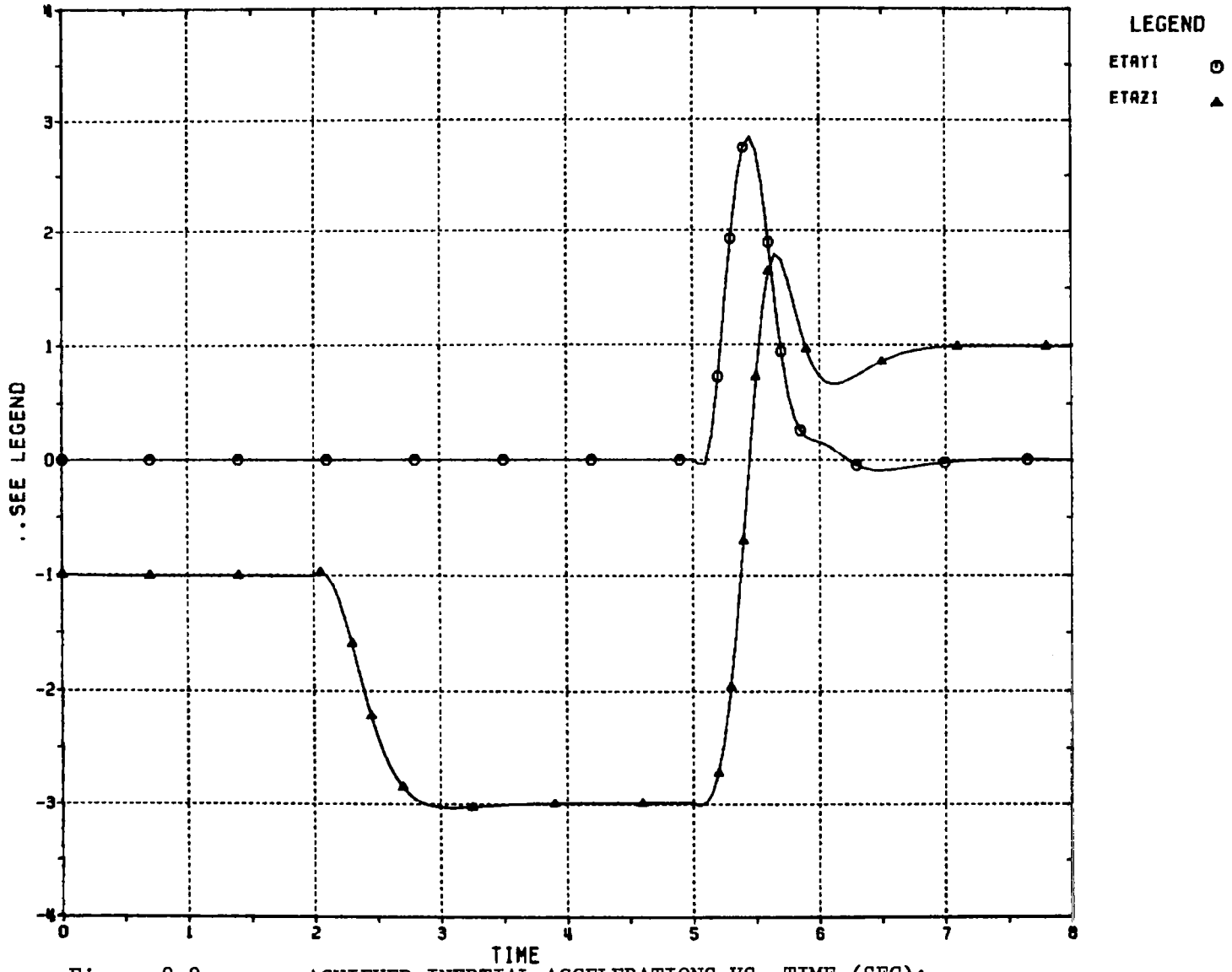

Figure 8.9 ACHIEVED INERTIAL ACCELERATIONS VS. TIME (SEC); CBTT OF ELLIPTICAL AIRFRAME WITHOUT AERODYNAMIC CROSS-COUPLING; 2 GEES (0^{o}, 180^{o})
ETAYI = CROSS-PLANE, ETAZI = MANEUVER PLANE (GEES)

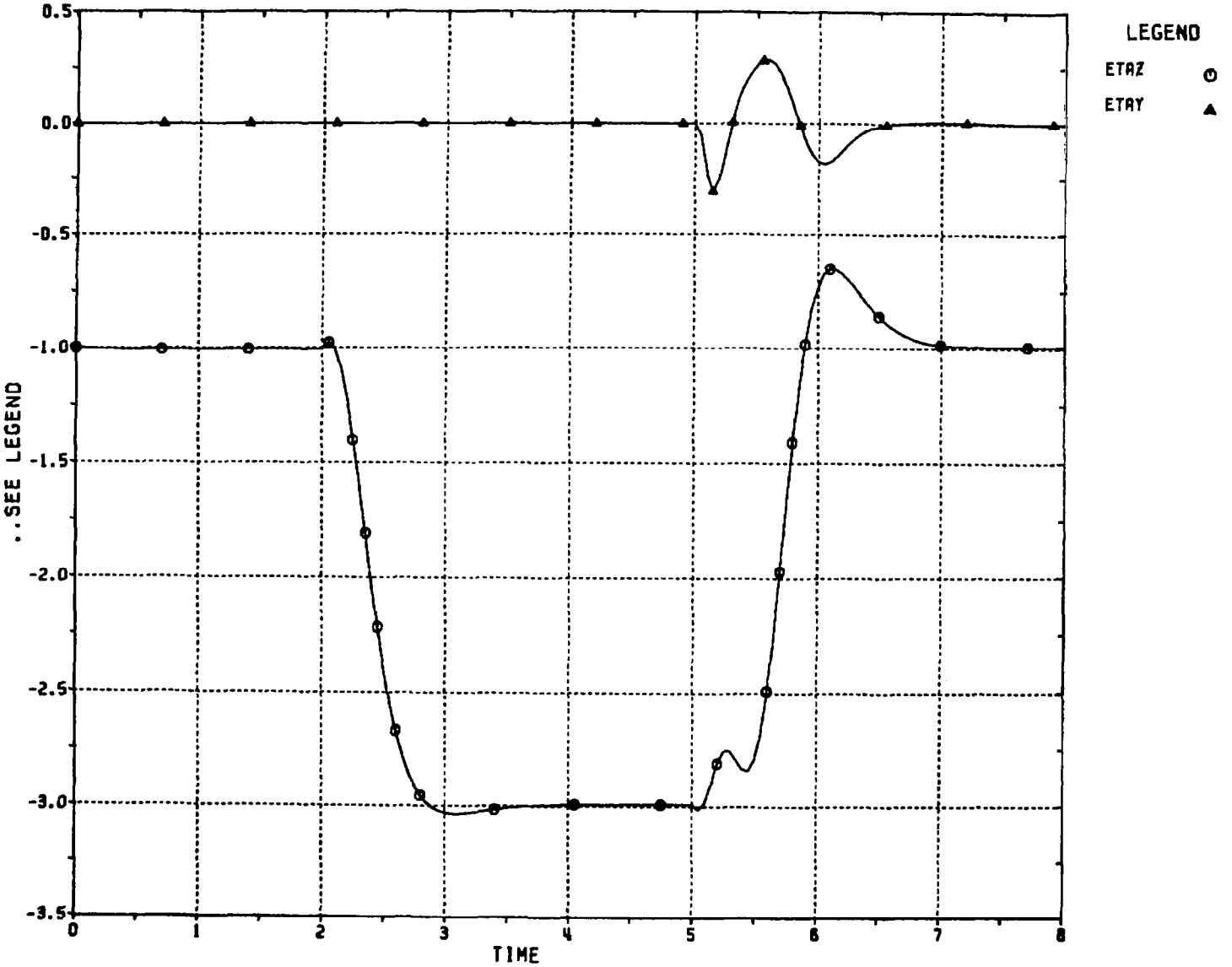

Figure 8.10 ACHIEVED BODY-FIXED ACCELERATIONS VS. TIME (SEC); CBTT OF ELLIPTICAL AIRFRAME WITHOUT AERODYNAMIC CROSS-COUPLING; 2 GEES (0^{o}, 180^{o})
ETAY = YAW (GEES), ETAZ = PITCH (GEES)

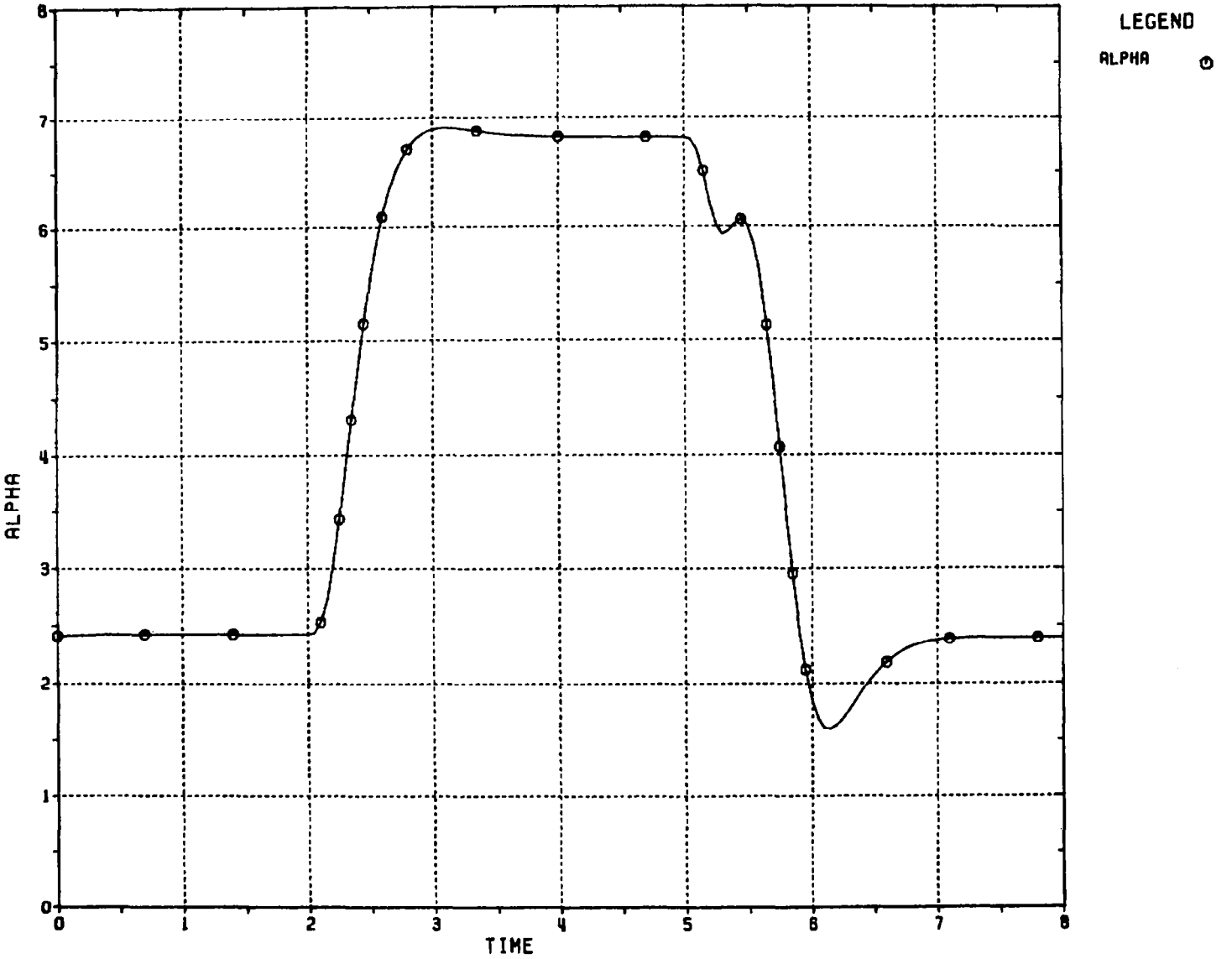

Figure 8.11 ANGLE OF ATTACK (DEG) VS. TIME (SEC); CBTT OF ELLIPTICAL AIRFRAME WITHOUT AERODYNAMIC CROSS-COUPLING; 2 GEES (0^{o}, 180^{o})

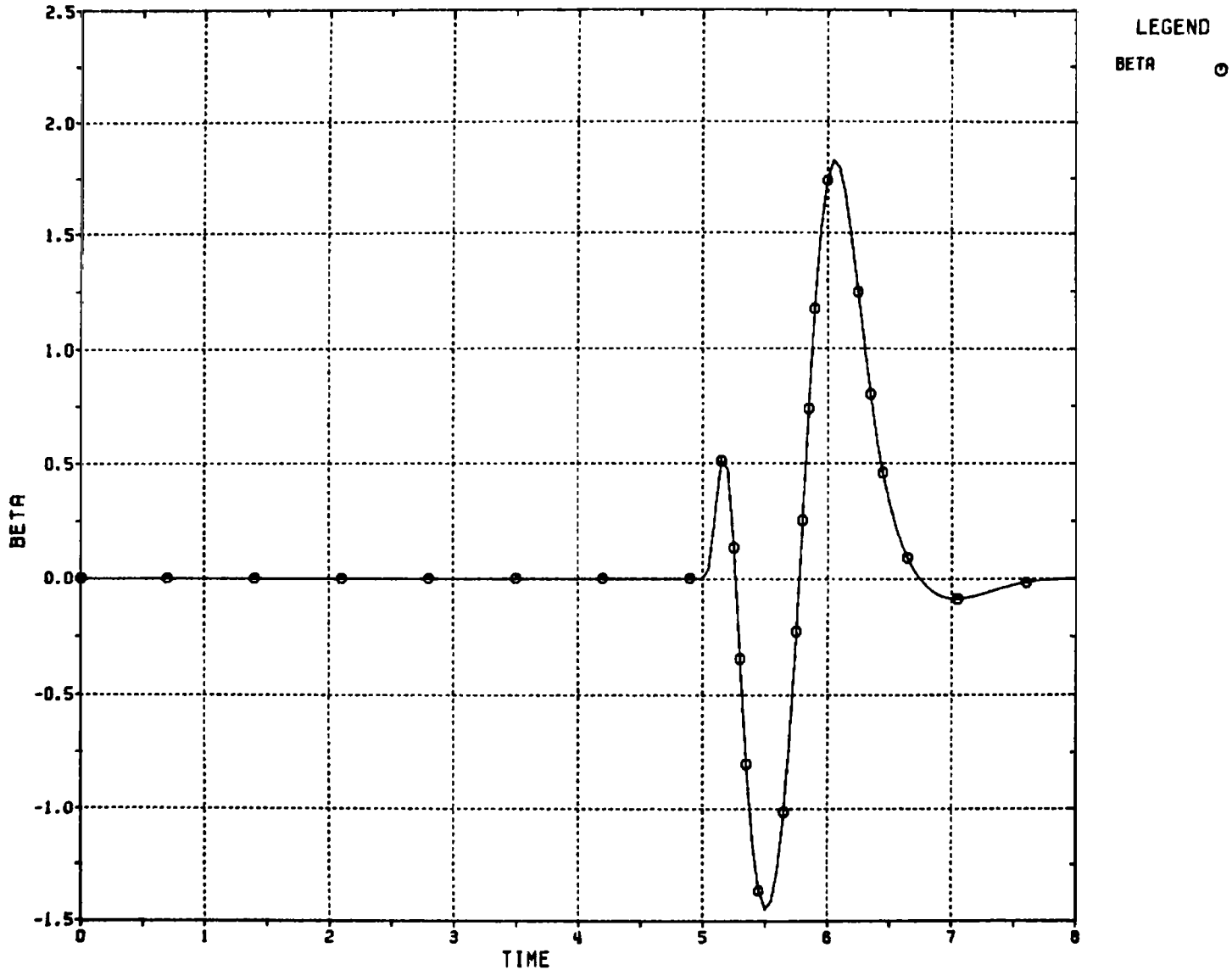

Figure 8.12 SIDESLIP ANGLE (DEG) VS. TIME (SEC);
CBTT OF ELLIPTICAL AIRFRAME WITHOUT
AERODYNAMIC CROSS-COUPLING;
2 GEES (0^{o}, 180^{o})

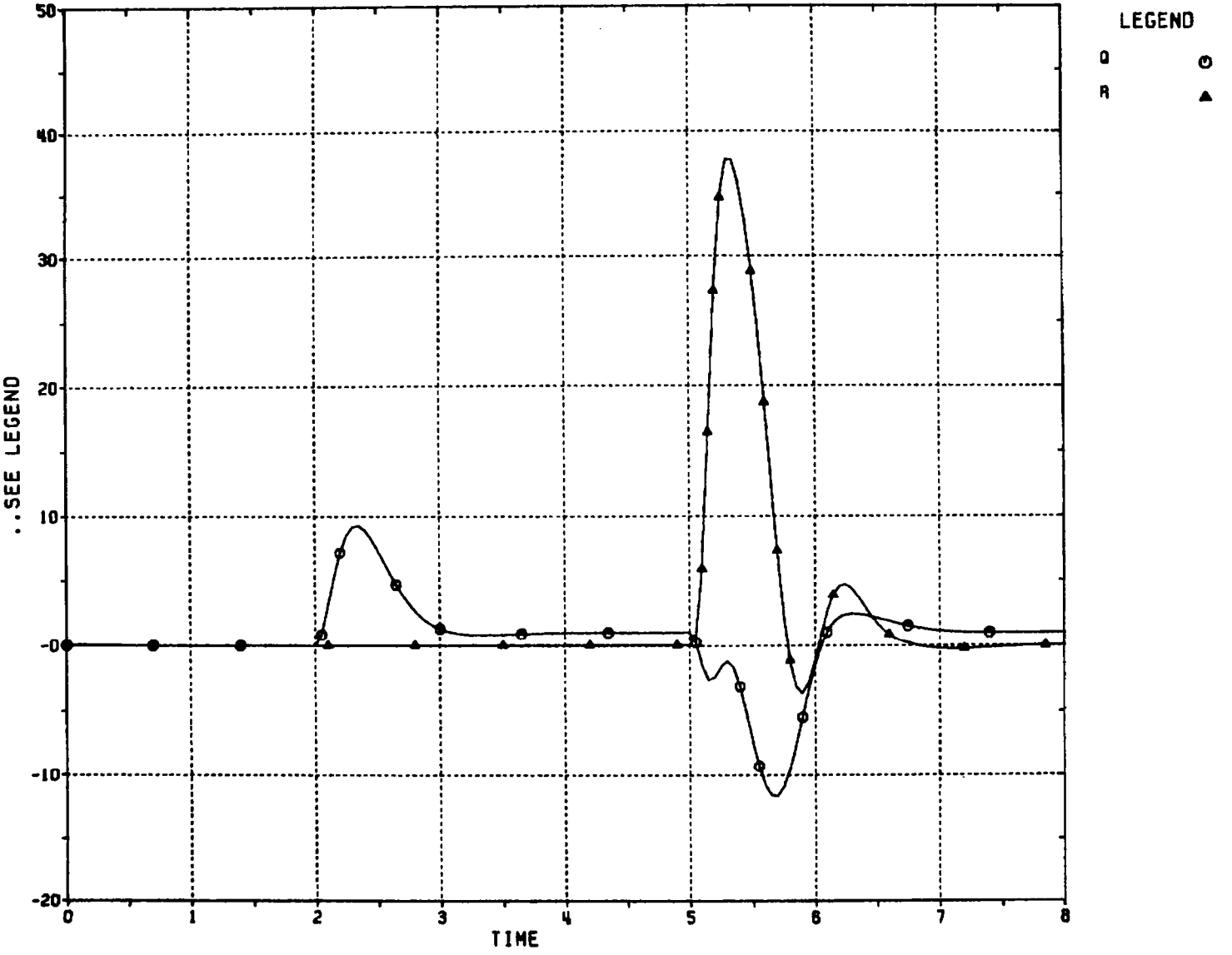

Figure 8.13 BODY ANGULAR RATES VS. TIME (SEC); CBTT OF ELLIPTICAL AIRFRAME WITHOUT AERODYNAMIC CROSS-COUPLING; 2 GEES (0^{o}, 180^{o})
Q = PITCH (DEG/SEC), R = YAW (DEG/SEC)

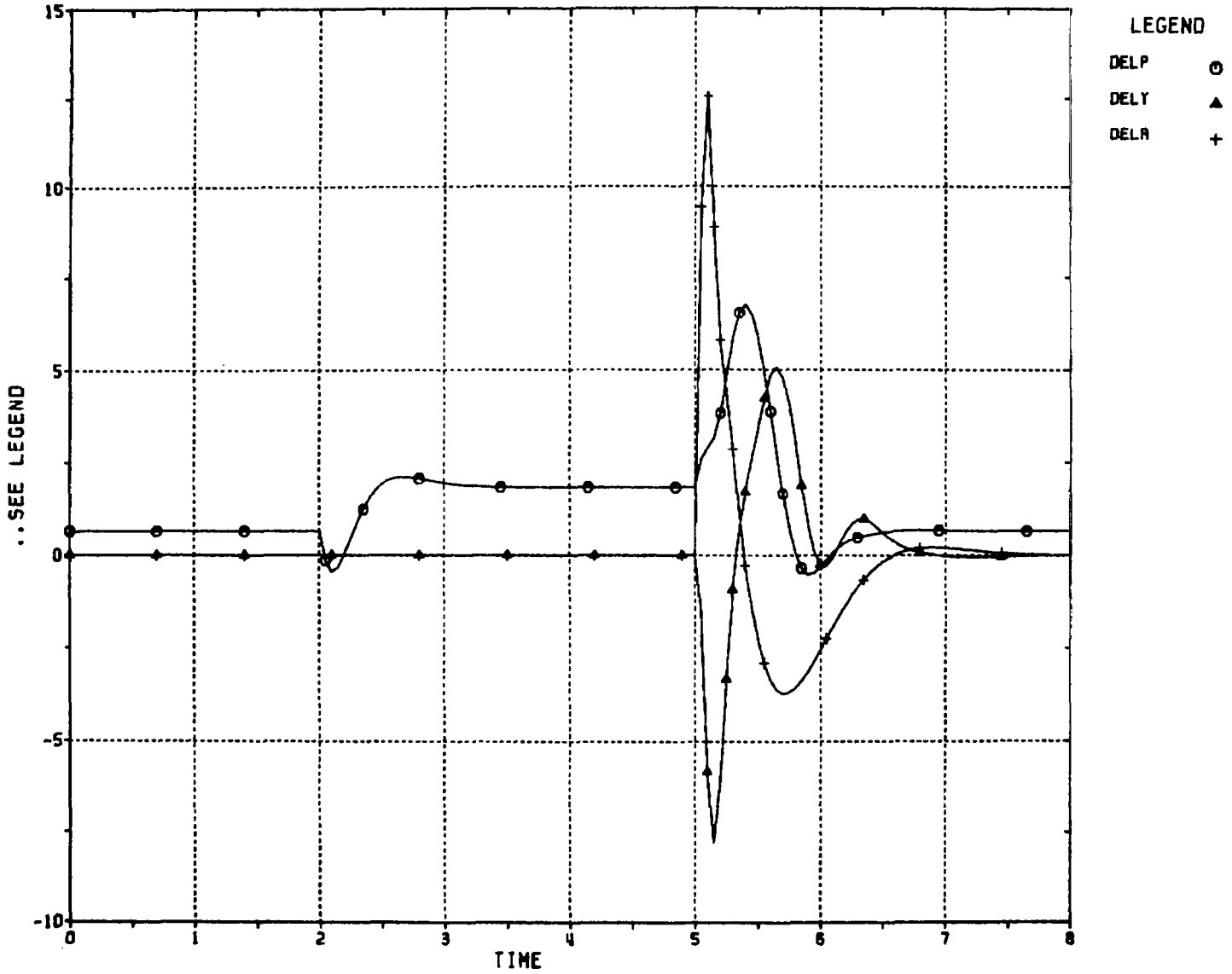

Figure 8.14 TAIL INCIDENCES VS. TIME (SEC); CBTT OF ELLIPTICAL AIRFRAME WITHOUT AERODYNAMIC CROSS-COUPLING; 2 GEES (0^{o}, 180^{o})
DELP = PITCH (DEG), DELY = YAW (DEG), DELR = ROLL (DEG)

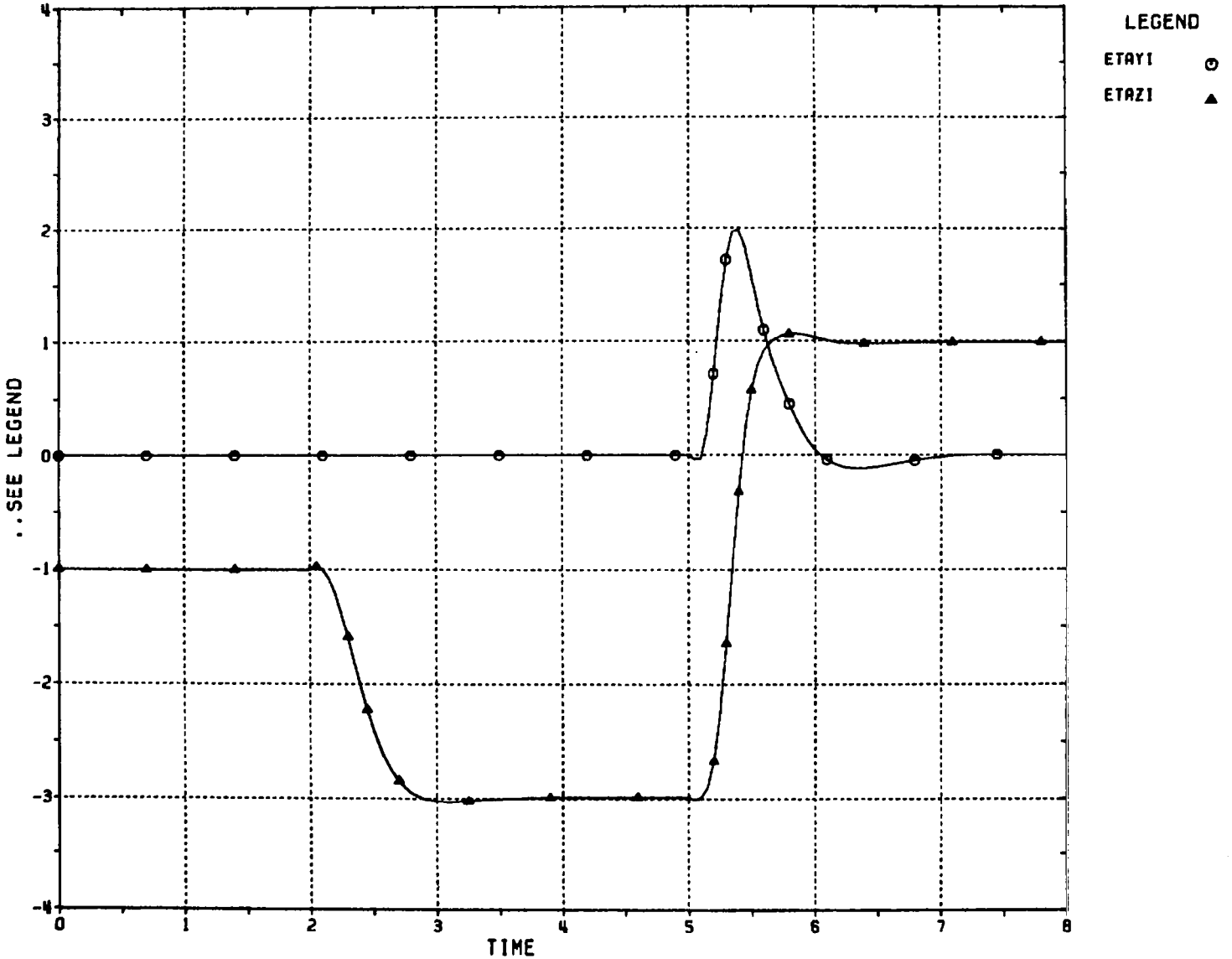

Figure 8.15 ACHIEVED INERTIAL ACCELERATIONS VS. TIME (SEC);
CBTT OF ELLIPTICAL AIRFRAME;
IDEAL AIRFRAME DYNAMICS; 2 GEES (0^{o}, 180^{o})
ETAYI = CROSS-PLANE (GEES), ETAZI = MANEUVER PLANE (GEES)

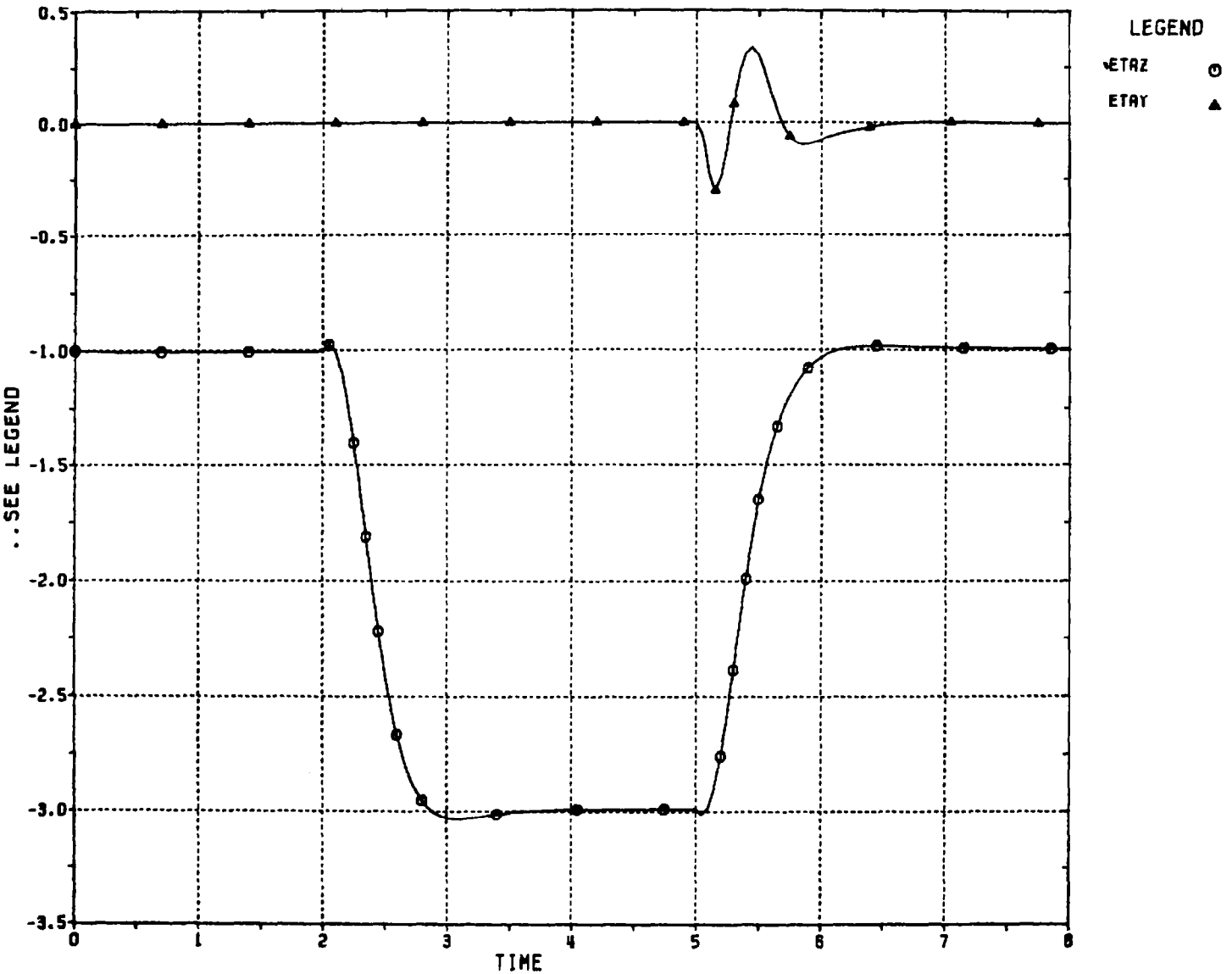

Figure 8.16 ACHIEVED BODY-FIXED ACCELERATIONS VS. TIME (SEC);
CBTT OF ELLIPTICAL AIRFRAME:
IDEAL AIRFRAME DYNAMICS; 2 GEES (0^{o}, 180^{o})
ETAY = YAW (GEES), ETAZ = PITCH (GEES)

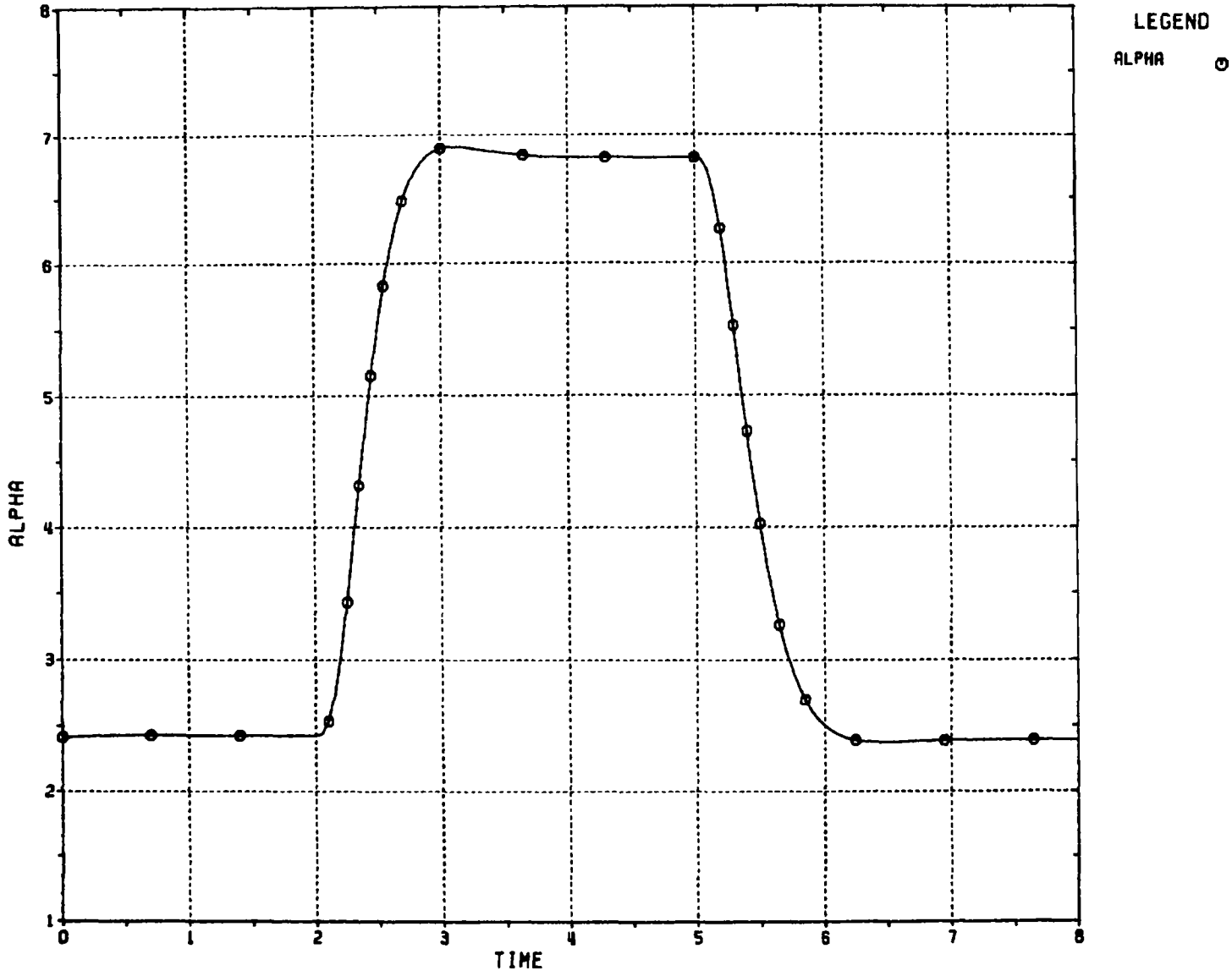

Figure 8.17 ANGLE OF ATTACK (DEG) VS. TIME (SEC); CBTT OF ELLIPTICAL AIRFRAME; IDEAL AIRFRAME DYNAMICS; 2 GEES (0^{o}, 180^{o})

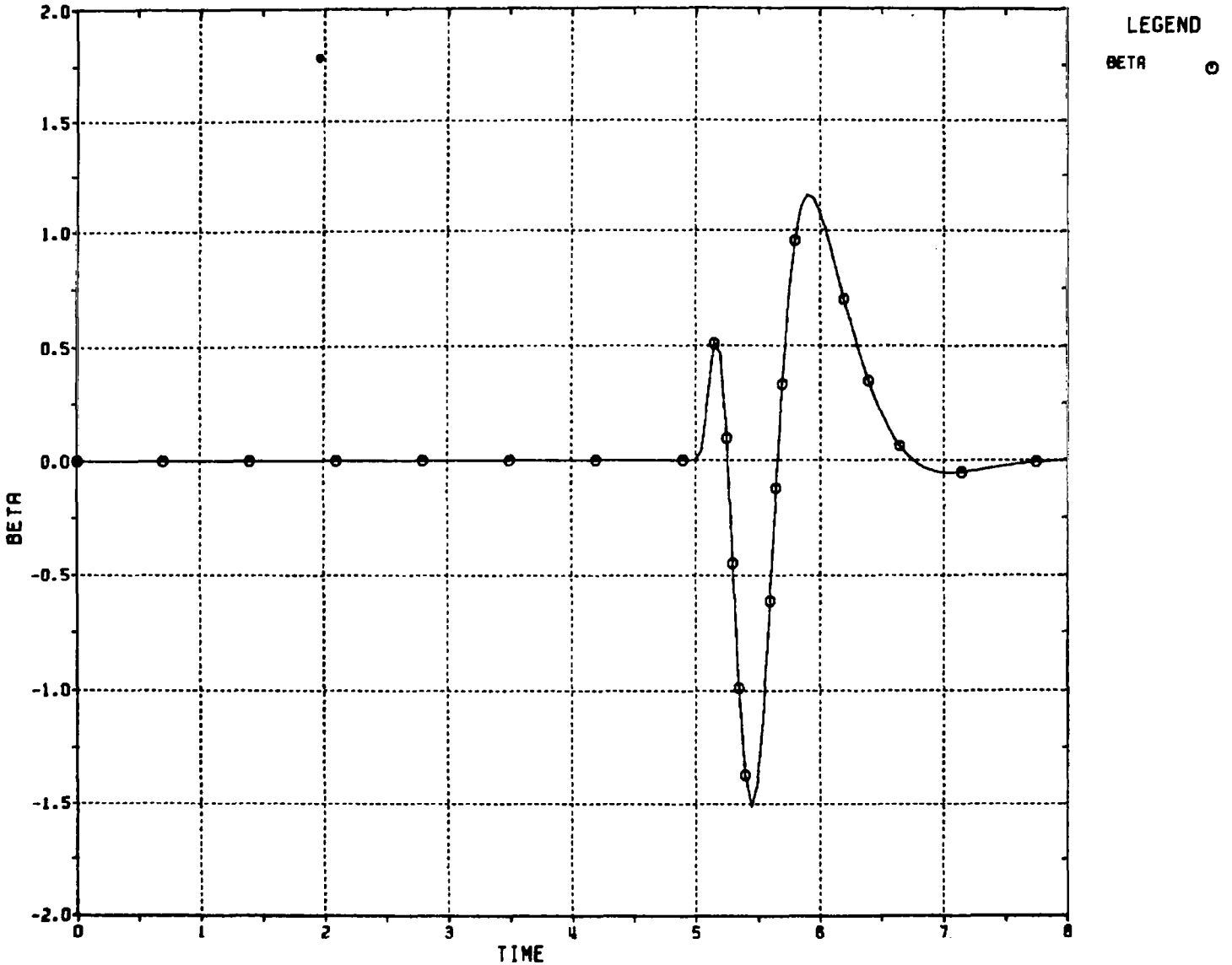

Figure 8.18 SIDESLIP ANGLE (DEG) VS. TIME (SEC); CBTT OF ELLIPTICAL AIRFRAME; IDEAL AIRFRAME DYNAMICS; 2 GEES (0^{o}, 180^{o})

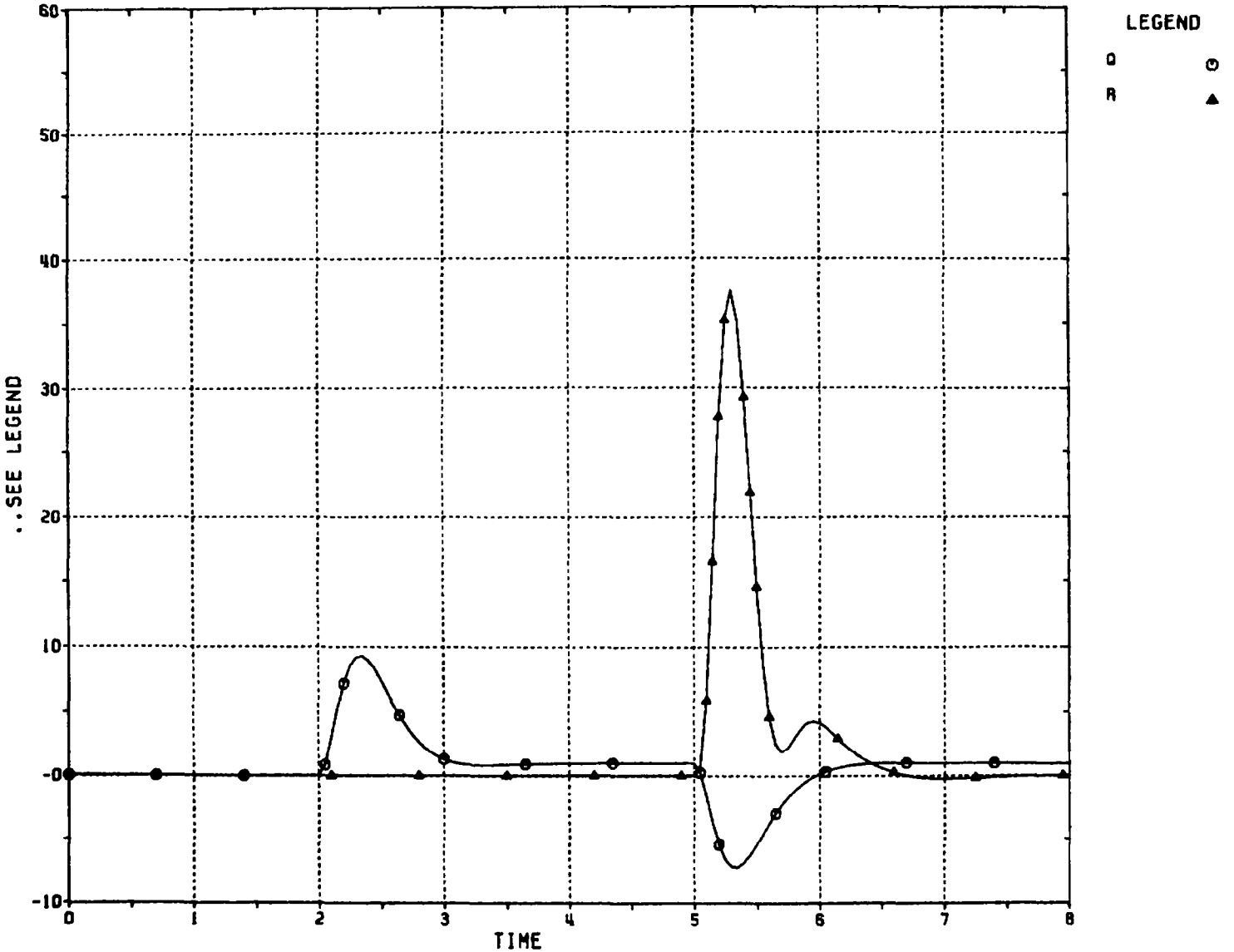

Figure 8.19 BODY ANGULAR RATES VS. TIME (SEC); CBTT OF ELLIPTICAL AIRFRAME; IDEAL AIRFRAME DYNAMICS; 2 GEES (0°, 180°) Q = PITCH (DEG/SEC), R = YAW (DEG/SEC)

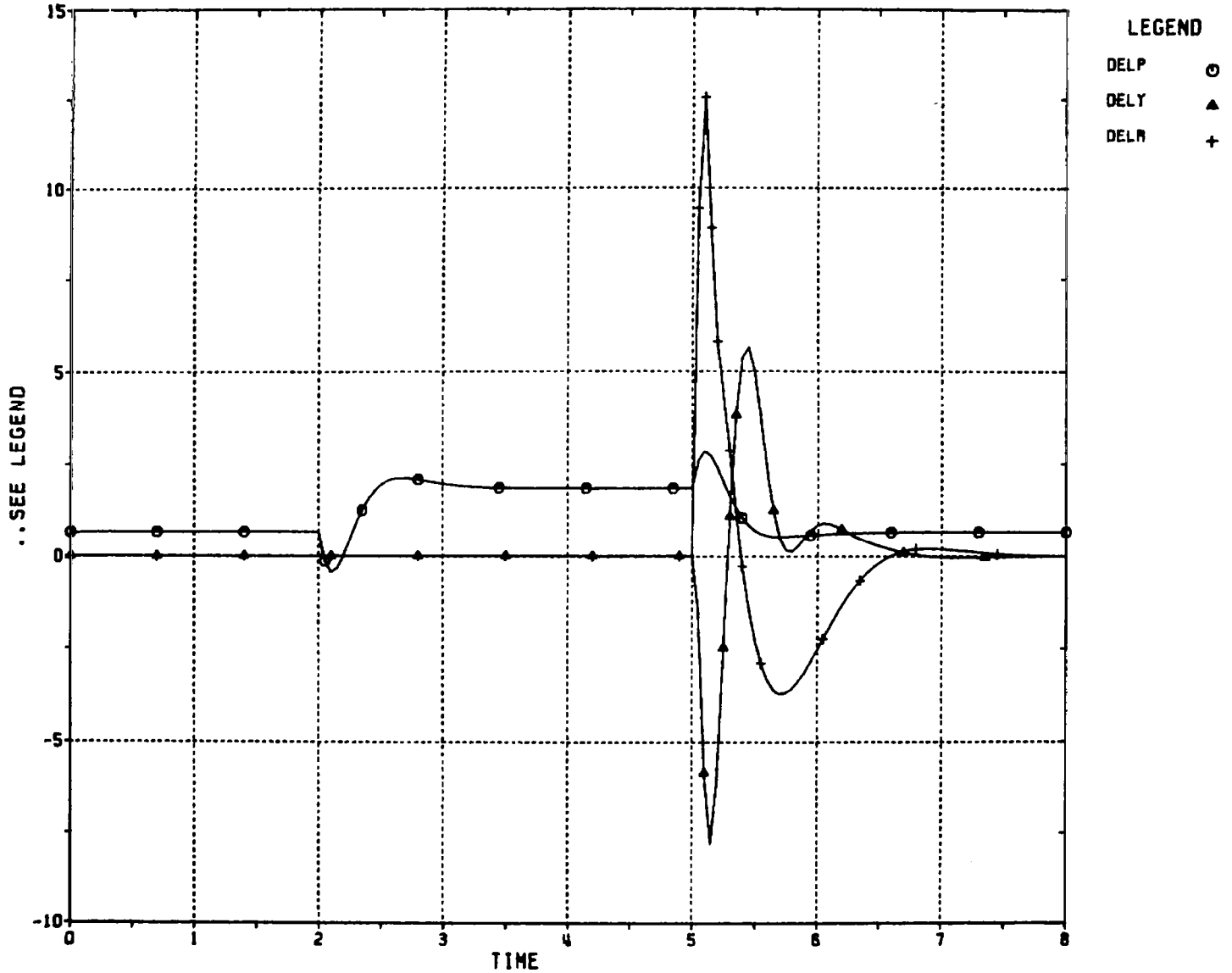

Figure 8.20 TAIL INCIDENCES VS. TIME (SEC);
CBTT OF ELLIPTICAL AIRFRAME; IDEAL
AIRFRAME DYNAMICS; 2 GEES (0°, 180°)
DELP = PITCH (DEG), DELY = YAW (DEG), DELR = ROLL (DEG)

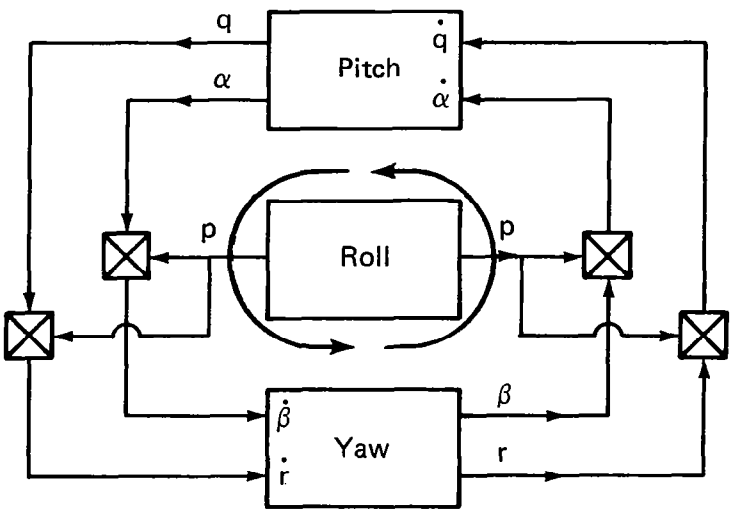

Fig. 8.21 Critical feedback loops for CBTT.

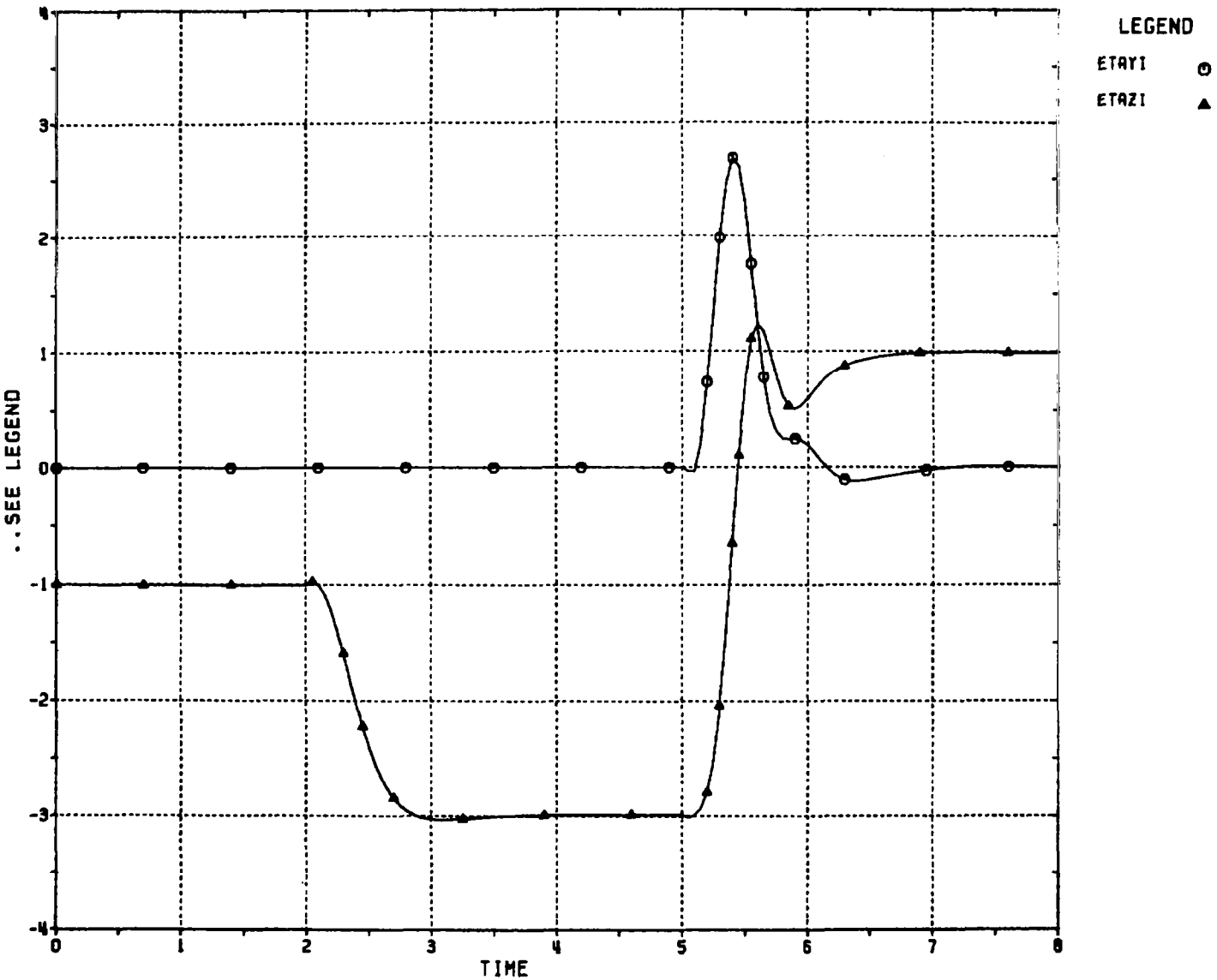

Figure 8.22 ACHIEVED INERTIAL ACCELERATIONS OF ELLIPTICAL AIRFRAME VS. TIME (SEC); AERODYNAMIC AND KINEMATIC (β p into $\dot{\alpha}$) CROSS-COUPLING REMOVED; INERTIAL COUPLING p r INTO $\dot{q}$ RETAINED;
ETAYI = CROSS-PLANE (GEES), ETAZI = MANEUVER PLANE (GEES)

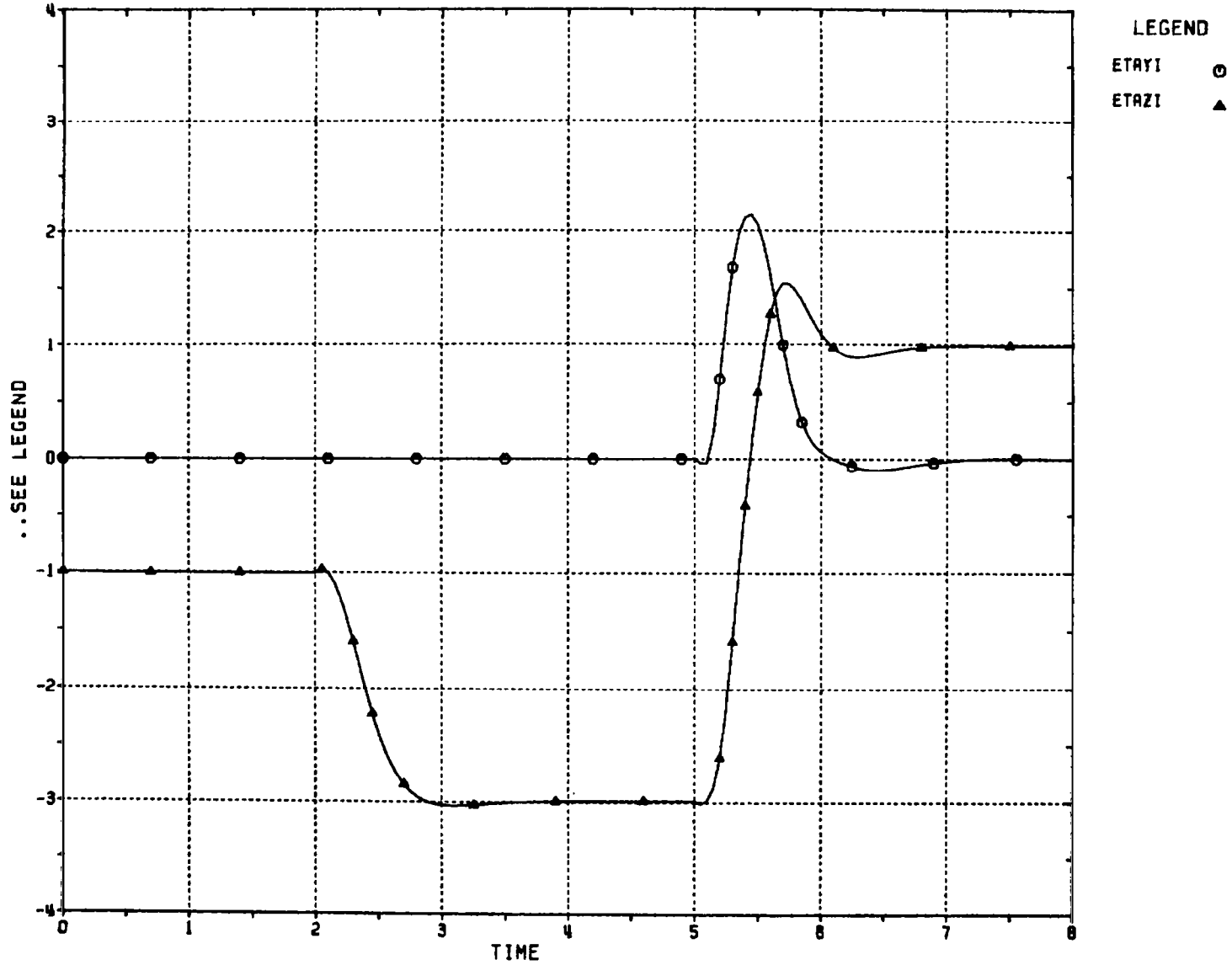

Figure 8.23 ACHIEVED INERTIAL ACCELERATIONS OF ELLIPTICAL AIRFRAME VS. TIME (SEC); AERODYNAMIC AND INERTIAL ($p\ r$ into $\dot{q}$) CROSS-COUPLING REMOVED; KINEMATIC COUPLING $\beta\ p$ into $\dot{\alpha}$ RETAINED;
ETAYI = CROSS-PLANE (GEES), ETAZI = MANEUVER PLANE (GEES)

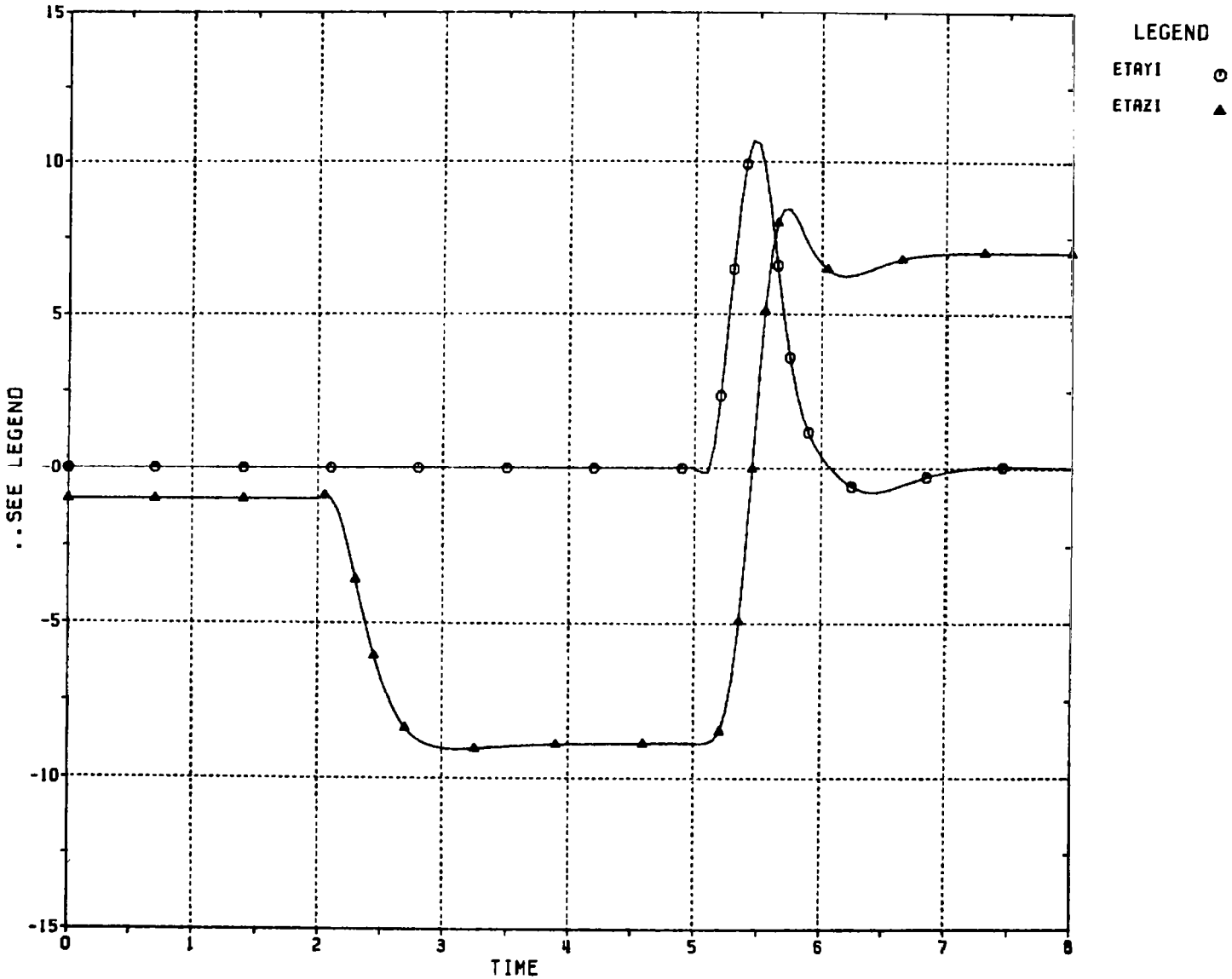

Figure 8.24 ACHIEVED INERTIAL ACCELERATIONS VS. TIME (SEC);
CBTT OF ELLIPTICAL AIRFRAME; AERODYNAMIC CROSS-COUPLING REMOVED;
8 GEES (0^{o}, 180^{o})
ETAYI = CROSS-PLANE (GEES), ETAZI = MANEUVER PLANE (GEES)

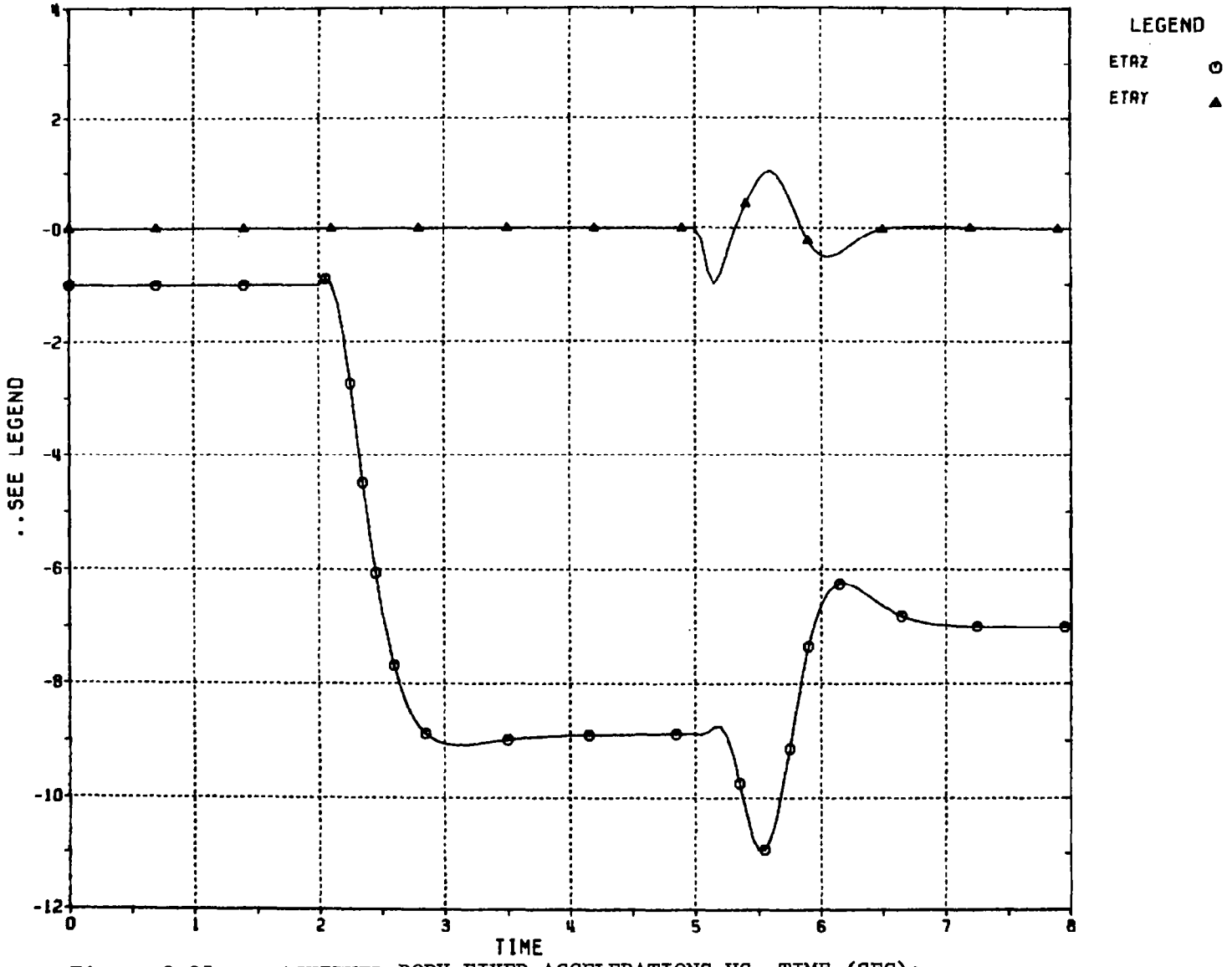

Figure 8.25 ACHIEVED BODY-FIXED ACCELERATIONS VS. TIME (SEC);
CBTT OF ELLIPTICAL AIRFRAME: AERODYNAMIC CROSS-COUPLING
REMOVED; 8 GEES (0^{o}, 180^{o})
ETAY = YAW (GEES), ETAZ = PITCH (GEES)

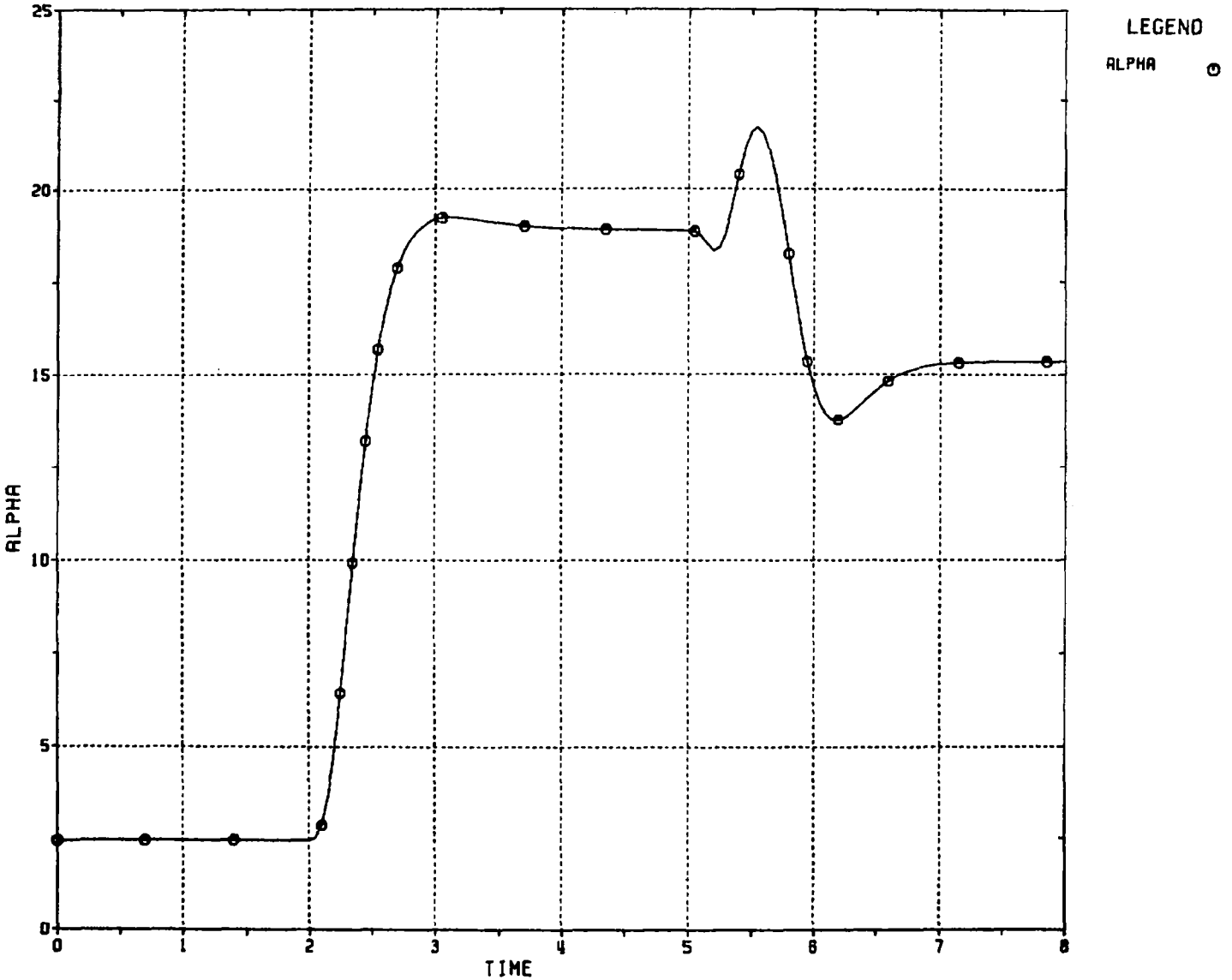

Figure 8.26 ANGLE OF ATTACK (DEG) VS. TIME (SEC);
CBTT OF ELLIPTICAL AIRFRAME;
AERODYNAMIC CROSS-COUPLING REMOVED;
8 GEES (0^{o}, 180^{o})

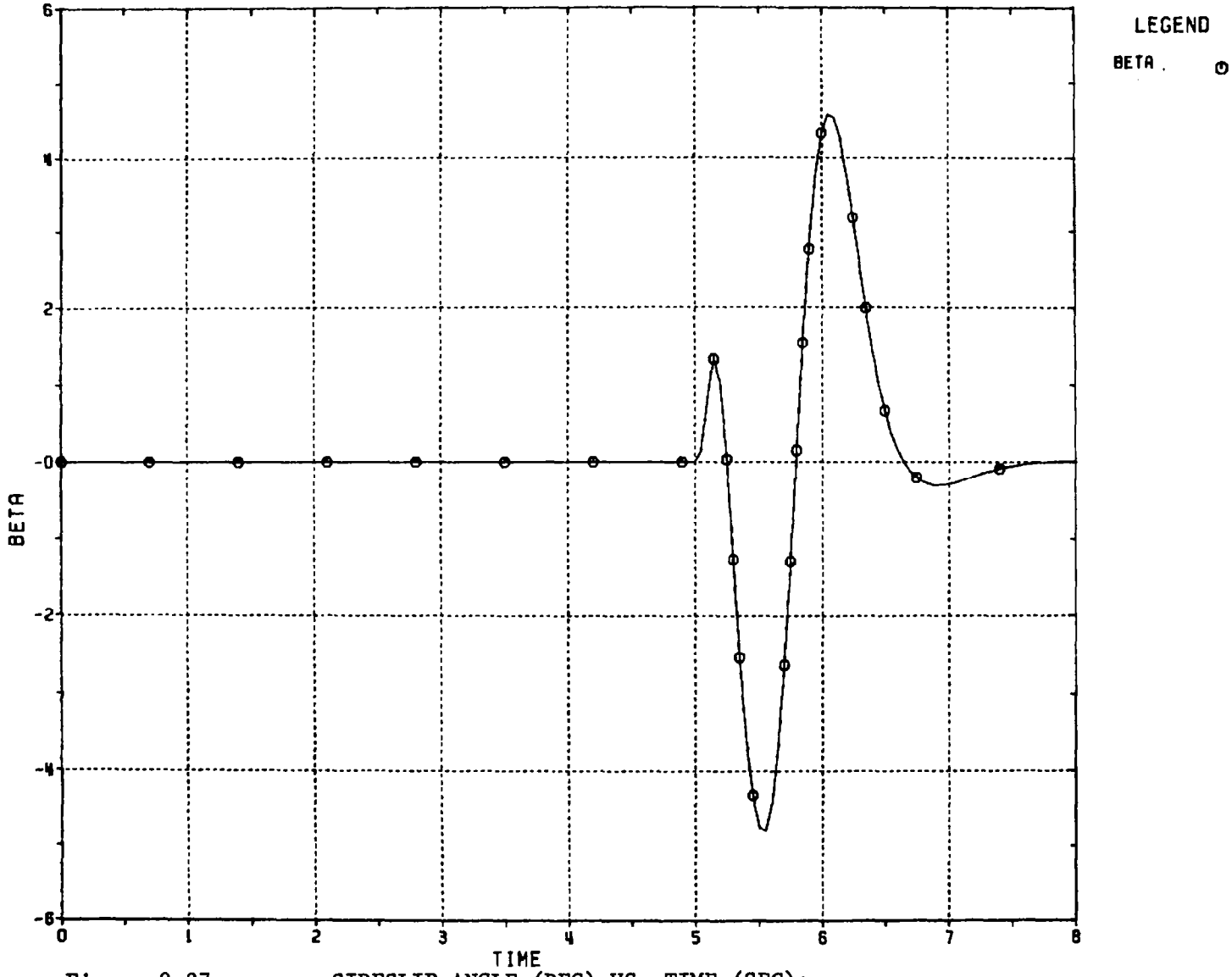

Figure 8.27 SIDESLIP ANGLE (DEG) VS. TIME (SEC);
CBTT OF ELLIPTICAL AIRFRAME;
AERODYNAMIC CROSS-COUPLING REMOVED;
8 GEES (0^{o}, 180^{o})

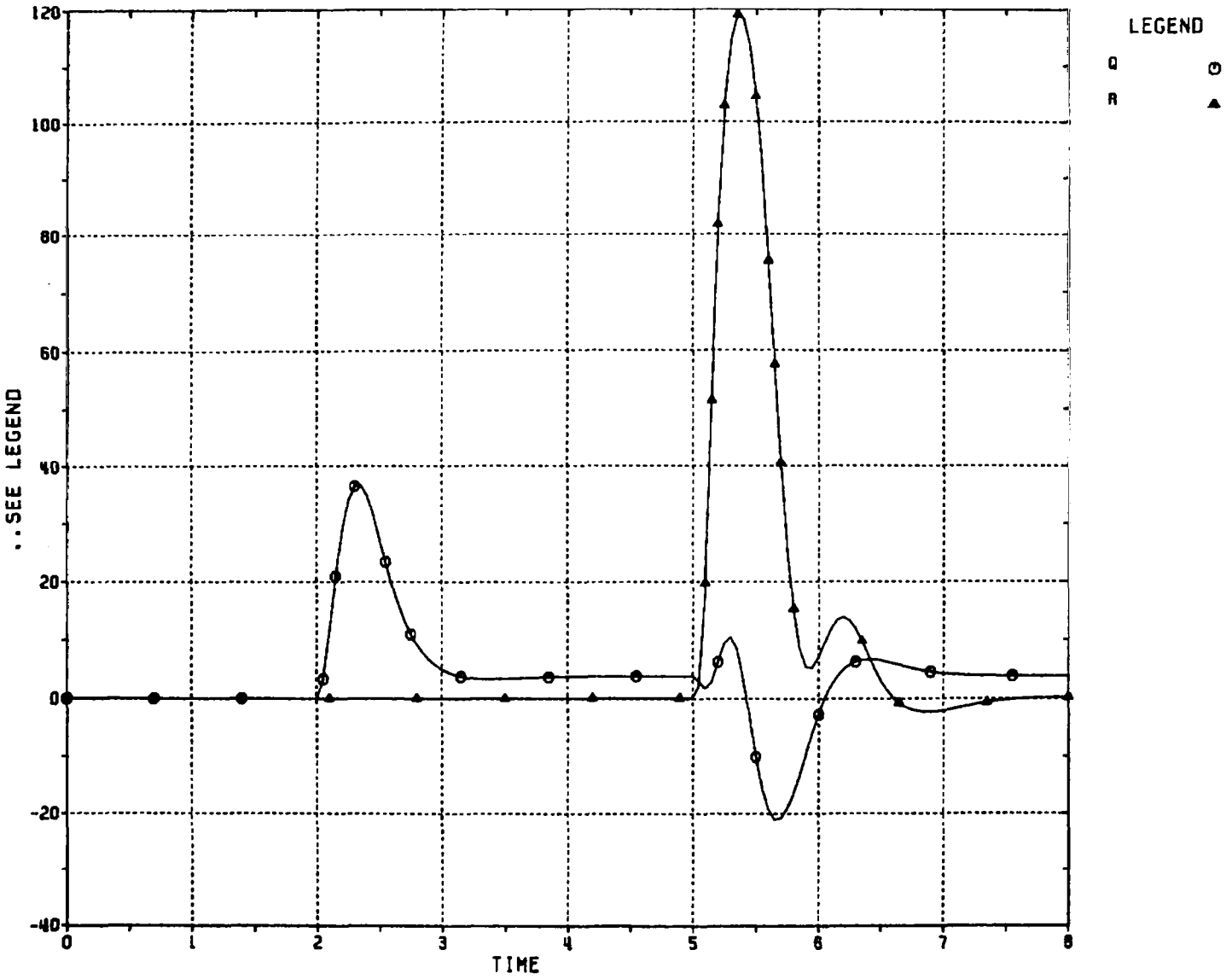

Figure 8.28 BODY ANGULAR RATES VS. TIME (SEC); CBTT OF ELLIPTICAL AIRFRAME; AERODYNAMIC CROSS-COUPLING REMOVED; 8 GEES (0^{o}, 180^{o})
Q = PITCH (DEG/SEC), R = YAW (DEG/SEC)

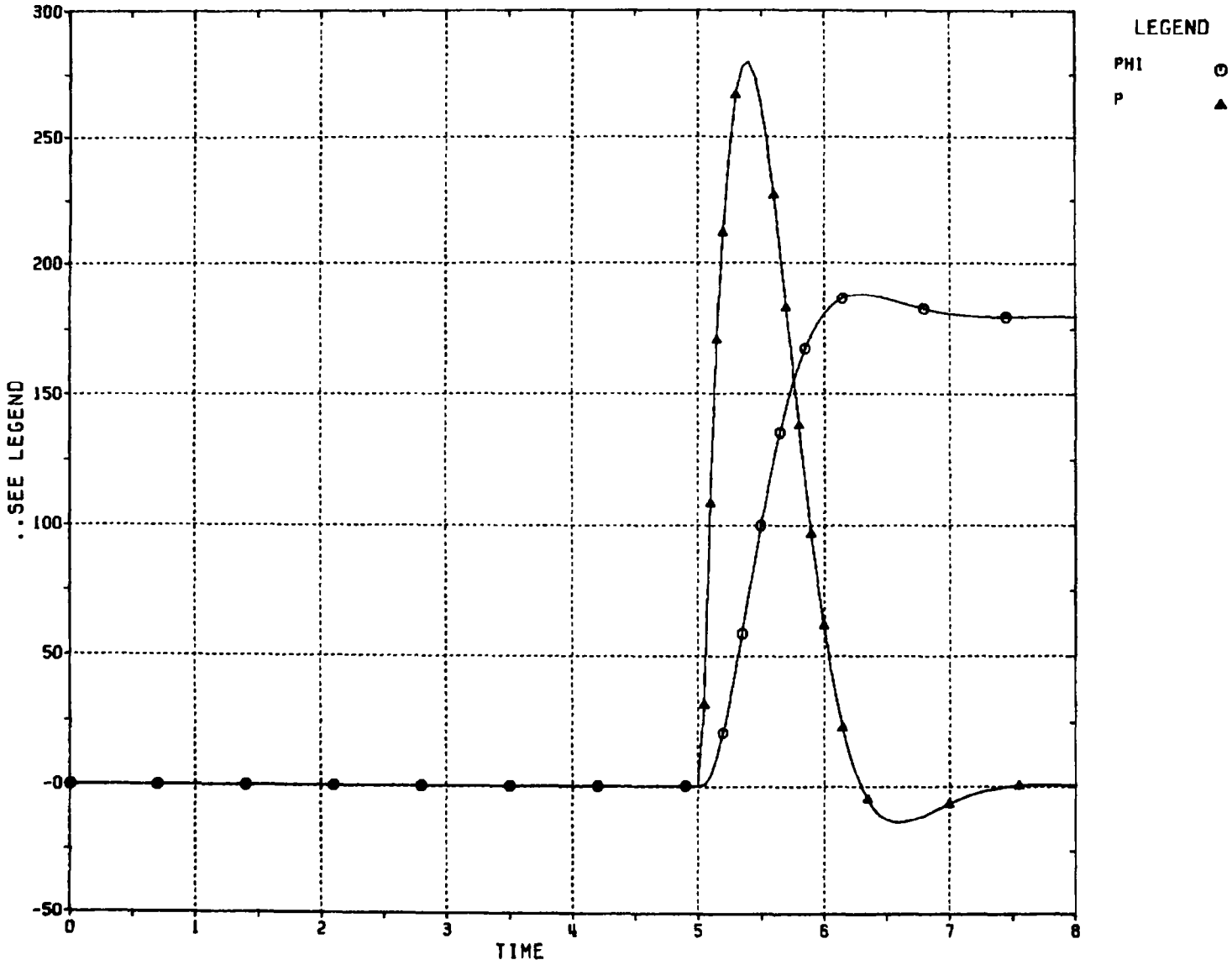

Figure 8.29 ROLL ANGLE AND ANGULAR RATE VS. TIME (SEC);
CBTT OF ELLIPTICAL AIRFRAME; AERODYNAMIC CROSS-COUPLING
REMOVED; 8 GEES (0^{o}, 180^{o})
PHI = ROLL ANGLE (DEG), P = ROLL ANGULAR RATE (DEG/SEC)

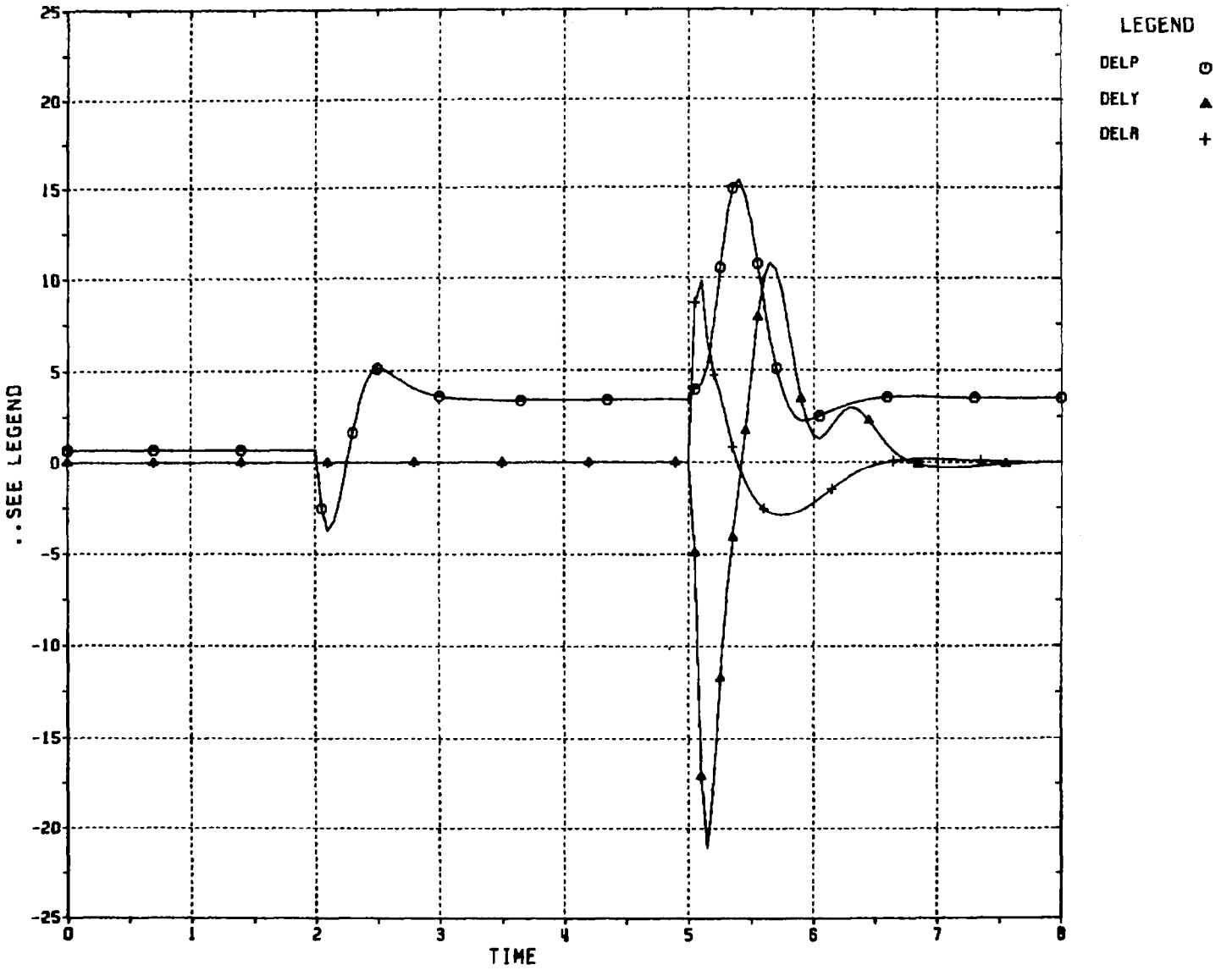

Figure 8.30 TAIL INCIDENCES VS. TIME (SEC);
CBTT OF ELLIPTICAL AIRFRAME;
AERODYNAMIC CROSS-COUPLING REMOVED; 8 GEES (0^{o}, 180^{o})
DELP = PITCH (DEG), DELY = YAW (DEG), DELR = ROLL (DEG)

9 NONLINEAR ANALYSIS OF CBTT AUTOPILOT FOR CIRCULAR AIRFRAME

Except for the aerodynamic and mass parameter changes consistent with the circular airframe, and the changes in the control law shown in Figures 7.1 and 7.2, the CBTT simulation was the same as used for the elliptical airframe in Section 8. Anti-gravity bias and the modification to the coordination gain $\bar{\alpha}$ was done the same way as described in Section 8.

9.1 CBTT PERFORMANCE

The same 2 gees (0^o, 180^o) guidance commands and flight condition were used for direct comparison with the performance results of the elliptical airframe. However, to decrease simulation run time, the first guidance command and anti-gravity bias were applied at zero time with no missile or autopilot initial conditions. The response to the first command was shown to be insensitive to the transient effects of gravity and anti-gravity bias.

The nonlinear 3-D simulation verified the linear studies of Section 7. The CBTT autopilot was unstable for a coordination gain K_{YP} of unity and the roll actuator command branch lead at the uncoupled roll autopilot design value of 110 rad/sec (Appendix F). Therefore it was necessary to set the gain of K_{YP} to 0.458 and the roll actuator command branch lead to 60 rad/sec as determined in the linear studies (Section 7) which in turn resulted in larger sideslip angles.

Figure 9.1 shows that the achieved maneuver plane acceleration has a good response to the first command which is applied at zero time. The missile with the circular airframe moves upward like a skid-to-turn missile, as did the elliptical airframe missile in Section 8, because the motion is in the desired maneuver direction and therefore the roll channel is not commanded. Comparing Tables 9.1 and 8.1, the time constants of the achieved maneuver plane

response (i.e., τ_1) of the two airframes are approximately the same. The circular is 6.5 percent slower. The achieved maneuver plane response due to the second guidance command applied at 3 seconds, shown in Figure 9.1, is reacting differently to the kinematic and inertial cross-coupling than the elliptical airframe in Figure 8.1. Rather than overshoots and undershoots, a slowing transient starts at 3.5 seconds. Figure 9.2 shows that the overshoot in the body-fixed pitch acceleration due to the kinematic and inertial cross-coupling during the second command is substantially more than it was for the elliptical airframe and occurs much sooner.

From Figures 9.4 and 9.6 it is seen that the maximum sideslip angle of 4.5 degrees occurs at the maximum roll rate when the roll angle is 90 degrees. The main contribution to the maximum sideslip angle is the same as it was for the elliptical airframe, namely, the kinematic cross-coupling input of αp into β which is nulled by the autopilot coordination command. The contributions to maximum sideslip angle from either gravity or yaw acceleration were negligible. The reason the maximum sideslip angle of the circular airframe is larger than that of the elliptical airframe is that the coordination gain of the autopilot could not be set at its proper value of unity. This is proven in Section 10. Even though the circular airframe has higher maximum angles-of-attack (Figures 9.3 and 8.3) during the first command, there is no initial delaying transient due to the kinematic and inertial cross-coupling and therefore when the maximum sideslip occurs the angle-of-attack is lower than it was for the elliptical airframe. As a result, the contribution of the kinematic cross-coupling (i.e., $p\alpha$) was larger for the elliptical airframe but the autopilot coordination which nulled its effects did a better job.

Comparing Figures 9.5 and 8.5, the pitch rates of the circular airframe are higher than those of the near neutrally stable elliptical airframe. This is due to the elliptical airframe being closer to being neutrally stable in pitch, as shown in the linear studies of Appendix D, Figures D.4 and D.5,

whereas the circular airframe is stable in pitch. Yaw angular rates are lower for the circular airframe because the airframe is closer to being neutrally stable in yaw, as shown in the linear studies of Appendix E, Figures E.5 and E.6 and the autopilot coordination gain is lower. Roll rates and angle response are not affected by the CBTT control for either circular or elliptical airframes due to the effectiveness of the autopilot roll acceleration feedback at the flight condition studied. Maximum rates are summarized in Table 9.2.

Comparison of Figures 9.7 and 8.7 show that the roll tail incidence δ_R of the circular airframe has been reduced due to larger aerodynamic roll control effectiveness. Pitch tail control incidence δ_P is higher for the circular airframe because of the more stable pitch aerodynamics as discussed in Appendix D. The yaw tail incidence of the circular airframe is very oscillatory while the sideslip angles are large. The elliptical airframe shows improved stability in both yaw and roll tail incidences. Smaller maximum yaw tail incidence δ_Y for the circular airframe is due to the same reasons mentioned above for yaw angular rate. The difference in lateral control incidences for circular and elliptical airframes are discussed further in Section 10.

9.2 EFFECT OF INCREASING PITCH CHANNEL SPEED OF RESPONSE

To reduce the effect of kinematic and inertial cross-coupling during the second guidance command, the response of the pitch channel of the CBTT autopilot for the circular airframe was made faster as shown in Appendix D. This was accomplished by increasing by 3 dB the acceleration error gain K_A (Figure 7.1). The effect of the change in K_A on achieved body-fixed accelerations (Figure 9.9) results in the achieved maneuver plane acceleration response (Figure 9.8). Figure 9.8 shows that the achieved maneuver plane acceleration response during the second guidance command has improved. Although the delay due to the transient is more pronounced, the acceleration

rises more rapidly to the plus one gee level. However, the resulting time constant is 24 percent larger than the desired value of 0.5 seconds (Table 9.1) and unacceptable. Improvement of both maneuver plane acceleration time constant and also coordination of the CBTT autopilot for the circular airframe is addressed in Section 10.

Table 9.1 shows that increasing the acceleration error gain in the pitch channel resulted in a 13 percent decrease in maximum sideslip angle and a slight decrease in yaw angular rates.

Since the faster pitch channel has improved performance it is used for the following studies.

9.3 EFFECT OF INERTIAL AND KINEMATIC CROSS-COUPLING IN PITCH CHANNEL

The cross-couplings, $-\beta p$ into $\dot{\alpha}$ and rp into $\dot{q}$, were removed in order to assess their effect on performance. The lateral aerodynamic cross-coupling was retained. Comparing Figures 9.10 and 9.11 with Figures 9.8 and 9.9 show that the undesirable transients are gone. Comparing Figures 9.12 and 9.3, the large undershoot in angle-of-attack is gone. Although sideslip angle (Figures 9.13 and 9.4) has increased, it is shown in Section 10 how it may be reduced. Table 9.1 shows that the achieved maneuver plane acceleration time constant for the second command has decreased to the desired value. Figure 9.14 and Table 9.2 show that the body angular rates in pitch and yaw have changed very little. Roll angle and angular rate responses are the same as Figure 9.6. The oscillations in yaw tail angle shown in Figure 9.15 still exist and are attributable to the lateral aerodynamic cross-coupling. Effects of lateral aerodynamic cross-coupling can be reduced as will be shown in Section 10.

The main contributor to the transients shown in Figures 9.1 through 9.7 was the kinematic coupling of βp into $\dot{\alpha}$.

9.4 CONCLUSIONS

1. The nonlinear 3-D performance study verifies the linear results that the CBTT autopilot is unstable when the coordination gain is unity and the roll actuator command lead is at the uncoupled system value of 110 rad/sec. In addition, it also shows that the maximum sideslip angle is determined primarily by the coordination gain. Lateral cross-coupling aerodynamics affects the magnitude of coordination gain and thereby affects maximum sideslip angle indirectly (Section 9.1).

2. When the CBTT autopilot of the circular airframe (which was determined by the linear studies of Section 7) is commanded to roll the missile through 180 degrees while at angle-of-attack, transients are caused by kinematic and inertial cross-coupling between pitch and yaw dynamics through missile roll rate. Although the time constant was only six percent larger than the desired value of 0.5 seconds (Table 9.1), the transients cause excessive slowdown in the achieved maneuver acceleration as the commanded level is approached (Figure 9.1). The response is unacceptable.

3. Kinematic and Inertial cross-coupling effects are due mainly to the kinematic coupling of βp into $\dot{\alpha}$ (Section 9.3).

4. A faster responding pitch channel, obtained by increasing the acceleration error gain, reduces the slow down effect of kinematic and inertial cross-coupling on maneuver plane acceleration and reduces maximum sideslip. Slowdown in the achieved maneuver plane acceleration is still more than desired (Section 9.2, Figure 9.8). Response is rapid until just before the time constant level when it slows down. The resulting time constant is twenty-four percent

larger than the desired value of 0.5 seconds (Table 9.1). Improvement in the response is addressed in Section 10.

Condition	τ_1	τ_2	α_{min}		α_{max}		β_{min}		β_{max}	
	(sec)	(sec)	(deg)	(sec)	(deg)	(sec)	(deg)	(sec)	(deg)	(sec)
K_A = -.0274	0.49	0.53	0.	0.	11.5	1.37	-0.46	4.29	4.47	3.47
K_A = -.0387	0.37	0.62	-.07	3.67	11.9	0.87	-0.39	4.29	3.9	3.47
*K_A = -.0387	0.37	0.52	0.	0.	11.9	0.87	-0.46	4.6	5.4	3.6

* = no inertial or kinematic cross-coupling into pitch channel
K_A = pitch autopilot acceleration error gain
τ_1 = 63 percent time constant of achieved maneuver plane acceleration due to first command
τ_2 = 63 percent time constant of achieved maneuver plane acceleration due to second command

TABLE 9.1 CBTT Performance Summary of Circular Airframe

Condition	q_{min}		q_{max}		p_{min}		p_{max}		r_{min}		r_{max}	
	deg/sec	sec	deg/sec	sec	deg/sec	sec	deg/sec	sec	deg/sec	sec	deg/sec	sec
K_A = -.0274	-9.2	3.24	20.3	0.29	-14.3	4.6	277.4	3.4	-1.6	4.56	23.9	3.3
K_A = -.0387	-14.6	3.24	28.1	0.27	-14.2	4.6	278.9	3.4	-1.46	4.55	22.3	3.3
*K_A = -0.0387	-17.8	3.26	28.1	0.27	-14.	4.6	275.6	3.4	-1.48	4.8	24.3	3.3

* = no inertial or kinematic cross-coupling into pitch channel
K_A = pitch autopilot acceleration error gain

TABLE 9.2 Range of CBTT Missile Body Angular Rates of Circular Airframe

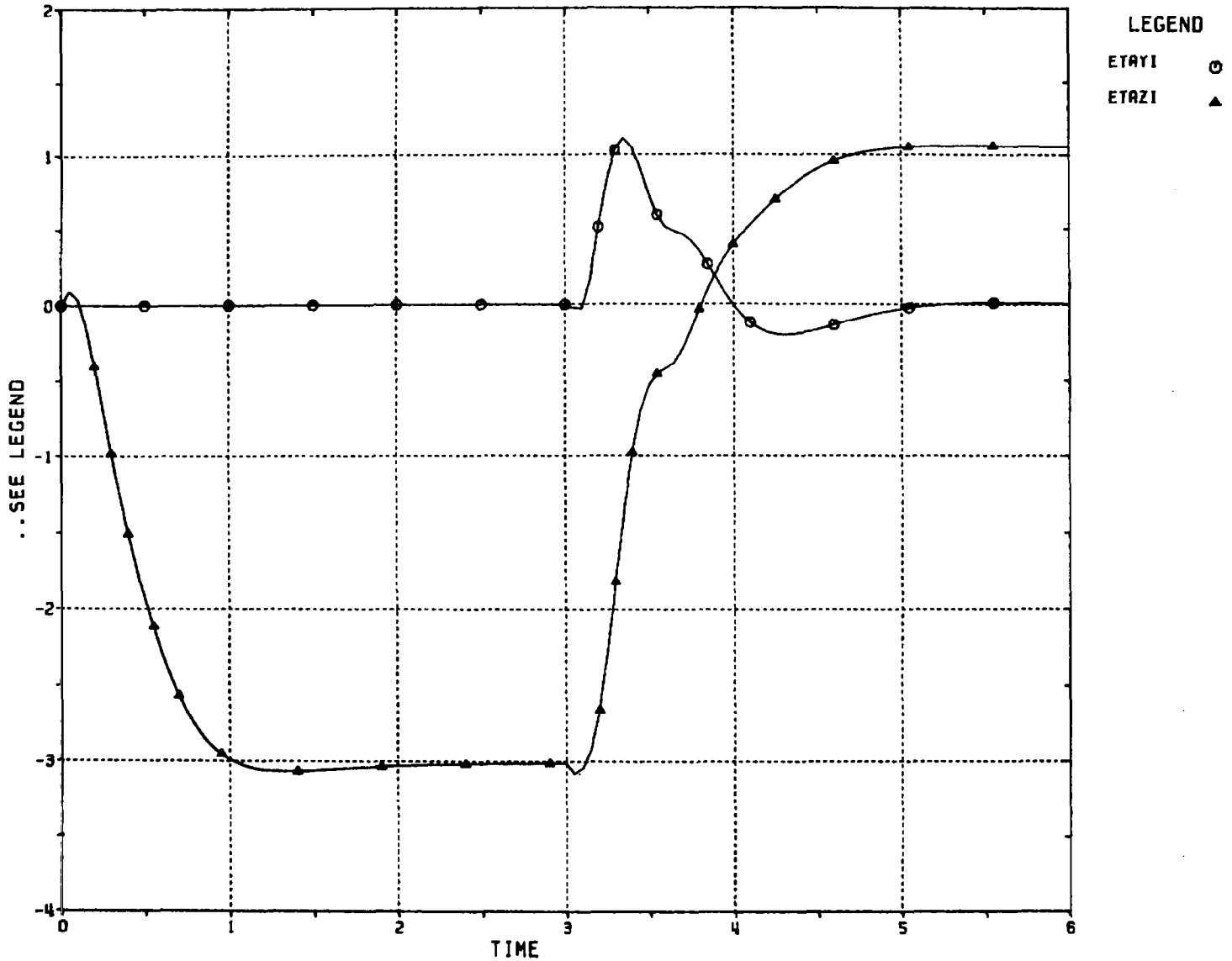

Figure 9.1 ACHIEVED INERTIAL ACCELERATIONS VS. TIME (SEC);
CBTT OF CIRCULAR AIRFRAME; 2 GEES (0^{o}, 180^{o})
ETAYI = CROSS-PLANE (GEES), ETAZI = MANEUVER PLANE (GEES)

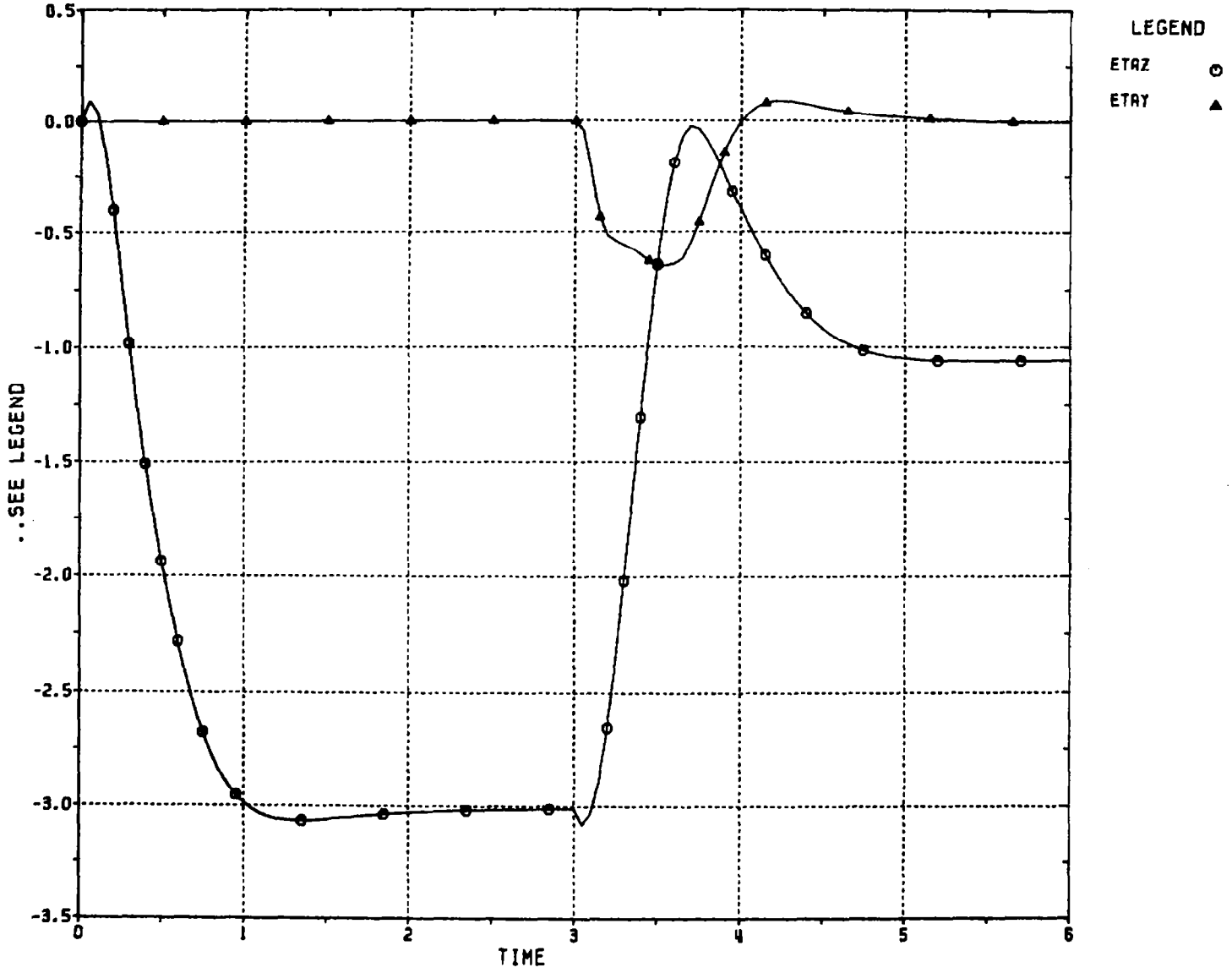

Figure 9.2 ACHIEVED BODY-FIXED ACCELERATIONS VS. TIME (SEC);
CBTT OF CIRCULAR AIRFRAME; 2 GEES (0^{o}, 180^{o})
ETAY = YAW (GEES), ETAZ = PITCH (GEES)

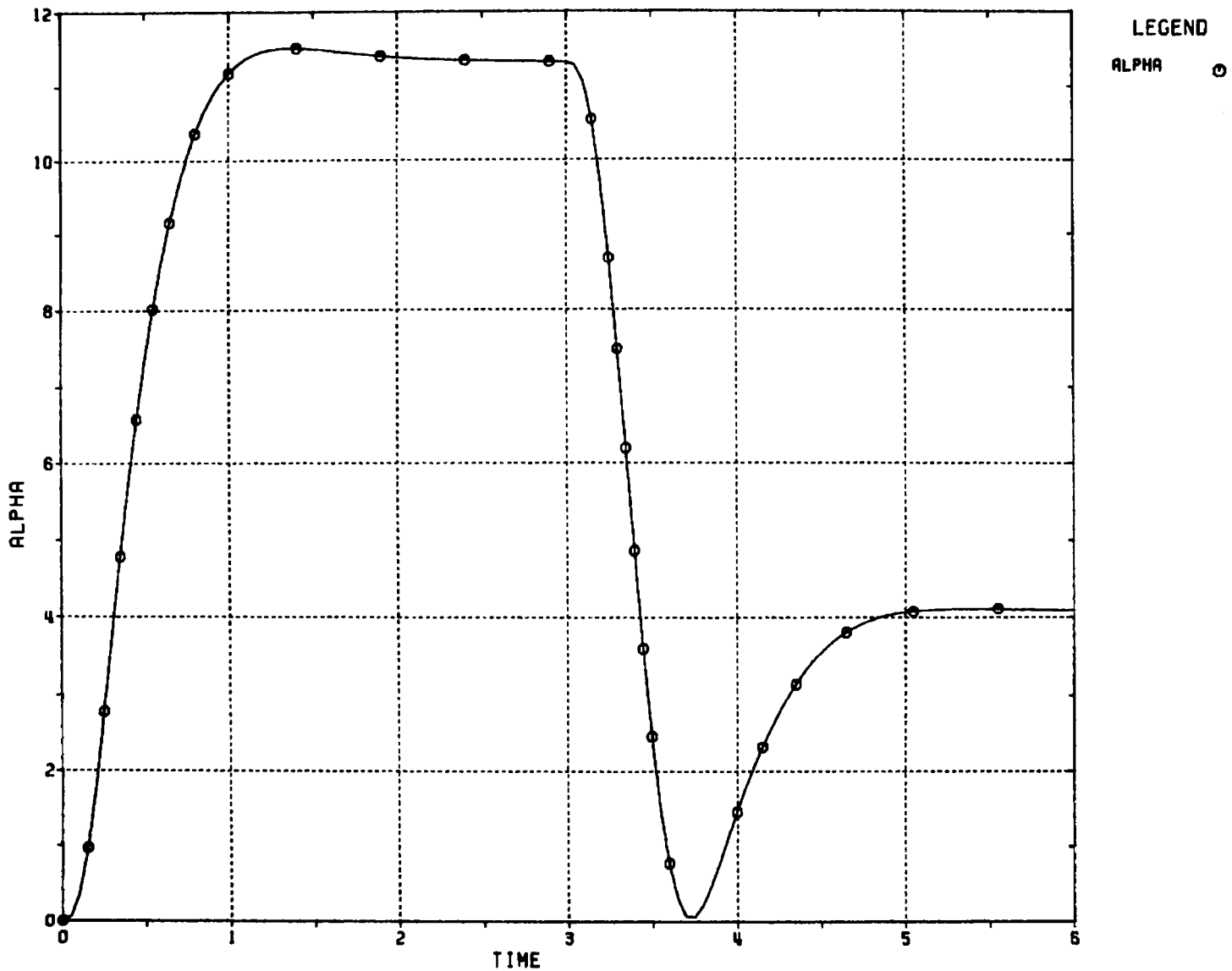

Figure 9.3 ANGLE OF ATTACK (DEG) VS. TIME (SEC);
CBTT OF CIRCULAR AIRFRAME;
2 GEES (0^{o}, 180^{o})

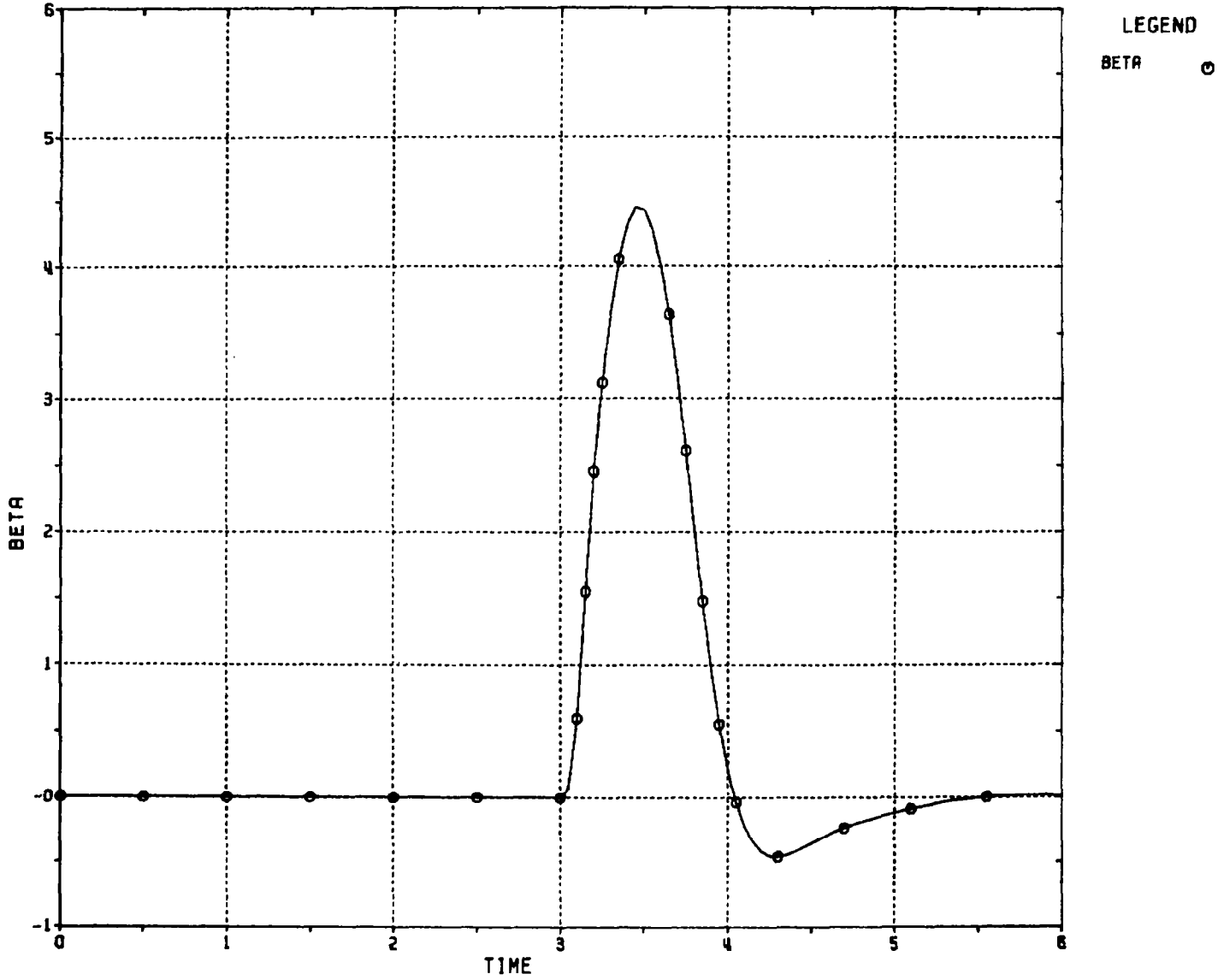

Figure 9.4 SIDESLIP ANGLE (DEG) VS. TIME (SEC);
CBTT OF CIRCULAR AIRFRAME;
2 GEES (0^{o}, 180^{o})

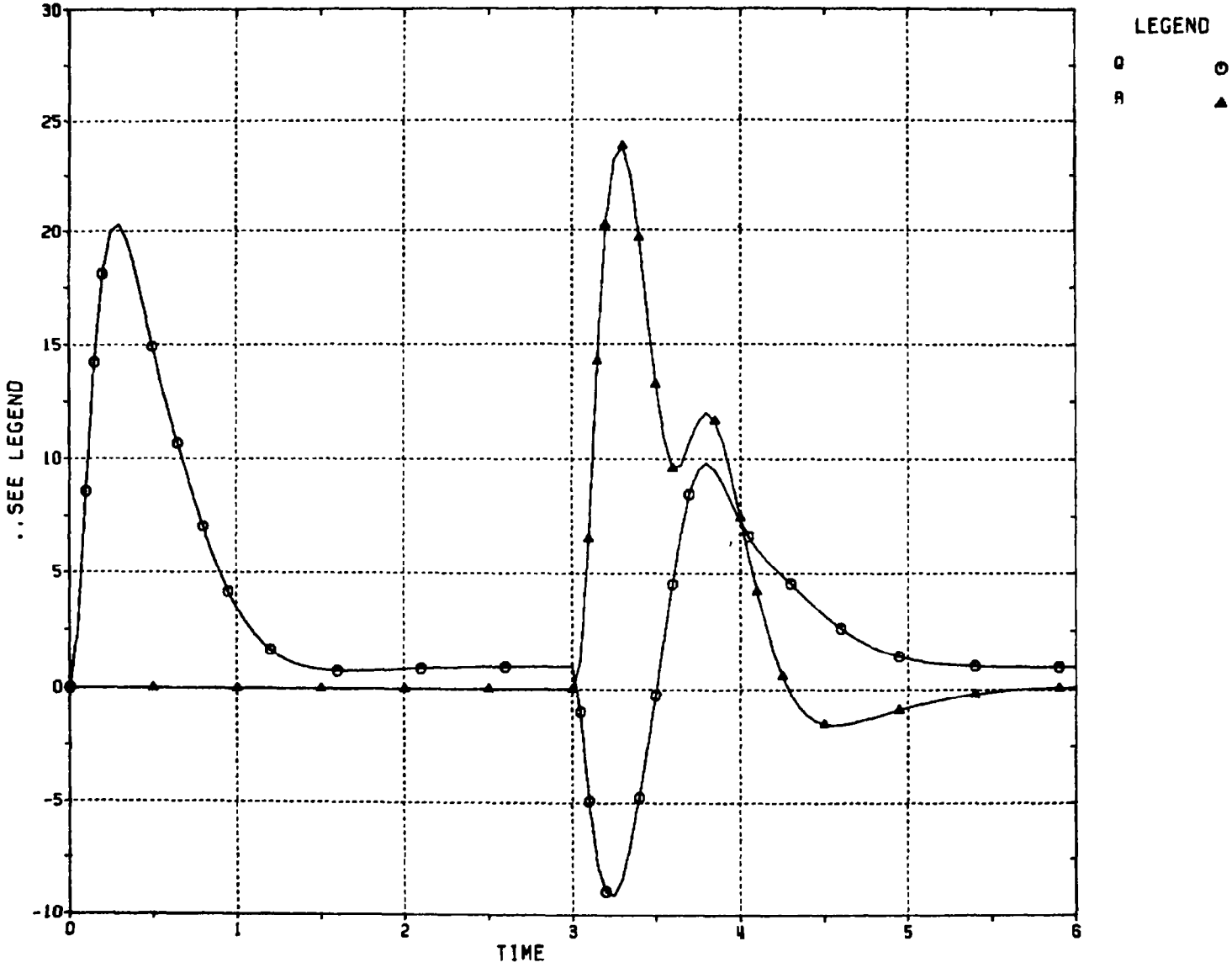

Figure 9.5 BODY ANGULAR RATES VS. TIME (SEC);
CBTT OF CIRCULAR AIRFRAME; 2 GEES (0^{o}, 180^{o})
Q = PITCH (DEG/SEC), R = YAW (DEG/SEC)

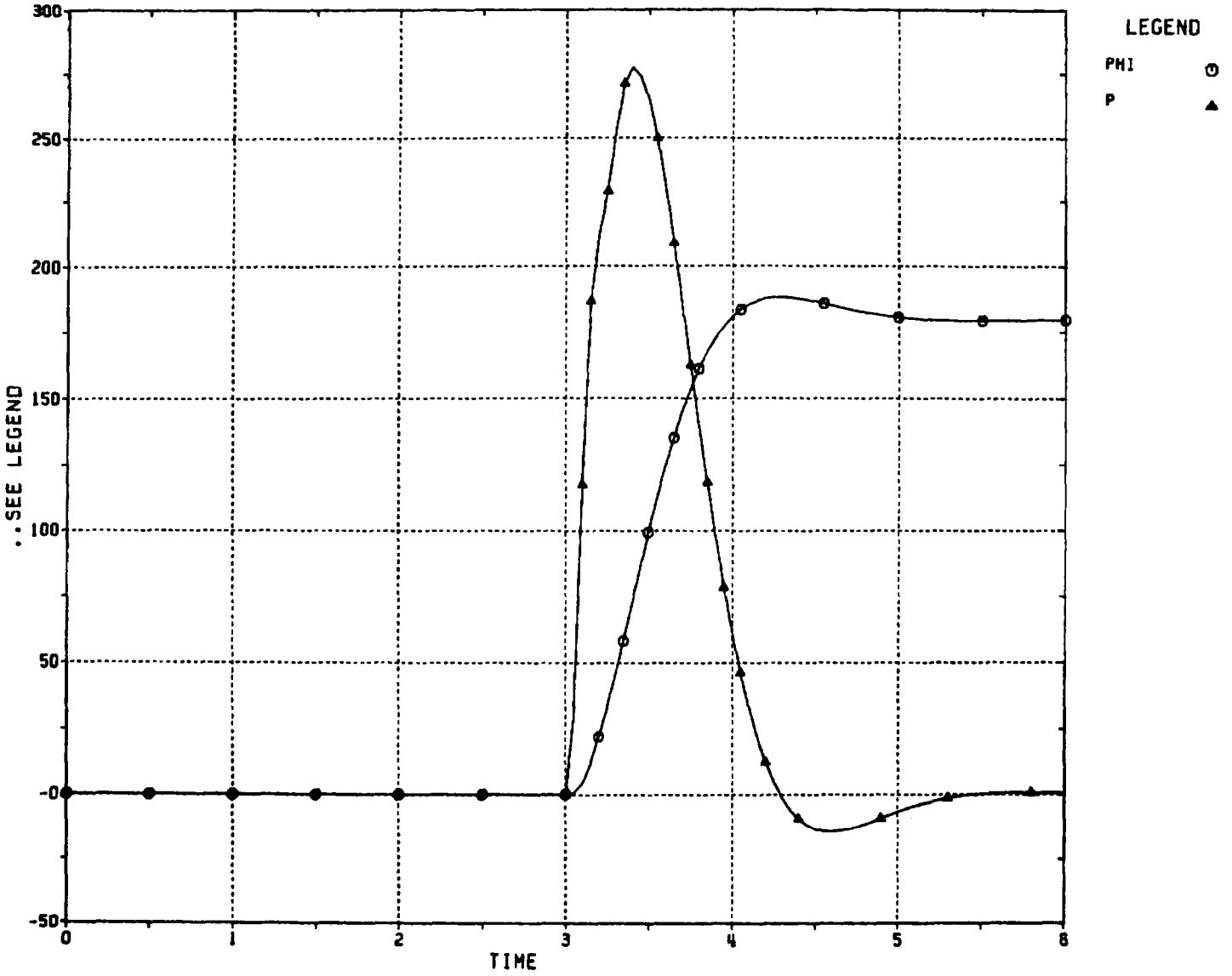

Figure 9.6 ROLL ANGLE AND ANGULAR RATE VS. TIME (SEC);
CBTT OF CIRCULAR AIRFRAME; 2 GEES (0^{o}, 180^{o})
PHI = ROLL ANGLE (DEG), P = ROLL ANGULAR RATE (DEG/SEC)

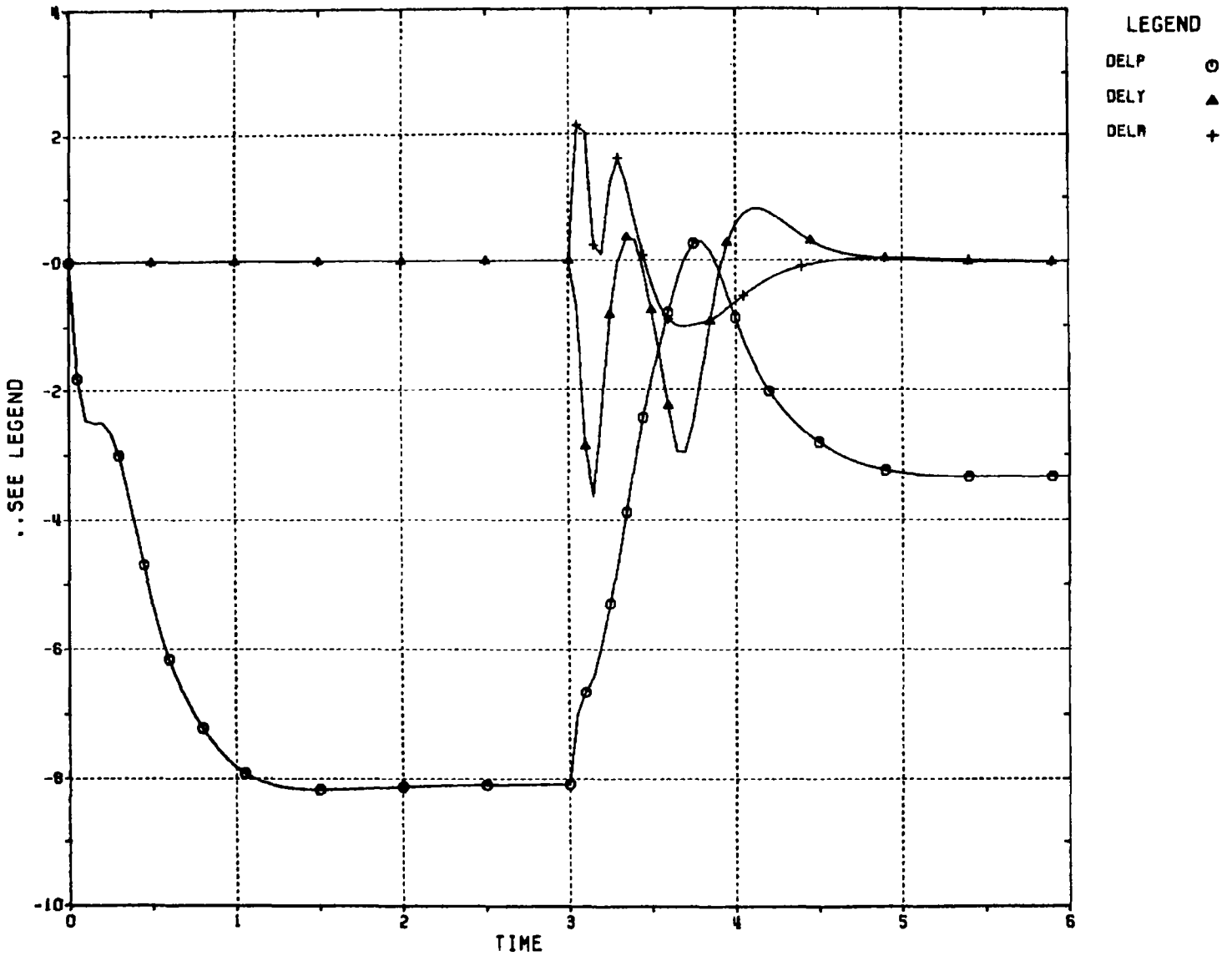

Figure 9.7 TAIL INCIDENCES VS. TIME (SEC);
CBTT OF CIRCULAR AIRFRAME; 2 GEES (0^{o}, 180^{o})
DELP = PITCH (DEG), DELY = YAW (DEG), DELR = ROLL (DEG)

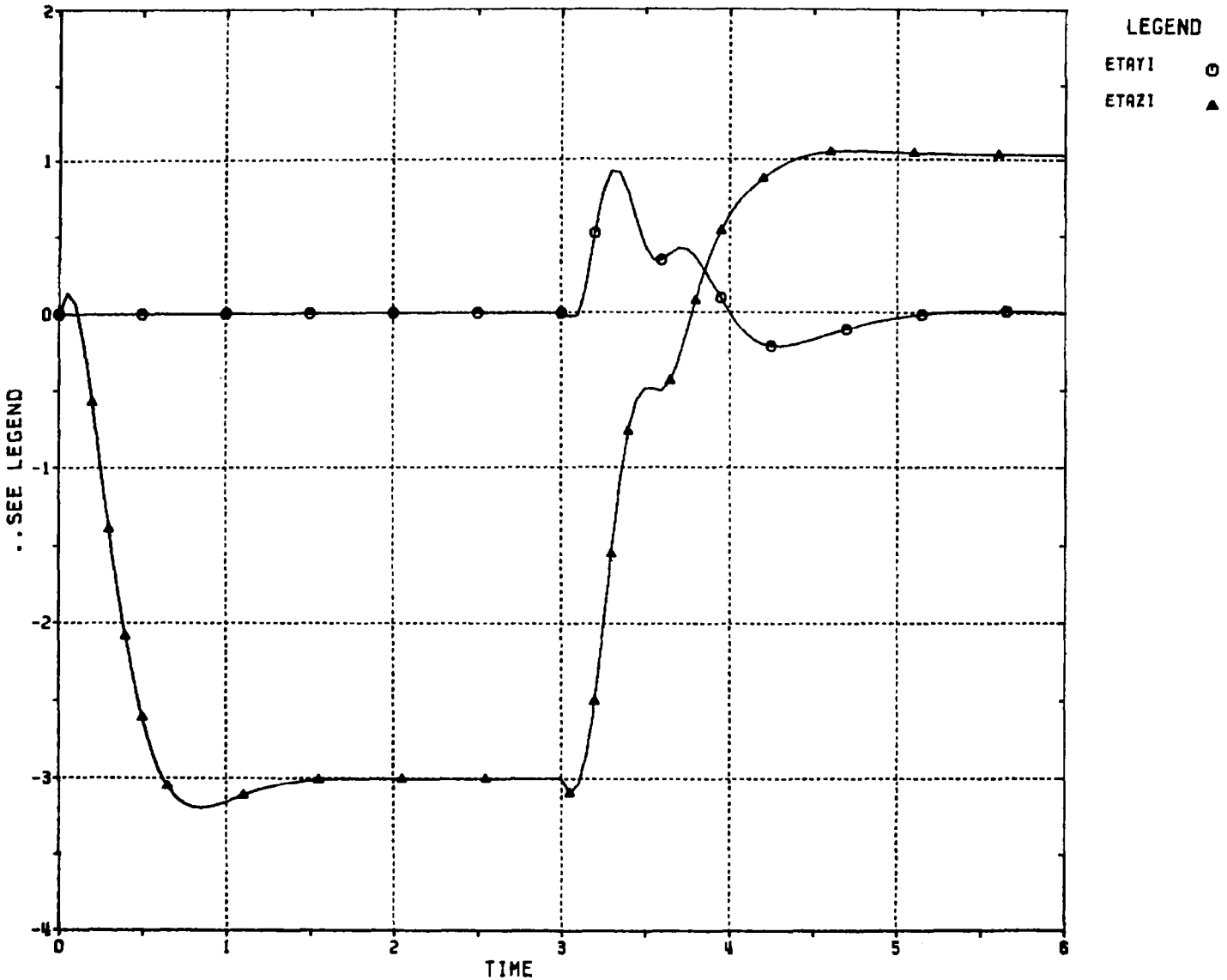

Figure 9.8 ACHIEVED INERTIAL ACCELERATIONS VS. TIME (SEC);
CBTT OF CIRCULAR AIRFRAME WITH FASTER RESPONDING PITCH CHANNEL;
2 GEES (0^{o}, 180^{o})
ETAYI = CROSS-PLANE (GEES), ETAZI = MANEUVER PLANE (GEES)

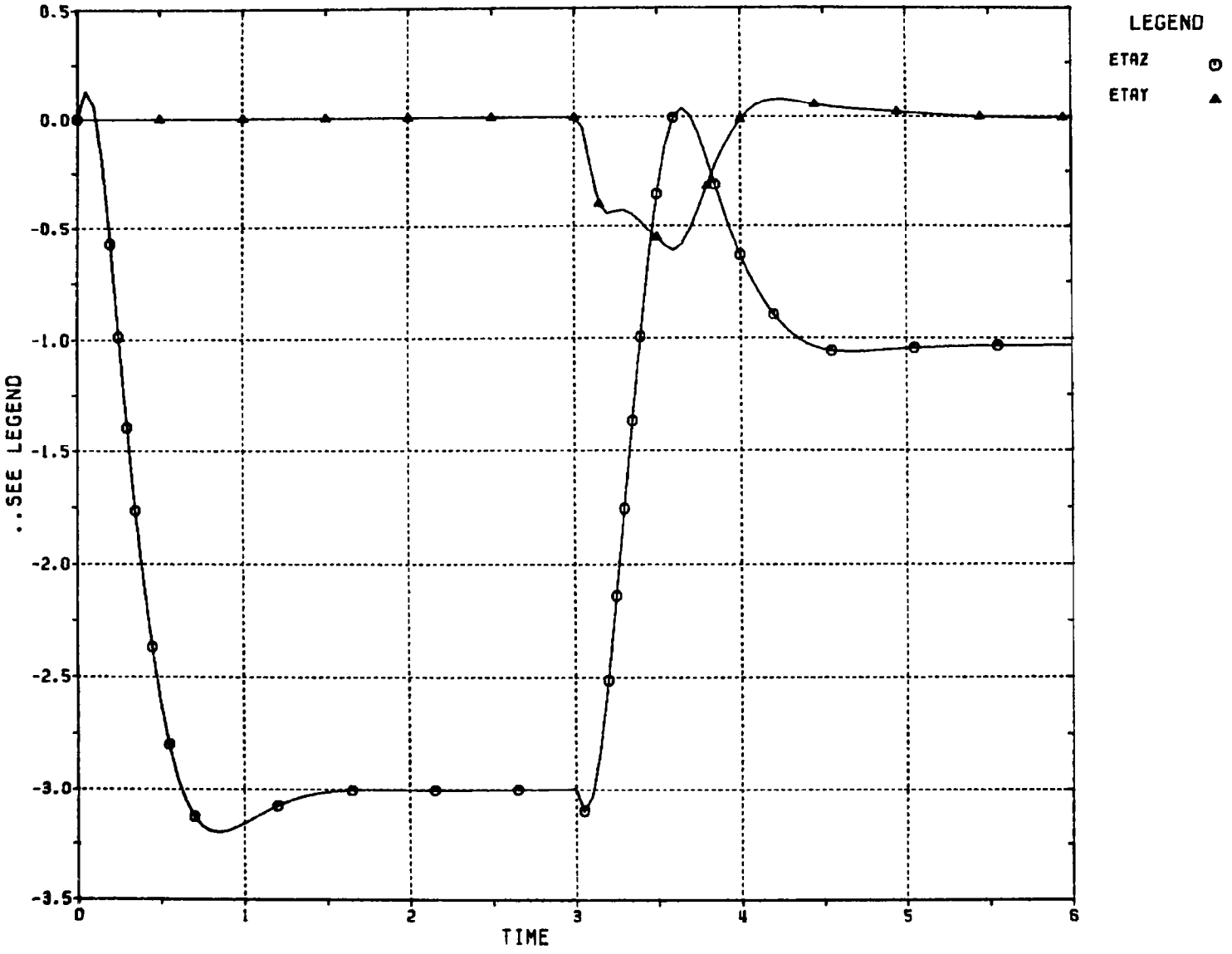

Figure 9.9 ACHIEVED BODY-FIXED ACCELERATIONS VS. TIME (SEC);
CBTT OF CIRCULAR AIRFRAME WITH FASTER RESPONDING PITCH CHANNEL;
2 GEES (0^{o}, 180^{o})
ETAY = YAW (GEES), ETAZ = PITCH (GEES)

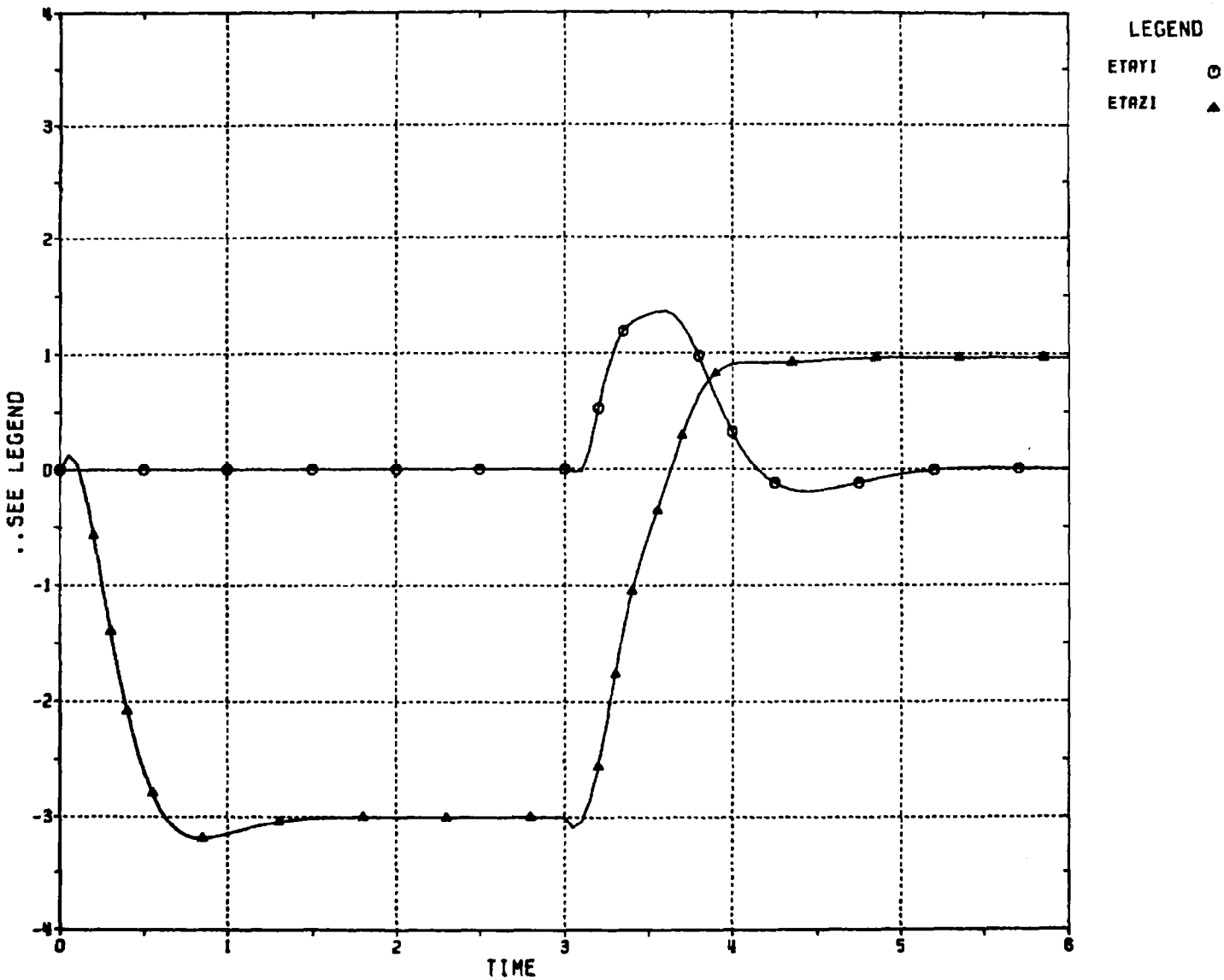

Figure 9.10 ACHIEVED INERTIAL ACCELERATIONS VS. TIME (SEC); CBTT OF CIRCULAR AIRFRAME; FASTER PITCH CHANNEL; INERTIAL AND KINEMATIC CROSS-COUPLING INTO PITCH CHANNEL REMOVED; 2 GEES (0^{o}, 180^{o})
ETAYI = CROSS-PLANE (GEES), ETAZI = MANEUVER PLANE (GEES)

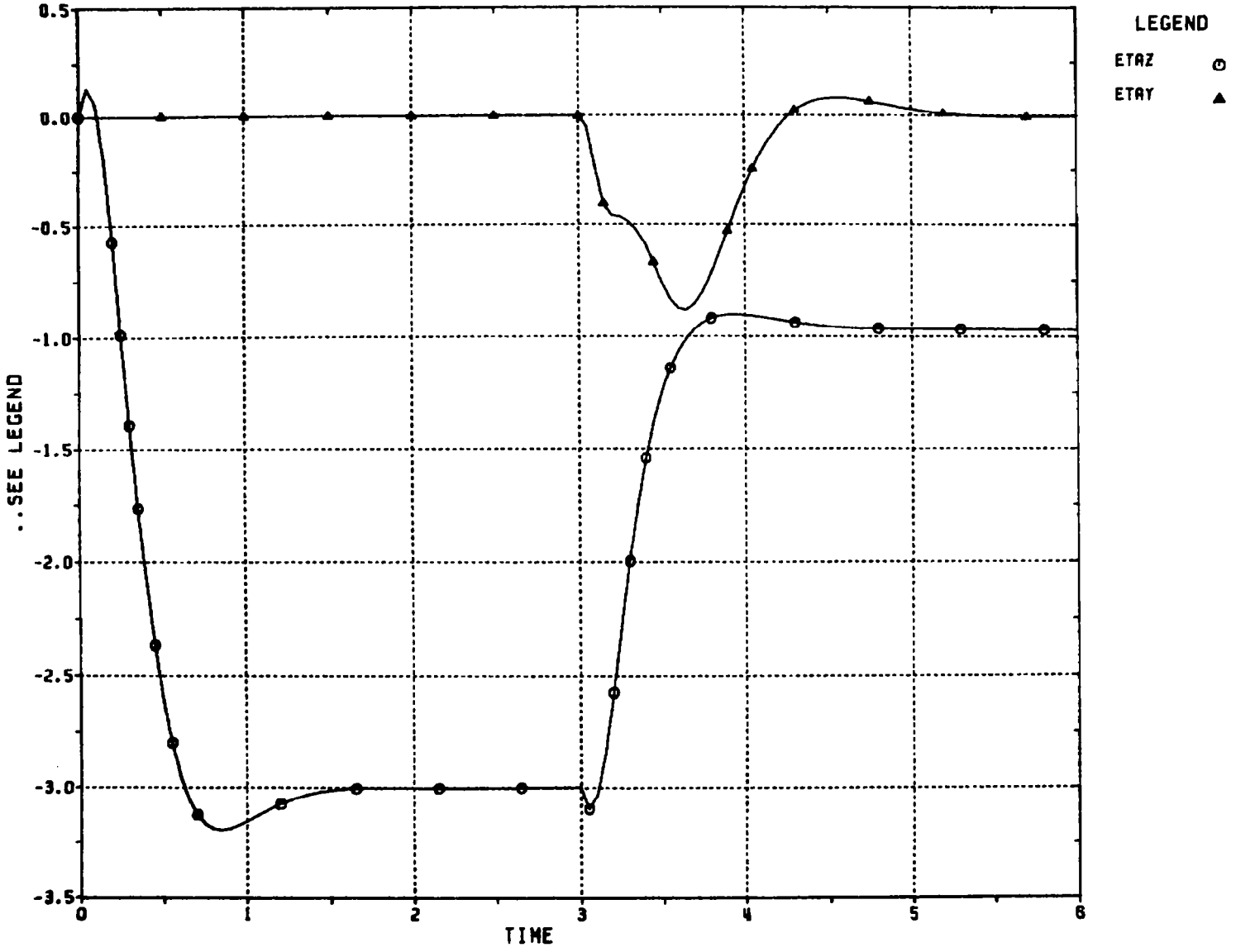

Figure 9.11 ACHIEVED BODY-FIXED ACCELERATIONS VS. TIME (SEC); CBTT OF CIRCULAR AIRFRAME; FASTER PITCH CHANNEL; INERTIAL AND KINEMATIC CROSS-COUPLING INTO PITCH CHANNEL REMOVED; 2 GEES (0°, 180°)
ETAY = YAW (GEES), ETAZ = PITCH (GEES)

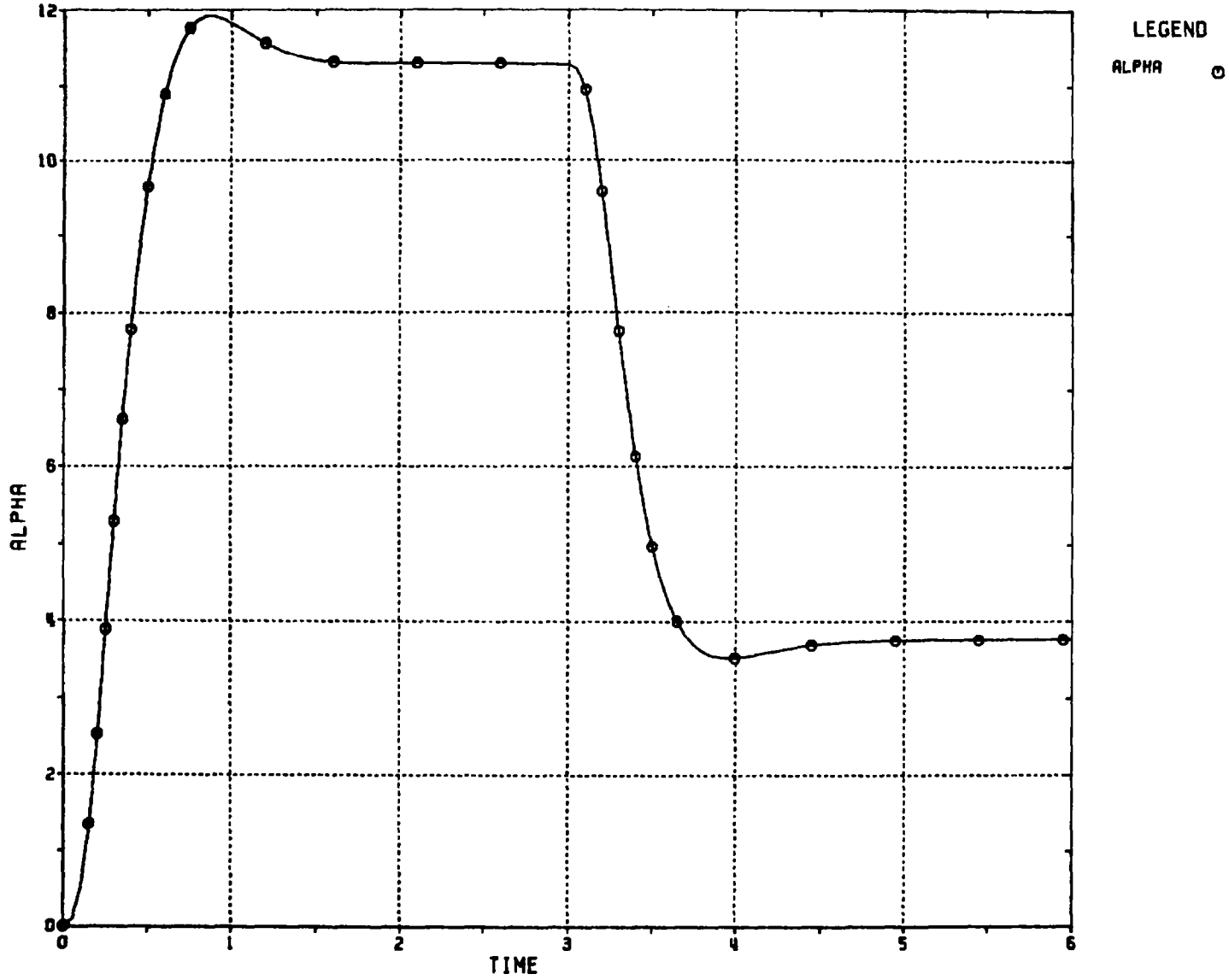

Figure 9.12 ANGLE OF ATTACK (DEG) VS. TIME (SEC); CBTT OF CIRCULAR AIRFRAME; FASTER PITCH CHANNEL; INERTIAL AND KINEMATIC CROSS-COUPLING INTO PITCH CHANNEL REMOVED; 2 GEES (0^{o}, 180^{o})

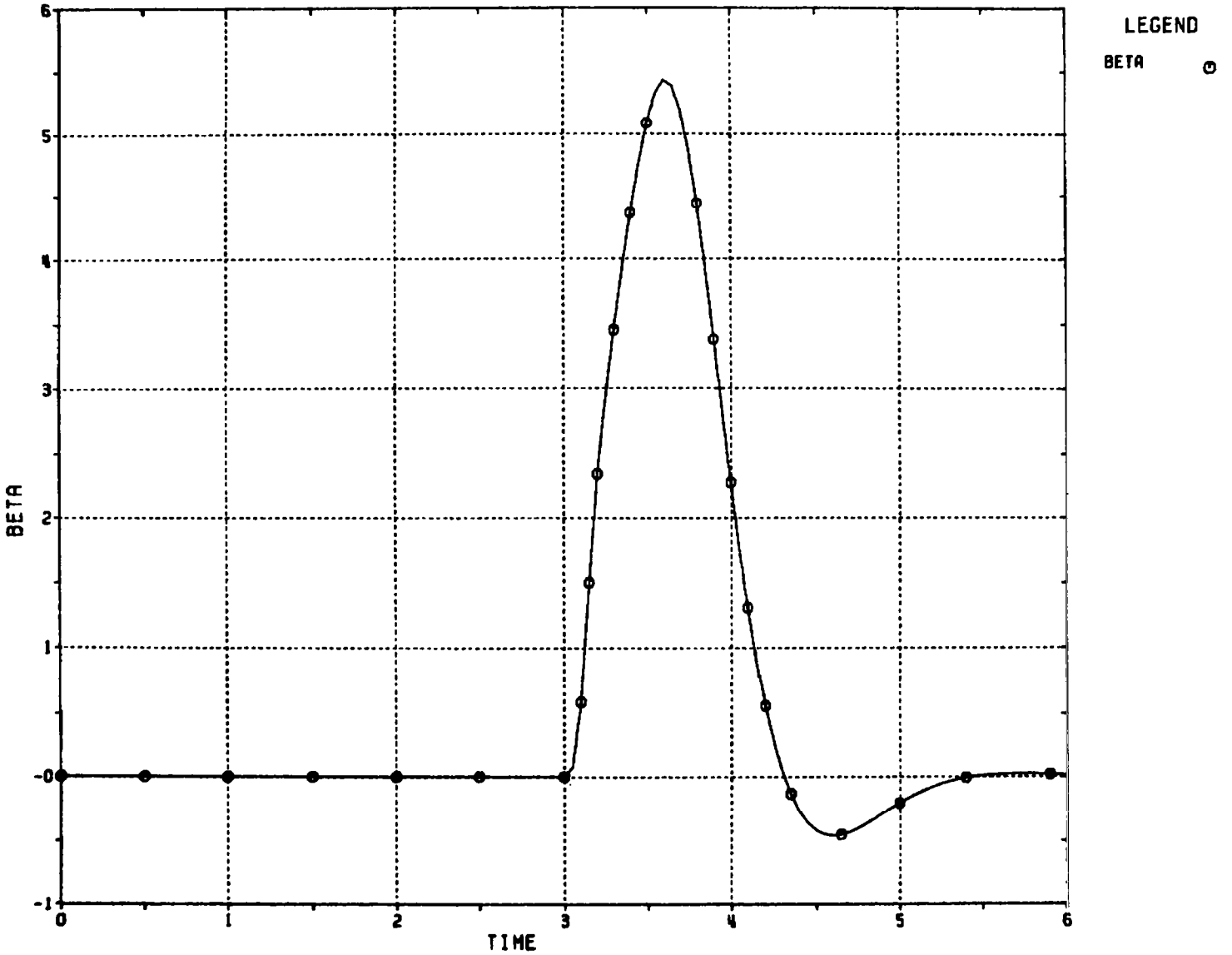

Figure 9.13 SIDESLIP ANGLE (DEG) VS. TIME (SEC); CBTT OF CIRCULAR AIRFRAME; FASTER PITCH CHANNEL; INERTIAL AND KINEMATIC CROSS-COUPLING INTO PITCH CHANNEL REMOVED; 2 GEES (0^{o}, 180^{o})

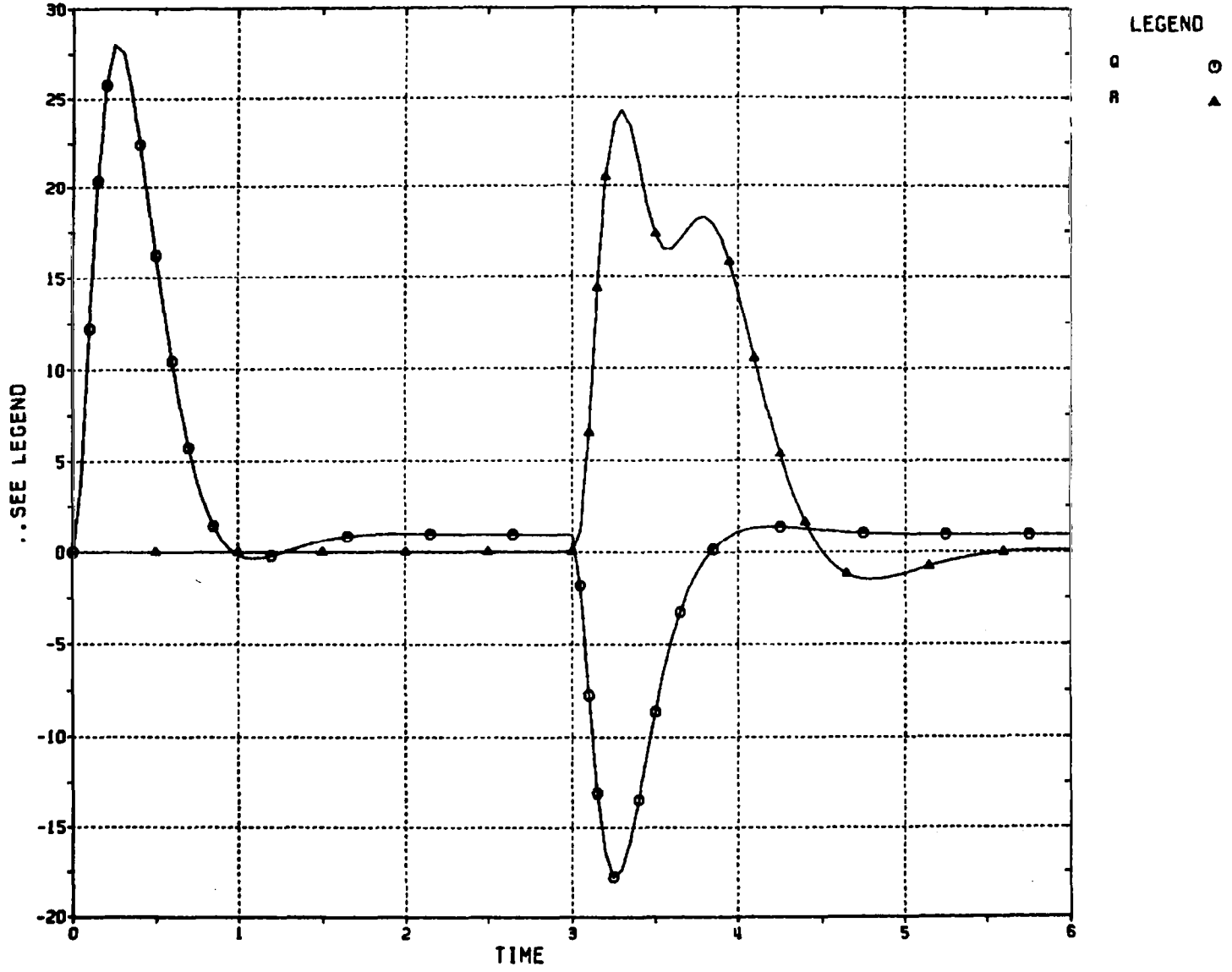

Figure 9.14 BODY ANGULAR RATES VS. TIME (SEC); CBTT OF CIRCULAR AIRFRAME; FASTER PITCH CHANNEL; INERTIAL AND KINEMATIC CROSS-COUPLING INTO PITCH CHANNEL REMOVED; 2 GEES (0^{o}, 180^{o})

Q = PITCH (DEG/SEC), R = YAW (DEG/SEC)

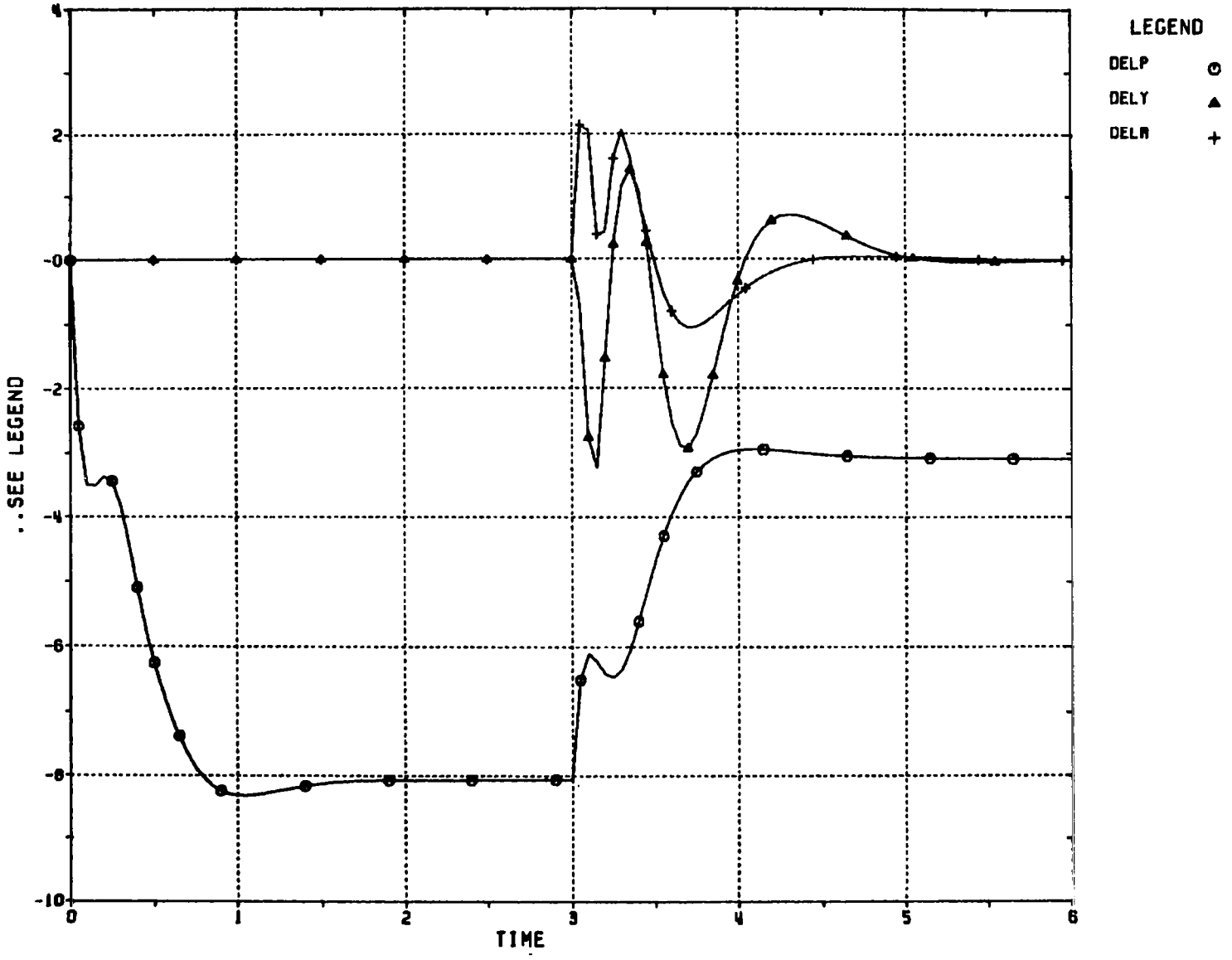

Figure 9.15 TAIL INCIDENCES VS. TIME (SEC);
CBTT OF CIRCULAR AIRFRAME; FASTER PITCH CHANNEL;
INERTIAL AND KINEMATIC CROSS-COUPLING INTO PITCH
CHANNEL REMOVED; 2 GEES (0^{o}, 180^{o})
DELP = PITCH (DEG), DELY = YAW (DEG), DELR = ROLL (DEG)

10. IMPROVING COORDINATION AND MANEUVER PLANE ACCELERATION RESPONSE OF CIRCULAR AIRFRAME

The CBTT autopilots of the elliptical airframe in Section 8 and the circular airframe in Section 9 were designed with the same bandwidths in the uncoupled channels (see Appendices D, E, and F) and the same coordination technique. However, the relative stability of the coordination command branch was lower for the circular airframe. In addition, inertial and kinematic cross-coupling caused the circular airframe to have a slower than desired maneuver plane acceleration response. If the coordination of the circular airframe can be improved, it will also reduce the inertial and kinematic cross-coupling effect.

The coordination of the circular airframe can be improved provided the coordination gain K_{YP} can be increased from 0.458 (as used in Table 7.2) to 1.0. Since this increase would lower the relative stability of the coordination branch, methods must be found for improving its stability. Section 10.1 identifies the critical aerodynamic cross-coupling which limits relative stability in the coordination branch. Methods for reducing the effect of the critical cross-coupling are addressed in Sections 10.2 and 10.3. The method in Section 10.2 modifies the roll channel whereas the method in Section 10.3 introduces autopilot cross-coupling between roll and yaw channels. Section 10.4 discusses whether the effects of coordination and inertial and kinematic cross-coupling change at high angles-of-attack.

10.1 Identifying the Problem

Figure 10.1 shows the cross-coupling between the roll and yaw channels. The autopilot coordination command branch is shown in dashed lines. Figure 10.1 shows that the only coupling which forms a feedback loop through the coordination branch and therefore affects stability are $C_{\ell_{\delta_Y}}$ and C_{ℓ_β}. The critical coupling path was identified by observing the

change in the frequency response of the coordination branch while removing aerodynamic cross-coupling. The only aerodynamic coupling which influences the stability is $C_{\ell_{\delta_Y}}$.

10.2 Increasing Synthetic Roll Control Effectiveness

The stability in the coordination branch of the autopilot can be improved by reducing the effect of $C_{\ell_{\delta_Y}}$ on missile roll angular acceleration. Reducing the effect of $C_{\ell_{\delta_Y}}$ on the roll channel, shown in Figure 10.1, will in turn reduce the effect of the critical feedback loop which determines the stability of the coordination command branch. Roll acceleration is as follows:

$$\dot{p} = \frac{\bar{q}Sd}{I_{xx}} \left(C_{\ell_{\delta_R}} \delta_R + C_{\ell_{\delta_Y}} \delta_Y + C_{\ell_\beta} \beta\right)$$

or

$$\dot{p} = \frac{\bar{q}Sd}{I_{xx}} C_{\ell_{\delta_R}} \left(\delta_R + \frac{C_{\ell_{\delta_Y}}}{C_{\ell_{\delta_R}}} \delta_Y + \frac{C_{\ell_\beta}}{C_{\ell_{\delta_R}}} \beta\right) . \qquad (10\text{-}1)$$

The relative effect on $\dot{p}$ of δ_Y compared with δ_R can be decreased by decreasing the ratio $C_{\ell_{\delta_Y}}/C_{\ell_{\delta_R}}$.

The elliptical airframe has more stability in the coordination branch because of an increase in the synthetic roll control effectiveness which is defined as,

$$\bar{C}_{\ell_{\delta_R}} = K\, C_{\ell_{\delta_R}} \qquad (10\text{-}2)$$

where $K = 4.17$ for elliptical airframe
$K = 1.0$ for circular airframe.

where K is the autopilot frequency independent gain in series with the roll actuator shown in Figure 7.2. The uncoupled roll autopilot for the elliptical airframe was designed in Appendix F by using the same control law as for the circular airframe except for the addition of frequency independent gain K in series with the roll actuator. This increase in gain K was added to balance out the decrease in the ratio of $C_{\ell_{\delta_R}}/I_{xx}$. Since both changes are in series with each other, there is no change in high frequency attenuation or control law. When changing from the circular to the elliptical airframe, $C_{\ell_{\delta_R}}$ decreased by a factor of 1.52 at α = 10 degrees and I_{xx} increased by a factor of 2.75. Therefore, the roll acceleration becomes,

$$\dot{p} = \frac{\bar{q}Sd}{I_{xx}} \bar{C}_{\ell_{\delta_R}} \left(\delta_R + \frac{C_{\ell_{\delta_Y}}}{\bar{C}_{\ell_{\delta_R}}} \delta_Y + \frac{C_{\ell_\beta}}{\bar{C}_{\ell_{\delta_R}}} \beta\right) \qquad (10\text{-}3)$$

The ratio of $C_{\ell_{\delta_Y}}/C_{\ell_{\delta_R}}$ decreases by only a factor of 1.05 when changing from the circular to the elliptical at α = 10 deg. However, there is a 1/K gain reduction from δ_Y to $\dot{p}$ and no change in the gain from δ_R to $\dot{p}$ due to the autopilot gain K. However, the penalty for forcing a missile with a larger roll inertia and lower roll control effectiveness to maintain the same speed of response is larger roll tail angular motion (i.e., factor of K larger). This may require a slower roll response at very low dynamic pressures to prevent exceeding the actuator command limits, which could in turn cause a nonlinear stability problem.

A linear stability study was done to show that the increased synthetic roll control effectiveness and missile roll inertia are the reasons for the larger stability in the coordination branch of the elliptical airframe. This was done by changing $C_{\ell_{\delta_Y}}$, $\bar{C}_{\ell_{\delta_R}}$ and I_{xx} in the circular airframe dynamic

model to be the same as the elliptical airframe. This may not be done physically without difficulty, but it was done here analytically to isolate these parameters as the critical ones for determining the relative stability in the coordination branch. Once the critical parameters are shown to improve stability and it is verified on the nonlinear 3-D simulation, practical methods for producing the same effects with the circular airframe are addressed. The roll inertia of the circular airframe was increased by a factor of 2.75 and the $C_{\ell_{\delta_R}}$ and $C_{\ell_{\delta_Y}}$ of the circular airframe were changed to be the same as the elliptical parameters at α = 10 deg . An autopilot gain of 4.17 was inserted in series with the roll actuator command. In addition, the coordination gain was increased from 0.458 to the desired value of 1.0. The linear autopilot model of Section 7.0 was used to compare the resulting autopilot stability with that of the elliptical airframe. Table 10.1 shows that the phase margins in the roll channel of the modified circular are now equivalent to the corresponding ones for the elliptical airframe. The roll actuator command gain margin for the modified circular does not have the decreasing gain margin of the elliptical which is an improvement. Table 10.2 shows that the modified circular has a decreasing gain margin in the yaw actuator command branch which is a potential nonlinear problem if limits are exceeded. All other margins have improved over the corresponding ones for the elliptical airframe. The attenuation at 100 rps for the yaw actuator command of the modified circular is still larger than the required 15 dB.

The nonlinear 3-D simulation of Section 9 was modified by increasing the roll inertia of the circular airframe by a factor of 4.17 and setting the dc gain in series with the roll actuator to 4.17. The aerodynamics of the circular airframe was not modified. In addition, the coordination gain of 1.0 was used and also the faster responding uncoupled pitch channel (K_A = -.0387). The results are shown in Figures 10.2 through 10.8, where all cross-coupling is present. The maneuver plane acceleration response of the modified circular (Figure 10.2) is more like the one for the elliptical (Figure 8.1). The same is true for the body-fixed acceleration (Figures 10.3 and 8.2). The slowness in the maneuver plane acceleration, of the circular airframe before the changes (Figure 9.8), has been removed and a 13.1 percent undershoot now occurs. The time constant of the maneuver plane acceleration response, during the second acceleration command (τ_2 in Table 10.3) when the

missile rolls through 180 degrees, is only 2.7 percent slower than that of the first command which required no roll motion. The large overshoot in the body-fixed achieved pitch acceleration at 3.8 sec. due to inertial and kinematic cross-coupling has been reduced (Figures 10.3 and 9.9) as well as the magnitude of body-fixed yaw acceleration (Figures 10.3 and 9.9) which is due to the improved sideslip response shown in Figure 10.5. The sideslip behavior of the two airframes is nearly identical even though the elliptical airframe is stable in yaw and the circular airframe is unstable (Figures 10.5 and 8.4). Although coordination is more difficult for the circular airframe due to larger angles-of-attack for the same maneuver, the yaw incidence is not appreciably different from that of the elliptical (Figures 10.8 and 8.7). It is not clear whether it is preferable to try to reduce yaw control requirements by having yaw stability or to strive for neutral yaw stability and greater control effectiveness. Further studies at higher angles-of-attack and lower dynamic pressure may resolve this issue. Angle-of-attack undershoot at 3.8 sec. due to kinematic and inertial cross-coupling (Figure 10.4) has been reduced (Figure 9.3). Figure 10.6 shows increased yaw angular rates over those of Figure 9.5 due to the improved coordination. The yaw rates are also higher than those of the elliptical in Figure 8.5, due to the higher angles-of-attack of the circular airframe. Pitch rates are higher than for the elliptical because the uncoupled pitch channel is faster. Roll angles and rates (Figures 10.7 and 9.6) remain the same. Figure 10.8 shows that the roll tail incidences are approximately as large as they were for the elliptical airframe in Figure 8.7 as might be expected since the parameters influencing roll were modified to match the elliptical. Yaw tail incidences are larger than for the elliptical due to higher coordination commands. Pitch tail incidences are larger because the circular airframe is more stable.

Therefore, it has been shown that the reason for the improved stability in the coordination branch of the elliptical is due to the increased synthetic roll control effectiveness which balanced out the increased missile roll inertia. The reduced effect of kinematic and inertial cross-coupling is attributed to the reduced sideslip angle and to the faster pitch channel.

Figures 10.9 and 10.10 show that removal of the kinematic and inertial cross-coupling into the pitch channel removes the transients. Sideslip angles changed a small amount.

The increased magnitude of $\bar{C}_{\ell_{\delta_R}}$ via an increase in K would alone, as shown in (10-3), reduce the effect of $C_{\ell_{\delta_Y}}$. However, an increase of K alone would also increase the gain from δ_R to $\dot{p}$ and the roll control law would no longer be valid. The increase in I_{xx} of the elliptical airframe is the same as the increase in $\bar{C}_{\ell_{\delta_R}}$ and as a result the gain from δ_R to $\dot{p}$ remained the same while the effect of $C_{\ell_{\delta_Y}}$ was decreased.

The synthetic roll control effectiveness can be increased for the circular airframe studied in this report, if the roll control law is modified. This will probably require additional high frequency filters to maintain high frequency attenuation in the actuator command branch for actuator and elastic mode frequencies. The redesign problem for the autopilot would be relieved and the roll tail incidence decreased if the increase in $\bar{C}_{\ell_{\delta_R}}$ is not as large as it was for the elliptical (i.e., 4.17). Therefore, the roll inertia in the dynamic model of the circular airframe was increased by a factor of 2 and the synthetic roll control effectiveness also was increased by the same factor [i.e., K = 2 in (10-2)]. The result is shown in Figures 10.11 through 10.17, where all circular airframe cross-coupling is present. The increased effect of lateral aerodynamic cross-coupling has resulted in slight changes in accelerations and sideslip angles, but the major effect is shown by comparing Figures 10.17 and 10.8. Roll tail angle motion has decreased considerably due to the lower roll inertia. There has also been a slight reduction in inertial and kinematic cross coupling effect due to the increased effect of lateral cross-coupling aerodynamics. Therefore, adjustment of the smallest K to provide sufficient coordination branch stability should not require a difficult autopilot redesign to satisfy requirements.

10.3 Autopilot Cross-Coupling

Section 10.1 has shown that the critical aerodynamic cross-coupling is $C_{\ell_{\delta_Y}}$. Section 10.2 has shown an in-channel method for decreasing the effect of $C_{\ell_{\delta_Y}}$. This section will now effectively change the characteristics of $C_{\ell_{\delta_Y}}$ via autopilot cross-coupling.

Assume the circular airframe is at a constant angle-of-attack and a positive sideslip angle occurs resulting in a negative yawing moment. Since $C_{n_{\delta_Y}}$ is negative, a negative δ_Y will be required to provide the positive restoring yawing moment. However, a negative δ_Y will result in a positive rolling moment, because $C_{\ell_{\delta_Y}}$ is negative, or a destabilizing condition which drives the missile away from the desired maneuver plane. Therefore, it is desirable to change the polarity of $C_{\ell_{\delta_Y}}$. Nyquist's stability criterion applied to the open $C_{\ell_{\delta_Y}}$ branch shows that the linear CBTT autopilot of the circular airframe is stable when the polarity of $C_{\ell_{\delta_Y}}$ is changed. The gain margin is greater than 20 dB at a frequency exceeding 100 rad/sec. Sections 8 and 9 have shown that the aerodynamic cross-coupling has only a minor effect on the response when changing desired maneuver plane. Thus a change in the polarity of $C_{\ell_{\delta_Y}}$ would have beneficial effect on stability without affecting response.

Figure 10.18 shows that by adding an autopilot cross-coupling branch from the yaw to roll actuator, a branch is placed in parallel with $C_{\ell_{\delta_Y}}$. The combined effect of both branches is to change the polarity of $C_{\ell_{\delta_Y}}$. Because the effects of $C_{\ell_{\delta_Y}}$ are not being nulled, the results should not be sensitive

to the exact knowledge of $C_{\ell_{\delta_Y}}$ and $C_{\ell_{\delta_R}}$. The new autopilot cross-coupling branch shown in Figure 10.18 is also creating a new feedback path through the roll channel to missile roll rate and through the autopilot coordination branch back to the yaw channel and then back to the new autopilot branch. This may have a detrimental effect on stability and coordination. For this investigation, the 3-D simulation was used to determine whether there were any obvious problems.

The autopilot cross-coupling was added to the nonlinear 3-D simulation with K_{YP} (the coordination gain) equal to unity and with the faster responding pitch autopilot (K_A = -.0387). The performance is summarized and compared with that of the modified circular airframe of Section 10.2 in Tables 10.3 and 10.4, which show that the time constants for maneuver plane acceleration and sideslip control are essentially the same. The autopilot cross-coupling has resulted in higher roll and yaw rates. The time responses are shown in Figures 10.19 through 10.25 are generally satisfactory. Figure 10.25 shows that the maximum roll tail incidence is less than 2 degrees. Maximum yaw tail incidence is 7.5 degrees.

10.4 Inertial and Kinematic Cross-Coupling Effects at Large Acceleration Levels

Guidance commands of 4 gees (0^o, 180^o) were applied to the CBTT autopilot of the circular airframe with the lateral aerodynamic cross-coupling removed to determine whether inertial and kinematic cross-coupling effects increase with acceleration level. Section 8.5 showed that the coupling effects do not become more severe for the CBTT autopilot of the elliptical airframe.

Figures 10.26 through 10.32 show the results when applying a 4 gee (0^o, 180^o) command with no aerodynamic cross-coupling and with coordination gain K_{YP} = 1.0. Body-fixed pitch acceleration (Figure 10.27) shows evidence of slowdown and overshoot after the second command due to inertial and kinematic cross-coupling. However, missile roll angle (Figure 10.31) removes the slowdown from the achieved maneuver plane acceleration (Figure 10.26). Overshoot and undershoot transients in the maneuver plane acceleration have not increased with larger acceleration commands and are within conservative requirements of ten percent. Sideslip angles (Figure 10-29) are well within 5 degrees. Roll angles and angular rates have not changed as shown in Figure 10-31 and the inertial and kinematic cross-coupling is evident in the pitch angular rate (Figure 10.30). Figure 10-32 shows missile roll tail incidences are less than 3 degrees and yaw tail incidences reach 12 degrees maximum. Therefore, the missile response is good with no apparent problems provided the effect of the aerodynamic cross-coupling is negligible. A summary of the performance in Table 10.5 shows that the maneuver plane acceleration time constants are much faster than the required 0.5 seconds (i.e., 26 percent faster for the first command and 22 percent faster for the second command). Table 10.5 also summarizes the ranges of missile body angular rates.

10.5 Conclusion

1. The critical aerodynamic cross-coupling is $C_{\ell_{\delta_Y}}$ for the stability in the autopilot coordination branch (Section 10.1, Figure 10.1)

2. $C_{\ell_{\delta_Y}}$ has less effect in the CBTT autopilot of the elliptical airframe than in the CBTT autopilot of the circular airframe, because higher synthetic roll control effectiveness $\bar{C}_{\ell_{\delta_R}}$ is

balanced by reduced actual roll control effectiveness $C_{\ell_{\delta_R}}$ and larger roll inertia (Section 10.2, Tables 10.1 and 10.2, Tables 10.3 and 10.4 with K = 4.17, Figures 10.2 through 10.8).

3. The CBTT autopilot for the circular airframe requires additional autopilot complexity to minimize the effects of $C_{\ell_{\delta_Y}}$ for the desired range of angles-of-attack. This may be accomplished by modifying the roll control law (Section 10.2, Tables 10.3 and 10.4 with K = 2, Figures 10.11 through 10.17) or via autopilot cross-coupling (Section 10.2, Tables 10.3 and 10.4, Figures 10.19 through 10.25).

4. Inertial and kinematic cross-coupling does not become more severe with higher acceleration levels (Section 10.4, Figures 10.26 through 10.32) provided the autopilot can be made to minimize the effects of the aerodynamic cross-coupling terms which tend to destabilize the system. Overshoots and undershoots in the maneuver plane acceleration response may exceed a ten percent requirement at low acceleration levels and be within ten percent at high acceleration levels. Therefore, overshoot and undershoot requirements for the larger transient effects in maneuver plane acceleration at lower acceleration levels must be determined in guidance level studies. Requirements for the smaller transient effects at high acceleration levels will be determined by structural limitations and typically vary from 10 to 20 percent overshoot.

5. Reducing inertial and kinematic cross-coupling into the pitch channel results in desirable CBTT performance (Figures 10.9 and 10.10).

6. The yaw aerodynamics of the elliptical airframe is not sufficiently stable to influence significantly the sideslip control for the guidance maneuver requiring a 180 degrees roll angle excursion (Section 10.2, Figures 8.4, 8.7, 10.5, and 10.8). The issue of stability vs neutral stability to reduce yaw incidence may be resolved by studying higher angle-of-attack and lower dynamic pressures.

Airframe	Branch	Gain (dB)	Margin (rad/sec)	Phase (deg)	Margin (rad/sec)	Attenuation at 100 rps (dB)
Modified Circular	Roll Actuator Command	>15.5	>100.	39.5	31.6	15.5
Elliptical		-30.9 >15.5	2.58 >100.	36.9	31.5	15.5
Modified Circular	Roll Rate Error	>23.	>100.	99.4	11.4	23.
Elliptical		>23.	>100.	101.1	14.7	23.
Modified Circular	Roll Angle Error	22.2	11.1	63.9	2.08	77.5
Elliptical		23.1	11.69	64.3	2.09	77.6

Note: α_e = 10 deg, P_e = 0, Q_e = 0
Modified Circular has faster pitch channel (K_A = -.0387)

TABLE 10.1 Comparison of Linear CBTT Roll Channel Stability Margins For Elliptical and Modified Circular Airframes

Airframe	Branch	Gain (dB)	Margin (rad/sec)	Phase (deg)	Margin (rad/sec)	Attenuation at 100 rps (dB)
Modified Circular	Yaw Actuator Command	-10.4	5.62	46.	15.49	19.4
Elliptical		>24.5	>100.	40.	14.2	24.5
Modified Circular	Yaw Acceleration Feedback	9.0	10.2	55.4	3.35	34.3
Elliptical		6.3	10.5	54.6	3.02	29.2
Modified Circular	Coordination	14.4	26.63	---	---	26.
Elliptical		15.69 13.	4.07 24.82	---	---	24.2

Note: $\alpha_e = 10$ deg, $P_e = 0$, $Q_e = 0$
Modified Circular has faster pitch channel ($K_A = -.0387$)

TABLE 10.2 Comparison of Linear CBTT Yaw Channel and Coordination Branch Stability Margins for Elliptical and Modified Circular Airframes

Condition	τ_1	τ_2	α_{min}		α_{max}		β_{min}		β_{max}	
	(sec)	(sec)	(deg)	(sec)	(deg)	(sec)	(deg)	(sec)	(deg)	(sec)
K_{YP} = 1.0, K = 4.17 K_A = -0.0387	0.37	0.38	0.	0.	11.9	0.9	-.9	3.4	1.7	3.9
K_{YP} = 1.0, K = 2.0 K_A = -.0387 /	0.37	0.38	0.	0.	11.9	0.87	-1.4	3.46	1.6	3.97
K_A = -.0387, K_{YP} = 1.0, Autopilot cross-coupling for $C_{\ell_{\delta_Y}}$	0.37	0.39	0.	0.	11.9	0.87	-1.5	3.53	1.76	4.0

τ_1 = 63 percent time constant of achieved maneuver plane acceleration due to first command.

τ_2 = 63 percent time constant of achieved maneuver plane acceleration due to second command.

TABLE 10.3 CBTT Performance Summary of Modified Circular Airframe and Circular Airframe With Autopilot $C_{\ell_{\delta_Y}}$ Cross-Coupling, 2 gees (0°, 180°).

Condition	q_{min}		q_{max}		p_{min}		p_{max}		r_{min}		r_{max}	
	deg/sec	sec	deg/sec	sec	deg/sec	sec	deg/sec	sec	deg/sec	sec	deg/sec	sec
$K = 4.17$, $K_{YF} = 1.0$, $K_A = -.0387$	-15.8	3.5	28.1	0.265	-14.6	5.6	278.	3.4	-1.2	4.7	45.3	3.3
$K = 4.17$, $K_{YP} = 1.0$, $K_A = -.0387$	-16.	3.49	28.1	0.265	-14.5	4.6	272.5	3.39	-0.96	4.76	47.8	3.27
$K_{YP} = 1.0$, $K_A = -.0387$, Autopilot Cross-Coupling for $C_{\ell_{\delta_Y}}$	-16.4	3.57	28.1	0.265	-14.3	4.6	310.4	3.4	-3.95	3.84	51.3	3.34

TABLE 10.4 Range of CBTT Missile Body Angular Rates for Modified Circular Airframe and Circular Airframe With Autopilot $C_{\ell_{\delta_Y}}$ Cross-Coupling, 2 gees (0°, 180°)

τ_1	τ_2	α_{min}		α_{max}		β_{min}		β_{max}	
(sec)	(sec)	(deg)	(sec)	(deg)	(sec)	(deg)	(sec)	(deg)	(sec)
0.36	0.43	0.	0.	19.4	0.79	-2.2	3.51	2.03	4.05

Performance Summary

q_{min}		q_{max}		p_{min}		p_{max}		r_{min}		r_{max}	
deg/sec	sec	deg/sec	sec	deg/sec	sec	deg/sec	sec	deg/sec	sec	deg/sec	sec
-19.1	3.6	47.3	0.27	-14.3	4.6	280.6	3.39	-1.9	4.75	86.6	3.3

Range of Missile Body Angular Rates

TABLE 10.5 Circular Airframe, 4 gees (0°, 180°), No Aerodynamic Cross-Coupling, $K_{YP} = 1.0$, $K_A = -0.0387$

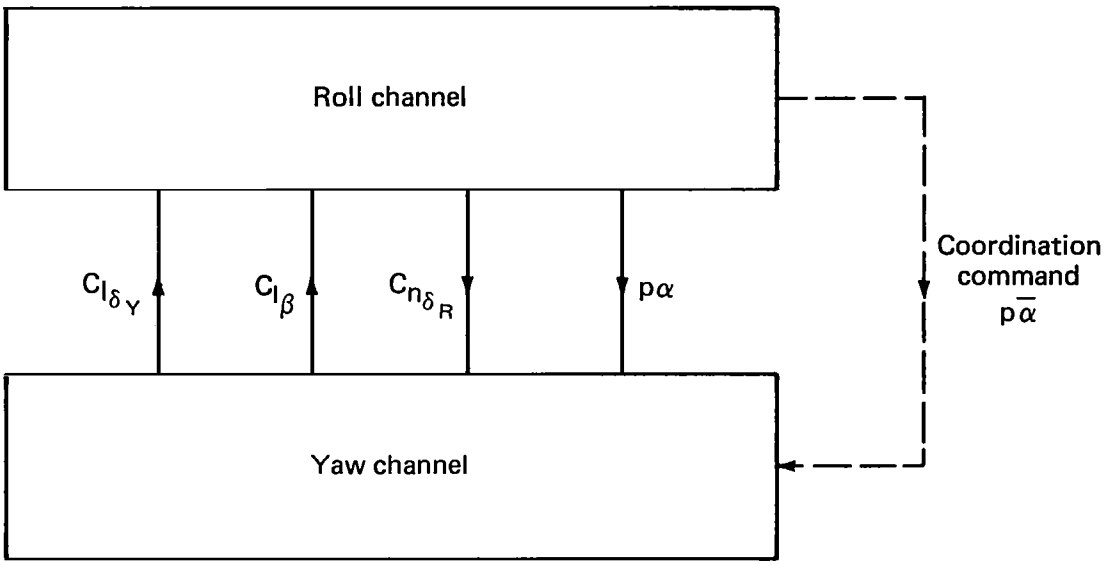

Cross-coupling between roll and yaw channels

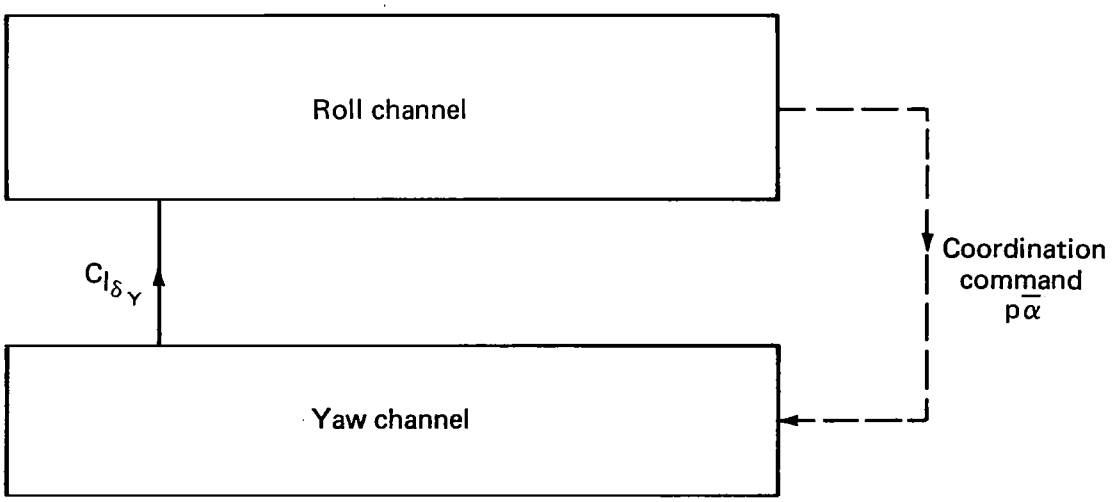

Critical cross-coupling path between roll and yaw channels

Fig. 10.1 Critical coupling loop which determines sideslip performance of CBTT for circular airframe.

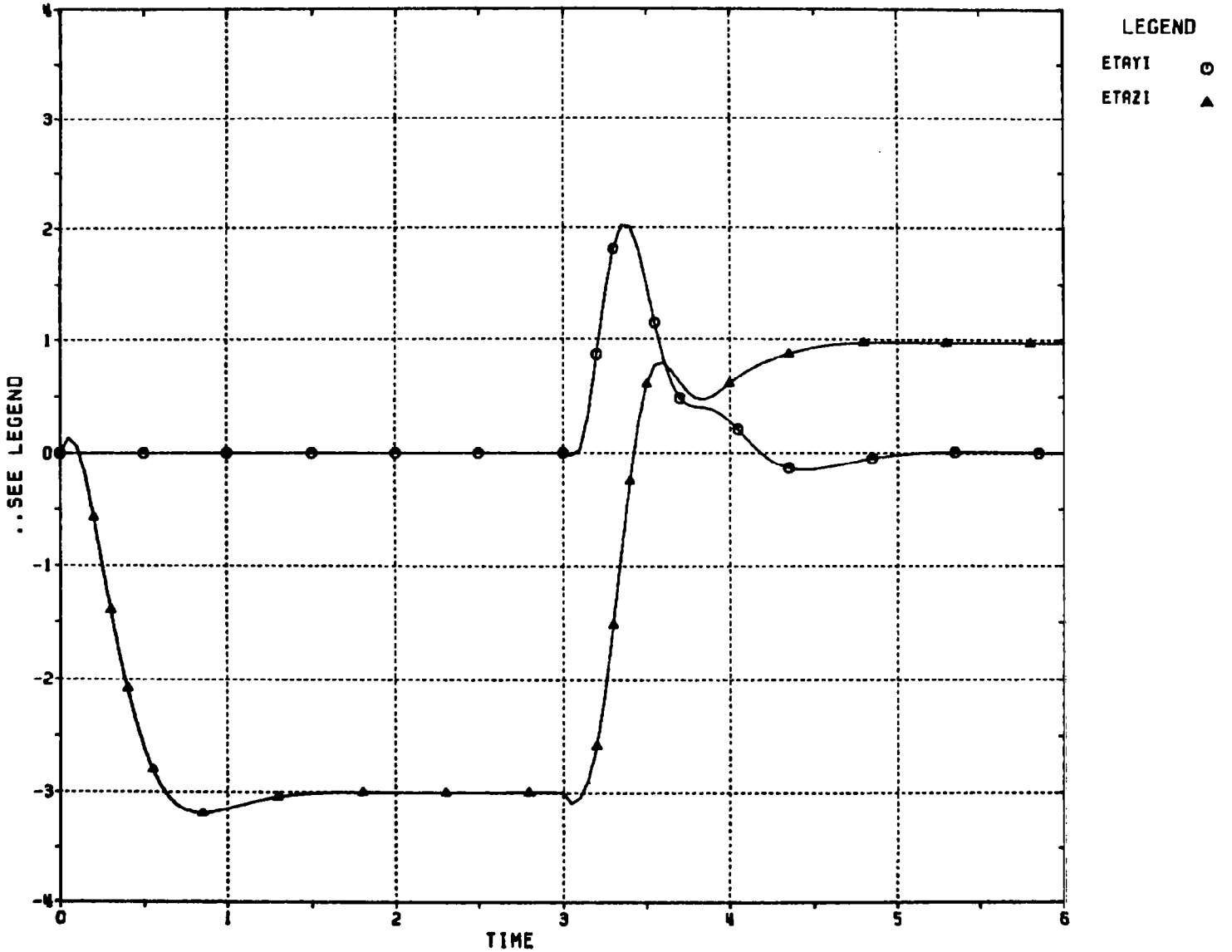

Figure 10.2 ACHIEVED INERTIAL ACCELERATIONS VS. TIME (SEC);
CBTT OF MODIFIED CIRCULAR AIRFRAME, K = 4.17;
2 GEES (0^{o}, 180^{o})
ETAYI = YAW (GEES), ETAZI = PITCH (GEES)

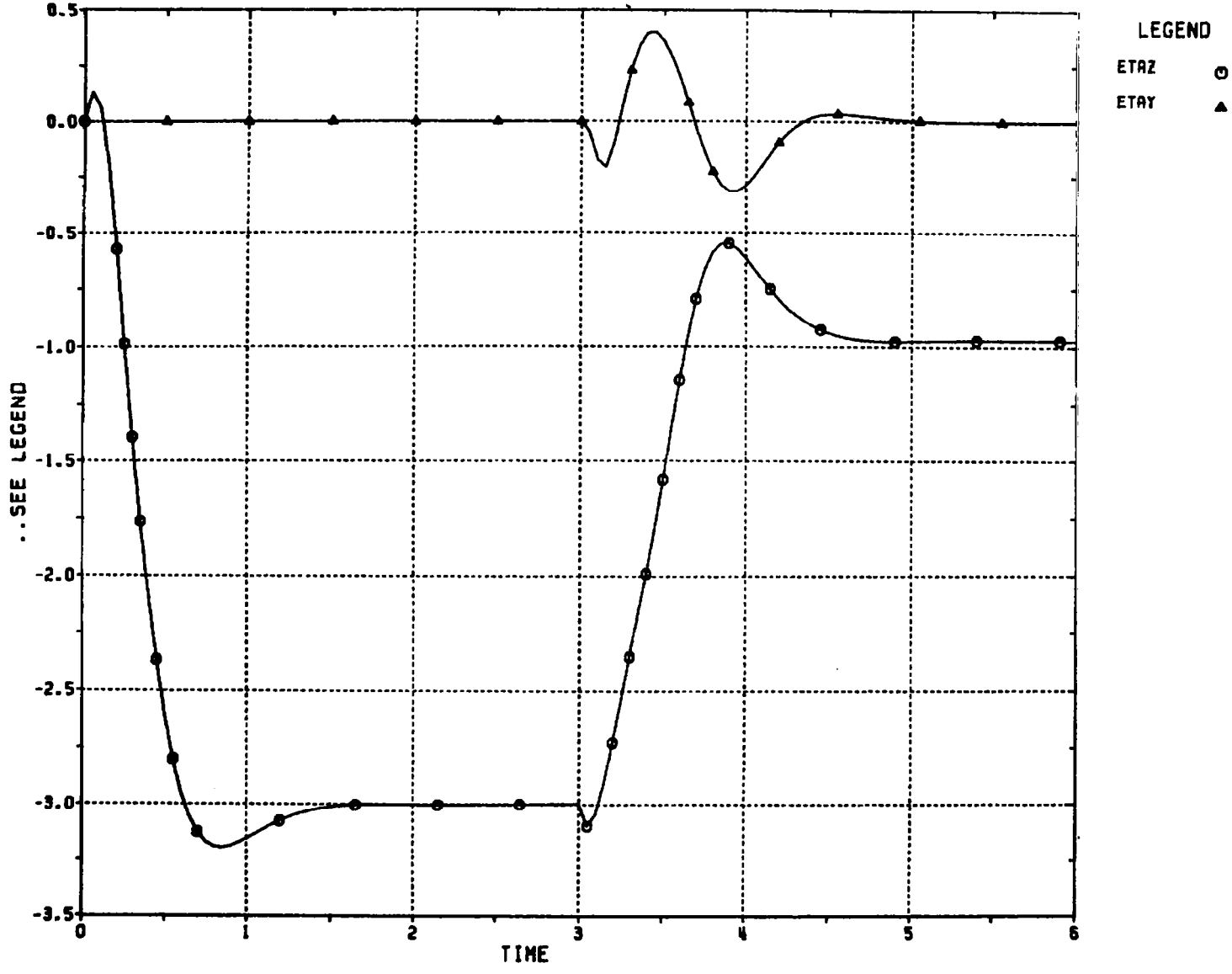

Figure 10.3 ACHIEVED BODY-FIXED ACCELERATIONS VS. TIME (SEC);
CBTT OF MODIFIED CIRCULAR AIRFRAME, K = 4.17;
2 GEES (0^{o}, 180^{o})
ETAY = YAW (GEES), ETAZ = PITCH (GEES)

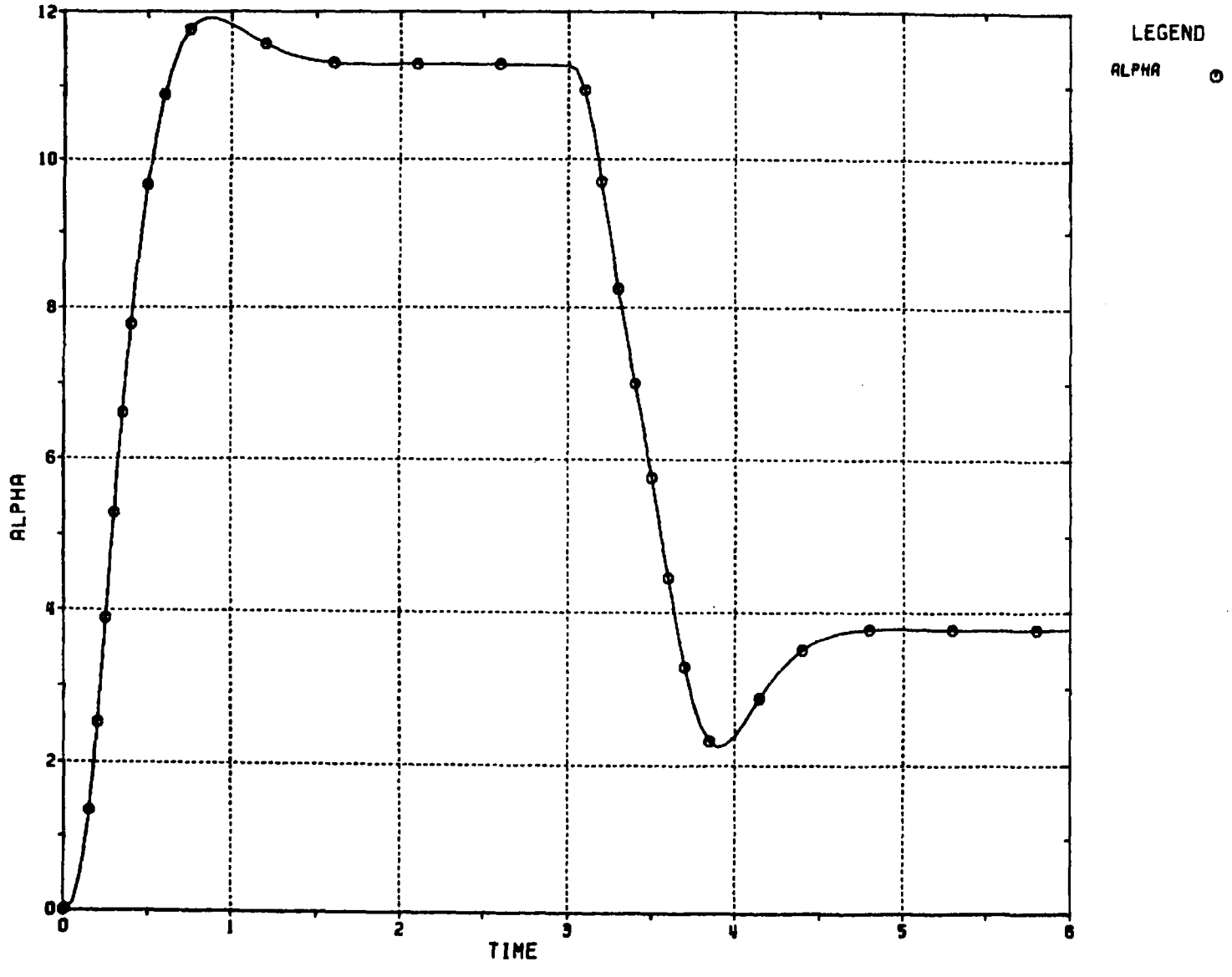

Figure 10.4 ANGLE OF ATTACK (DEG) VS. TIME (SEC);
CBTT OF MODIFIED CIRCULAR AIRFRAME, K = 4.17;
2 GEES(0^{o}, 180^{o})

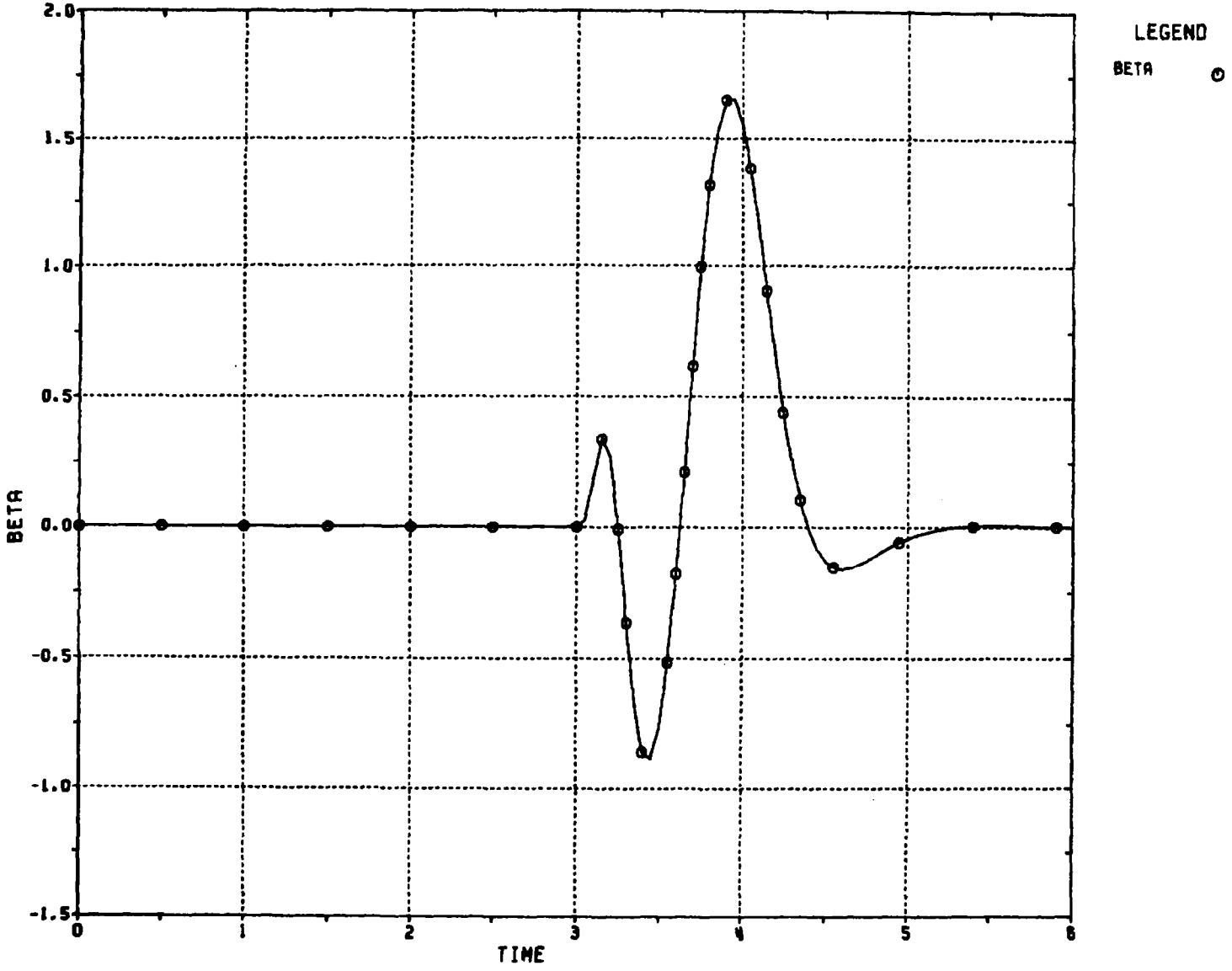

Figure 10.5 SIDESLIP ANGLE (DEG) VS. TIME (SEC);
CBTT OF MODIFIED CIRCULAR AIRFRAME, K = 4.17;
2 GEES (0°, 180°)

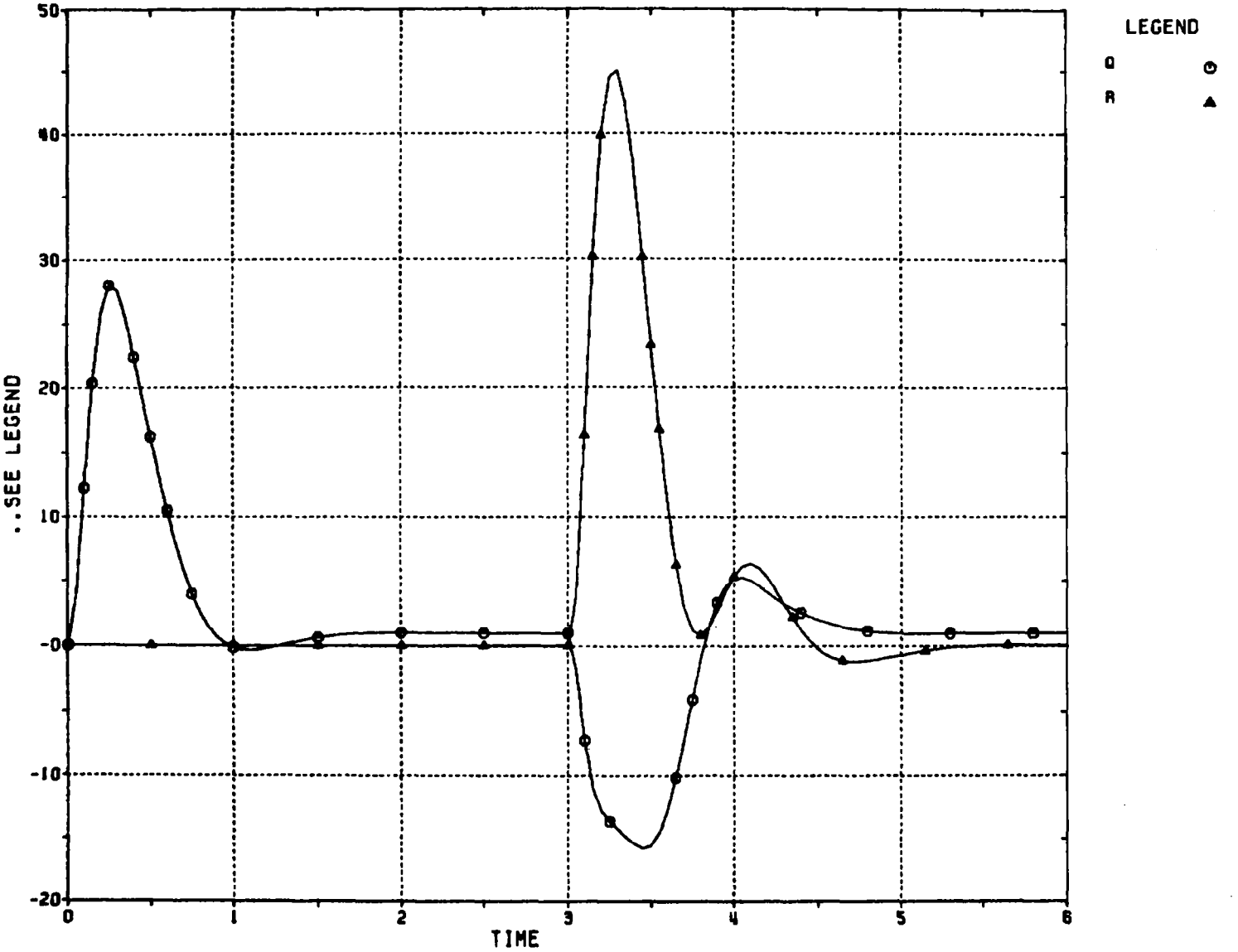

Figure 10.6 BODY ANGULAR RATES VS. TIME (SEC);
CBTT OF MODIFIED CIRCULAR AIRFRAME, K = 4.17;
2 GEES (0^{o}, 180^{o})
Q = PITCH (DEG/SEC), R = YAW (DEG/SEC)

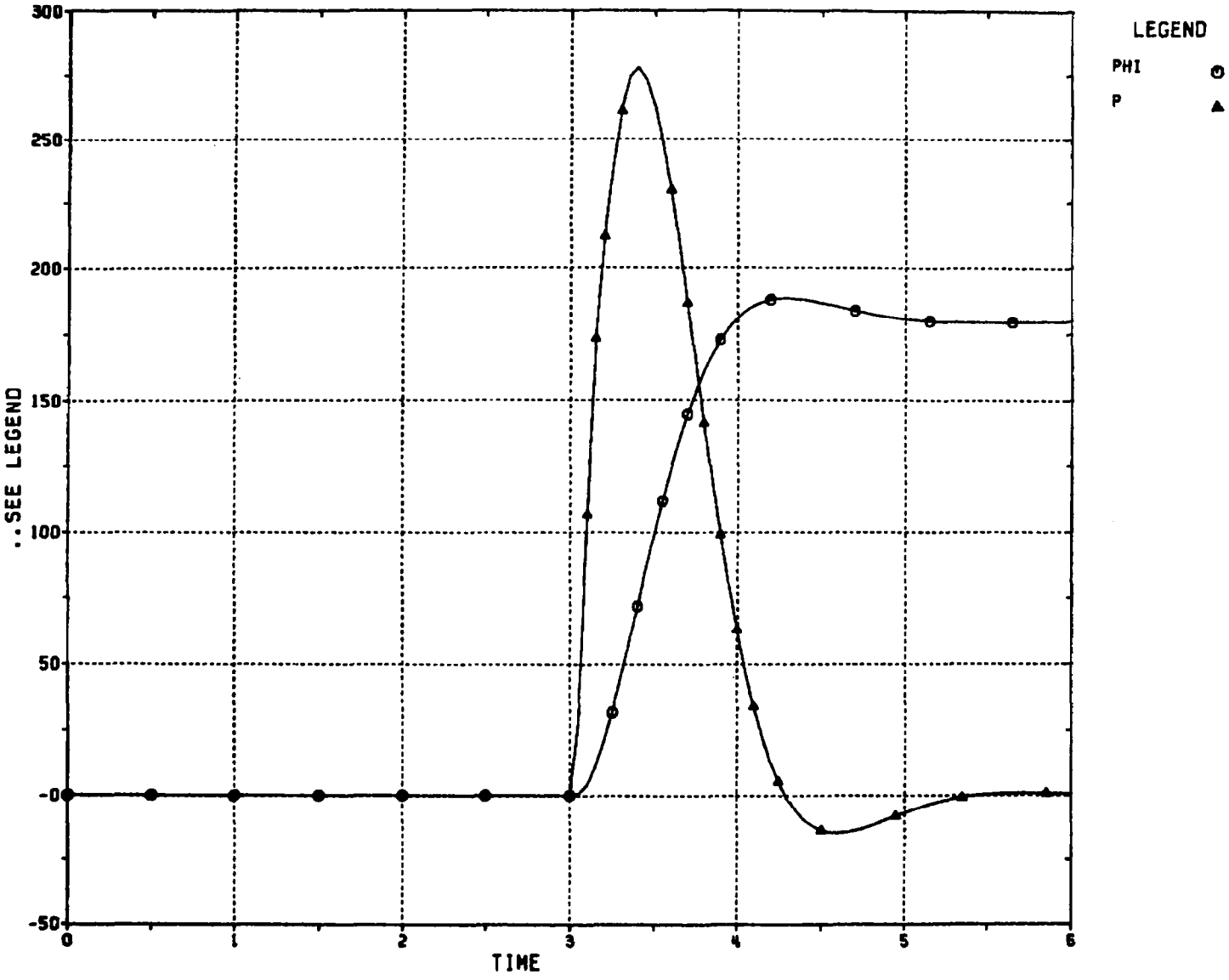

Figure 10.7 ROLL ANGLE AND ANGULAR RATE VS. TIME (SEC);
CBTT OF MODIFIED CIRCULAR AIRFRAME, K = 4.17;
2 GEES (0^{o}, 180^{o})
PHI = ROLL ANGLE, P = ROLL ANGULAR RATE (DEG/SEC)

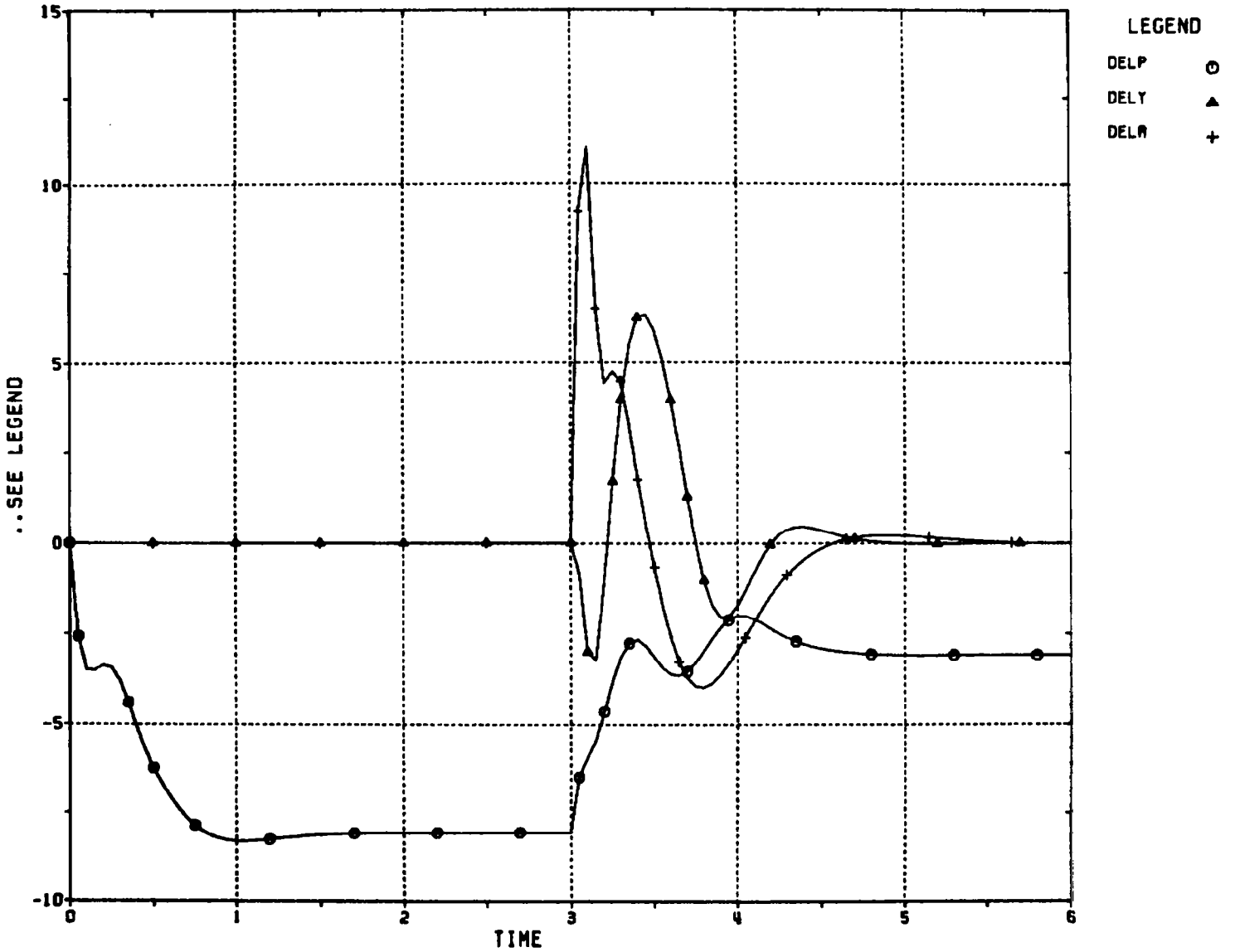

Figure 10.8 TAIL INCIDENCES;
CBTT OF MODIFIED CIRCULAR AIRFRAME, K = 4.17;
2 GEES (0^{o}, 180^{o})
DELP = PITCH (DEG), DELY = RUDDER (DEG), DELR = ROLL (DEG)

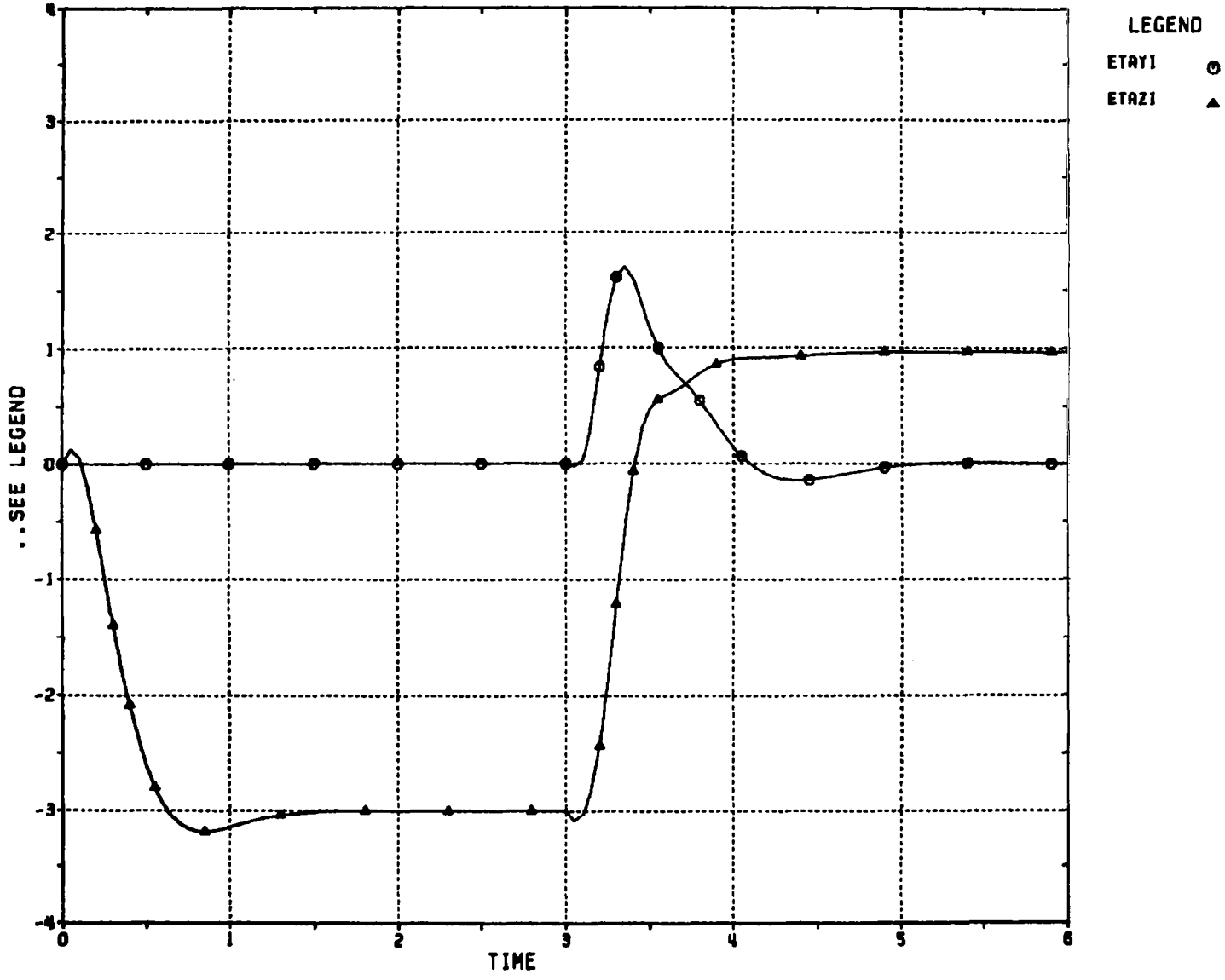

Figure 10.9 ACHIEVED INERTIAL ACCELERATIONS VS. TIME (SEC);
CBTT OF MODIFIED CIRCULAR AIRFRAME, K = 4.17;
INERTIAL AND KINEMATIC CROSS-COUPLING INTO PITCH
CHANNEL REMOVED; 2 GEES (0^{o}, 180^{o})
ETAYI = CROSS-PLANE (GEES), ETAZI = MANEUVER PLANE (GEES)

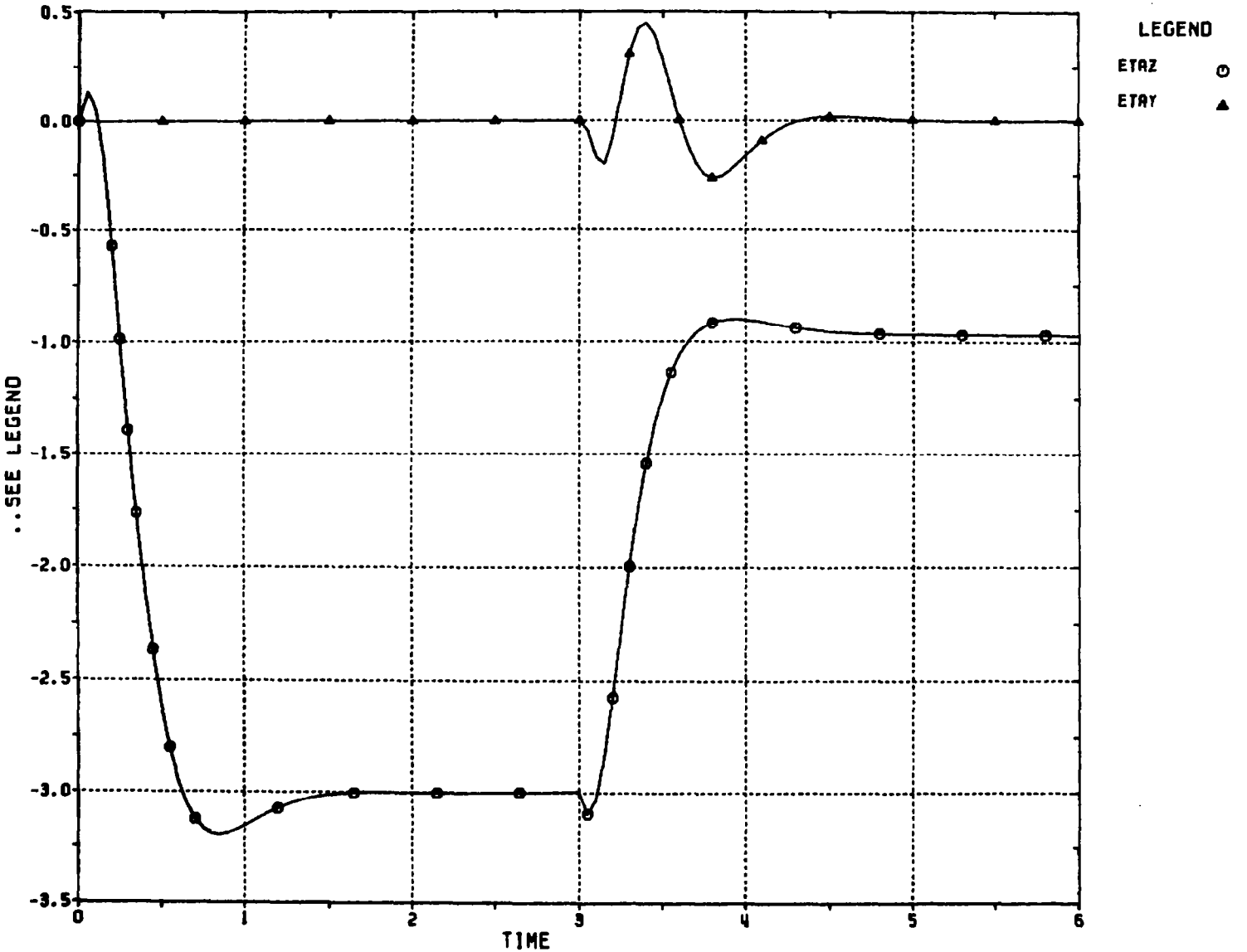

Figure 10.10 ACHIEVED BODY-FIXED ACCELERATIONS VS. TIME (SEC);
CBTT OF MODIFIED CIRCULAR AIRFRAME, K = 4.17;
INERTIAL AND KINEMATIC CROSS-COUPLING INTO PITCH
CHANNEL REMOVED; 2 GEES(0^{o}, 180^{o})
ETAY = YAW (GEES), ETAZ = PITCH (GEES)

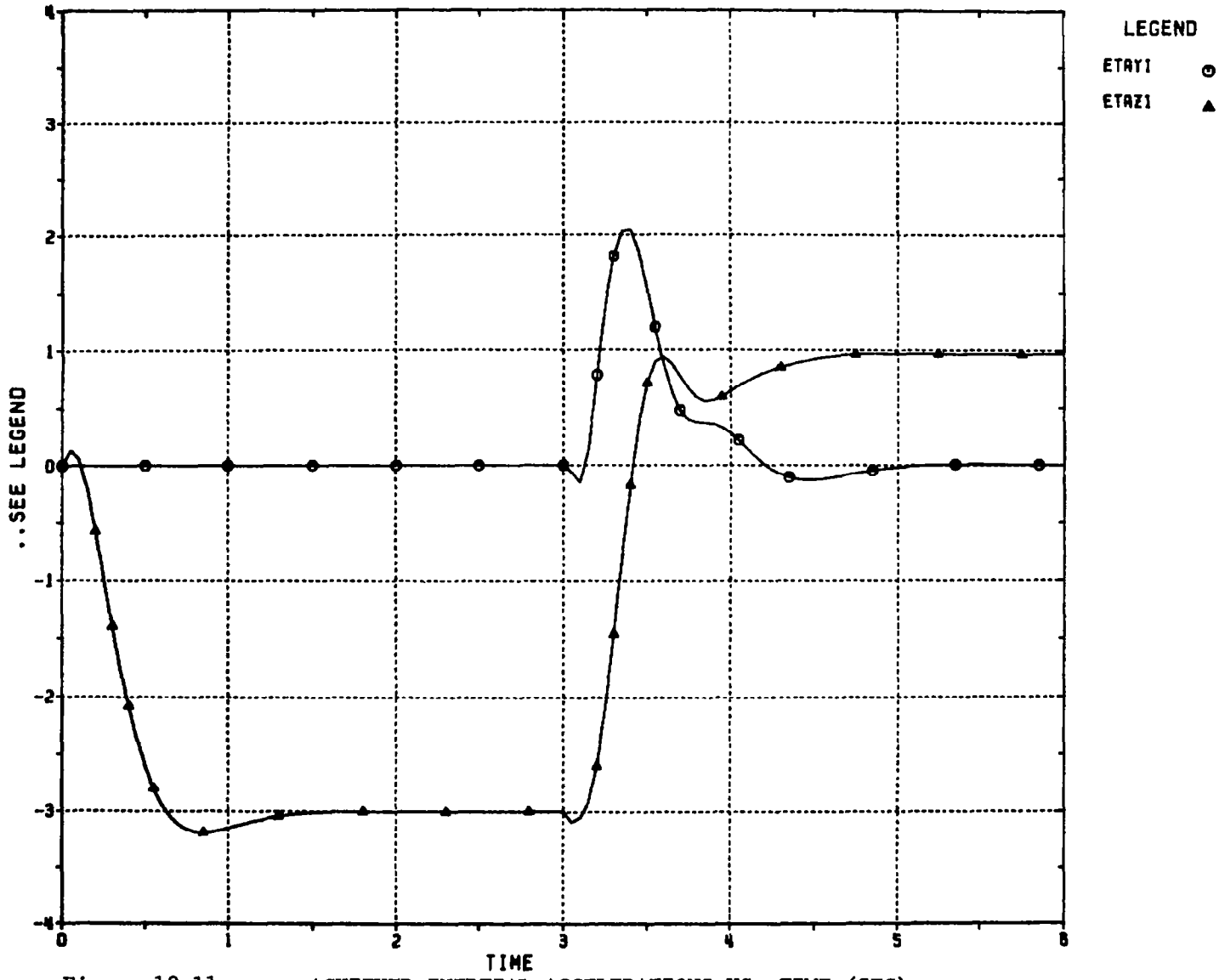

Figure 10.11 ACHIEVED INERTIAL ACCELERATIONS VS. TIME (SEC);
CBTT OF MODIFIED CIRCULAR AIRFRAME, K = 2
2 GEES (0^{o}, 180^{o})
ETAYI = CROSS-PLANE (GEES), ETAZI = MANEUVER PLANE (GEES)

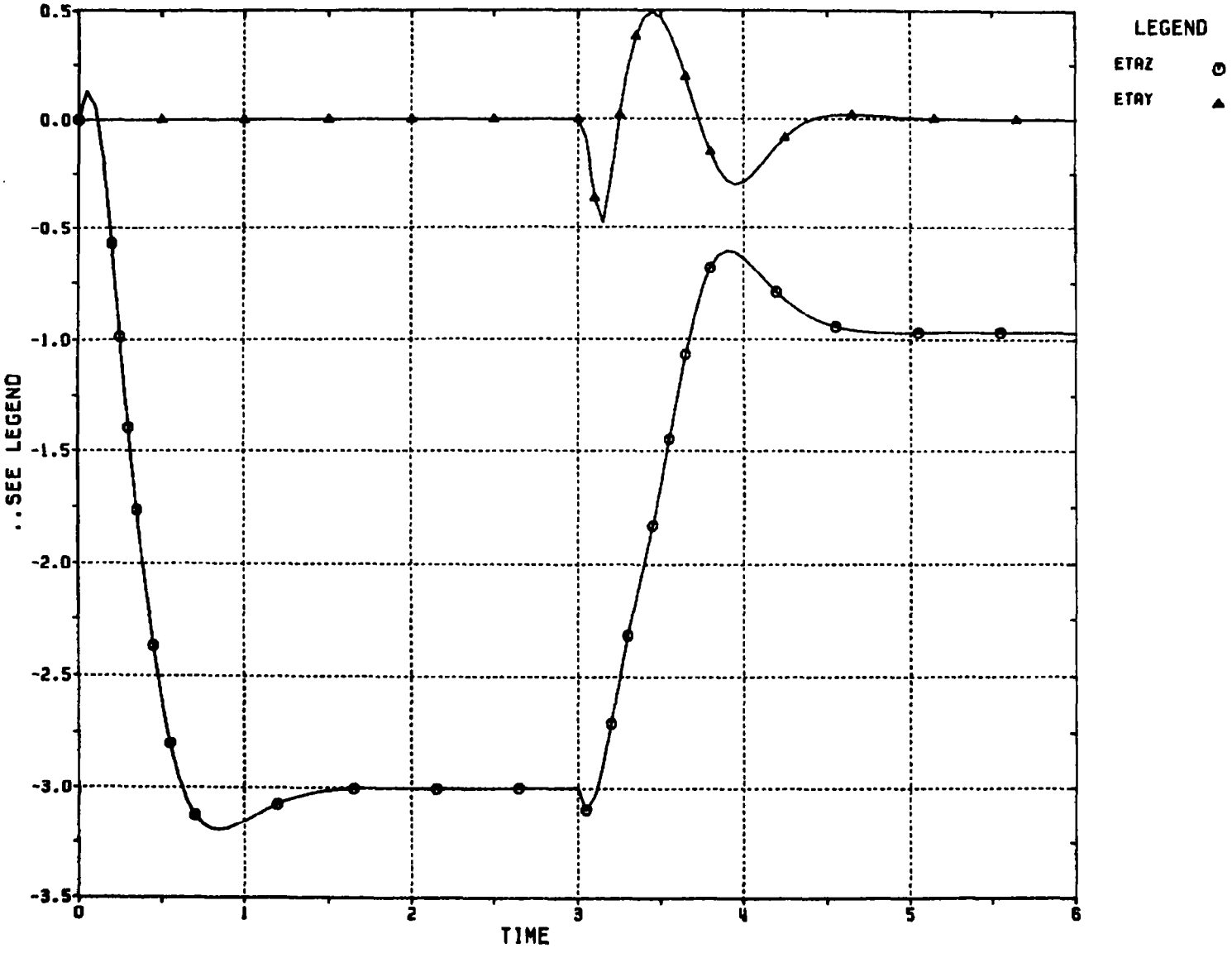

Figure 10.12 ACHIEVED BODY-FIXED ACCELERATIONS VS. TIME (SEC);
CBTT OF MODIFIED CIRCULAR AIRFRAME, K = 2
2 GEES (0^{o}, 180^{o})
ETAY = YAW (GEES), ETAZ = PITCH (GEES)

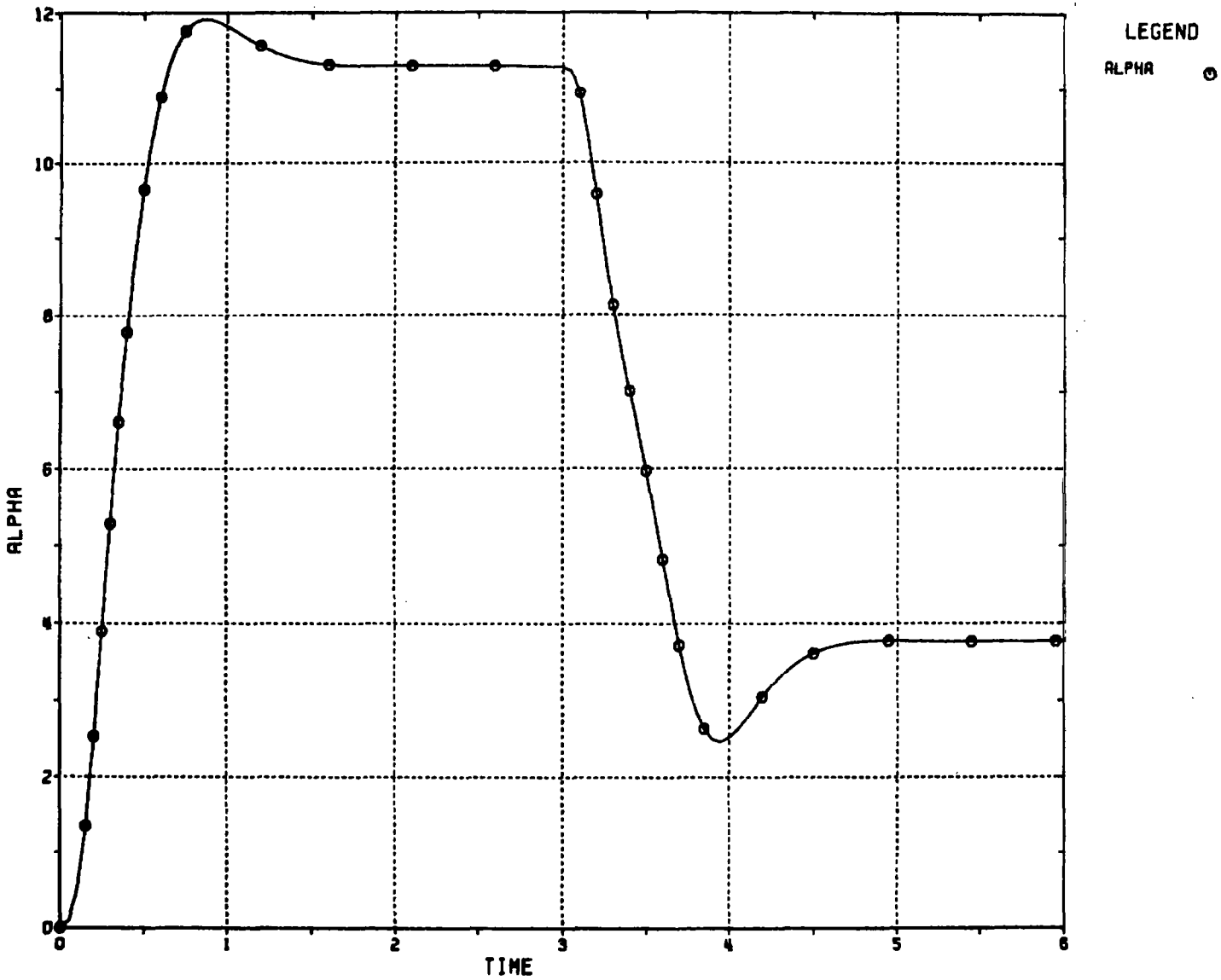

Figure 10.13 ANGLE OF ATTACK (DEG) VS. TIME (SEC);
CBTT OF MODIFIED CIRCULAR AIRFRAME, K = 2;
2 GEES (0^{o}, 180^{o})

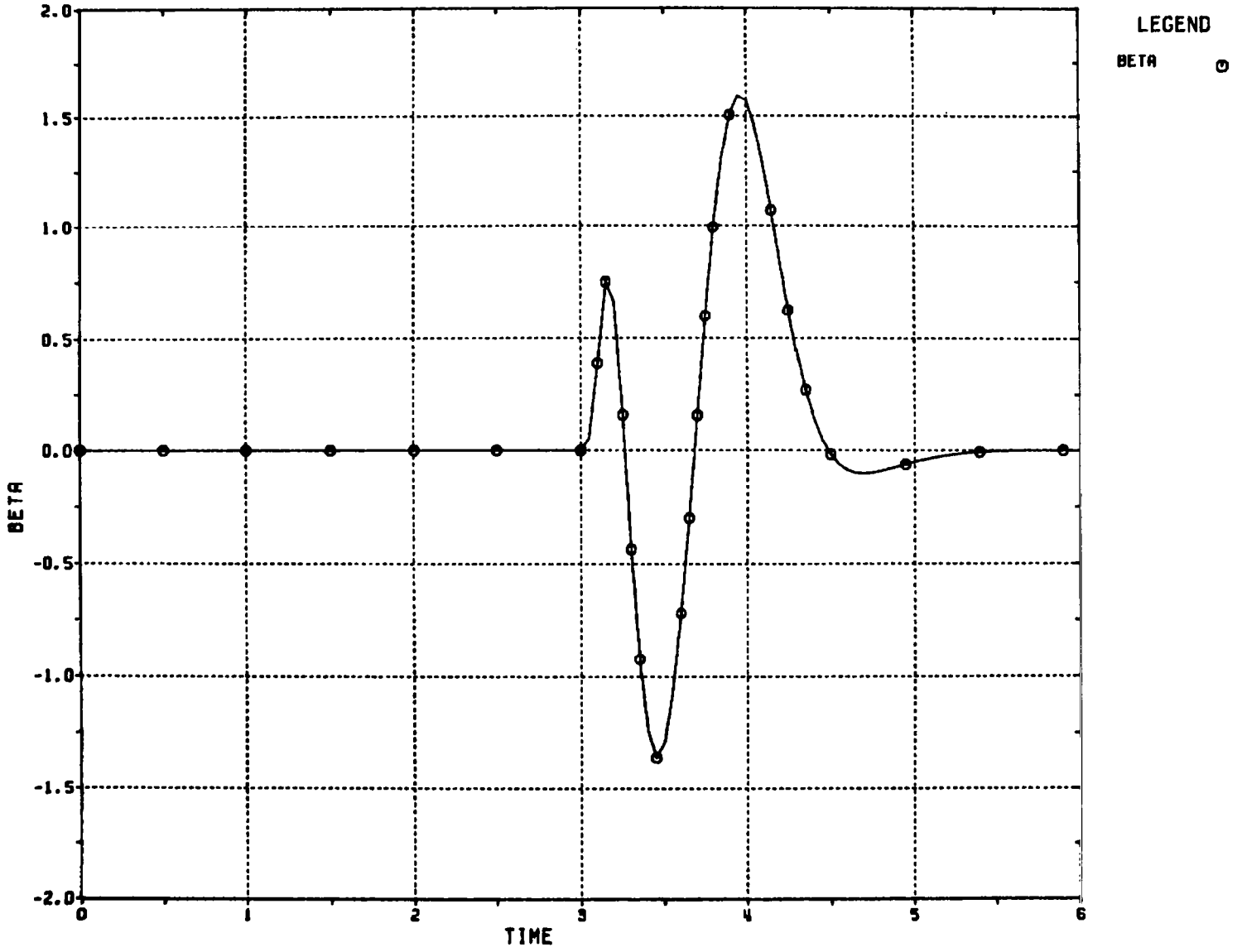

Figure 10.14 SIDESLIP ANGLE (DEG) VS. TIME (SEC);
CBTT OF MODIFIED CIRCULAR AIRFRAME, K = 2;
2 GEES (0^{o}, 180^{o})

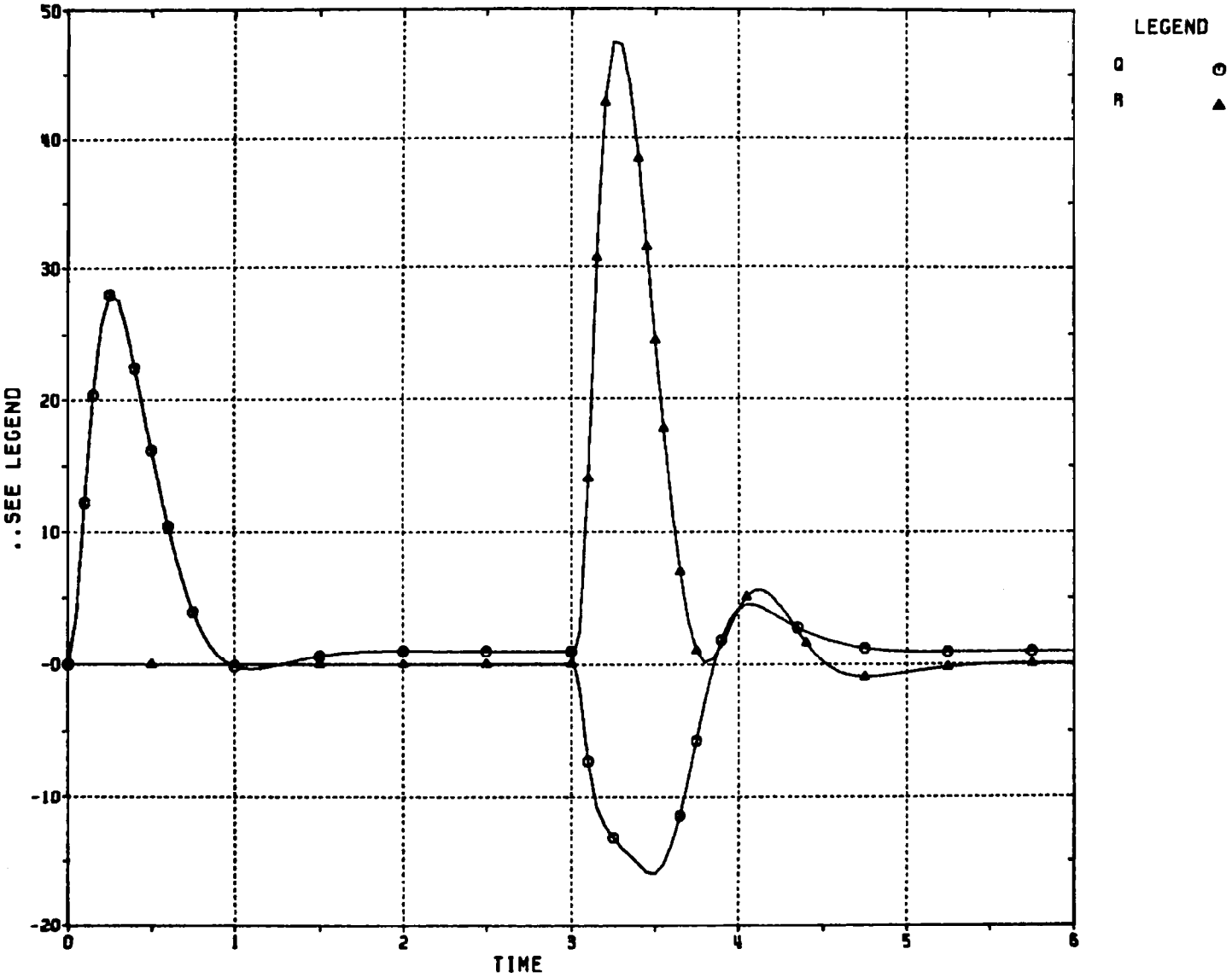

Figure 10.15 BODY ANGULAR RATES VS. TIME (SEC);
CBTT OF MODIFIED CIRCULAR AIRFRAME, K = 2;
2 GEES (0^{o}, 180^{o})
Q = PITCH (DEG/SEC), R = YAW (DEG/SEC)

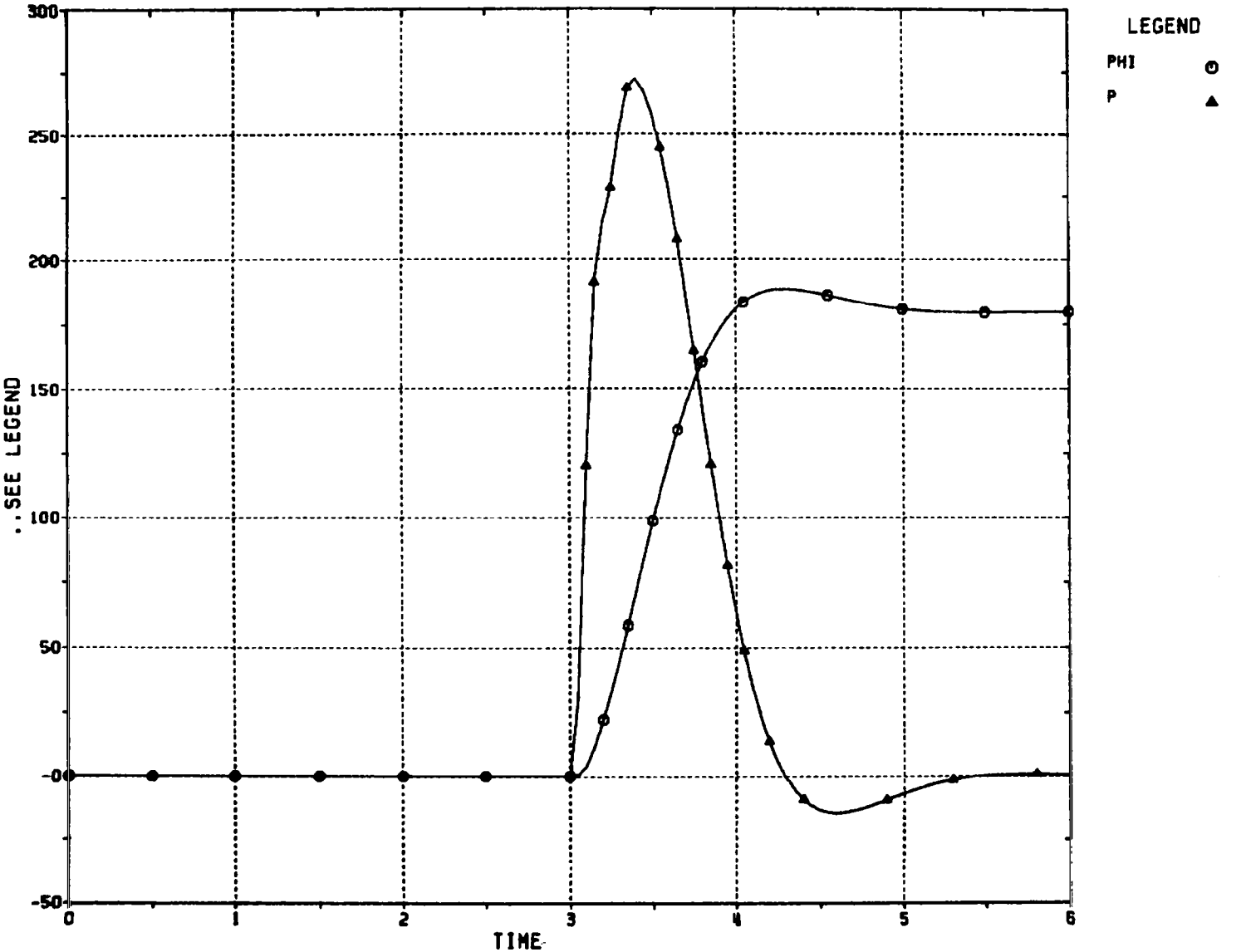

Figure 10.16 ROLL ANGLE AND ANGULAR RATE VS. TIME (SEC);
CBTT OF MODIFIED CIRCULAR AIRFRAME, K = 2;
2 GEES (0^{o}, 180^{o})
PHI = ROLL ANGLE (DEG), P = ROLL ANGULAR RATE (DEG/SEC)

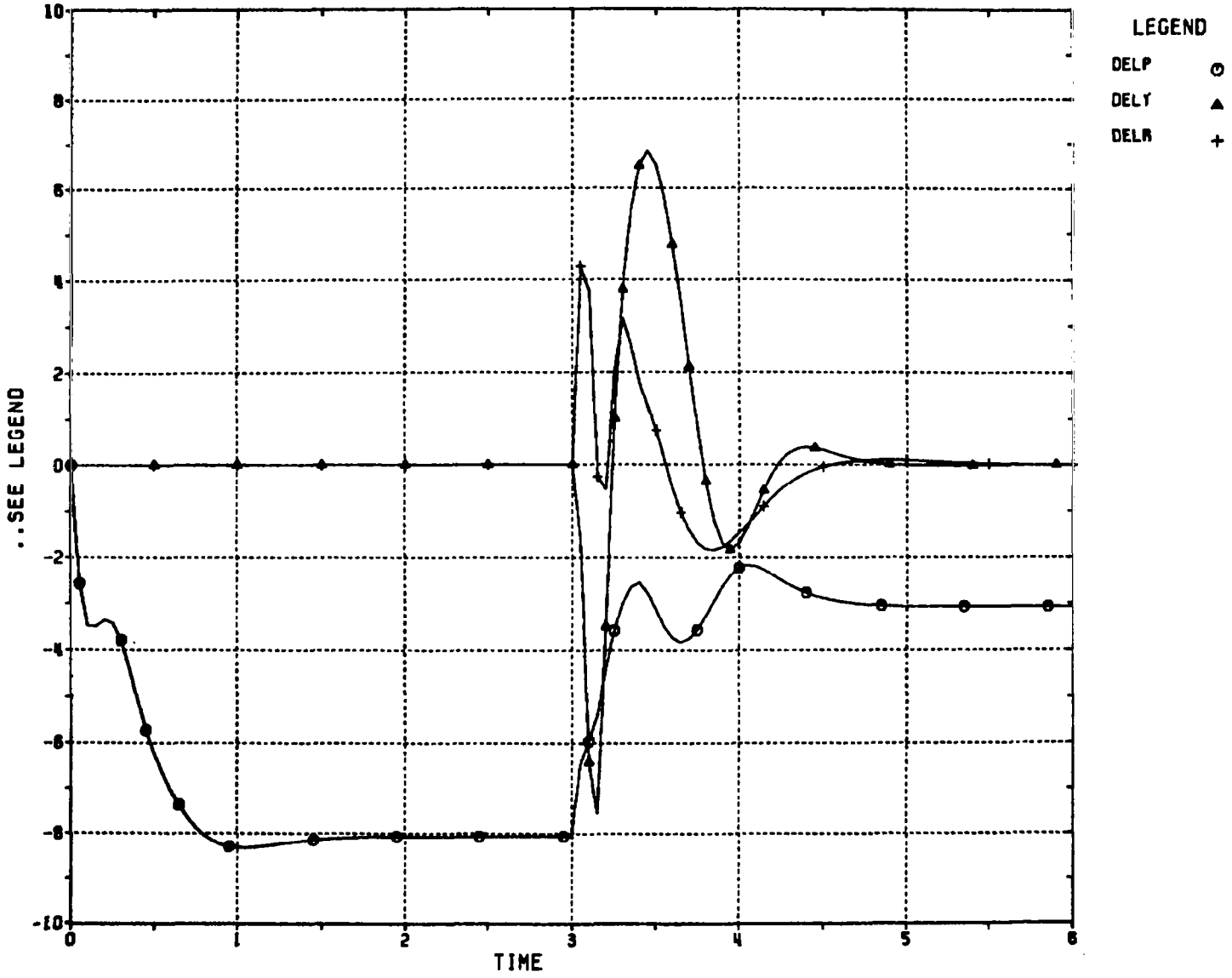

Figure 10.17 TAIL INCIDENCES VS. TIME (SEC);
CBTT OF MODIFIED CIRCULAR AIRFRAME, K = 2;
2 GEES (0^{o}, 180^{o})
DELP = PITCH (DEG), DELY = YAW (DEG), DELR = ROLL (DEG)

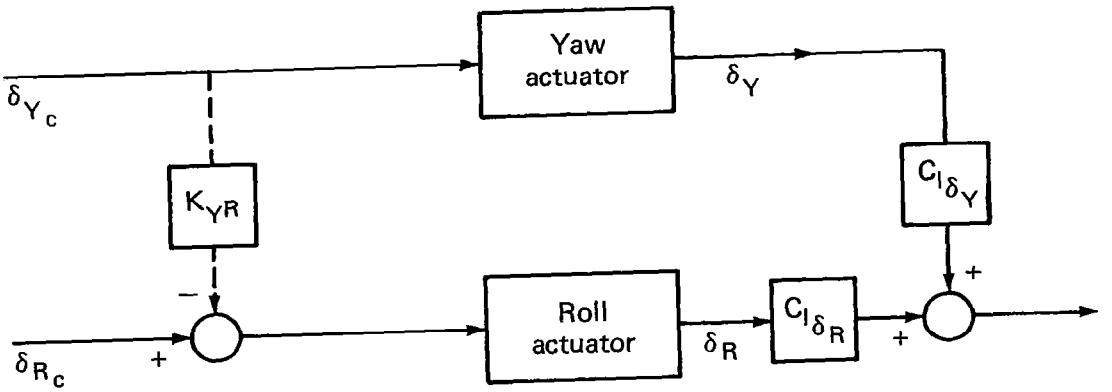

$$K_{YR} = 2\frac{C_{l_{\delta_Y}}}{C_{l_{\delta_R}}}$$

Fig. 10.18 Changing sign of $C_{l_{\delta_Y}}$ via autopilot cross-coupling.

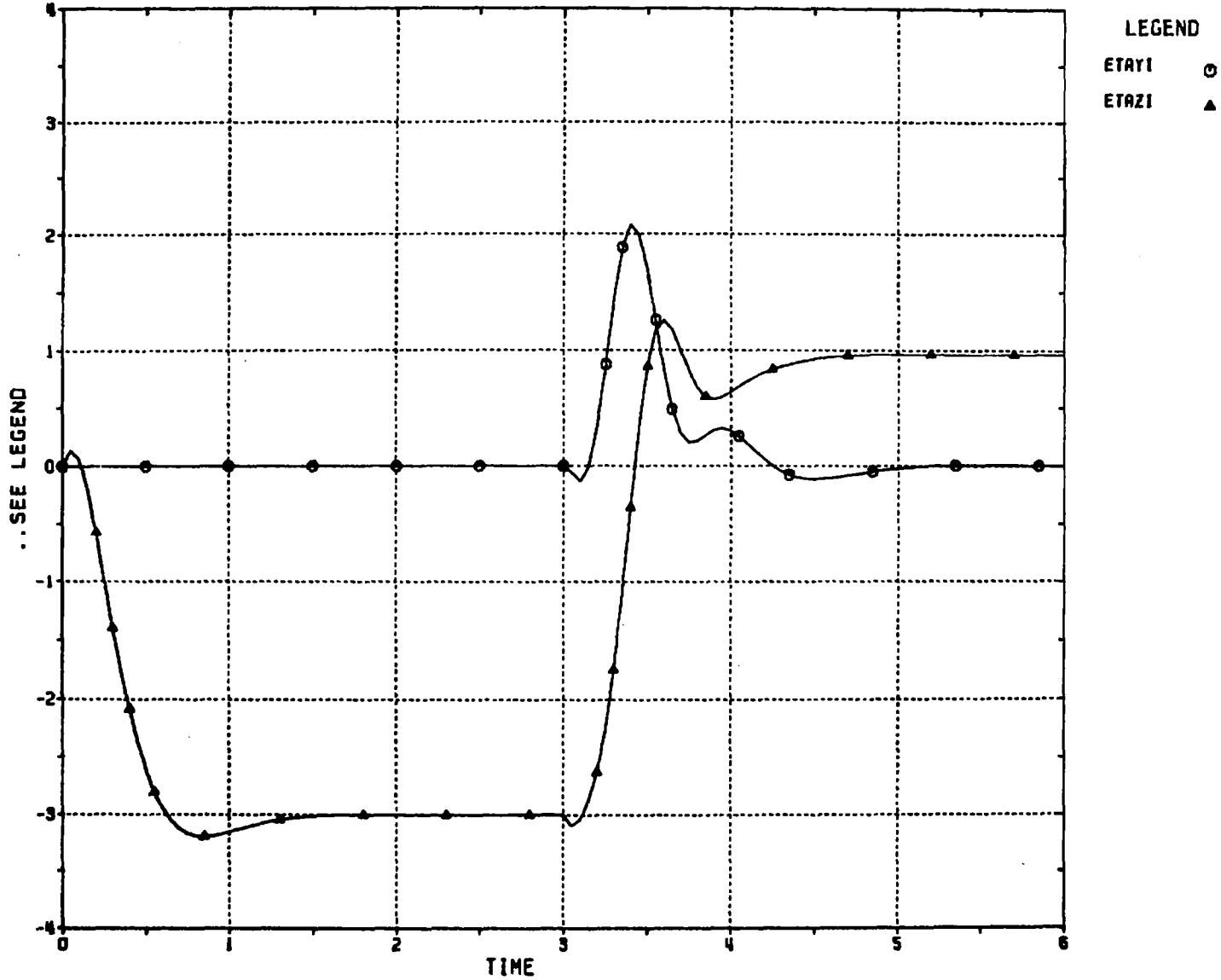

Figure 10.19 ACHIEVED INERTIAL ACCELERATIONS VS. TIME (SEC);
CBTT OF CIRCULAR AIRFRAME WITH AUTOPILOT CROSS-COUPLING FOR $C_{\ell_{\delta_Y}}$;
2 GEES (0°, 180°)
ETAYI = CROSS-PLANE (GEES), ETAZI = MANEUVER PLANE (GEES)

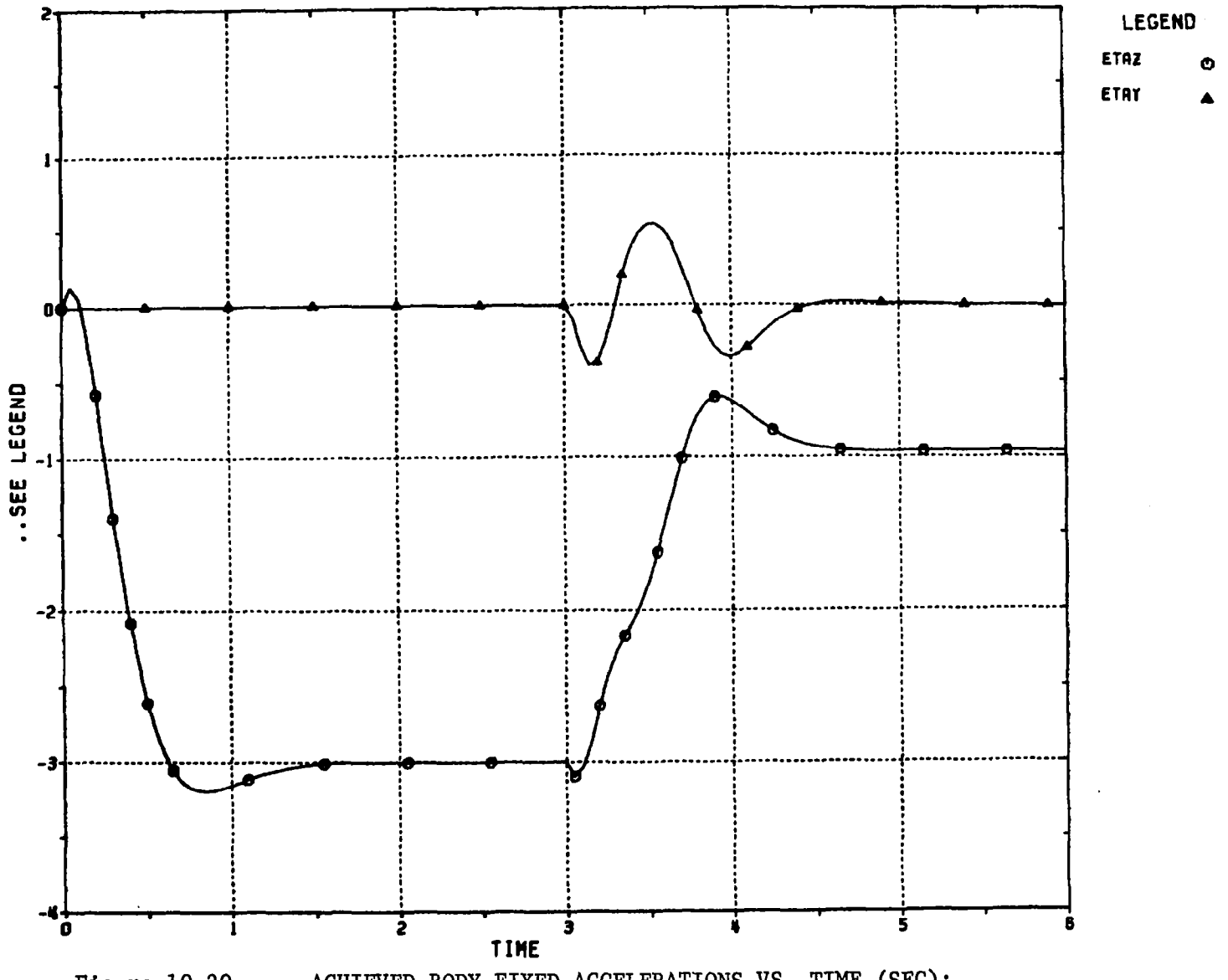

Figure 10.20 ACHIEVED BODY-FIXED ACCELERATIONS VS. TIME (SEC);
CBTT OF CIRCULAR AIRFRAME WITH AUTOPILOT CROSS-COUPLING FOR $C_{\ell_{\delta_Y}}$;
2 GEES (0^o, 180^o)
ETAY = YAW (GEES), ETAZ = PITCH (GEES)

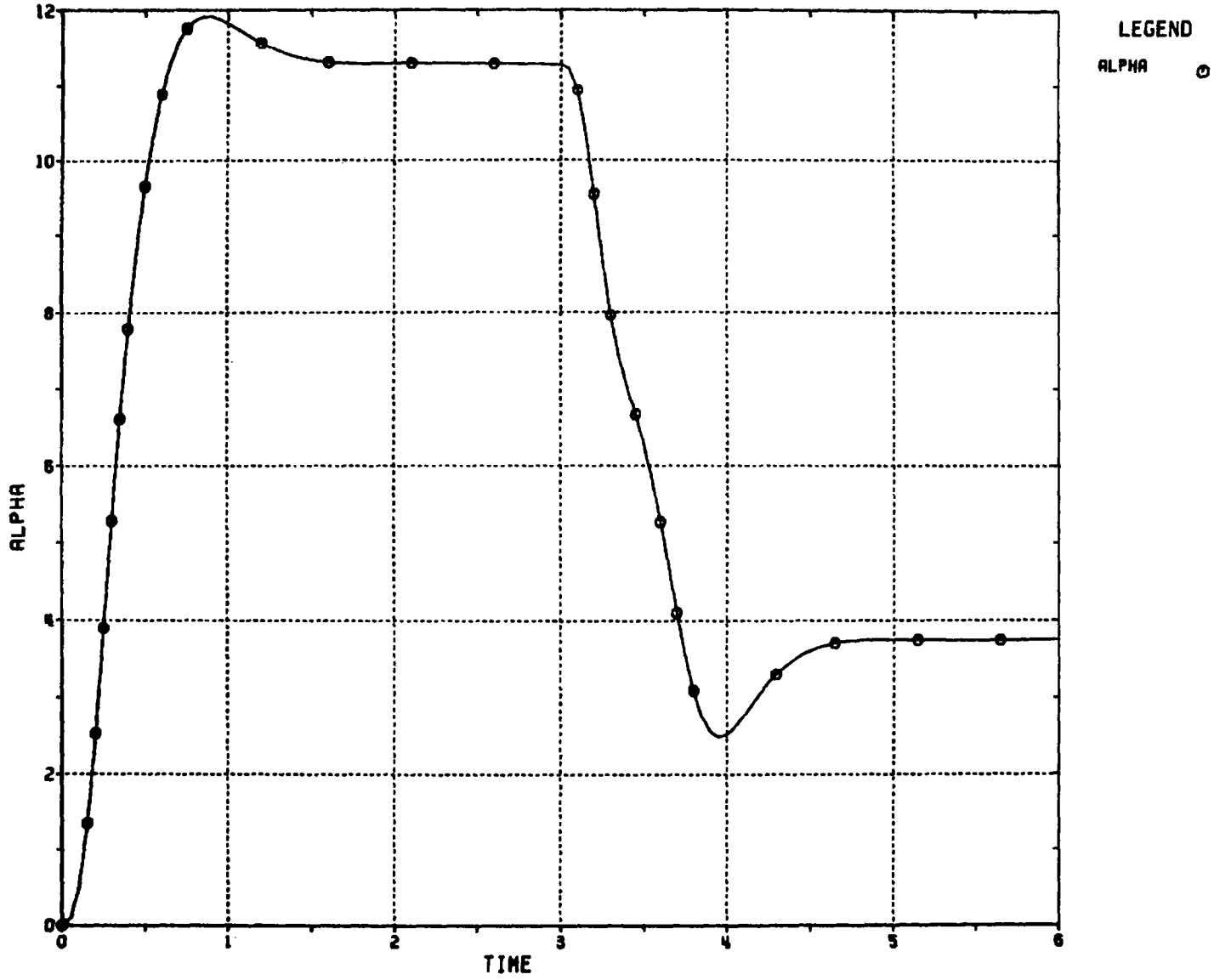

Figure 10.21 ANGLE OF ATTACK (DEG) VS. TIME (SEC);
CBTT OF CIRCULAR AIRFRAME WITH AUTOPILOT CROSS-COUPLING FOR $C_{\ell_{\delta_Y}}$;
2 GEES (0^o, 180^o)

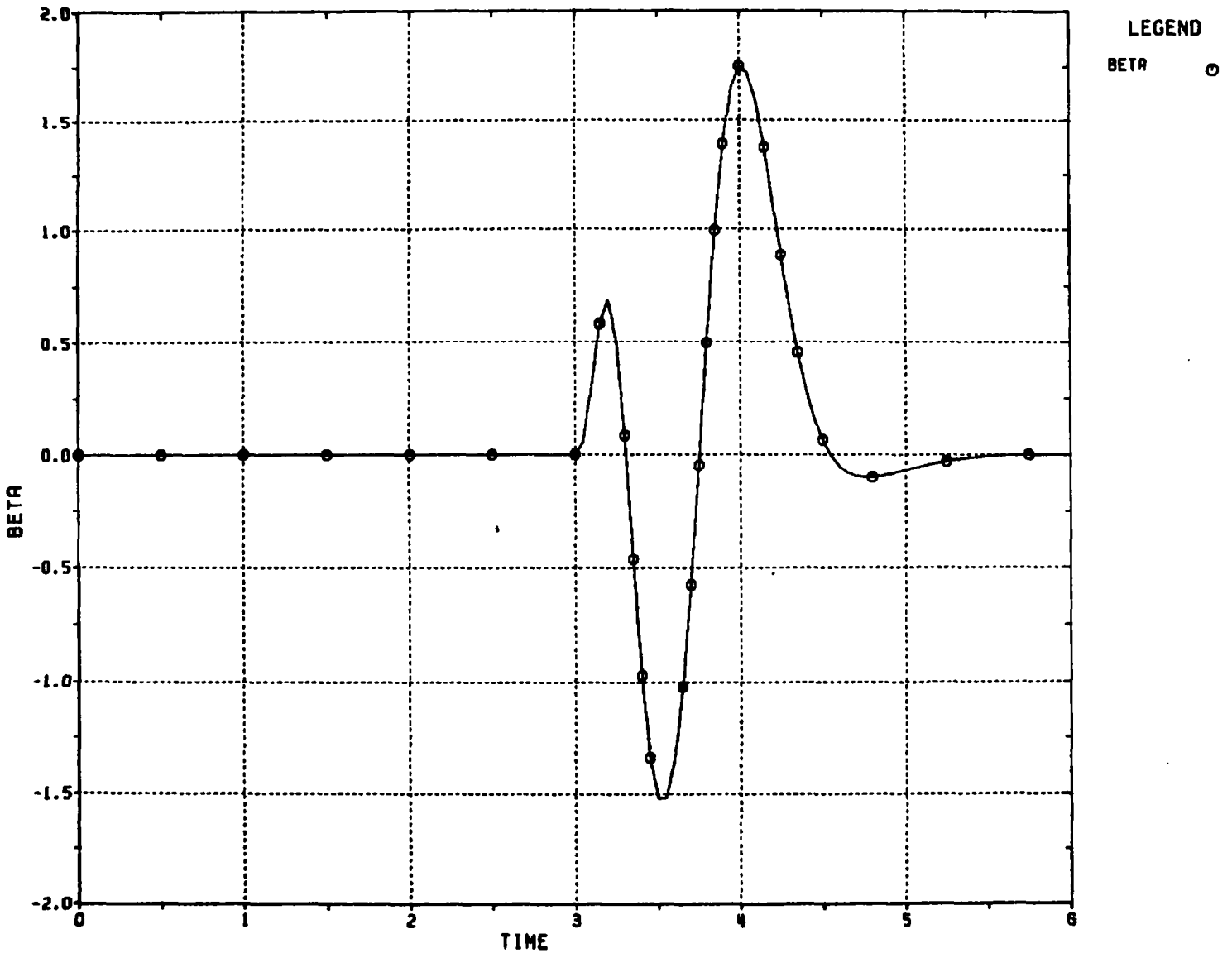

Figure 10.22 SIDESLIP ANGLE (DEG) VS. TIME (SEC);
CBTT OF CIRCULAR AIRFRAME WITH AUTOPILOT CROSS-COUPLING FOR $C_{\ell_{\delta_Y}}$;
2 GEES (0°, 180°)

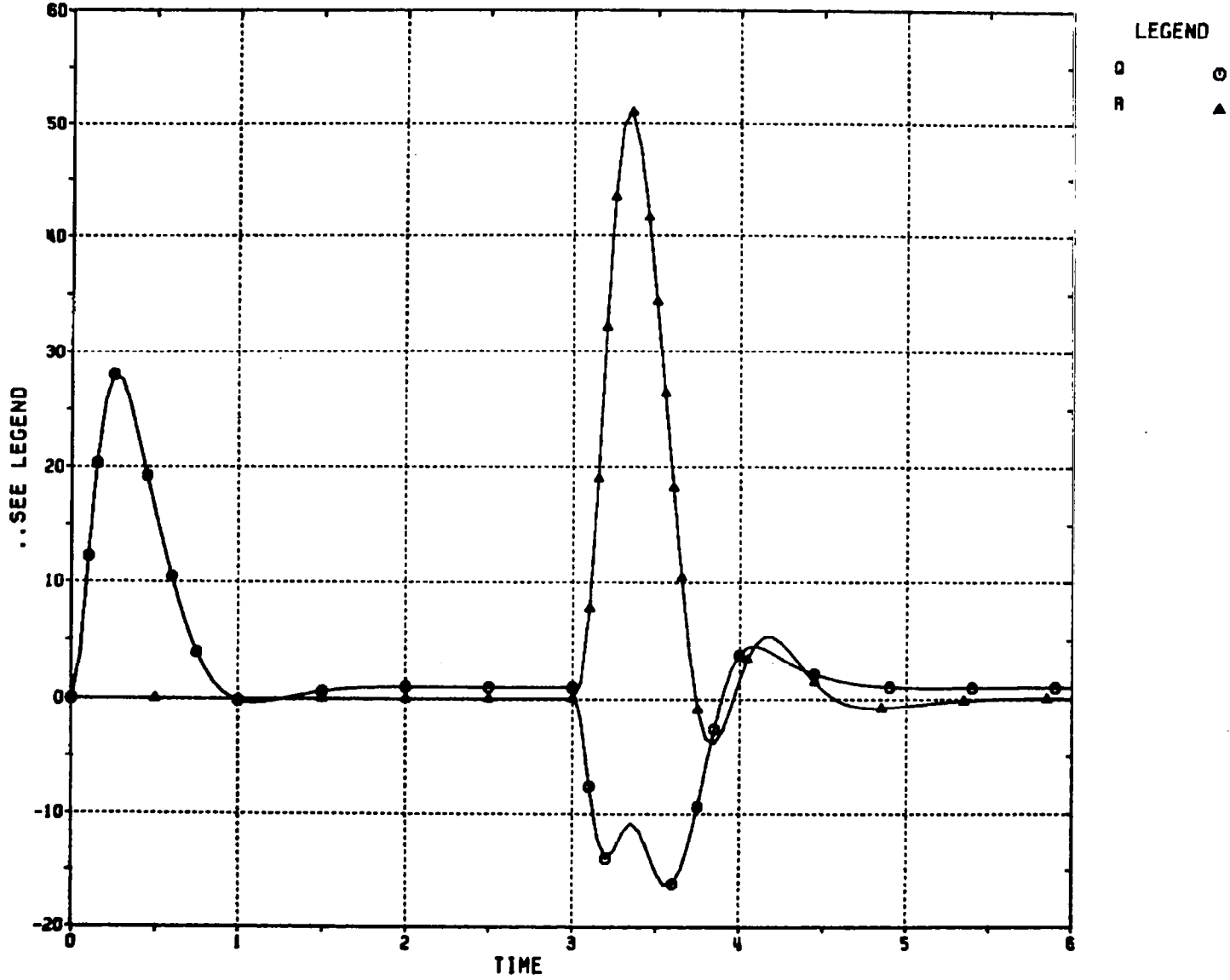

Figure 10.23 BODY ANGULAR RATES VS. TIME (SEC);
CBTT OF CIRCULAR AIRFRAME WITH AUTOPILOT CROSS-COUPLING FOR $C_{\ell_{\delta_Y}}$;
2 GEES (0^o, 180^o)
Q = PITCH (DEG/SEC), R = YAW (DEG/SEC)

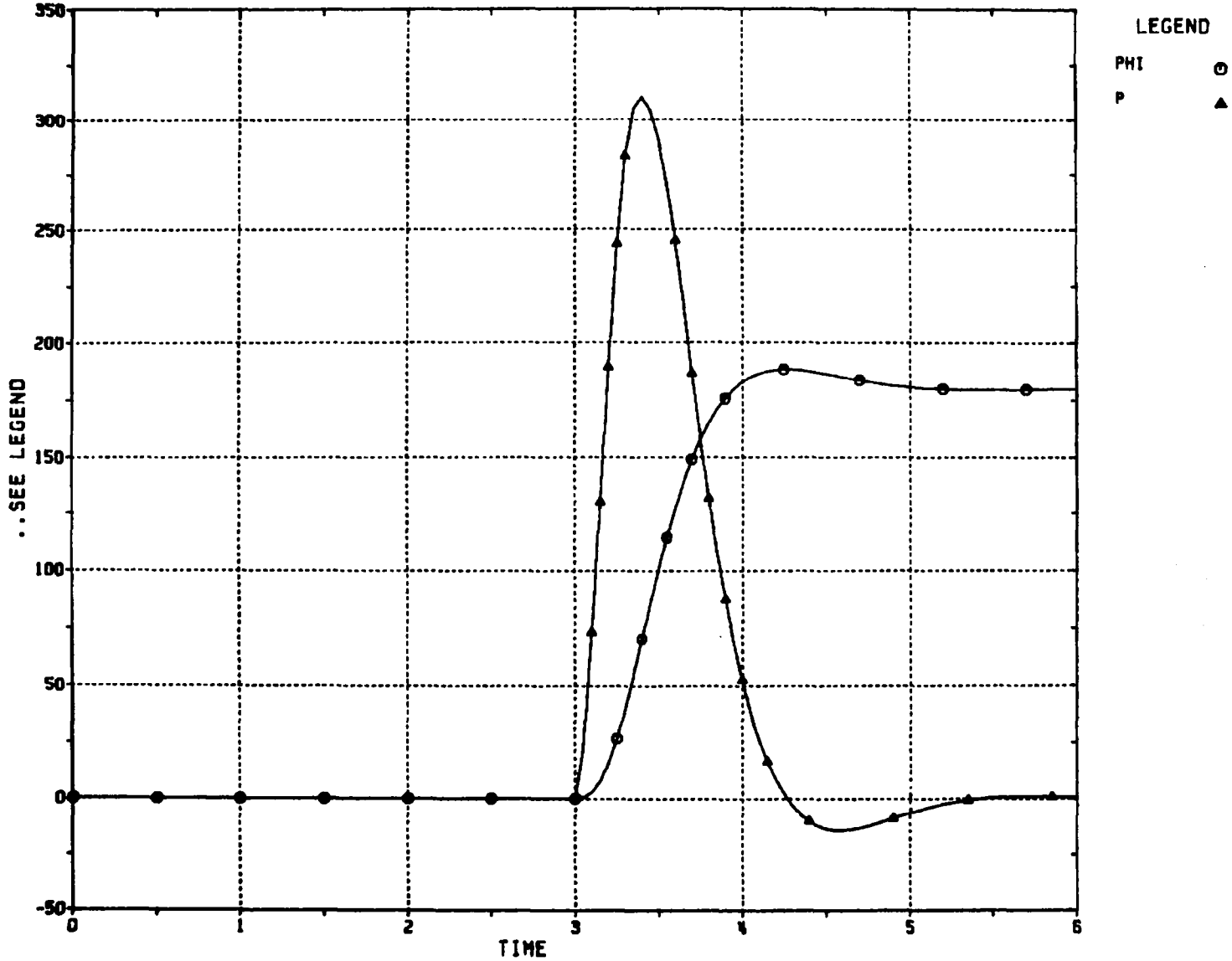

Figure 10.24 ROLL ANGLE AND ANGULAR RATE VS. TIME (SEC);
CBTT OF CIRCULAR AIRFRAME WITH AUTOPILOT CROSS-COUPLING FOR $C_{\ell_{\delta_Y}}$;
2 GEES (0^o, 180^o)
PHI = ROLL ANGLE (DEG), P = ROLL ANGULAR RATE (DEG/SEC)

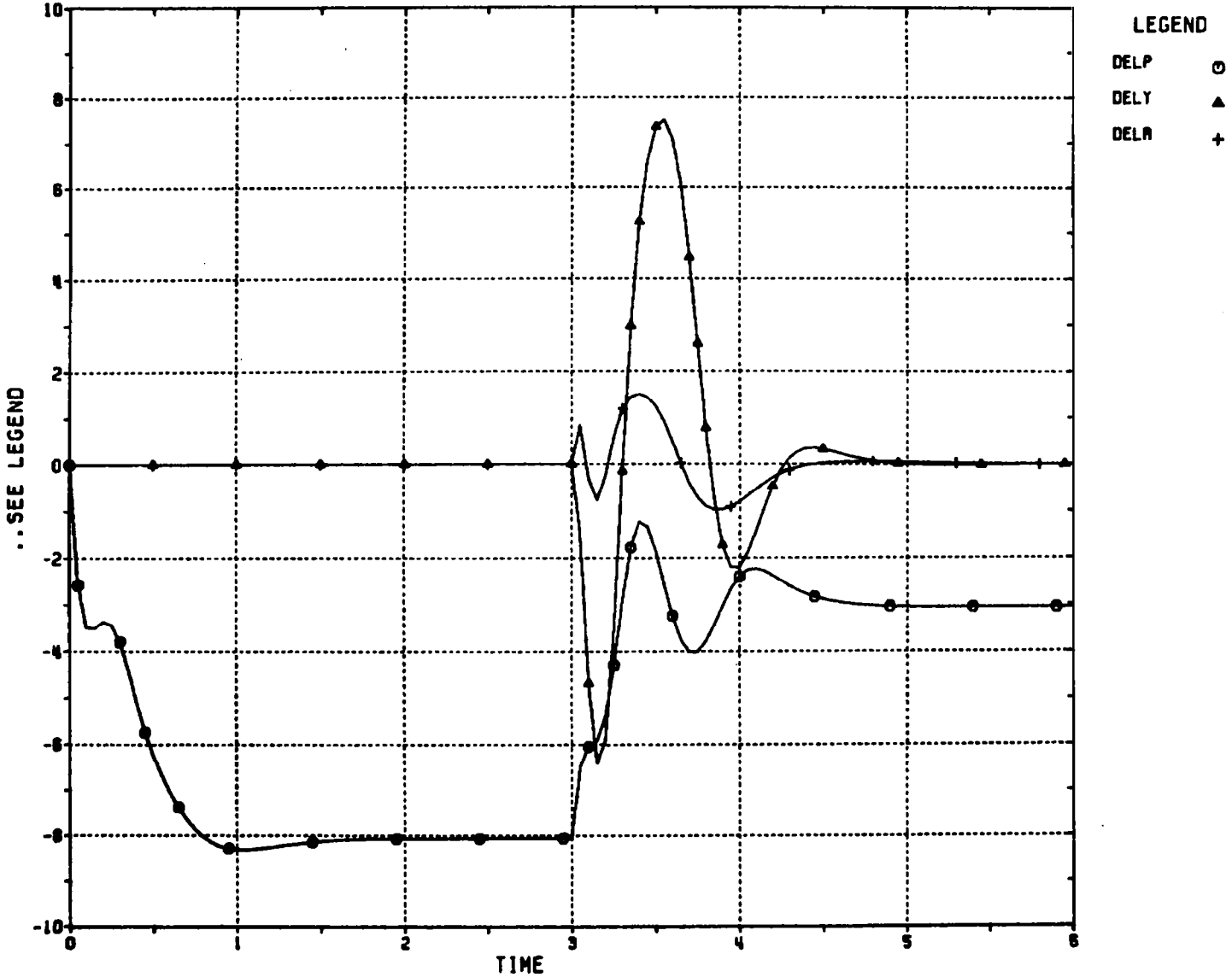

Figure 10.25 TAIL INCIDENCES;
CBTT OF CIRCULAR AIRFRAME WITH AUTOPILOT CROSS-COUPLING FOR $C_{\ell_{\delta_Y}}$;
2 GEES (0°, 180°)
DELP = PITCH (DEG), DELY = YAW (DEG), DELR = ROLL (DEG)

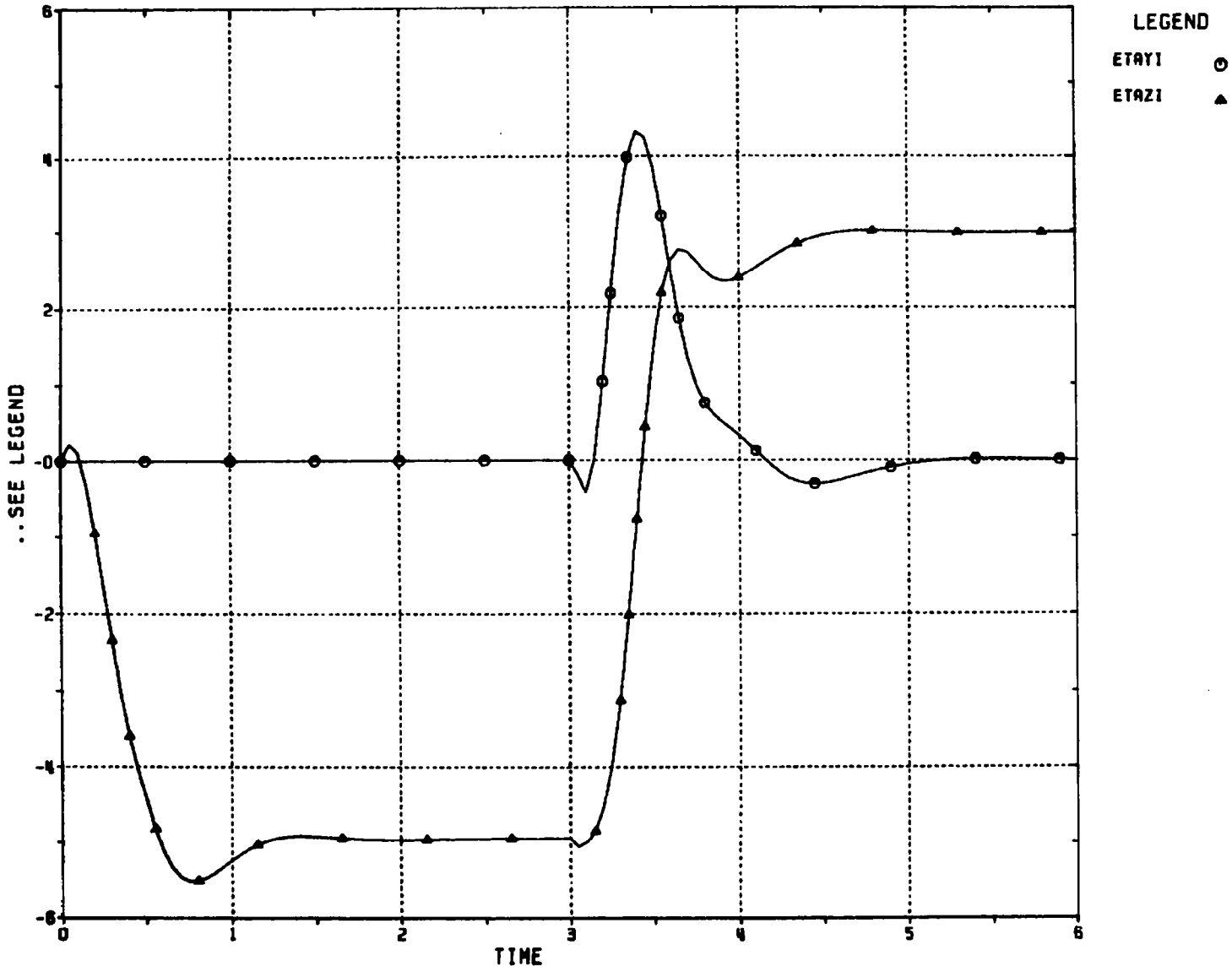

Figure 10.26 ACHIEVED INERTIAL ACCELERATIONS VS. TIME (SEC);
CBTT OF CIRCULAR AIRFRAME; AERODYNAMIC CROSS-COUPLING REMOVED, K_{YP} = 1.0;
4 GEES (0^{o}, 180^{o})
ETAYI = CROSS-PLANE (GEES), ETAZI = MANEUVER PLANE (GEES)

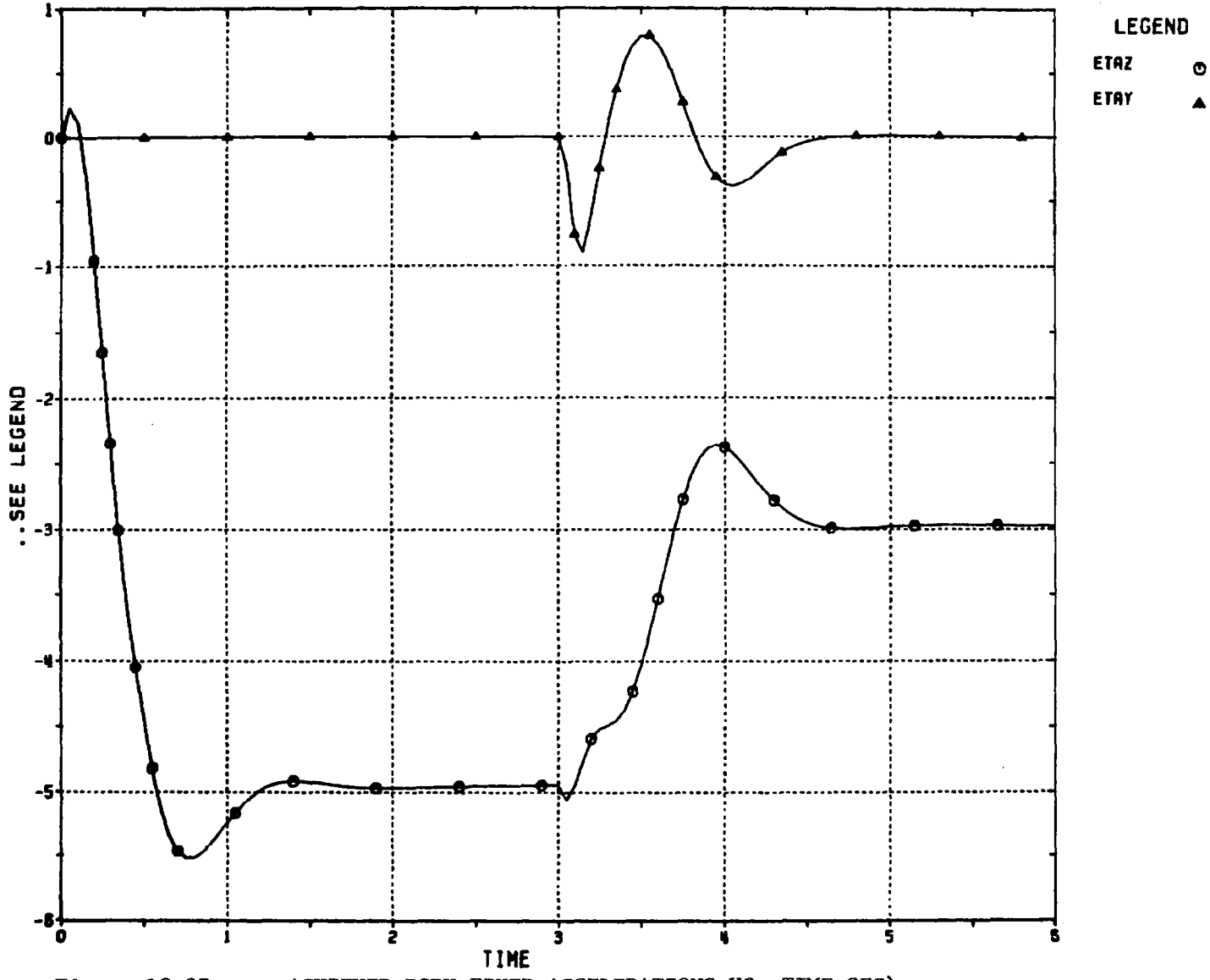

Figure 10.27 ACHIEVED BODY-FIXED ACCELERATIONS VS. TIME SEC);
CBTT OF CIRCULAR AIRFRAME; AERODYNAMIC CROSS-COUPLING REMOVED, K_{YP} = 1.0;
4 GEES (0^{o}, 180^{o})
ETAY = YAW (GEES), ETAZ = PITCH (GEES)

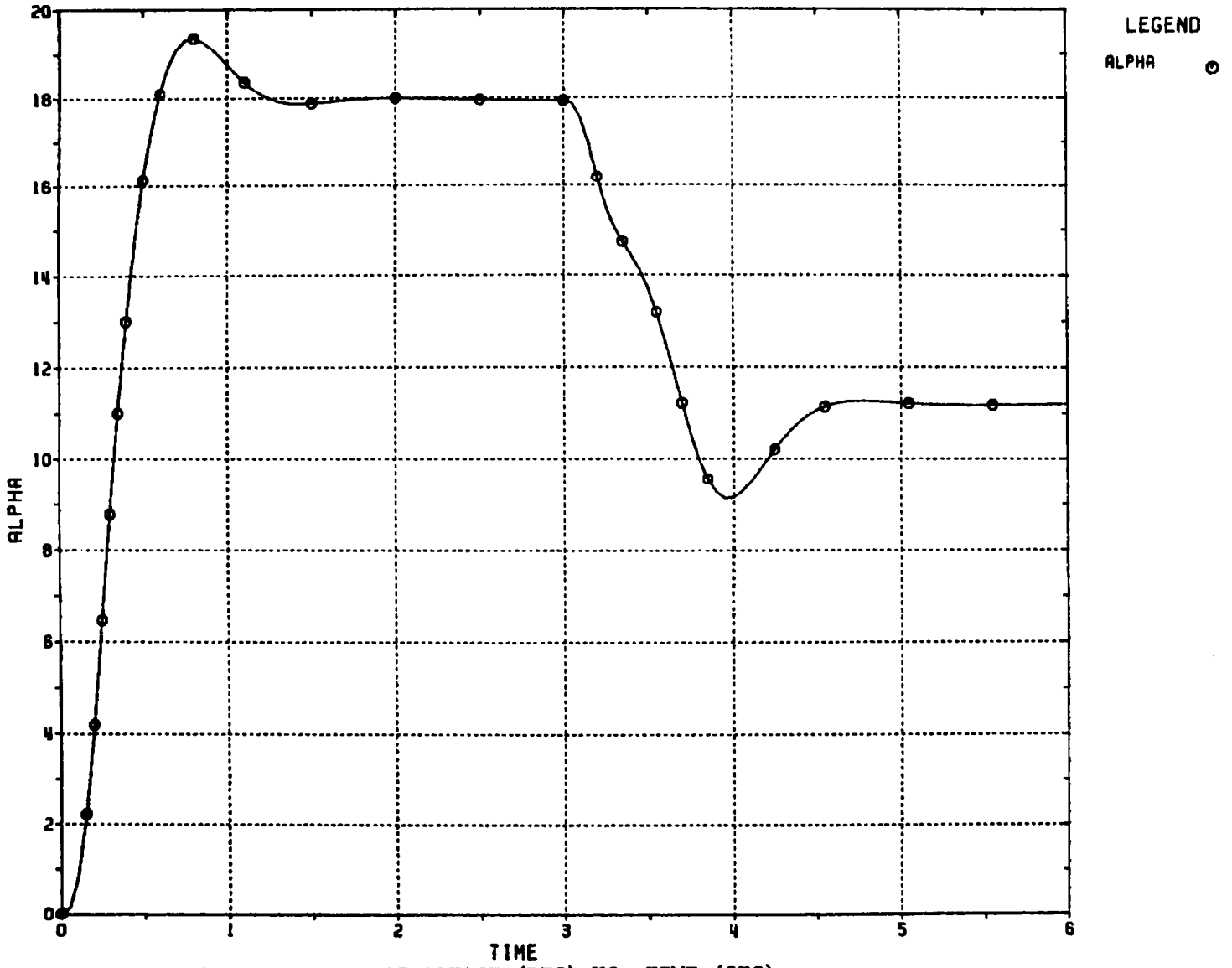

Figure 10.28 ANGLE OF ATTACK (DEG) VS. TIME (SEC);
CBTT OF CIRCULAR AIRFRAME;
AERODYNAMIC CROSS-COUPLING REMOVED, K_{YP} = 1.0;
4 GEES (0^{o}, 180^{o})

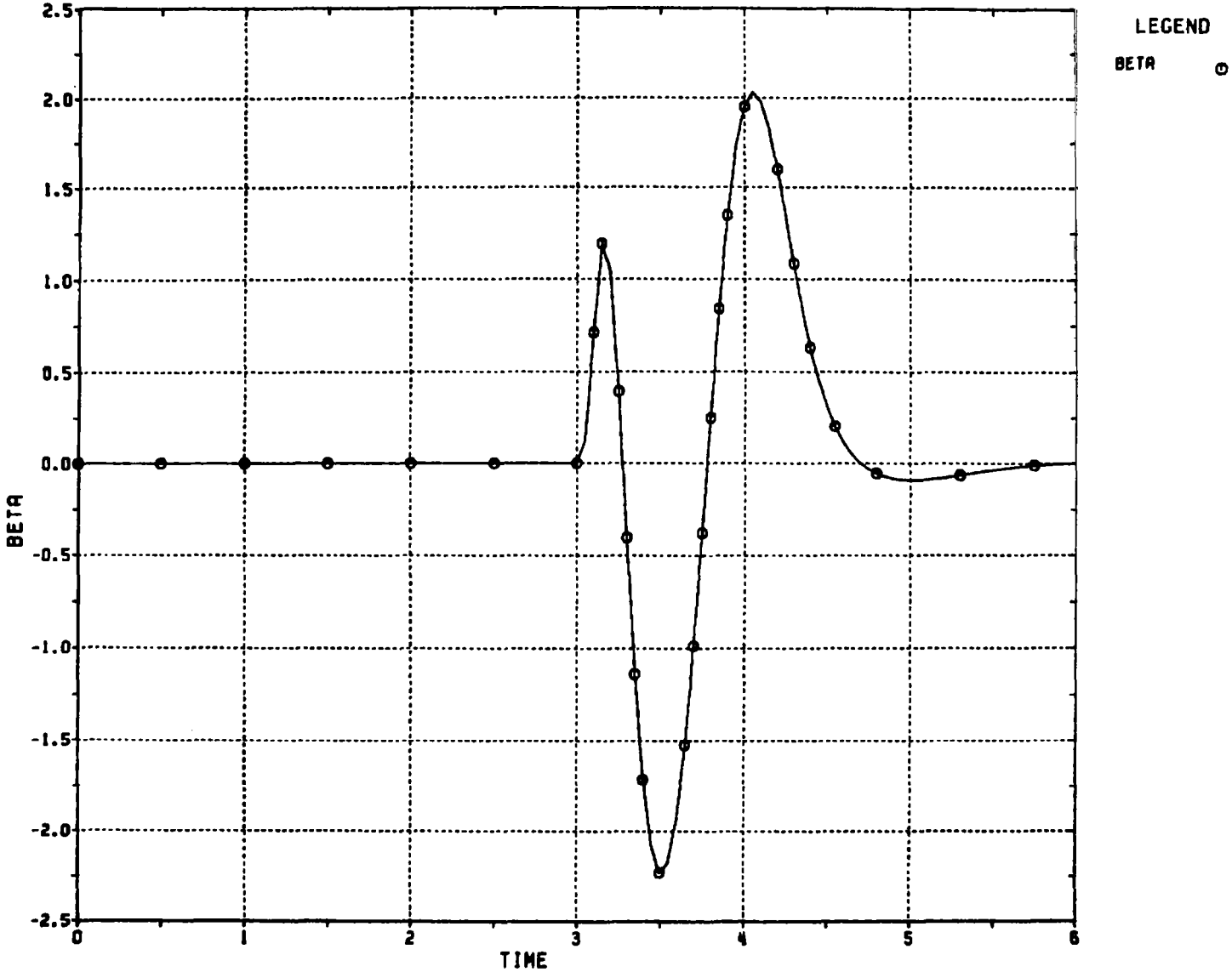

Figure 10.29 SIDESLIP ANGLE (DEG) VS. TIME (SEC);
CBTT OF CIRCULAR AIRFRAME;
AERODYNAMIC CROSS-COUPLING REMOVED, $K_{YP} = 1.0$;
4 GEES (0^{o}, 180)

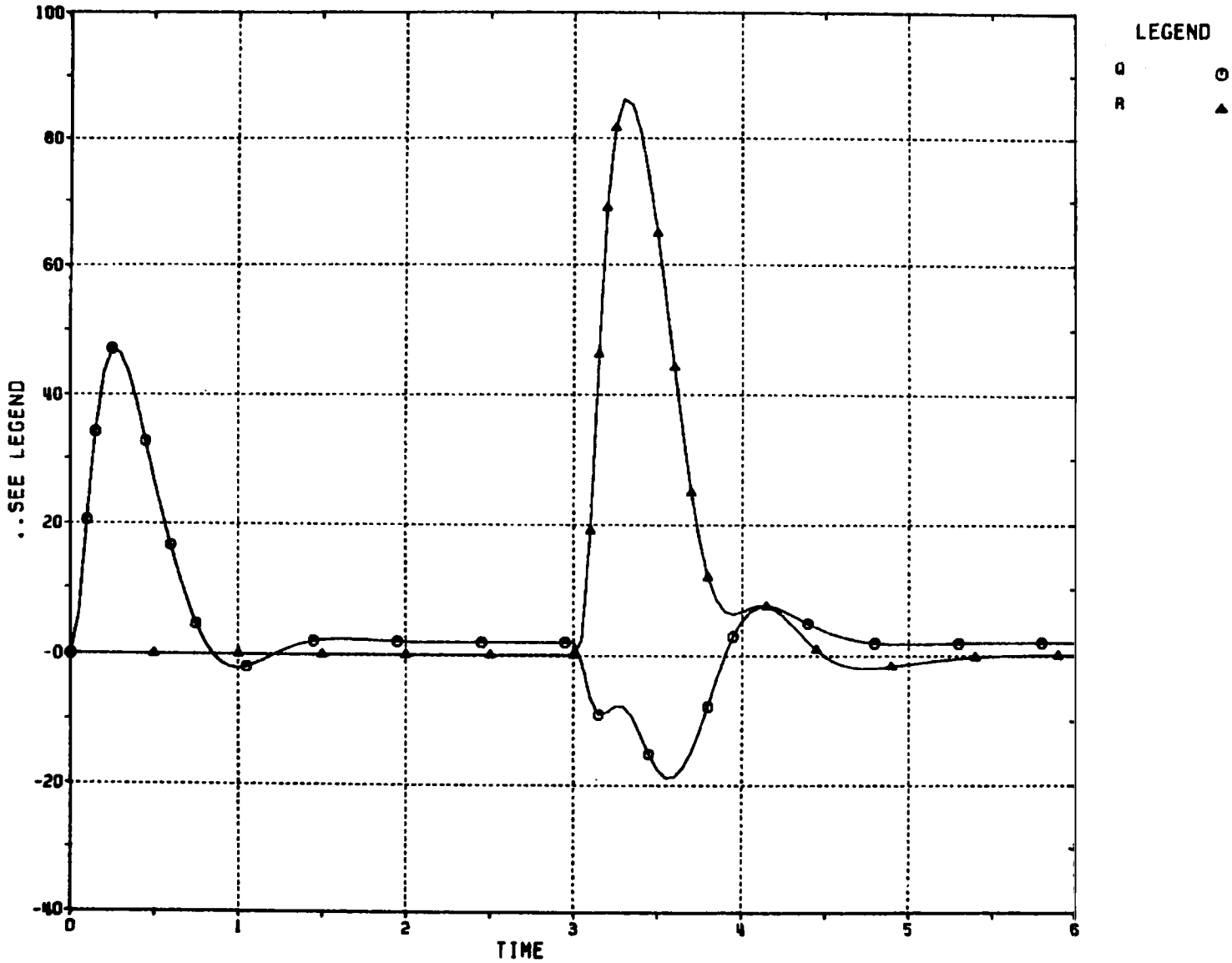

Figure 10.30 BODY ANGULAR RATES VS. TIME (SEC);
CBTT OF CIRCULAR AIRFRAME;
AERODYNAMIC CROSS-COUPLING REMOVED, K_{YP} = 1.0;
4 GEES (0^{o}, 180^{o})
Q = PITCH (DEG/SEC), R = YAW (DEG/SEC)

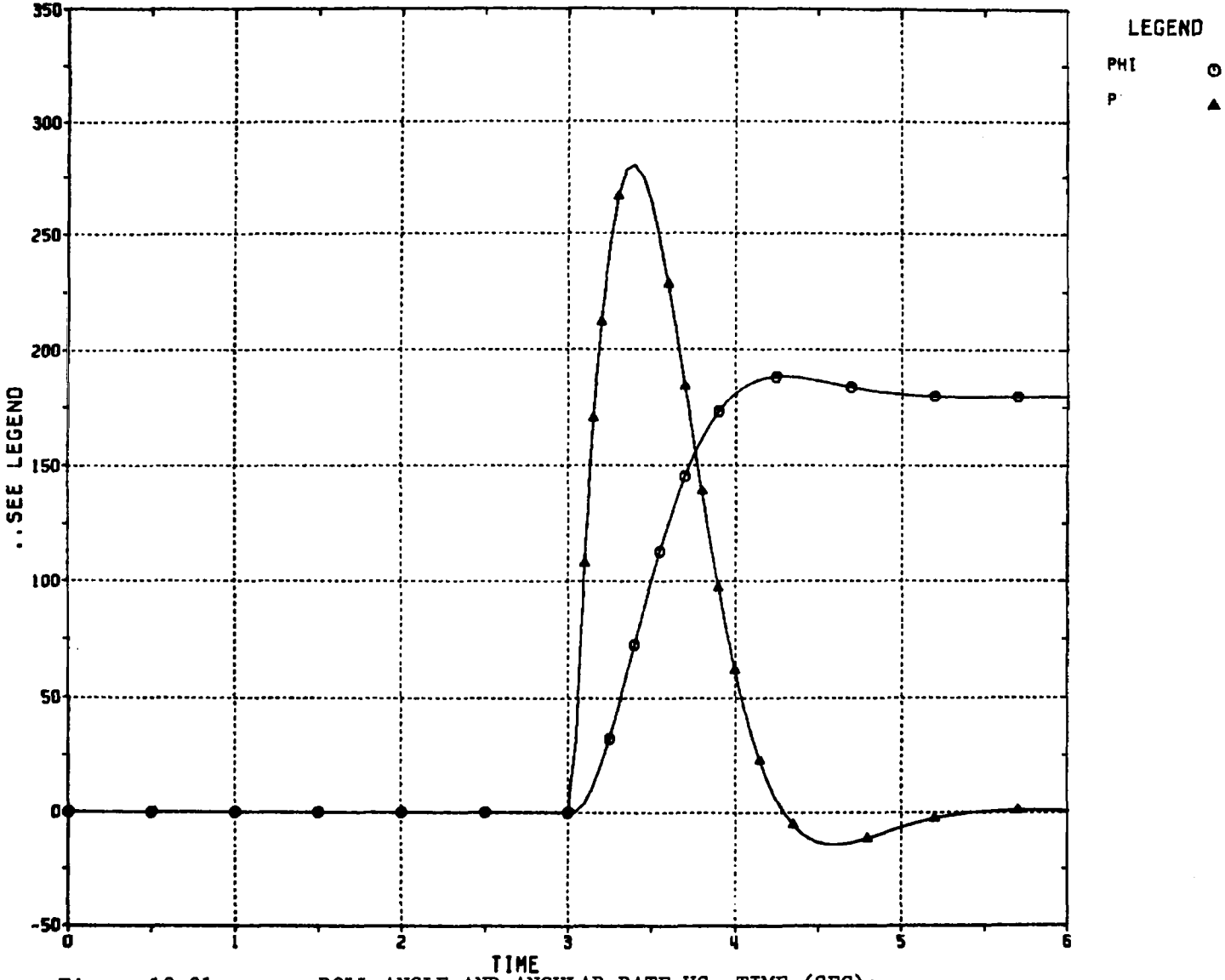

Figure 10.31 ROLL ANGLE AND ANGULAR RATE VS. TIME (SEC);
CBTT OF CIRCULAR AIRFRAME;
AERODYNAMIC CROSS-COUPLING REMOVED, $K_{YP} = 1.0$;
4 GEES (0^{o}, 180^{o})
PHI - ROLL ANGLE (DEG), P = ROLL ANGULAR RATE (DEG/SEC)

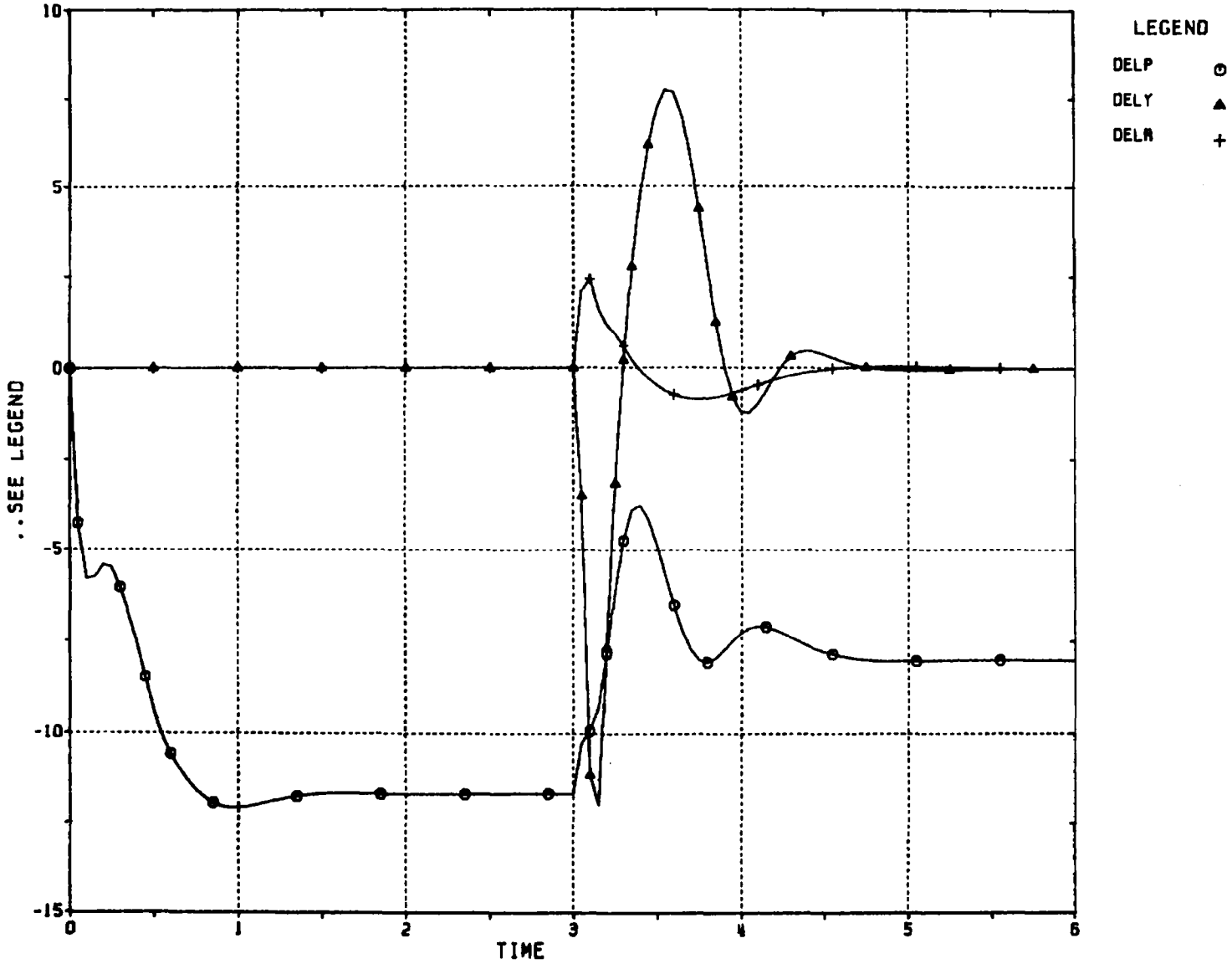

Figure 10.32 TAIL INCIDENCES VS. TIME (SEC);
CBTT OF CIRCULAR AIRFRAME;
AERODYNAMIC CROSS-COUPLING REMOVED, K_{YP} = 1.0;
4 GEES (0^{o}, 180^{o})
DELP = PITCH (DEG), DELY = YAW (DEG), DELR = ROLL (DEG)

11 CONCLUSIONS AND RECOMMENDATIONS

The conclusions that follow are based on a single representative flight condition (Mach 3.95 and 60K ft altitude) with moderate maneuver requirements and should be regarded as guidance in the design of CBTT autopilots.

Performance of coordinated bank-to-turn (CBTT) autopilots is limited by aerodynamic, kinematic, and inertial cross-coupling. To improve such performance by aerodynamic configuration changes or autopilot control law techniques will require minimizing the effects of these couplings.

Analysis of the CBTT performance of the circular and elliptical planar airframes has revealed desirable aerodynamic properties for an efficient CBTT autopilot (i.e., small control surface effort, small sideslip, high relative autopilot stability for a required acceleration response in the desired maneuver plane). Sections 11.1 and 11.2 contain the conclusions pertaining to desirable aerodynamic properties. Section 11.3 covers kinematic and inertial cross-coupling. Section 11.4 covers the CBTT autopilot. Section 11.5 contains recommendations.

11.1 Desired In-Channel Aerodynamics For CBTT Control

11.1.1 Force Derivatives

Large yaw force derivative C_{Y_β} is desirable to simplify design of rapidly responding yaw autopilot by increasing the zeros in the η_y/δ_Y transfer function (Sections E.1, 4.1.2).

Large pitch force derivative C_{N_α} is desirable in that a smaller angle-of-attack is required for a given maneuver which decreases coordination commands (Sections 7.1, 8.1) and may result in

less severe aerodynamic cross-coupling (Section 4.1.1). In addition, large C_{N_α} simplifies the design of a rapidly responding yaw autopilot by increasing the zeros in the n_z/δ_P transfer function (Sections D.1, 4.1.1, 8.2, 9.1).

11.1.2 Control Derivatives

Large control derivatives $C_{\ell_{\delta_R}}$, $C_{n_{\delta_Y}}$, $C_{m_{\delta_P}}$ are desirable to reduce control effort and aerodynamic cross-coupling effects (Sections D.1, E.1, F.1, 4, 11.2).

11.1.3 Stability Derivatives

Neutral yaw stability ($C_{n_\beta} = 0$) vs stable yaw ($C_{n_\beta} > 0$) for reducing yaw control required for coordination is still an issue. The yaw stability of the elliptical airframe was not sufficient to influence significantly the sideslip control (Sections E.1, 10.2).

Neutral pitch stability($C_{m_\alpha} = 0$) is desirable in that it requires less pitch control (Section 4.1.1, D.1) but the effects of kinematic and inertial cross-coupling must be reduced entirely by control surfaces. Large pitch stability helps to attenuate the effects of kinematic and inertial coupling at the expense of increased pitch control (Sections D.1, 4.2).

11.2 Desired Aerodynamic Cross-Coupling For CBTT Control

Maximum attenuation is desired for the induced rolling moment coefficient due to yaw control ($C_{\ell_{\delta_Y}} = 0$ or $C_{\ell_{\delta_Y}}/C_{\ell_{\delta_R}}$ small). $C_{\ell_{\delta_Y}}$ is the

critical cross-coupling parameter for autopilot stability in the coordination branch (Section 10.1). It is less critical for the elliptical airframe at the expense of increased roll incidence (Section 10.2). The autopilot for the circular airframe requires more complex changes to insure stability, such as modification to the roll control law or autopilot cross-coupling (Sections 10.2, 10.3).

Increased stability in roll ($C_{\ell_\beta} < 0$) has robust stability properties for a CBTT autopilot (Section 7.4). In addition, negative C_{ℓ_β} is helpful in reducing transients in the maneuver plane acceleration response resulting from kinematic and inertial cross-coupling between pitch and yaw channels through roll rate (Section 8.3). However, increased stability in roll requires more roll control effort to achieve the desired roll rate.

Induced yaw moment due to roll control $C_{n_{\delta_R}}$ was not a limiting factor for sideslip control or autopilot stability for the angles-of-attack which were studied (Section 7.4).

11.3 Kinematic and Inertial Cross-Coupling

1. Transients in maneuver plane acceleration are caused by kinematic and inertial coupling between pitch and yaw dynamics through missile roll rate. Transients are in the form of overshoots and undershoots (Sections 8.4, 10.2, 10.3) which are less pronounced at higher acceleration levels (Sections 8.5 and 10.4). Transients may also result in a slower maneuver plane acceleration response (Section 8.2).

2. Coupling transients may be reduced by increasing pitch stability (Section 4.2), by the techniques listed in Section 8.6, and by increasing pitch channel speed of response (Section 9.2).

11.4 CBTT Autopilot

1. Nonlinear 3-D studies of the autopilot verified the basic results on stability and sideslip control found in the linear studies.

2. Autopilot stability is only slightly sensitive to roll rate (Section 7.3.4). Aerodynamic cross-coupling sensitivity increases with roll rate (Section 7.4).

3. The magnitude of sideslip can be minimized by commanding yaw angular rate to be equal to kinematic cross-coupling α p (i.e., coordination gain K_{YP} equal to unity (Section 7.2.1)). For any given K_{YP} value the magnitude of sideslip is not sensitive to aerodynamic cross-coupling (Sections 7.2.1, 8.3).

4. Maneuver plane response, which is the combined result of body-fixed pitch and yaw accelerations and roll angle, may have a response which is not evident from the responses of its component parts (Section 8.2).

5. The CBTT autopilot of the elliptical airframe has achieved less than the required 0.5 second speed of response for maneuver plane acceleration. Acceptable sideslip, missile body angular rates and control surface rates and incidences were obtained for the commands applied (Sections 8.6, 8.2).

6. The CBTT autopilot of the circular airframe may achieve less than the required 0.5 second speed of response for maneuver plane acceleration; and acceptable sideslip, missile body angular rates and incidences for commands applied; however, additional autopilot complexity is required (Sections 10.2, 10.3).

11.5 Recommendations

1. Further analyses of CBTT control should be made for a broad range of dynamic pressures (Mach number and altitude conditions). Lower dynamic pressures, requiring higher angles-of-attack to achieve desired maneuvers, may make sideslip control more difficult and intensify the effect of aerodynamic cross-coupling on autopilot stability. Higher dynamic pressures will result in higher missile angular rates and thus intensify the effects of kinematic and inertial coupling. To compensate for these effects, one might consider slower responses in roll attitude and pitch acceleration at low dynamic pressures and a change in control to limited bank-to-turn (LBTT) at high dynamic pressures.

2. The effect of requirements for inertial and kinematic coupling transients in the maneuver plane acceleration due to step functions applied in autopilot design studies must be assessed in guidance level studies.

3. To decrease kinematic and inertial cross-coupling effects, future autopilot studies should consider feedbacks of both angle-of-attack and rate of angle-of-attack for the pitch autopilot, which would have the effect of increasing the pitch stability C_{m_α}. Another possibility is to increase the pitch and yaw bandwidths via increase in acceleration error gains while maintaining or relieving the high frequency attenuation requirement in the actuator command branches.

4. Optimal control design techniques may reduce the time required and/or reveal simpler autopilot control laws for achieving desired stability and performance results and should therefore be investigated.

Appendix A. Missile Sizing and Mass Properties - L. L. Cronvich

In order to provide a realistic missile based on the configuration concepts tested aerodynamically in Ref. 5, the models were assumed to be 1/6-scale so that the full missile lengths were 168 in. The maximum diameter of the circular body, whose fineness ratio is 7:1, then becomes 24 in. For the elliptical body the maximum major and minor axes become 41.57 in. and 13.86 in., respectively.

In both cases the center-of-gravity for the investigation was taken to be at 0.6 body length from the nose, or 100.8 in. from the nose.

Since the main purpose of the study was to compare the capabilities of the two configurations to perform with bank-to-turn steering policies, no effort was expended on a detailed design of missile components. Instead mass properties were developed corresponding to mass distribution which might be expected for missiles of this size. These properties are presented in Table A-1.

TABLE A-1

Geometric and Mass Properties of Missile Configurations

	Circular	Elliptical
Weight (lbs.)	2525	2475
I_{xx} (Slug Ft^2)	40	110
I_{yy} (Slug Ft^2)	804	790
I_{zz} (Slug Ft^2)	810	853
Length (in.), ℓ	168	168
Center of Gravity Distance from Nose (in.)	100.8 (0.6 ℓ)	100.8 (0.6 ℓ)
Max. Diameter (in.)	24	
Max. Major Axis (in.)		41.57
Max. Minor Axis (in.)		13.86

Appendix B. Aerodynamic Data (Non-Linear Representation) - L. L. Cronvich

Source of Data and Their Application

The aerodynamic data were extracted from Ref. 5. The entire study was conducted at M = 3.95. The aerodynamic coefficients are defined in Section 3 and are based on a body-fixed axis system of Fig. 5.1. Note that the sign conventions chosen for the control surface deflections differ from those given in the Ref. 5. The reference length and area for the coefficients are 2 ft and π ft^2, respectively, which correspond to maximum diameter and cross-sectional area of the circular body.

For reference, the normal force and pitching moment curves of Ref. 5 at M = 3.95 have been reproduced in Figs. B.1 and B.2 for the two configurations. The aerodynamic derivatives of C_Y, C_n, and C_ℓ with respect to sideslip angle β, yaw control δ_Y, and roll control δ_R are presented in Figs. B.3, B.4, and B.5 as they were used in the computer simulation, namely, as piecewise linear segments for ease in interpolation.

A unique feature of the control surfaces (which were identical for both configurations) should be noted as described in Ref. 5: "In order for tail deflection to be compatible with the complex surfaces of the after-body of the elliptical configuration, the tail hinge line was skewed such that a 10^o deflection measured at the body-tail juncture had a resultant 7.04^o surface deflection". Thus one might expect control derivatives for the elliptical configuration (which were based on the 10^o rotation of the hinge line) to be lower than those obtained for the circular configuration and more in proportion to the actual surface deflection. In turn, this geometrical effect may result in apparently larger surface deflections to achieve desired control.

It should also be noted that data for the effect of pitch control on the β-derivatives was not available and was not included in the study.

Character of the Data at M = 3.95

The normal force generated by the elliptical configuration is about 30% higher than that generated by the circular configuration at the same angle of attack. Thus for the same called-for normal force the elliptical

configuration will operate at a smaller angle of attack. Furthermore, since the elliptical configuration is nearly neutrally stable in pitch and the circular configuration is stable the difference in trim angle of attack will be even greater for the same maneuver and thus the circular configuration may be subject to slightly more severe aerodynamic coupling among the pitch, yaw, and roll modes of motion than the elliptical configuration.

The control parameters are not too greatly different for the same true panel deflection but are nearly related by a 0.7 factor for the same panel-deflection at the body-tail juncture.

On the other hand, the β-derivatives, C_{n_β} and C_{ℓ_β} are significantly different. The elliptical configuration is approximately half a reference diameter stable in yaw whereas the circular configuration is unstable in yaw. Also the elliptical configuration is a factor of 2 to 3 more stable in roll.

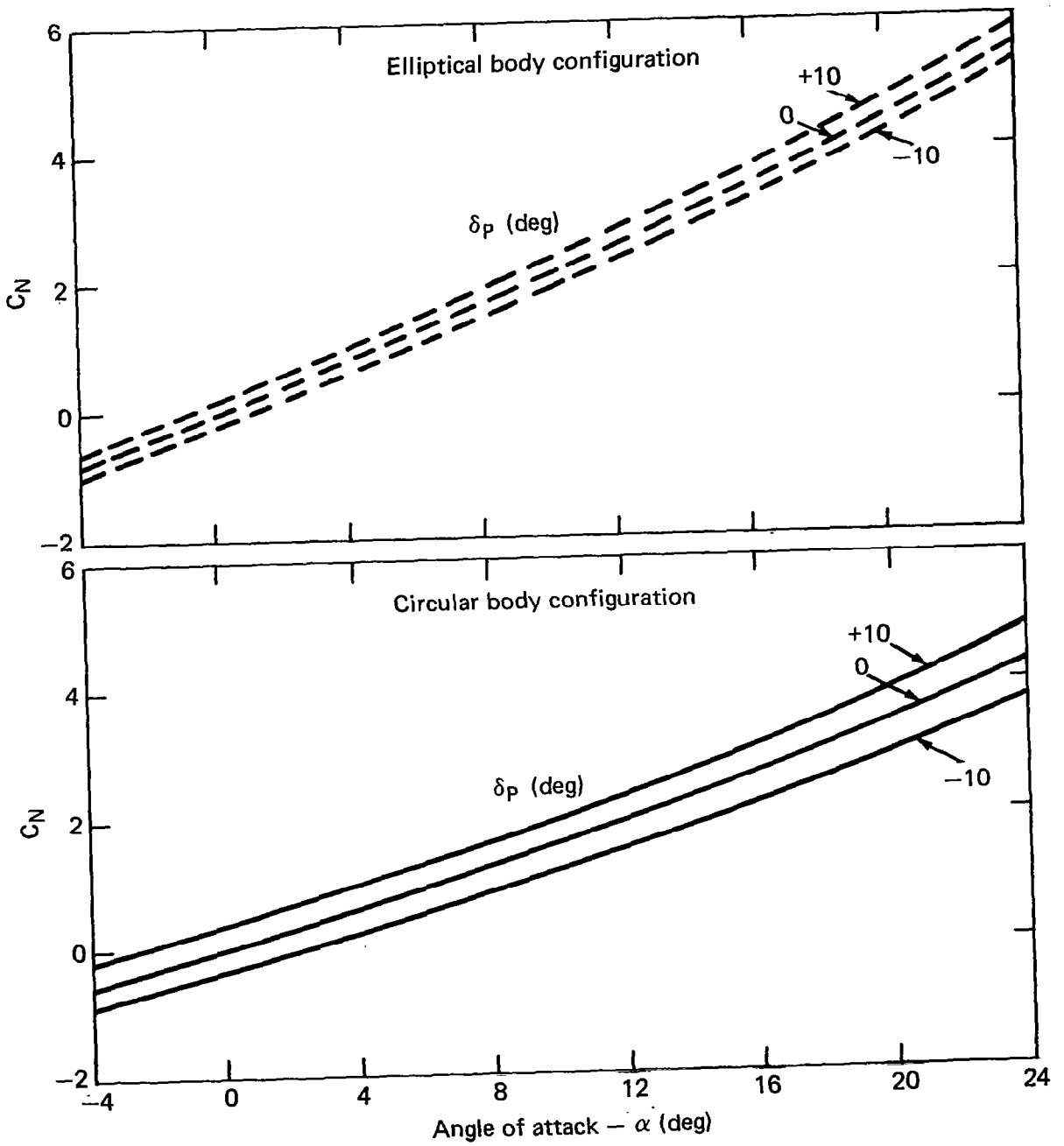

Fig. B.1 Normal force coefficients ~ M = 3.95.

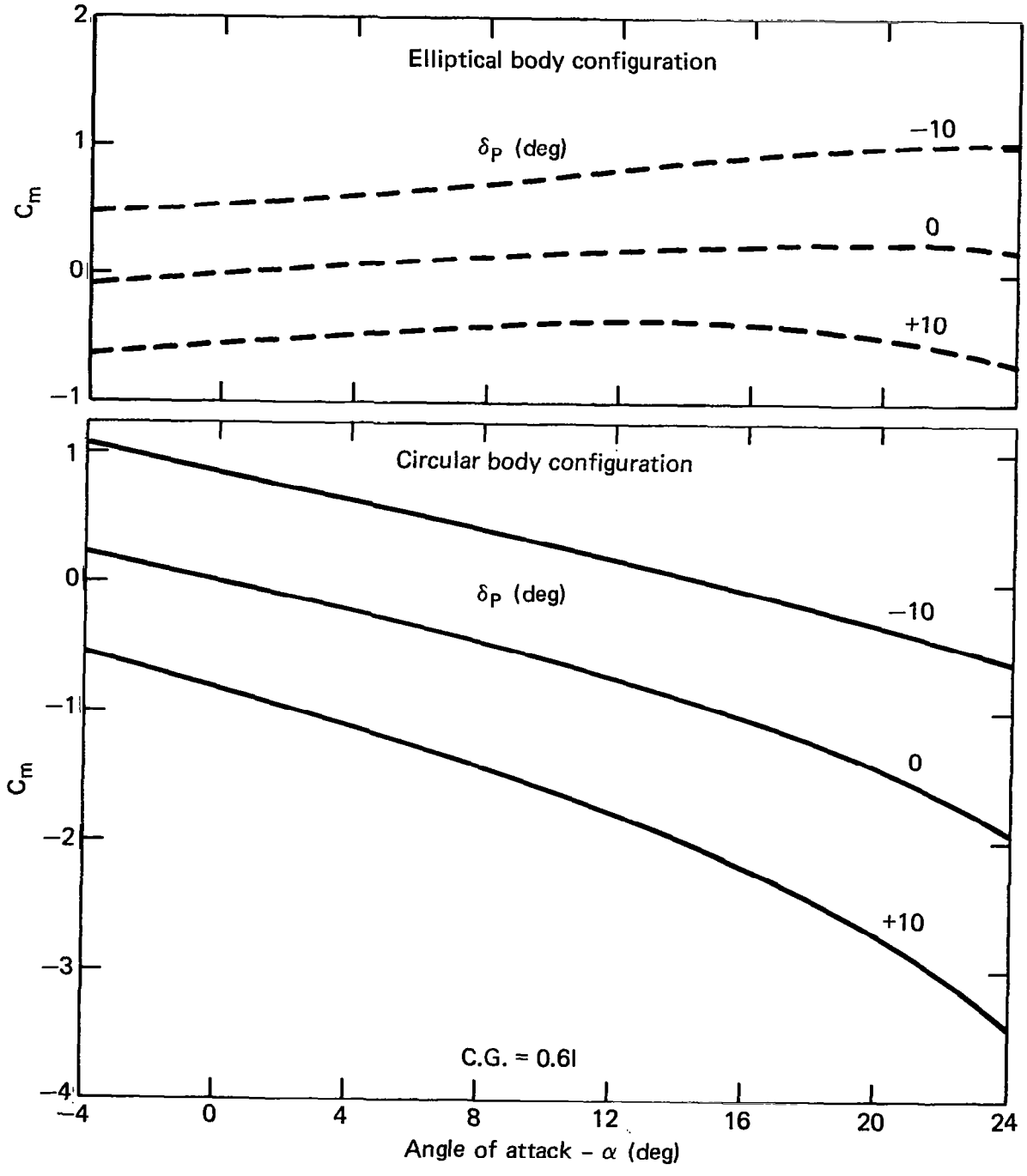

Fig. B.2 Pitching moment coefficients ~ M = 3.95.

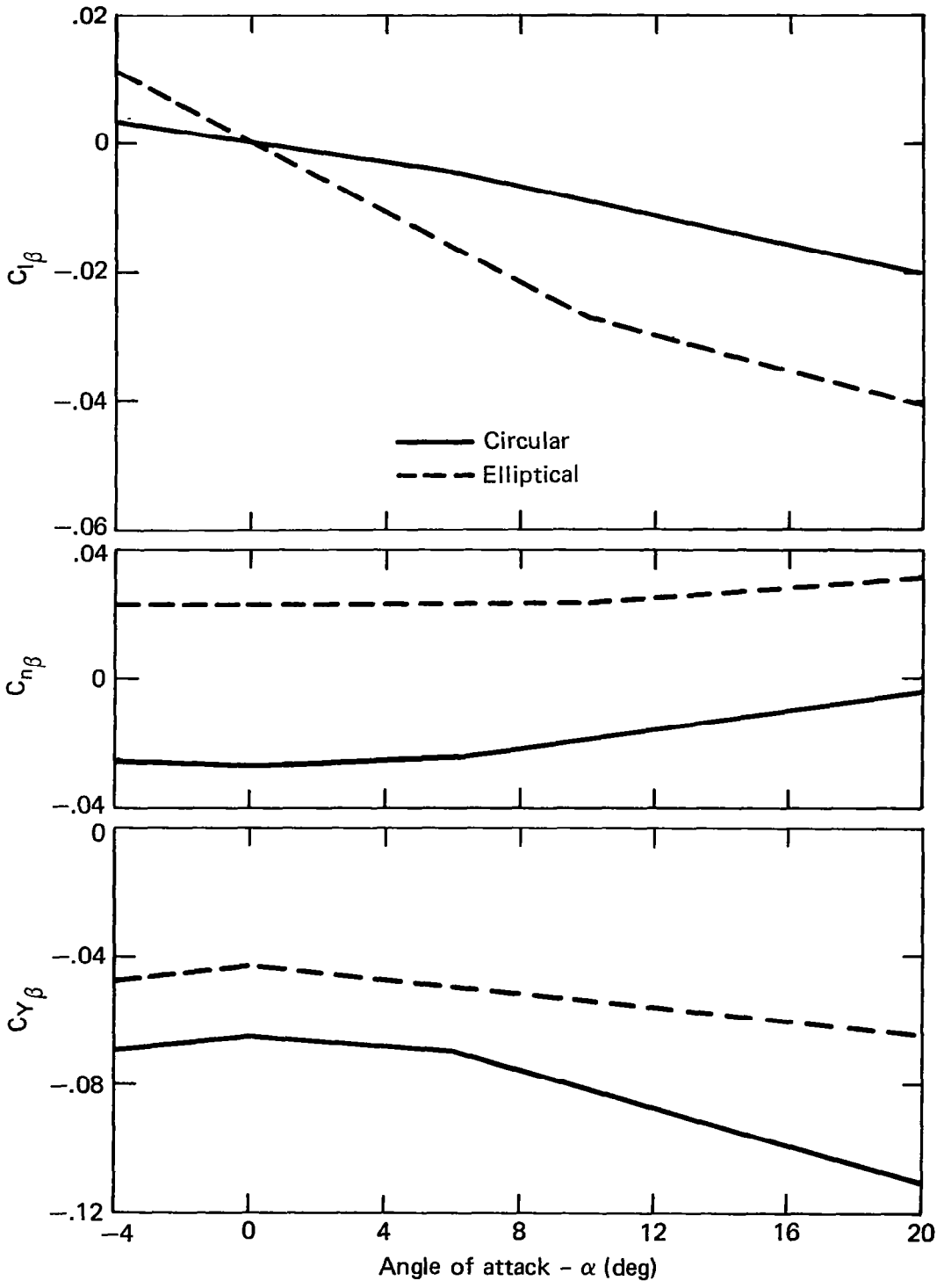

Fig. B.3 Sideslip derivatives.

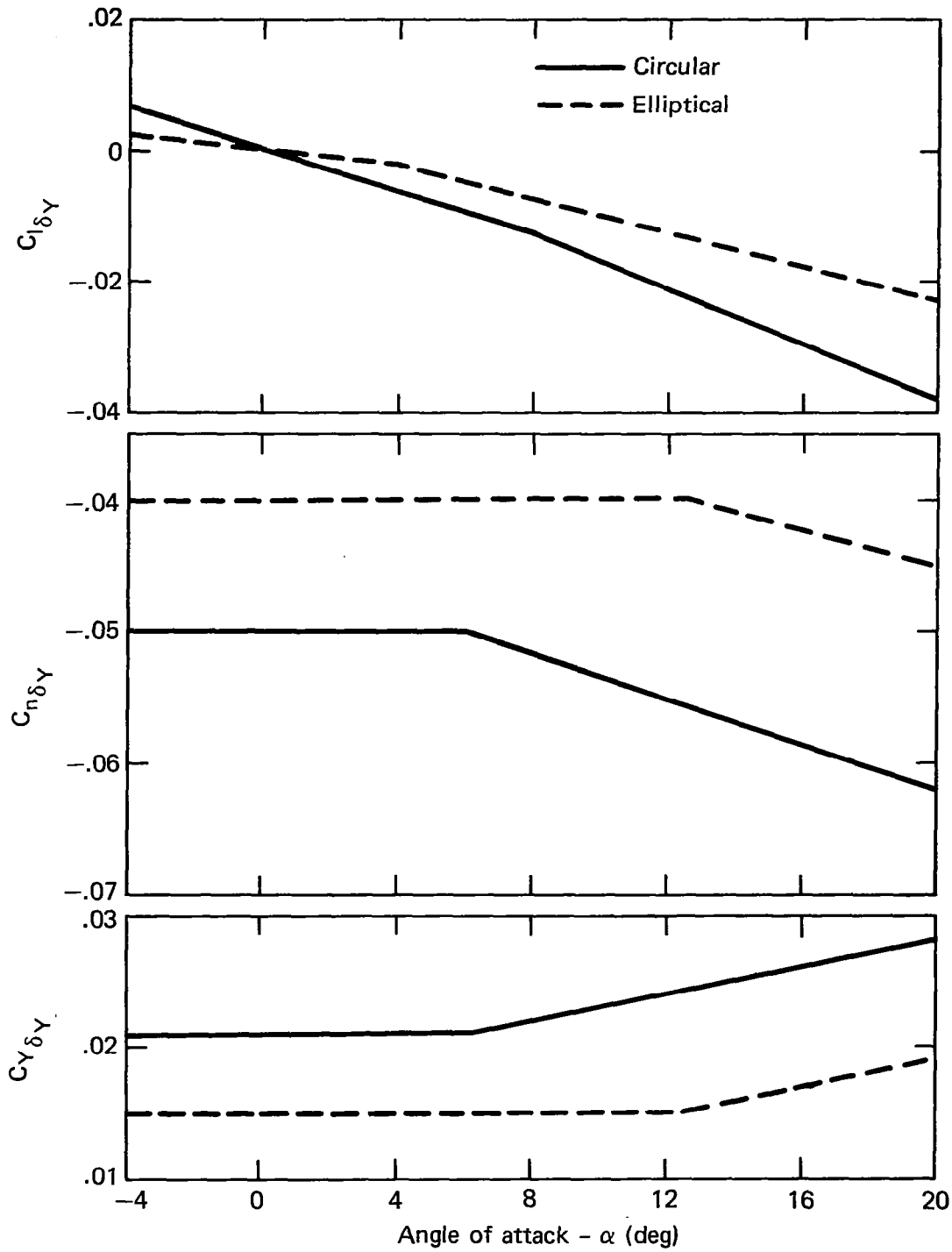

Fig. B.4 Yaw control derivatives.

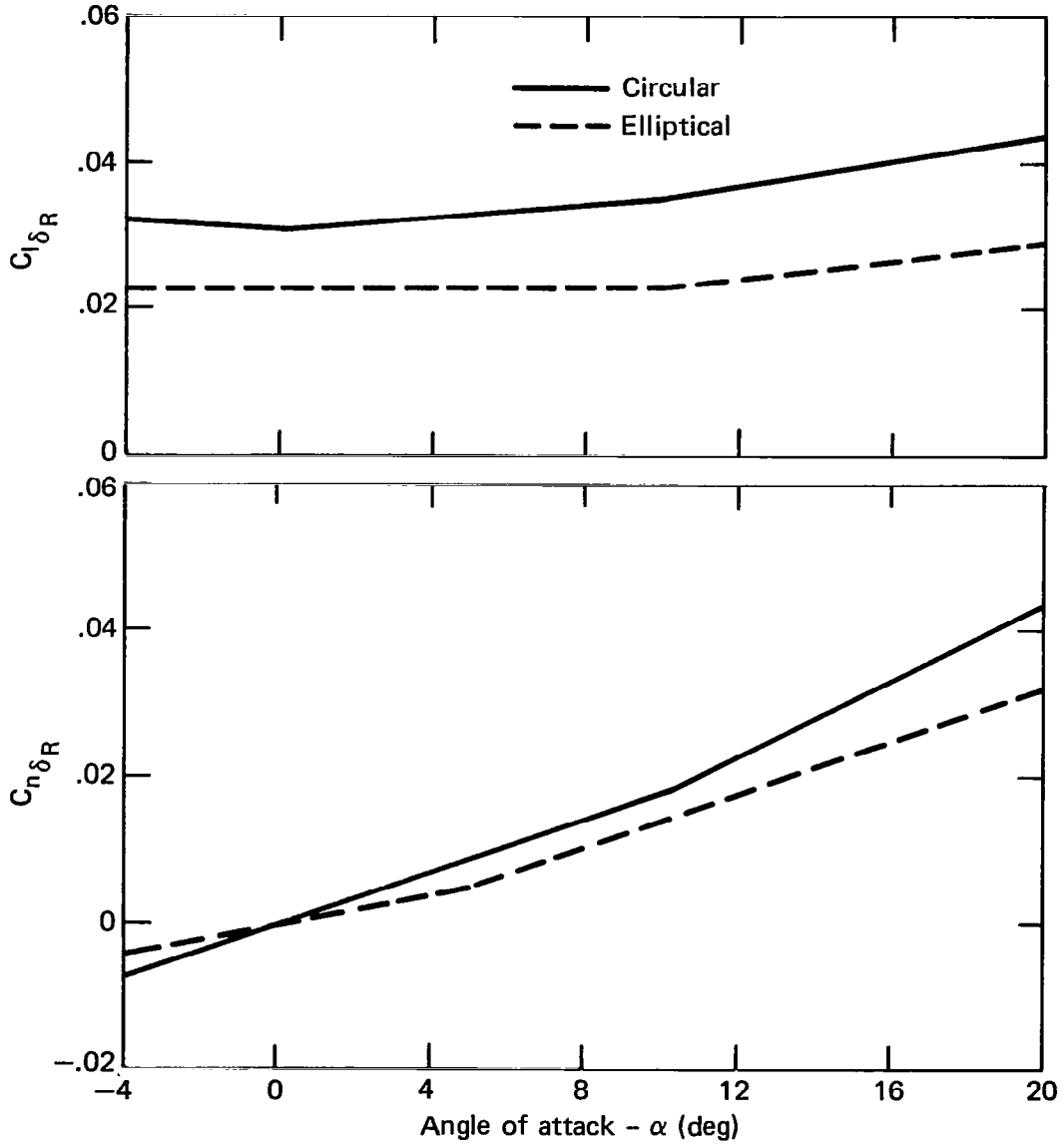

Fig. B.5 Roll control derivatives.

Appendix C. Aerodynamic Data - Linear Approximation - L. L. Cronvich

A linear approach was used in the design and stability analysis of the autopilots of the pitch, yaw, and roll channels, both uncoupled and coupled. Accordingly, a linear approximation of the aerodynamic derivatives at M = 3.95 was provided for each configuration at three angles-of-attack, about which the system could be perturbed. These linearized aerodynamic derivatives are presented in Table C.1.

TABLE C.1

Linearized Aerodynamic Derivatives (M = 3.95)

	Circular			Elliptical		
	$\alpha = 0^o$	$\alpha = 10^o$	$\alpha = 20^o$	$\alpha = 0^o$	$\alpha = 10^o$	$\alpha = 20^o$
C_{Y_β}	- .065	- .082	- .111	- .043	- .054	- .064
C_{n_β}	- .025	- .019	- .003	+ .024	+ .024	+ .032
C_{ℓ_β}	0	- .009	- .020	0	- .027	- .040
$C_{Y_{\delta_Y}}$	+ .021	+ .022	+ .028	+ .016	+ .015	+ .019
$C_{n_{\delta_Y}}$	- .050	- .053	- .062	- .042	- .039	- .045
$C_{\ell_{\delta_Y}}$	0	- .016	- .038	0	- .010	- .023
$C_{Y_{\delta_R}}$	0	- .009	- .022	0	- .006	- .014
$C_{n_{\delta_R}}$	0	+ .018	+ .044	0	+ .014	+ .032
$C_{\ell_{\delta_R}}$	+ .031	+ .035	+ .044	+ .023	+ .023	+ .029
C_{N_α}	+ .15	+ .17	+ .22	+ .18	+ .22	+ .30
$C_{N_{\delta_P}}$	+ .04	+ .04	+ .05	+ .02	+ .02	+ .025
C_{m_α}	- .060	- .065	- .118	+ .015	+ .0137	- .0125
$C_{m_{\delta_P}}$	- .080	- .095	- .115	- .055	- .055	- .075

Reference C.G. at 0.6 ℓ

APPENDIX D

LINEAR DESIGN AND ANALYSIS OF UNCOUPLED PITCH CHANNEL AUTOPILOTS FOR CIRCULAR AND ELLIPTICAL AIRFRAMES

The initial phase in the design of the CBTT autopilots involved the design of individual, uncoupled channels, pitch, yaw, and roll, with prescribed relationships between speeds-of-response which would meet the CBTT requirements when coupled.

The following appendix addresses the linear design and analysis of the uncoupled pitch channel autopilots of the circular and elliptical airframes. A general block diagram of an uncoupled pitch channel autopilot is shown in Figure D.1. A normal acceleration command (η_{z_c}, gees) is applied to the pitch control law which uses measurements of missile body pitch angular rate (q) and pitch normal acceleration (η_z) to determine the required actuator command (δ_{p_c}). The actuator is modeled as a first order lag at 30 Hz. (188.4 rad/sec).[c] The dynamic model is linearized about a trim angle-of-attack as described in Section 5.

The first section of this Appendix uses transfer functions to show what type of aerodynamics is desired for control and to compare the desired results with the circular and elliptical airframe aerodynamics. Section D.2 covers the autopilot design requirements and design technique and presents the pitch control laws. Section D.3 contains a time and frequency domain analysis the results of which serve as a useful comparison with the corresponding results of the coupled system.

D.1 Aerodynamic Transfer Functions

Uncoupled pitch aerodynamic transfer functions are

$$\frac{q}{\delta_P} = \frac{k(AE-BC)}{-C} \frac{\frac{Es}{k(AE-BC)}+1}{\frac{s^2}{-C}+\frac{Ak}{-C}s+1}, \qquad \text{deg/sec/deg} \qquad \text{D1}$$

$$\frac{n_z}{\delta_P} = \frac{AE-BC}{-C} \frac{\frac{B}{AE-BC}s^2+1}{\frac{s^2}{-C}+\frac{Ak}{-C}s+1}, \qquad \text{g's/deg} \qquad \text{D2}$$

$$A = \frac{\bar{q}S}{W} C_{N_\alpha}, \quad B = \frac{\bar{q}S}{W} C_{N_{\delta_p}}, \quad C = \frac{(57.3)\bar{q}Sd}{I_{yy}} C_{m_\alpha}$$

$$E = \frac{(57.3)\bar{q}Sd}{I_{yy}} C_{m_{\delta_p}}, \quad k = \frac{1845}{V}$$

Ideally, minimum control surface effort to achieve a particular acceleration is obtained by a neutrally stable airframe (i.e., $C_{m_\alpha} = 0$). In such a case the transfer functions shown in D1 and D2 reduce to

$$\frac{q}{\delta_P} = \frac{E}{s} \qquad \text{D3}$$

$$\frac{n_z}{\delta_P} = \frac{E}{k} \frac{\frac{B}{AE}s^2+1}{s(\frac{s}{Ak}+1)} \qquad \text{D4}$$

For a neutrally stable airframe D3 and D4 show that it is desirable to maximize A and E to minimize control incidences and increase speed of response. This will in-turn maximize the dc gains of D3 and D4 and move the leads and lag of D4 to higher frequencies. These desirable attributes will

result in the airframe doing most of the work required by the guidance commands and therefore it will be less likely for the control surfaces to be reaching their limits of rate and angle which would cause autopilot stability problems.

Table D.1 compares the uncoupled pitch aerodynamic transfer functions for the circular and elliptical airframes for a flight condition at M = 3.95 and altitude = 60 Kft. The circular airframe is stable for all angles-of-attack. The elliptical airframe is slightly unstable at zero and ten degrees angle-of-attack and becomes slightly stable at twenty degrees. The elliptical airframe transfer functions have a higher dc gain and poles which are located at a lower frequency due mainly to a more neutrally stable airframe. The dc gain in the pitch channel (i.e., (AE-BC)/-C) is directly proportional to pitch control moment $C_{m_{\delta_P}}$ and inversely proportional to magnitude of stability margin in pitch (i.e., $C_{m_\alpha}/C_{N_\alpha}$ or distance from center of pressure to center of gravity). Thus the nearly neutrally stable elliptical airframe is expected to have a higher gain than the stable circular airframe even though its control moment coefficient is slightly smaller. Higher dc gain will require less control surface incidences. The zeros of η_z/δ_P are directly porportional to C_{N_α} and the ratio $C_{m_{\delta_P}}/C_{N_{\delta_P}}$ or the distance from the point of action of tail forces to the center of gravity. Hence, for the elliptical airframe which has larger C_{N_α}, the zeros of η_z/δ_P are located at a higher frequency. Lower control surface incidences and higher frequency η_z/δ_p zeros of the elliptical airframe will simplify the design of a rapidly responding pitch autopilot.

D.2 Design Technique, Requirements and Control Laws

The design technique for all channels was classical, using a combination of Frequency Response and Root Locus techniques, to achieve practical bandwidths and in-turn provide the range of required missile body angular rates and control motions. In addition, the resulting design is

robust ,i.e., for which the influence of aerodynamic variations on response is minimized. Finally, and most important, the design technique has been proven by many missile programs to produce desired results.

Requirements for the classical design technique are:

1. High Frequency Attenuation in Actuator Command Branch

$\geq$ 15 dB at 100 rad/sec and zero angle-of-attack.

This requirement will provide sufficient high frequency attenuation for $\geq$ 30 Hz actuator and for body bending modes when high frequency filters are added. This requirement also limits autopilot speeds of response.

2. Relative Stability

Gain margins $\geq$ 6 dB , phase margins $\geq$ 30 deg with a goal of 12 dB and 50 deg.

3. Acceleration Time Response

a) 63 percent time constant of 0.5 seconds for a step command of acceleration at the flight condition of interest (M = 3.95, altitude 60 Kft) and small angles-of-attack. This response is representative of a tactical missile of this size.

b) Overshoot $\leq$ 10 percent.

c) Zero steady state error in acceleration to reduce variations of guidance navigation gain.

The resulting pitch control laws for the circular and elliptical airframes are shown in Figure D.2. Lag-leads were used to prevent guidance noise saturation problems. The design approach was similar for both airframes. The rate error compensation determines the high frequency attenuation and was used to minimize the effect of aerodynamic variations on acceleration time response. The acceleration error compensation determines the acceleration time response. An integrator was used in the acceleration error branch of the circular control law to satisfy the guidance requirement of zero steady state error. The same approach was initially used for the elliptical control law; however, to reduce the acceleration response overshoot below 10 percent the integrator was placed in the rate error path and a gain was placed in series with the acceleration command for zero steady state acceleration error. Actually the technique used for the elliptical control law has worked well for many missile systems.

D.3 Analysis

Figure D.3 compares the pitch acceleration responses of the circular and elliptical airframes due to a one gee acceleration command when the missile aerodynamics are linearized about zero angle-of-attack. The responses are approximately the same having a 0.5 second time constant and negligible overshoot. Figures D.4 through D.7 show that to achieve the acceleration response the elliptical airframe requires less body angular rate and control surface deflection because of reasons described in D.1.

When the aerodynamic data are linearized at 20 degrees, the time constant of the acceleration response decreases to approximately 0.4 sec with negligible overshoot. Although the elliptical airframe is slightly stable at this angle-of-attack, it is closer to neutral stability than the circular airframe (Table D.1) and therefore requires less body angular rate and control surface deflection.

Tables D.2 and D.3 compare the relative stability of the circular and elliptical pitch autopilot branches. The stability margins are excellent. The gain margin in the actuator command branch for the elliptical airframe is negative which corresponds to a decreasing gain margin. Potential nonlinear stability problems will be avoided by preventing the actuator command from limiting. The actuator command gain margin for the circular airframe occurs at a frequency greater than 100 rad/sec, which was the highest frequency calculated. The corresponding frequency response shown in Figure D.9 shows that the gain margin will be greater than the 15 dB attenuation at 100 rad/sec. Frequency responses corresponding to Table D.2 or $\alpha = 0$ are provided in Figures D.8 through D.11. Figures D.9 and D.10 show that both autopilots have at least 15 dB attenuation at 100 rad/sec. At $\alpha = 20$ degrees, the actuator branch of the circular loses 3 dB attenuation at 100 rad/sec but the remainder of the gain and all of the phase remains the same. The slightly stable elliptical airframe at $\alpha = 20$ degrees has an actuator response which loses 1 dB attenuation at 100 rad/sec as shown in Figure D.12. Acceleration feedback frequency responses at $\alpha = 20$ degrees have the same shape in gain and phase with more bandwidth as shown for the elliptical in Figure D.3. The frequency responses will be used to determine the influence of coupling the system together in Section 8.

A faster version of the pitch autopilot for the circular airframe was used in coupled system studies to improve time response. The faster version was obtained by increasing the acceleration error dc gain by 3 dB. The resulting time constant was 0.38 sec with 2.5 percent overshoot. Relative stability is still excellent as shown in Table D.4.

q/δ_p (1/sec)

Angle-of-Attack (α,deg)	Circular Airframe	Elliptical Airframe
0	$\dfrac{(-0.159)\left(\frac{s}{0.119}+1\right)}{\frac{s^2}{(6.66)^2}+\frac{2(0.0112)s}{6.66}+1}$	$\dfrac{(0.688)\left(\frac{s}{0.188}+1\right)}{\left(\frac{s}{3.27}+1\right)\left(\frac{s}{-3.45}+1\right)}$
10	$\dfrac{(-.207)\left(\frac{s}{0.14}+1\right)}{\left(\frac{s^2}{(6.93)^2}\right)+\frac{2(0.0122)s}{6.93}+1}$	$\dfrac{(1.15)\left(\frac{s}{0.288}+1\right)}{\left(\frac{s}{3.08}+1\right)\left(\frac{s}{-3.36}+1\right)}$
20	$\dfrac{(-0.163)\left(\frac{s}{0.167}+1\right)}{\frac{s^2}{(9.34)^2}+\frac{2(0.0117)s}{9.34}+1}$	$\dfrac{(-1.8)\left(\frac{s}{0.299}+1\right)}{\frac{s^2}{(3.07)^2}+\frac{2(0.0495)s}{3.07}+1}$

η_z/δ_p (g's/rad)

0	$\dfrac{(-18.82)\left(\frac{s}{13.32}+1\right)\left(\frac{s}{-13.32}+1\right)}{\frac{s^2}{(6.66)^2}+\frac{2(0.0112)s}{6.66}+1}$	$\dfrac{(81.6)\left(\frac{s}{19.6}+1\right)\left(\frac{s}{-19.6}+1\right)}{\left(\frac{s}{3.27}+1\right)\left(\frac{s}{-3.45}+1\right)}$
10	$\dfrac{(-24.52)\left(\frac{s}{15.82}+1\right)\left(\frac{s}{-15.82}+1\right)}{\frac{s^2}{(6.93)^2}+\frac{2(0.0122)s}{6.93}+1}$	$\dfrac{(136.8)\left(\frac{s}{24.3}+1\right)\left(\frac{s}{-24.3}+1\right)}{\left(\frac{s}{3.08}+1\right)\left(\frac{s}{-3.36}+1\right)}$
20	$\dfrac{(-19.34)\left(\frac{s}{16.93}+1\right)\left(\frac{s}{-16.93}+1\right)}{\frac{s^2}{(9.34)^2}+\frac{2(0.0117)s}{9.34}+1}$	$\dfrac{(-213)\left(\frac{s}{25.83}+1\right)\left(\frac{s}{-25.83)}+1\right)}{\frac{s^2}{(3.07)^2}+\frac{2(0.0495)s}{3.07}+1}$

TABLE D.1 Comparison of Uncoupled Pitch Channel Transfer Functions

Airframe	Branch	Gain (dB)	Margin (rad/sec)	Phase (deg)	Margin (rad/sec)
Circular	Actuator Command	---	---	66.2	20.9
Elliptical		-13.3	3.87	57.3	15.9
Circular	Acceleration Feedback	14.6	11.5	70.5	2.0
Elliptical		15.6	9.5	76.	1.92

TABLE D.2 Comparison of Uncoupled Pitch Channel Stability Margins (α = 0)

Airframe	Branch	Gain (dB)	Margin (rad/sec)	Phase (deg)	Margin (rad/sec)
Circular	Actuator Command	---	---	69.1	29.8
Elliptical		-21.7	4.6	62.8	21.9
Circular	Acceleration Feedback	15.6	14.2	68.4	2.5
Elliptical		15.7	11.7	71.9	2.6

TABLE D.3 Comparison of Uncoupled Pitch Channel Stability Margins (α = 20 deg)

Angle-of-attack (deg)	Branch	Gain Margin (dB)	Gain Margin (rad/sec)	Phase Margin (deg)	Phase Margin (rad/sec)
0	Actuator Command	---	---	65.3	20.2
20		---	---	69.	28.8
0	Acceleration Feedback	11.6	11.5	63.5	2.8
20		12.6	14.2	60.9	3.5

TABLE D.4 Stability Margins of Faster Uncoupled Pitch Channel for Circular Airframe

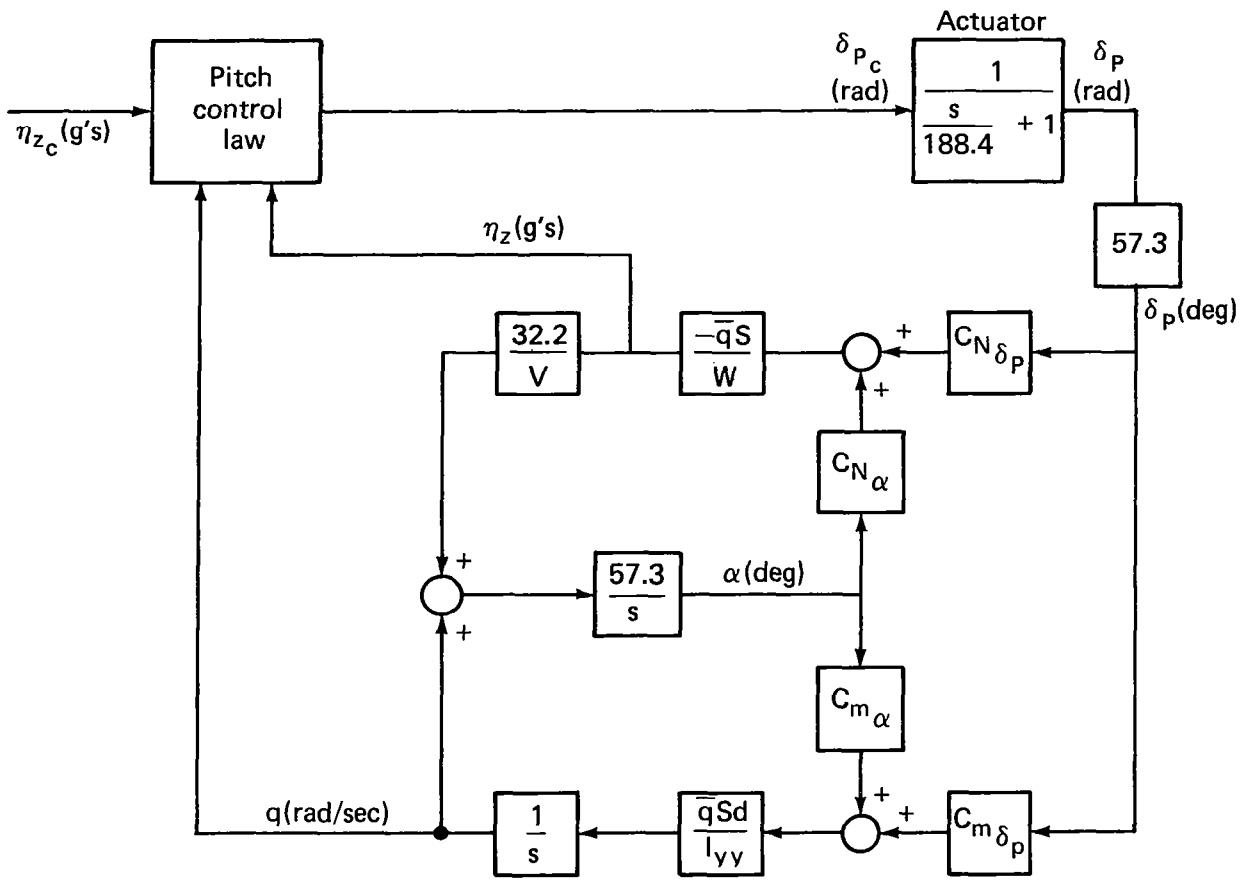

Fig. D.1 Uncoupled pitch channel autopilot.

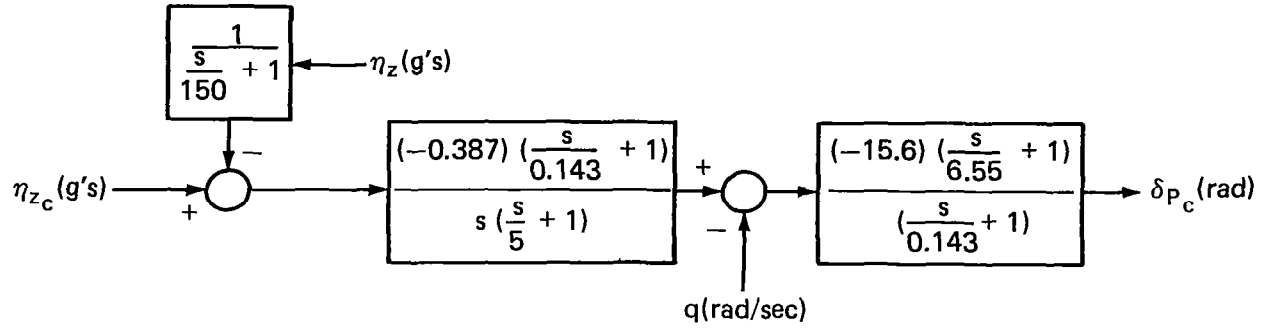

Circular airframe

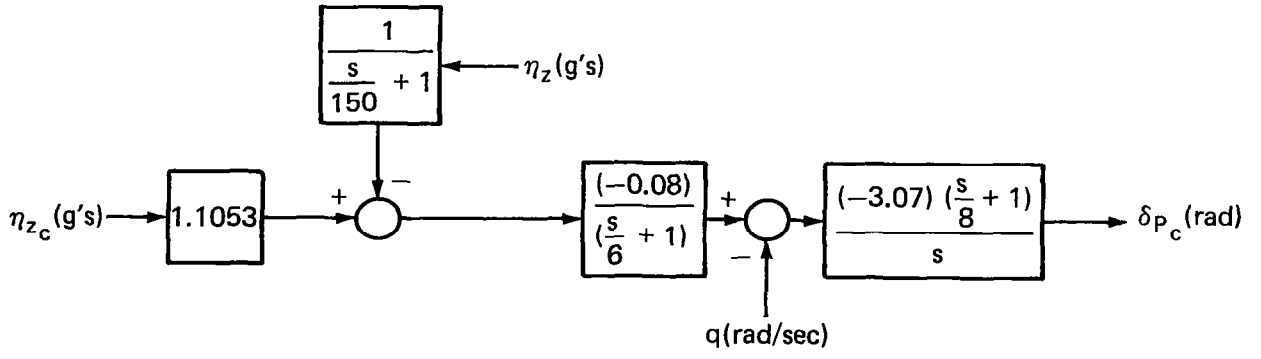

Elliptical airframe

Fig. D. 2 Pitch control laws.

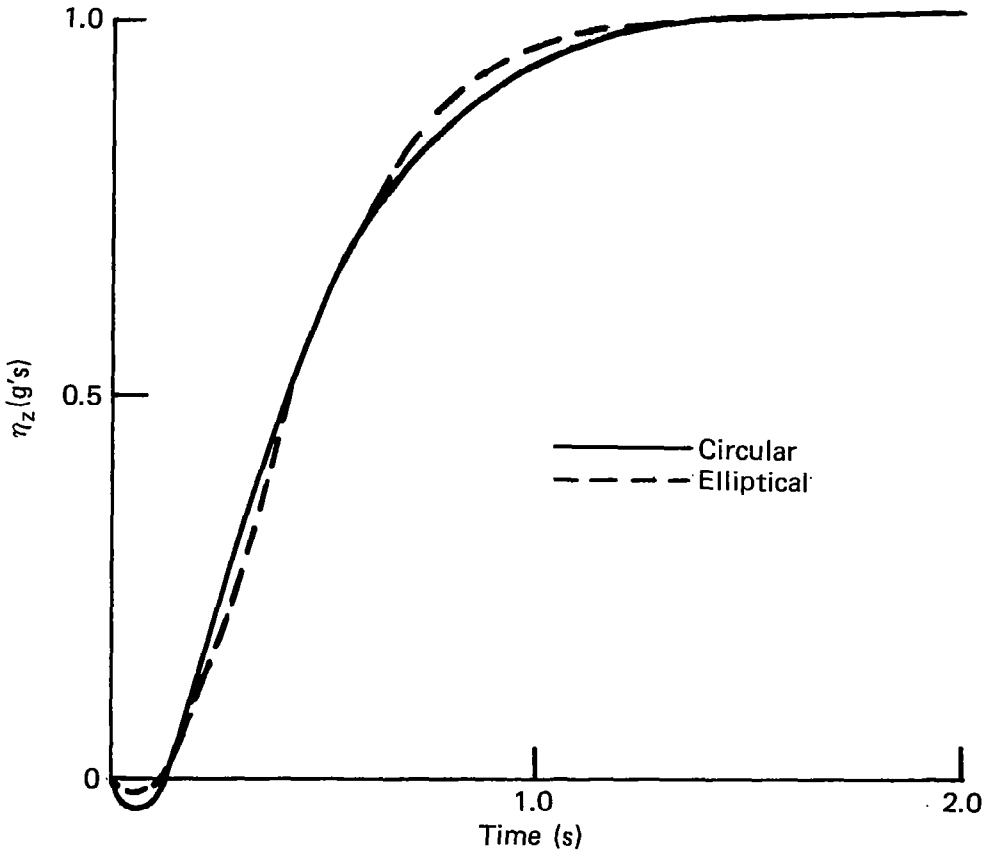

Fig. D.3 Comparison of pitch normal acceleration response; uncoupled pitch channel (α_e = 0, 1 gee command).

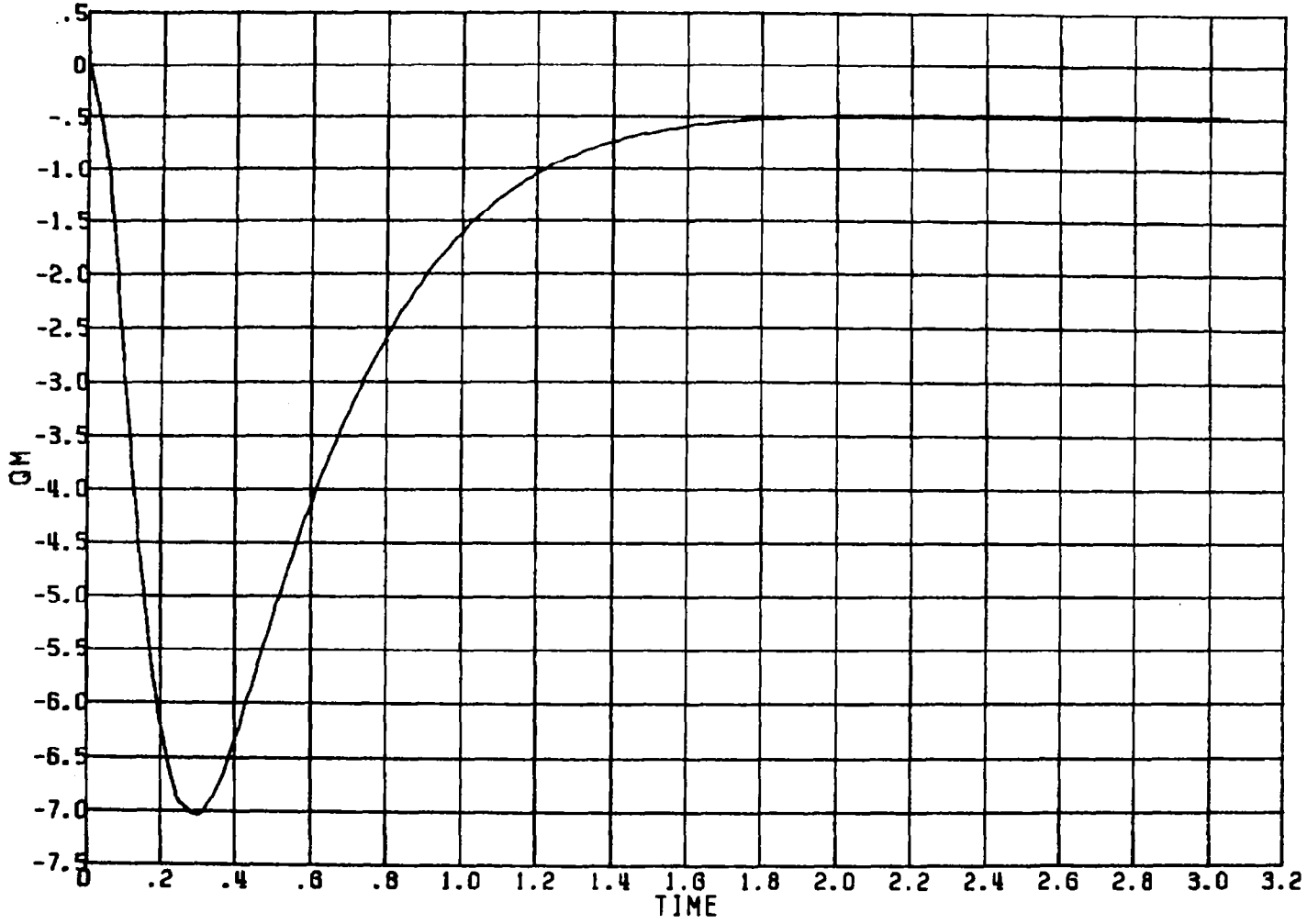

Figure D.4 PITCH BODY ANGULAR RATE (DEG/SEC) VS. TIME (SEC);
UNCOUPLED PITCH CHANNEL;
CIRCULAR AIRFRAME (α_e = 0, 1 GEE COMMAND)

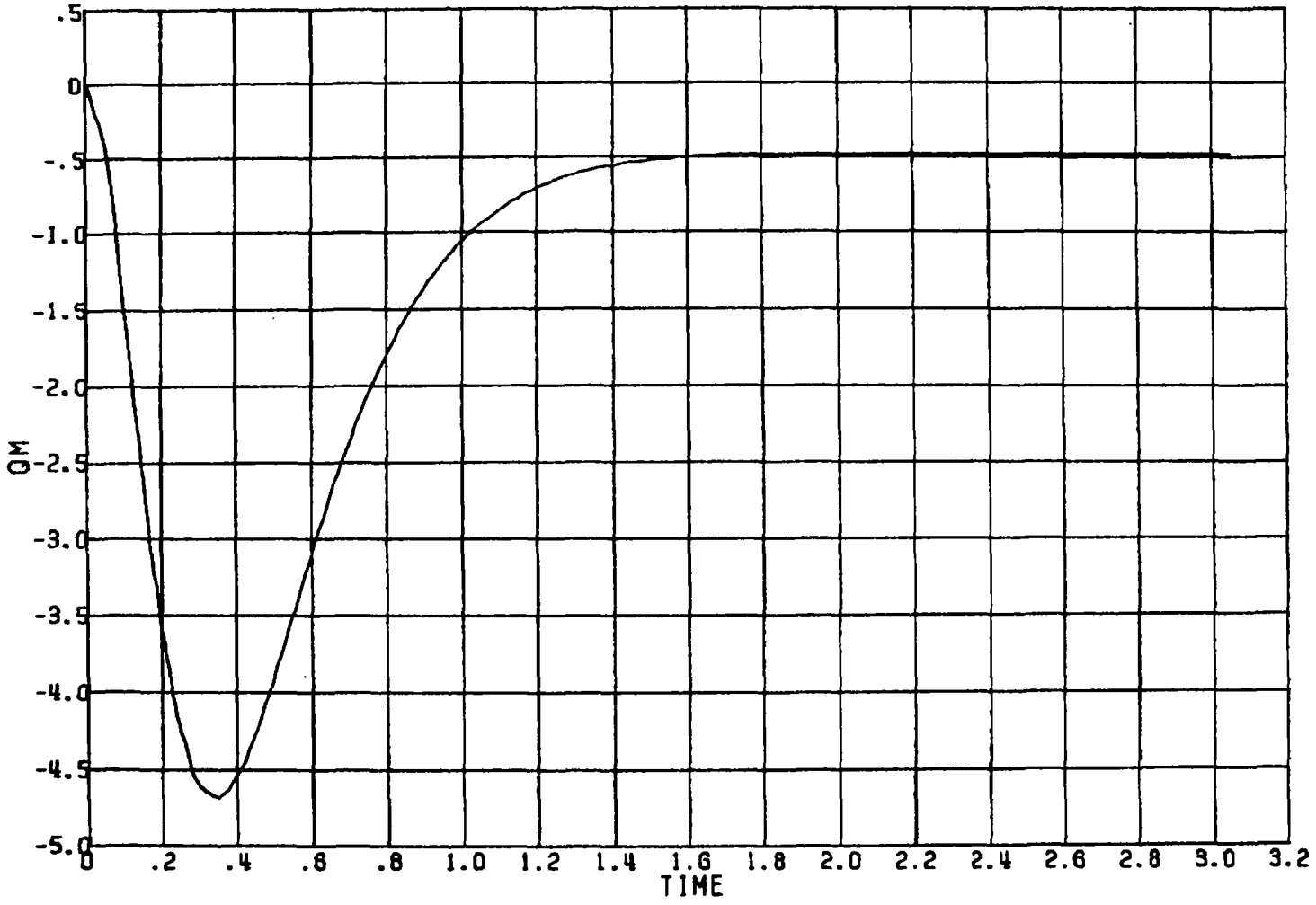

Figure D.5 PITCH BODY ANGULAR RATE (DEG/SEC) VS. TIME (SEC);
UNCOUPLED PITCH CHANNEL;
ELLIPTICAL AIRFRAME (α_e = 0, 1 GEE COMMAND)

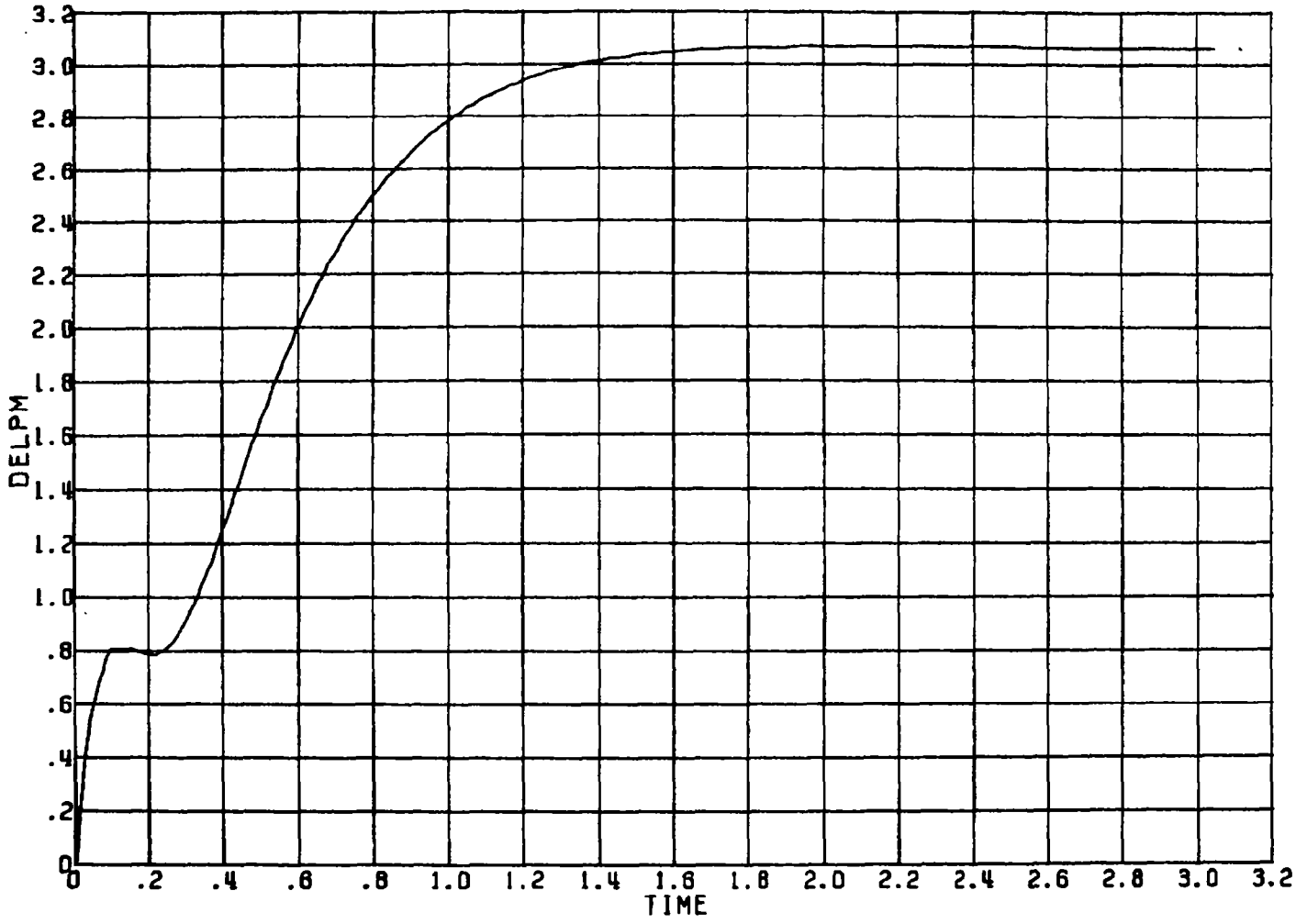

Figure D.6 PITCH TAIL INCIDENCE (DEG) VS. TIME (SEC);
UNCOUPLED PITCH CHANNEL;
CIRCULAR AIRFRAME (α_e = 0, 1 GEE COMMAND)

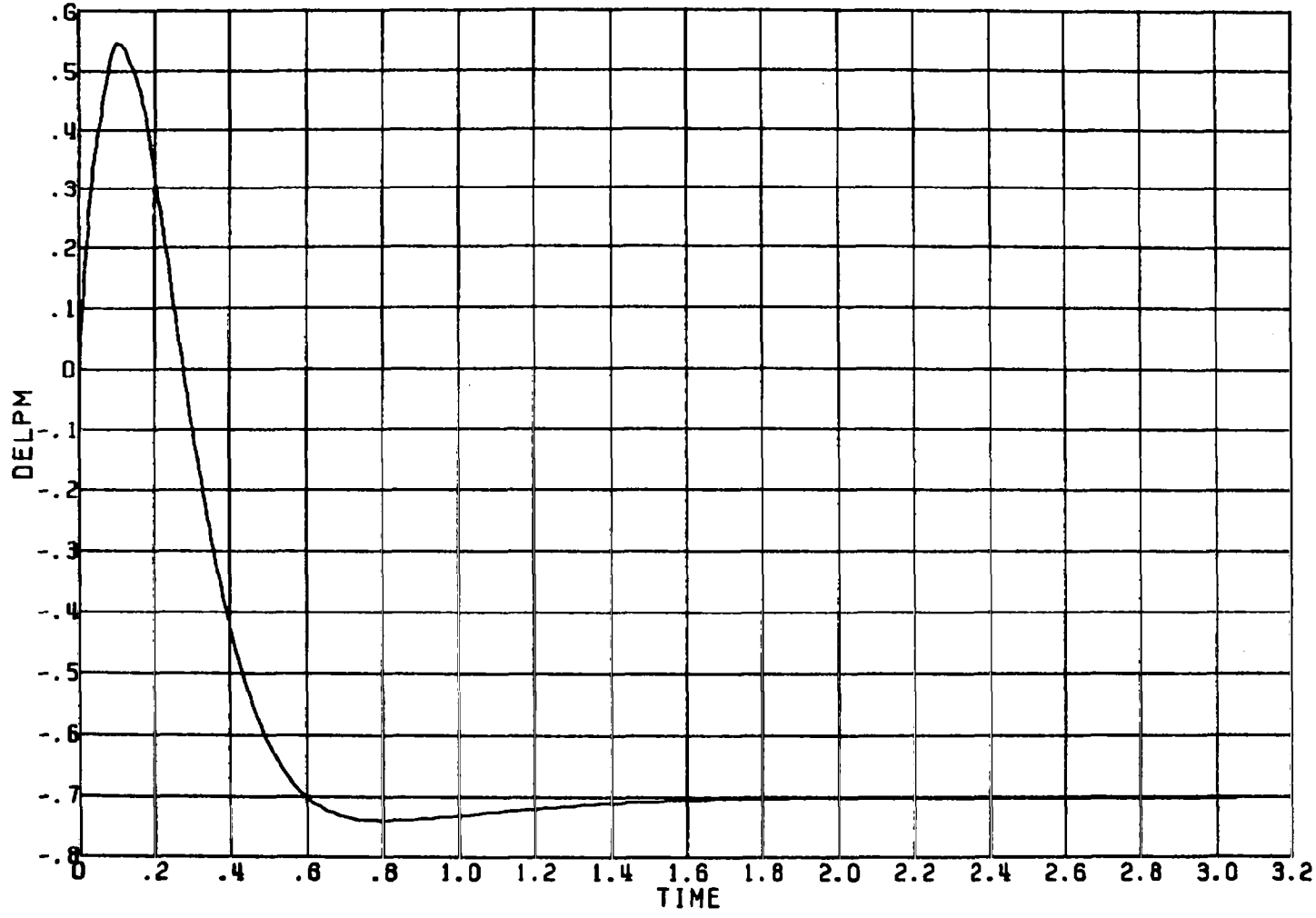

Figure D.7 PITCH TAIL INCIDENCE (DEG) VS. TIME (SEC);
UNCOUPLED PITCH CHANNEL;
ELLIPTICAL AIRFRAME (α_e = 0, 1 GEE COMMAND)

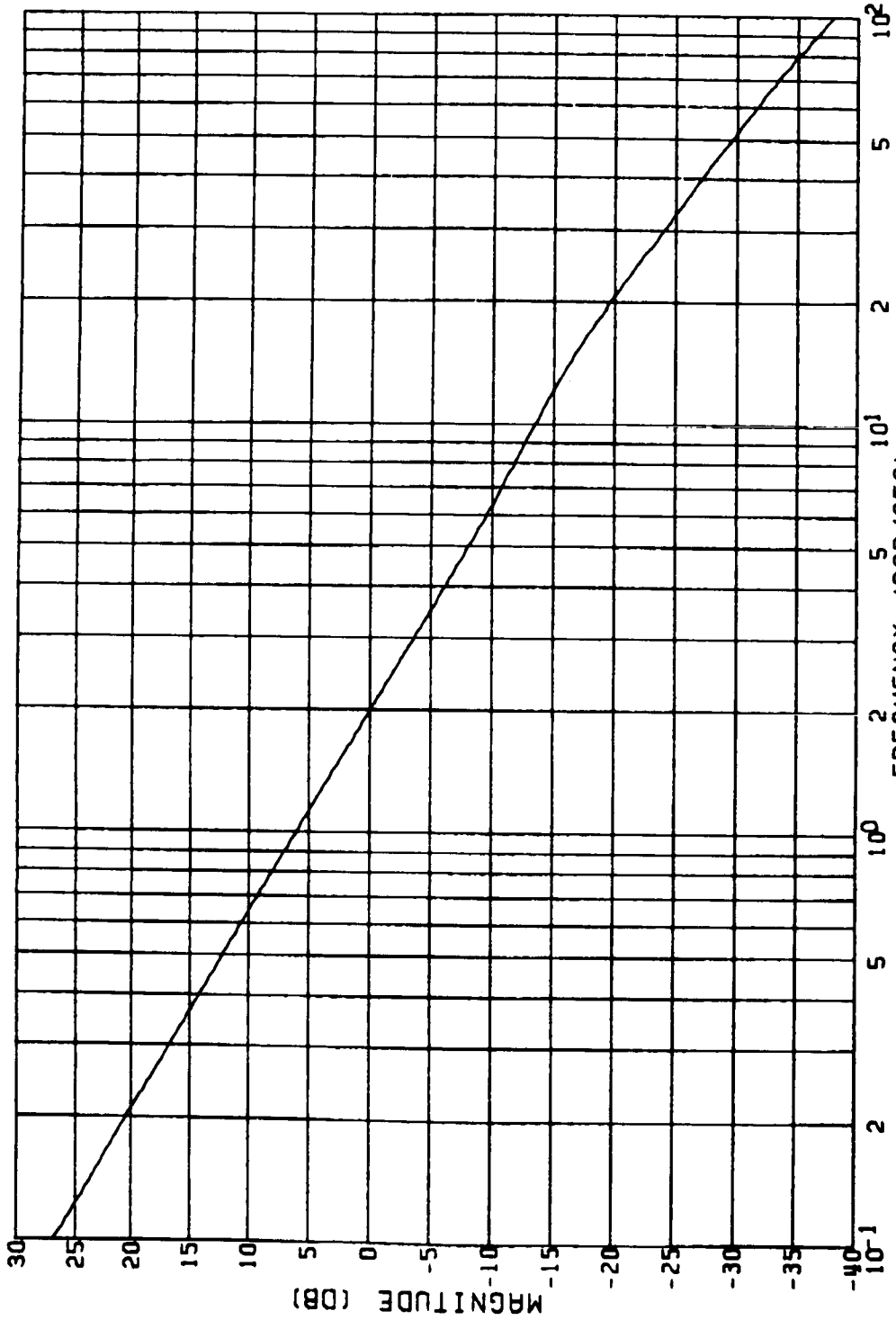

Figure D.8(a) PITCH ACCELERATION FEEDBACK; UNCOUPLED PITCH CHANNEL; CIRCULAR AIRFRAME ($\alpha_e = 0$) GAIN VS. FREQUENCY

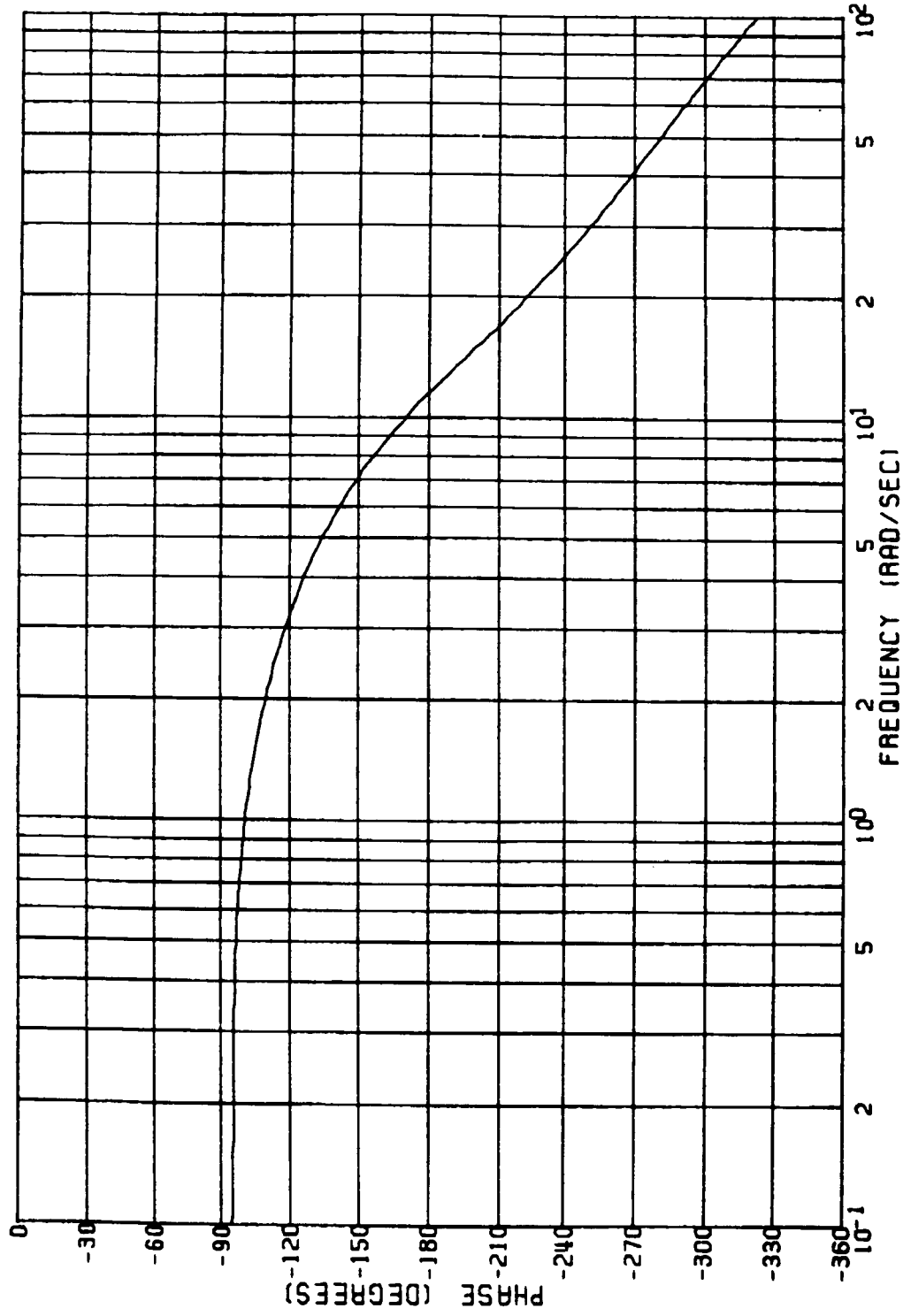

Figure D.8(b) PITCH ACCELERATION FEEDBACK; UNCOUPLED PITCH CHANNEL; CIRCULAR AIRFRAME ($\alpha_e = 0$) PHASE VS. FREQUENCY

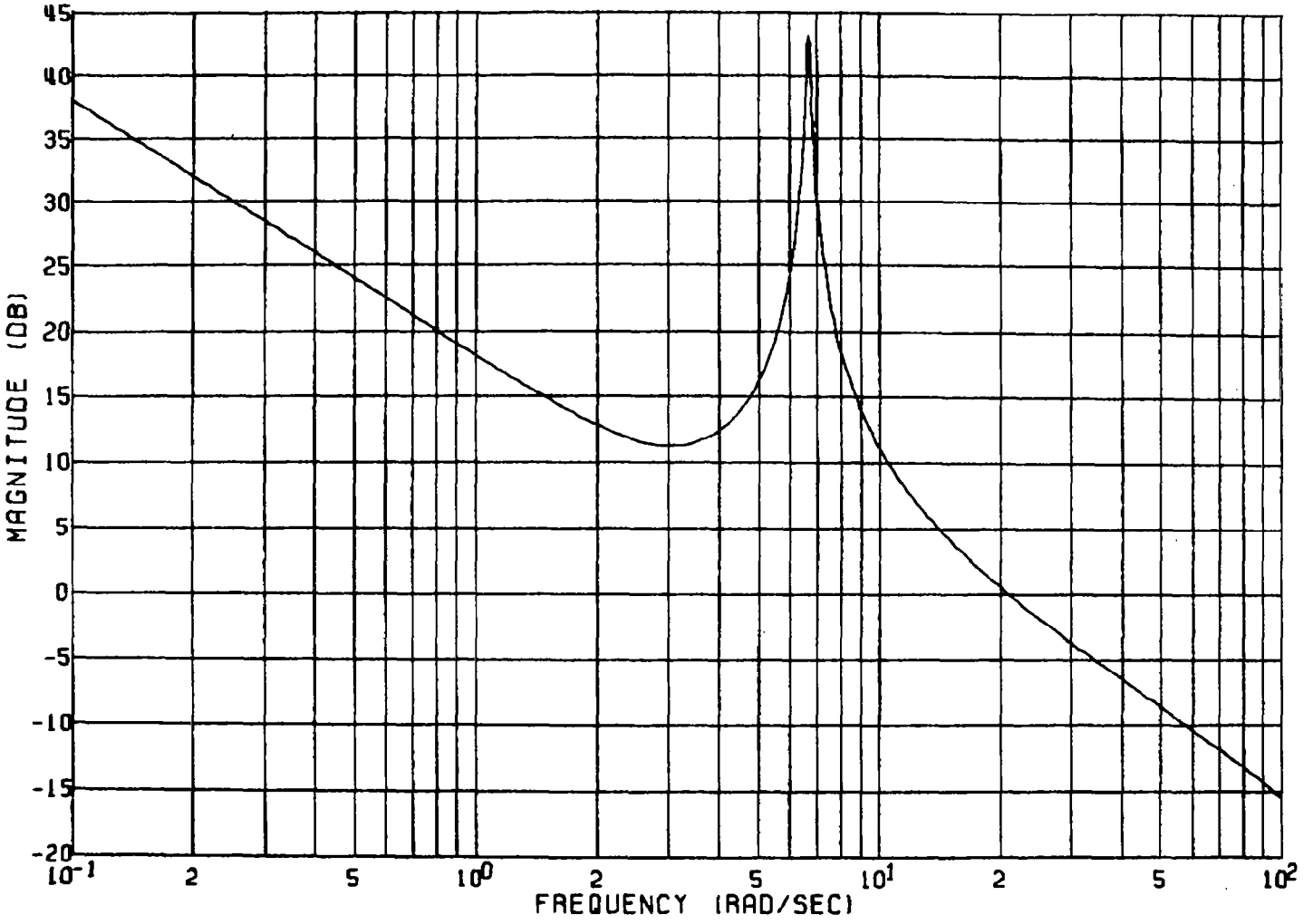

Figure D.9(a) PITCH ACTUATOR COMMAND; UNCOUPLED PITCH CHANNEL; CIRCULAR AIRFRAME ($\alpha_e = 0$) GAIN VS. FREQUENCY

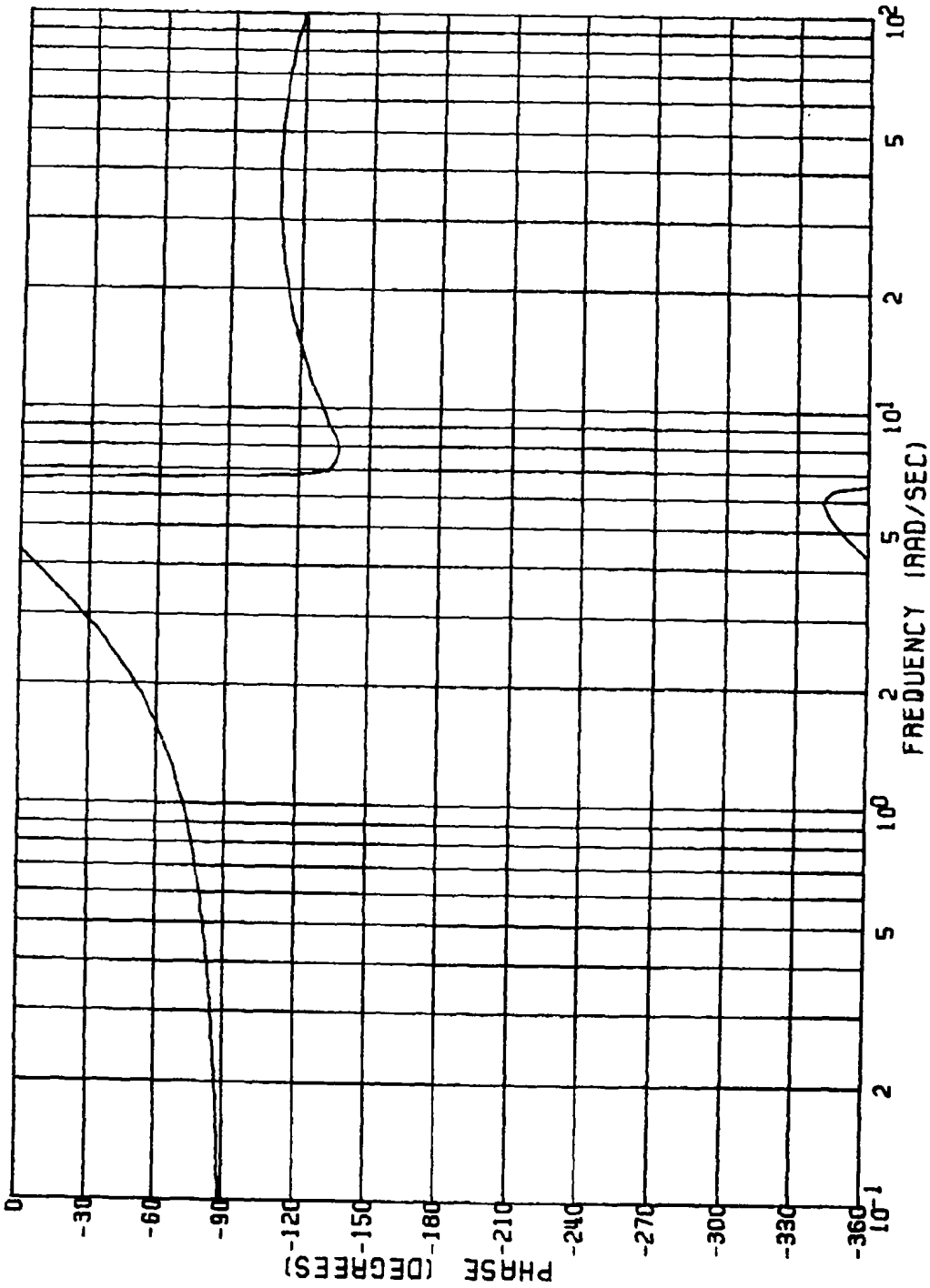

Figure D.9(b) PITCH ACTUATOR COMMAND; UNCOUPLED PITCH CHANNEL; CIRCULAR AIRFRAME ($\alpha_e = 0$) PHASE VS. FREQUENCY

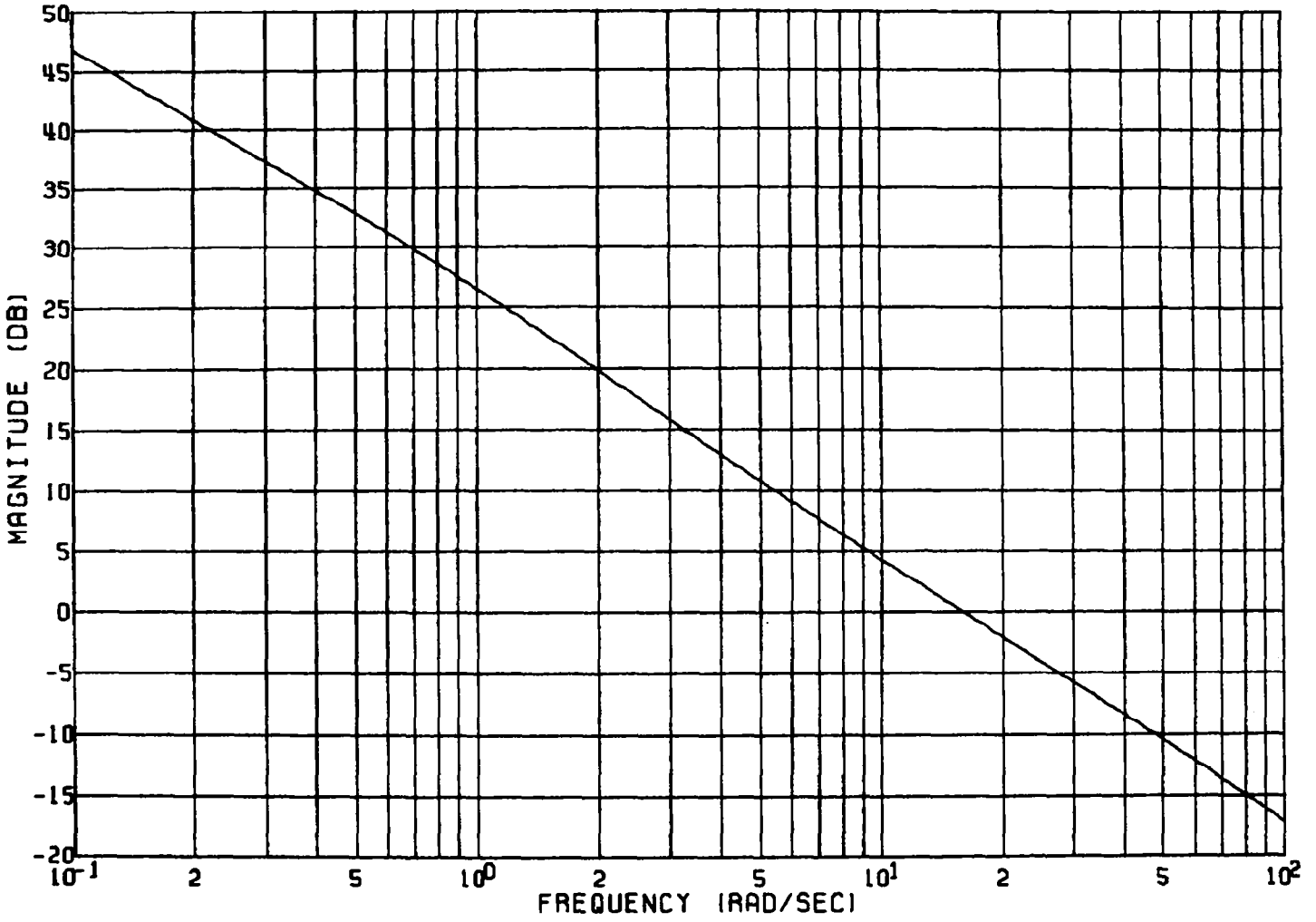

Figure D.10(a) PITCH ACTUATOR COMMAND; UNCOUPLED PITCH CHANNEL; ELLIPTICAL AIRFRAME ($\alpha_e = 0$) GAIN VS. FREQUENCY

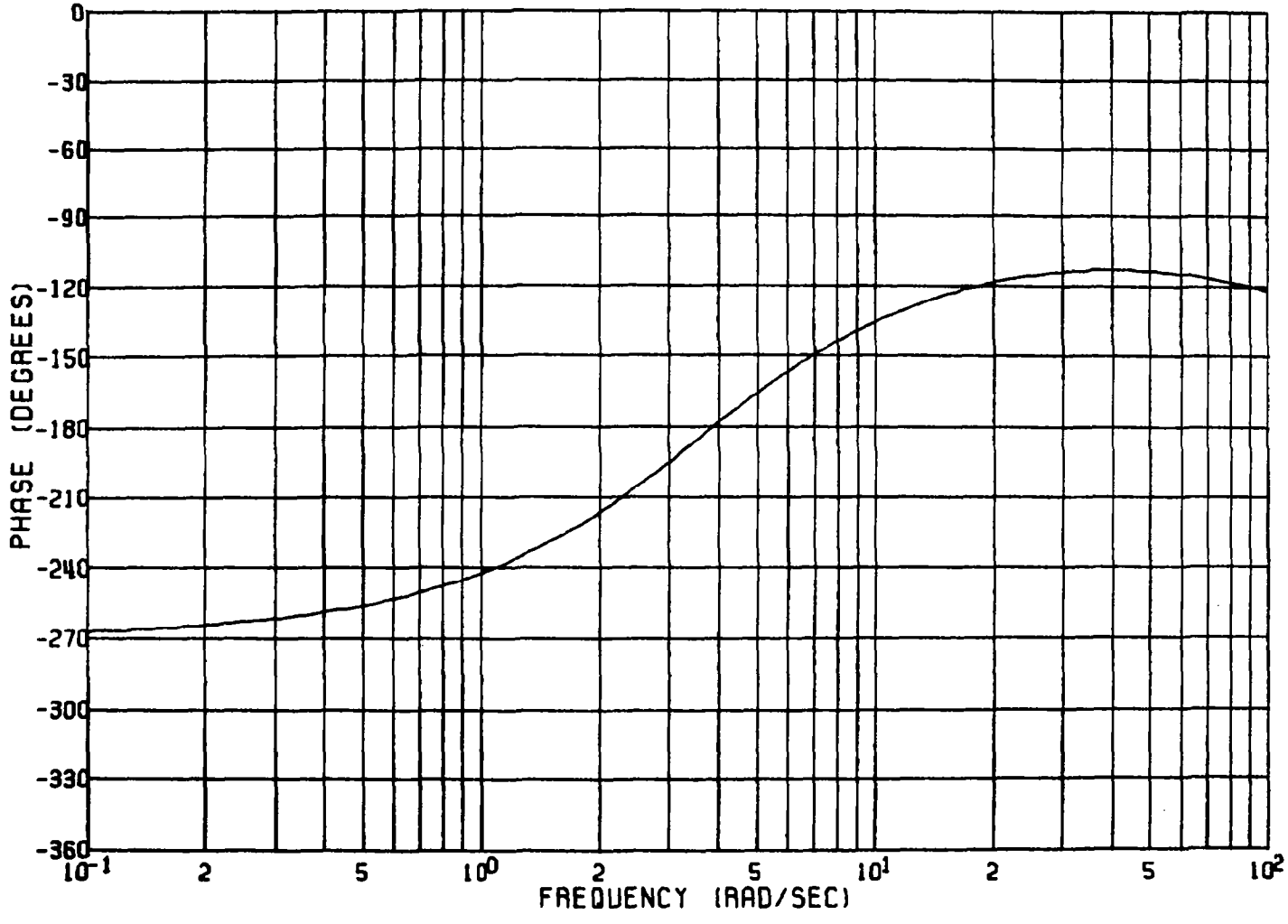

Figure D.10(b) PITCH ACTUATOR COMMAND; UNCOUPLED PITCH CHANNEL; ELLIPTICAL AIRFRAME (α_e = 0) PHASE VS. FREQUENCY

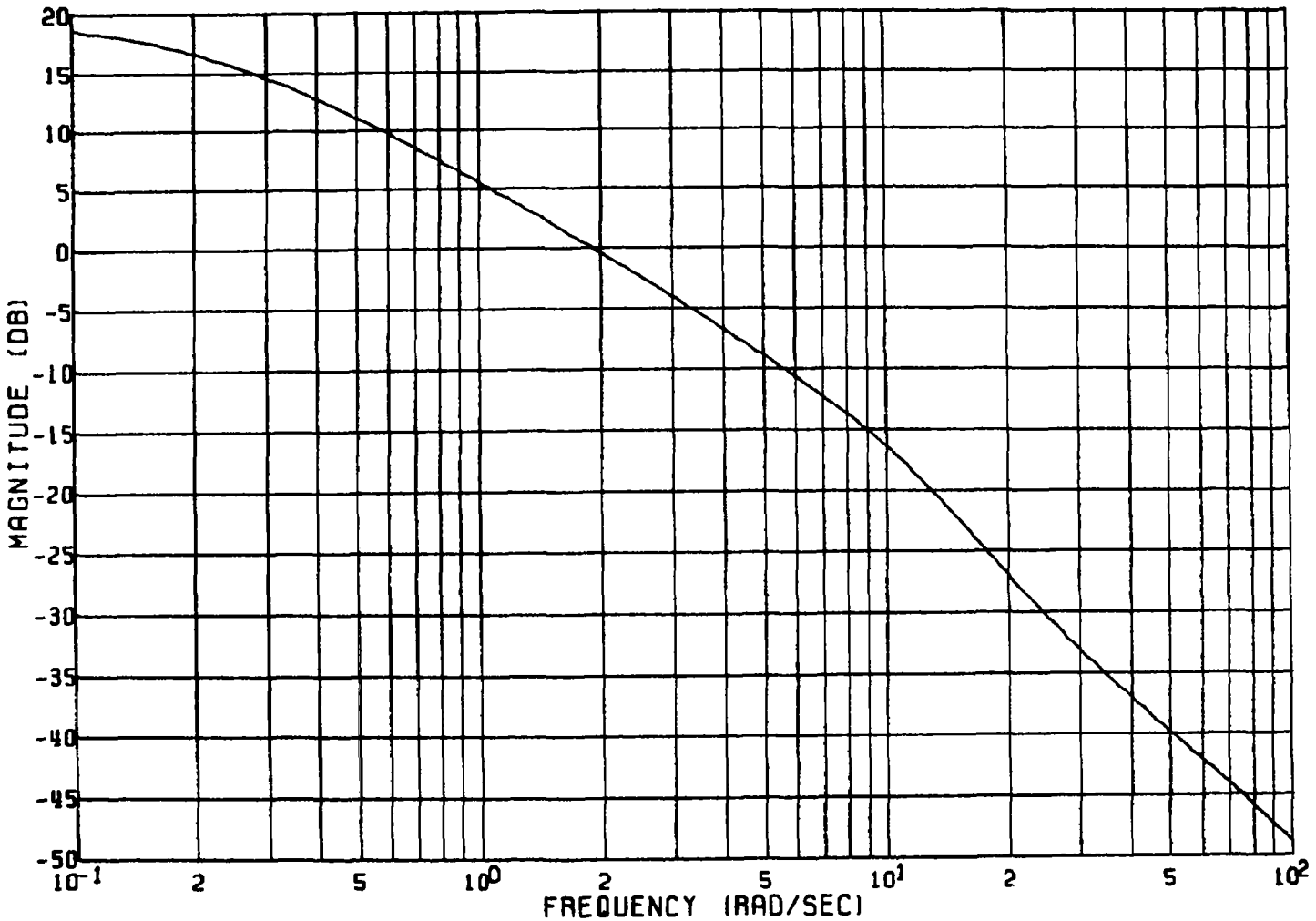

Figure D.11(a) PITCH ACCELERATION FEEDBACK; UNCOUPLED PITCH CHANNEL; ELLIPTICAL AIRFRAME ($\alpha_e = 0$) GAIN VS. FREQUENCY

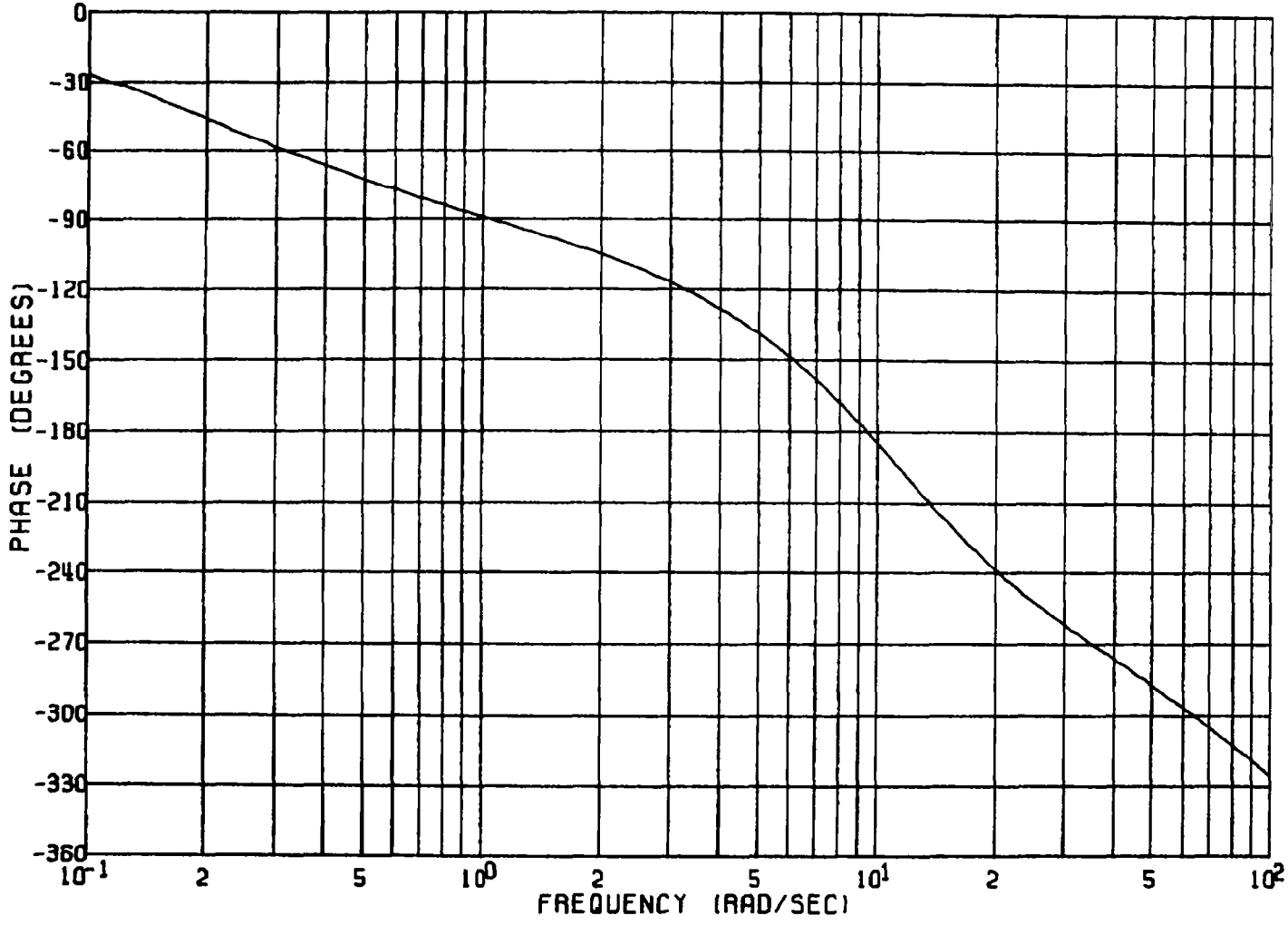

Figure D.11(b) PITCH ACCELERATION FEEDBACK; UNCOUPLED PITCH CHANNEL; ELLIPTICAL AIRFRAME ($\alpha_e = 0$) PHASE VS. FREQUENCY

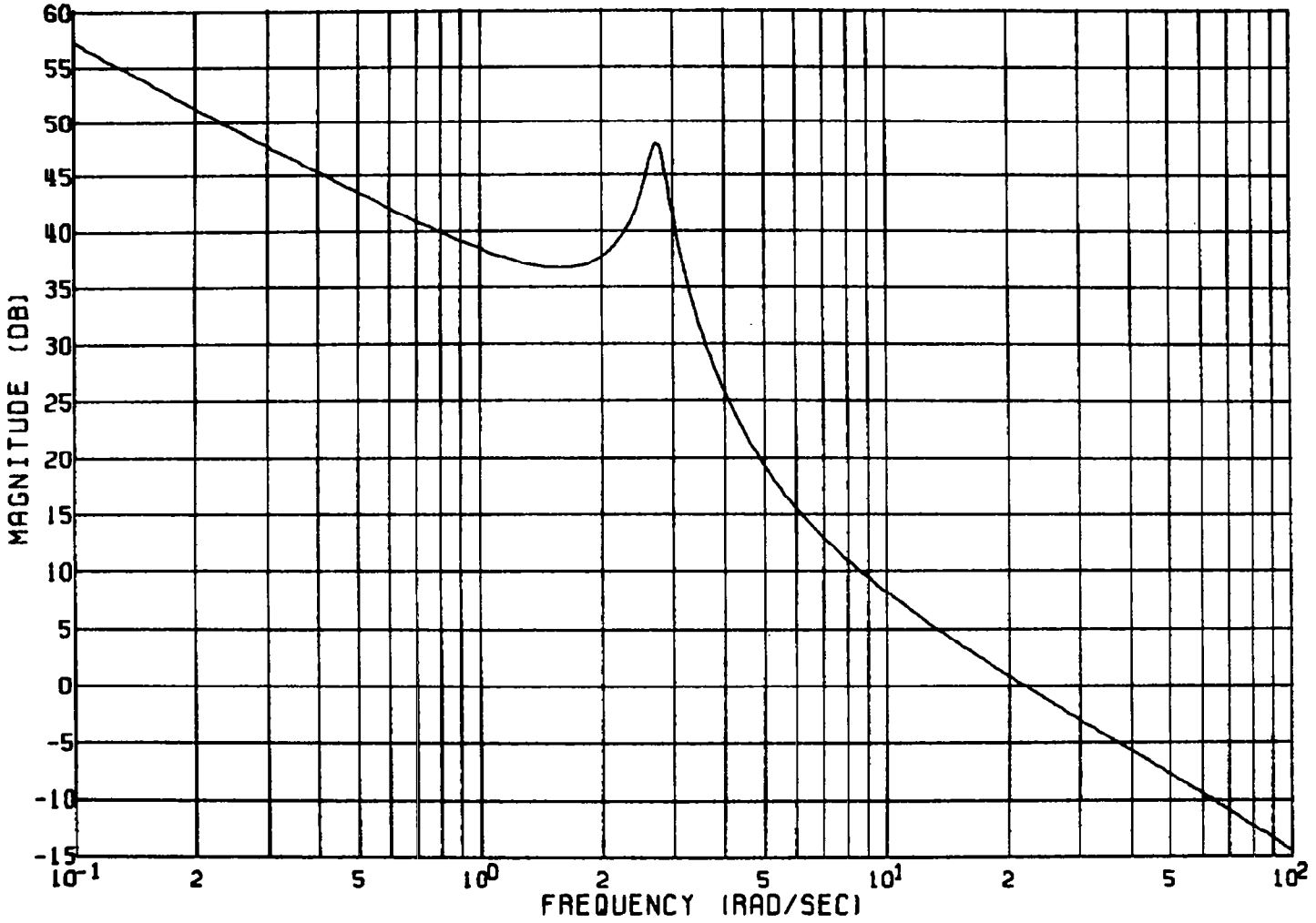

Figure D.12(a) PITCH ACTUATOR COMMAND; UNCOUPLED PITCH CHANNEL; ELLIPTICAL AIRFRAME (α_e = 20 DEG) GAIN VS. FREQUENCY

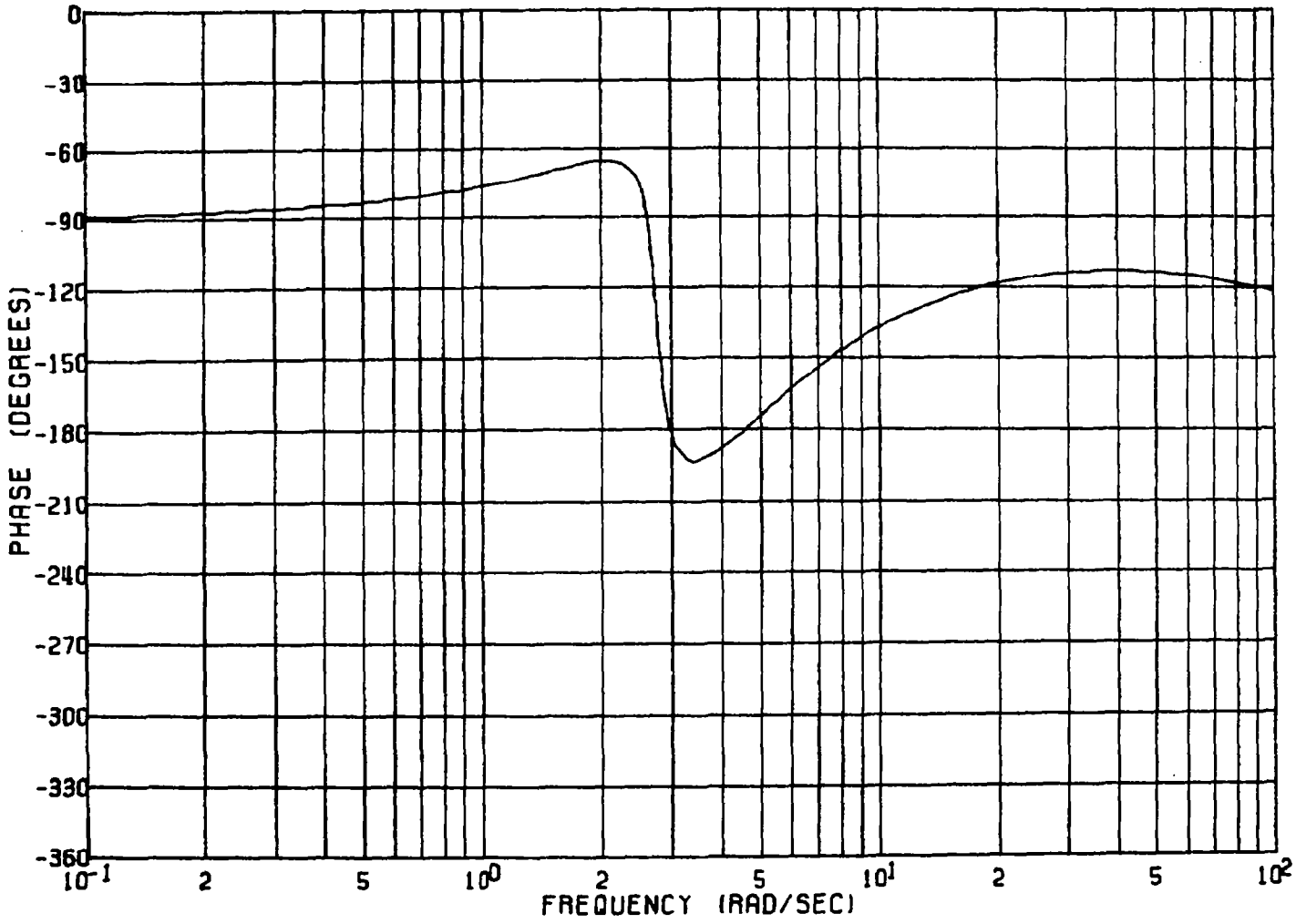

Figure D.12(b) PITCH ACTUATOR COMMAND: UNCOUPLED PITCH CHANNEL; ELLIPTICAL AIRFRAME (α_e = 20 DEG) PHASE VS. FREQUENCY

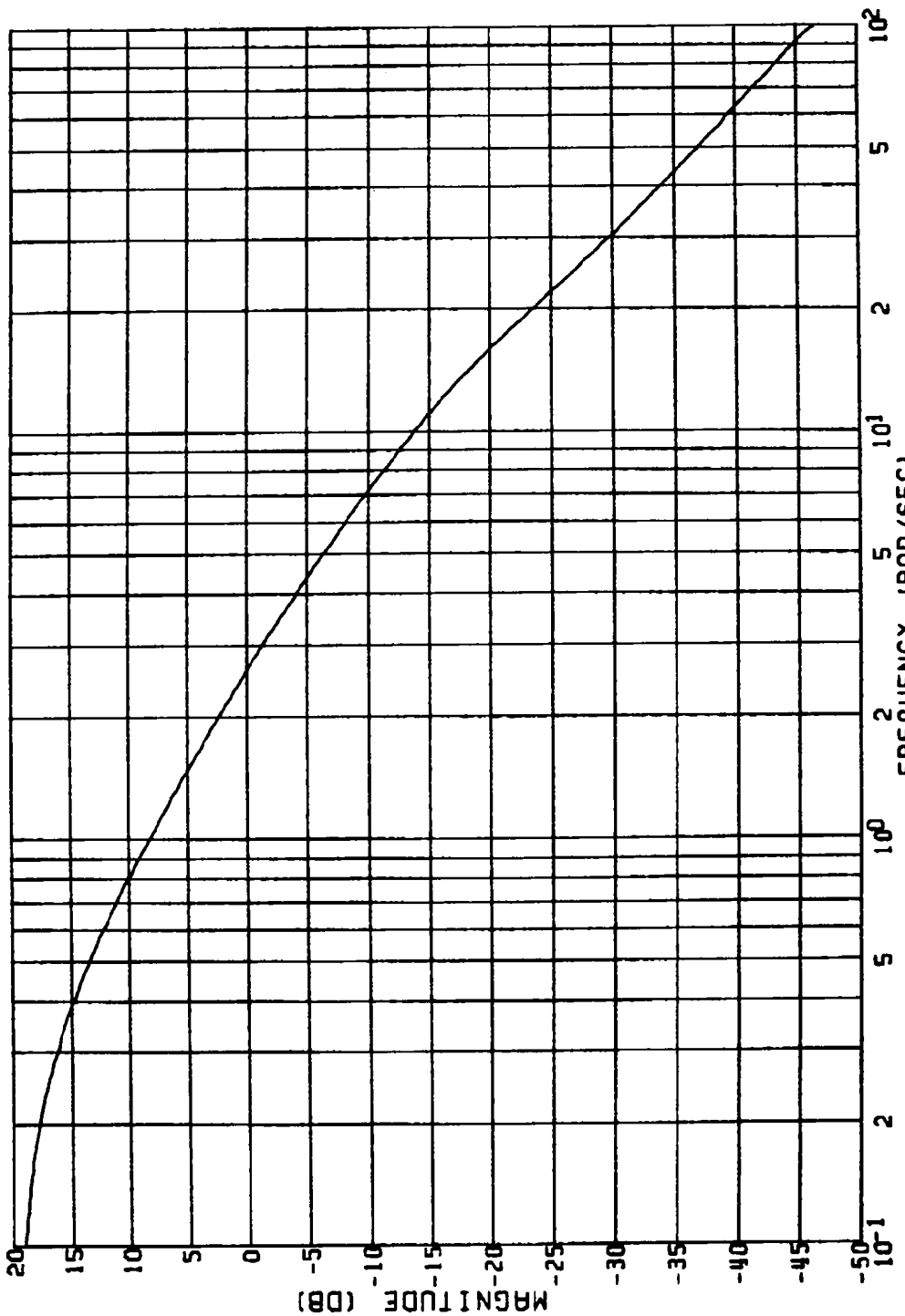

Figure D.13(a) PITCH ACCELERATION FEEDBACK; UNCOUPLED PITCH CHANNEL; ELLIPTICAL AIRFRAME (α_e = 20 DEG) GAIN VS. FREQUENCY

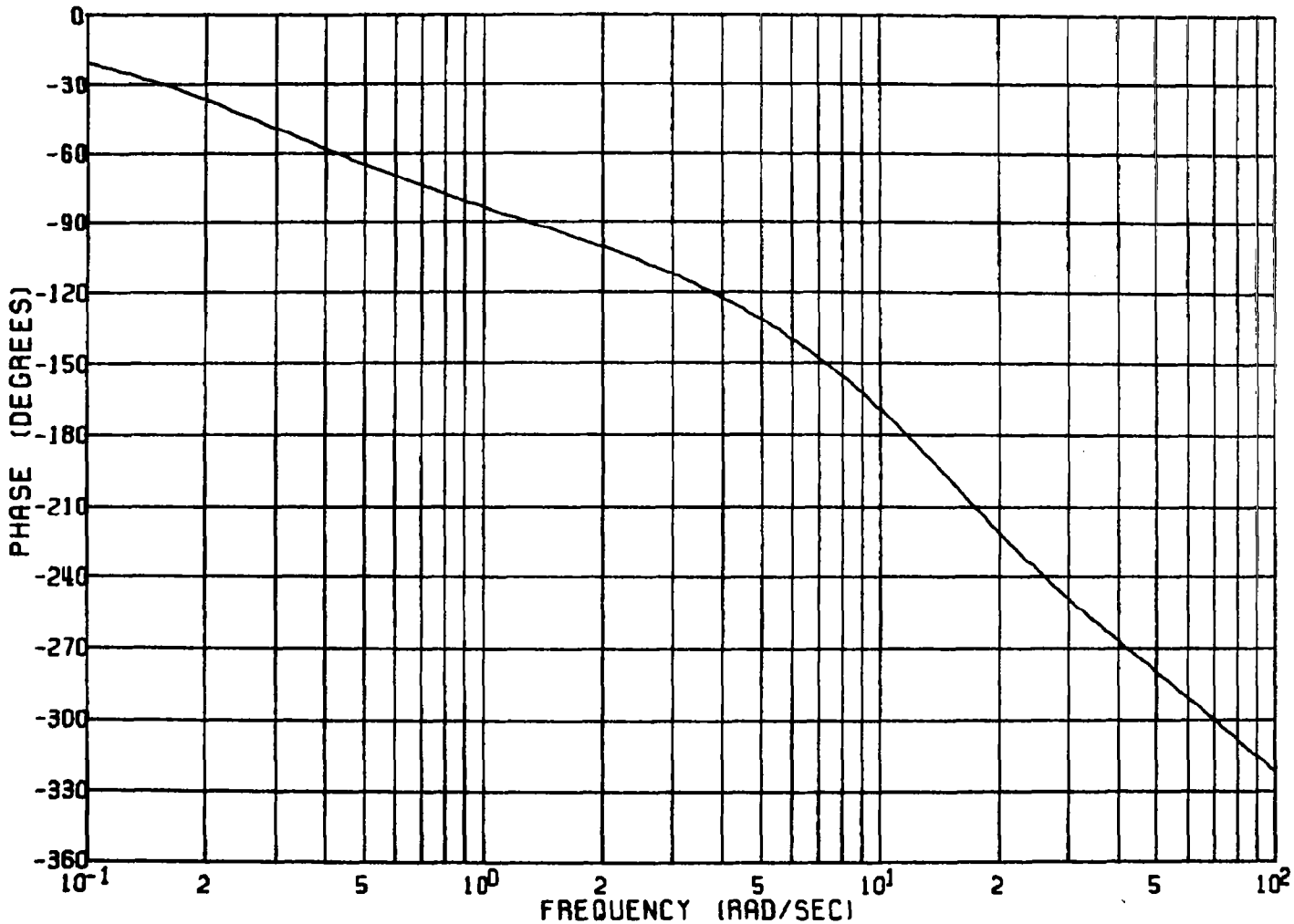

Figure D.13(b) PITCH ACCELERATION FEEDBACK; UNCOUPLED PITCH CHANNEL; ELLIPTICAL AIRFRAME (α_e = 20 DEG) PHASE VS. FREQUENCY

APPENDIX E

LINEAR DESIGN AND ANALYSIS OF UNCOUPLED YAW AUTOPILOTS

The purpose of the yaw channel autopilot of a CBTT autopilot is to minimize sideslip angle or provide coordinated motion between roll and yaw channels. This was accomplished in two ways. First, the uncoupled yaw channel autopilot (i.e., roll and pitch dynamic effects neglected) was designed as a regulator (i.e., no guidance command and with rate and acceleration feedback) to help minimize sideslip angle. Second, to aid in sideslip control, the regulator was commanded from the roll channel as explained in Section 7.

A block diagram of the uncoupled yaw channel is shown in Figure E.1. The normal acceleration n_{Y_c} is not used to command the CBTT autopilot. Instead, it is used for the design and analysis of the uncoupled channel. The command used by the coupled system is shown in dashed lines and is a yaw angular rate command, r_c. The yaw control law is governed by missile body yaw angular rate (r) and yaw normal acceleration (n_y). The yaw control law determines the required command (δ_{y_c}) to an actuator which is approximated as a first order lag at 30 Hz. The aerodynamics, linearized about a trim angle-of-attack is described in Section 5.

The first section of this Appendix uses transfer functions to discuss what are desired yaw aerodynamics for CBTT control and to compare the circular and elliptical airframes. Section E.2 covers the design requirements and technique and presents the yaw control laws. A time and frequency domain analysis is covered in Section D.3.

E.1 Aerodynamic Transfer Functions

Uncoupled yaw aerodynamic transfer functions are

$$\frac{r}{\delta_Y} = \frac{k(-\bar{A}\bar{E}+\bar{B}\bar{C})}{\bar{C}} \frac{\frac{\bar{E}}{k(\bar{B}\bar{C}-\bar{A}\bar{E})}s + 1}{\frac{s^2}{\bar{C}} - \frac{\bar{A}k}{\bar{C}}s + 1}, \qquad \text{deg/sec/deg} \qquad \text{E1}$$

$$\frac{n_y}{\delta_Y} = \frac{-\bar{A}\bar{E}+\bar{B}\bar{C}}{\bar{C}} \frac{\frac{\bar{B}}{-\bar{A}\bar{E}+\bar{B}\bar{C}}s^2 + 1}{\frac{s^2}{\bar{C}} - \frac{\bar{A}k}{\bar{C}}s + 1}, \qquad \text{g's/deg} \qquad \text{E2}$$

$$\bar{A} = \frac{\bar{q}S}{W} C_{Y_\beta} \qquad \bar{B} = \frac{\bar{q}S}{W} C_{Y_{\delta_Y}} \qquad \bar{C} = \frac{(57.3)\bar{q}Sd}{I_{zz}} C_{n_\beta}$$

$$\bar{E} = \frac{(57.3)\bar{q}Sd}{I_{zz}} C_{n_{\delta_Y}} \qquad k = \frac{1845}{V}$$

Because the yaw channel will act as a regulator to minimize sideslip angle, there is a question as to whether it is desirable to have a neutrally stable airframe ($C_{n_\beta} = 0$) which will minimize control surface motion due to the coordinating rate command from the roll channel or to have a stable airframe to help minimize sideslip angle. Table E.1 compares the linearized yaw aerodynamics of the circular and elliptical airframes in transfer function form. The circular airframe is unstable in yaw at all angles-of-attack whereas the elliptical airframe is stable. At 20 degrees angles-of-attack, the circular airframe is closer to neutral stability (i.e., C_{n_β} is numerically smaller). At zero angle-of-attack, C_{n_β} is approximately numerically the same for both airframes. The dc gain in the yaw channel

(i.e., $(-\overline{AE} + \overline{BC})/\overline{C}$) is directly proportional to the yaw control moment $C_{n_{\delta_Y}}$ and inversely proportional to magnitude of stability margin in yaw (i.e., C_{n_β}/C_{Y_β} or the distance from center of pressure to center of gravity). In this case the magnitude of stability margins are smaller for the circular configuration which coupled with its slightly larger yaw control moment coefficients result in higher gains in the yaw channel for the circular airframe. Higher dc gain will require less control surface incidences. The zeros of η_z/δ_P are directly proportional to C_{Y_β} and the ratio $C_{n_{\delta_Y}}/C_{Y_{\delta_Y}}$ or the distance from the point of action of the tail forces to the center of gravity. Hence, for the circular airframe which has larger C_{Y_β}, the zeros of η_y/δ_Y are located at a higher frequency which will simplify the design of a rapidly responding yaw autopilot. Hence, the circular airframe will have lower control surface incidences for the coordinating commands from the roll channel with no help from the unstable airframe for minimizing sideslip angle. On the other hand, the elliptical airframe will have help from the stable airframe for minimizing sideslip angle but will require larger control surface incidences for the coordinating commands from the roll channel. Which is best for the CBTT autopilot will be addressed in Section 10.

E.2 Requirements and Control Laws

Requirements for the classical design approach are:

1. High Frequency Attenuation in Actuator Command Branch

$\geq$ 15 dB at 100 rad/sec and zero angles-of-attack and sideslip. This requirement will provide sufficient high frequency attenuation for $\geq$ 30 Hz actuation and for body bending modes when high frequency filters are added, but it limits the ability of the yaw autopilot to minimize sideslip angle.

2. Relative Stability

Gain margins $\geq$ 6 dB, phase margins $\geq$ 30 deg with a goal of 12 dB and 50 deg.

3. Acceleration Time Response

a) 63 percent time constant of approximately 0.4 seconds for a step command of acceleration n_{y_c} at the flight condition of interest and at $\alpha = 0$, $\beta = 0$. This is a measure of yaw autopilot bandwidth. The time constant was arbitrarily set. The yaw autopilot must follow the roll channel command and therefore must be faster than the roll channel. The roll channel is designed to have the same time constant as the pitch channel. The limitation as to how small the yaw time constant should be made is partly due to the high frequency attenuation requirement and partly due to the need to avoiding large actuator commands leading to nonlinear stability problems. The requirement for the acceleration time constant of the uncoupled yaw channel autopilot will therefore be determined by an iterative procedure between uncoupled and nonlinear CBTT studies.

b) Overshoot $\leq$ 10 percent should provide for better sideslip control or regulation. This choice depends on the results of nonlinear coupled studies.

c) Steady state error need not be zero. The other above mentioned requirements will determine the steady state error which is not important to sideslip regulation.

The resulting yaw control laws for the circular and elliptical airframes at the flight condition of interest (i.e., Mach 3.95, 60 Kft or

18.3 Km altitude) are shown in Figure E.2. The rate compensation determines the high frequency attenuation and is used to minimize aerodynamic variations on the quality of regulation. The acceleration compensation determines the acceleration bandwidth via the time constant of the acceleration response due to a step command of acceleration at η_{y_c} .

E.3 Analysis

Figures E.3 and E.4 compare the yaw acceleration responses of the circular and elliptical airframes due to a one gee acceleration command in yaw when missile aerodynamics is linearized at zero angle-of-attack. The time constant of the elliptical is 0.36 seconds compared to 0.39 seconds for the circular.

Figures E.5 through E.8 show that the circular yaw angular rate and yaw tail deflection is lower because the airframe is closer to being neutrally stable as explained in Section E.1.

Figures E.9 through E.12 are frequency response plots from which the stability margins of Table E.2 and be obtained. Relative stability for angles-of-attack of zero and 20 degrees, shown in Tables E.2 and E.3, is satisfactory. The negative gain margins in the actuator command branches show that there are potential nonlinear stability problems for large amplitude actuator commands which exceed limits. There is 17.1 dB attenuation at 100 rad/sec for the actuator command branch of the circular airframe and 18.2 dB for the elliptical. At 20 degrees angle-of-attack, the circular attenuation decreases to 15.3 dB and the elliptical to 17.9 dB which satisfy the 15 dB attenuation requirement. At 20 degrees angle-of-attack, the low frequency gain of the circular actuator command branch increases substantially while there is a small increase for the elliptical. The phase of the actuator branch for both airframes does not change. The yaw acceleration feedback frequency responses at 20 degrees angle-of-attack has a slight increase in gain for both airframes and no change in phase.

The frequency responses of the uncoupled yaw autopilot is compared to the corresponding ones for the CBTT autopilot in Section 7.

Angle-of-attack (α, deg)	Circular Airframe	Elliptical Airframe
	r/δ_y (1/sec)	
0	$\frac{(0.15)(\frac{s}{0.0748}+1)}{(\frac{s}{4.3}+1)(\frac{s}{-4.25}+1)}$	$\frac{(-0.0598)(\frac{s}{0.0342}+1)}{\frac{s^2}{(4.088)^2}+\frac{2(0.0053)s}{4.088}+1}$
10	$\frac{(0.249)(\frac{s}{0.089}+1)}{(\frac{s}{3.77}+1)(\frac{s}{-3.69}+1)}$	$\frac{(-0.0735)(\frac{s}{0.0453}+1)}{\frac{s^2}{(4.088)^2}+\frac{2(0.0067)s}{4.088}+1}$
20	$\frac{(2.3)(\frac{s}{0.011}+1)}{(\frac{s}{1.54}+1)(\frac{s}{-1.43}+1)}$	$\frac{(-0.0718)(\frac{s}{0.051}+1)}{\frac{s^2}{(4.72)^2}+\frac{2(0.0069)s}{4.72}+1}$
	η_y/δ_y (g's/rad)	
0	$\frac{(17.76)(\frac{s}{11.48}+1)(\frac{s}{-11.48}+1)}{(\frac{s}{4.3}+1)(\frac{s}{-4.25}+1)}$	$\frac{(-7.1)(\frac{s}{7.87}+1)(\frac{s}{-7.87}+1)}{\frac{s^2}{(4.088)^2}+\frac{2(0.0053)s}{4.088}+1}$
10	$\frac{(29.49)(\frac{s}{12.6}+1)(\frac{s}{-12.6}+1)}{(\frac{s}{3.77}+1)(\frac{s}{-3.69}+1)}$	$\frac{(-8.73)(\frac{s}{9}+1)(\frac{s}{-9}+1)}{\frac{s^2}{(4.088)^2}+\frac{2(0.0067)s}{4.088}+1}$
20	$\frac{(273.1)(\frac{s}{13.5}+1)(\frac{s}{-13.5}+1}{(\frac{s}{1.54}+1)(\frac{s}{-1.43}+1)}$	$\frac{(-8.52)(\frac{s}{9.13}+1)(\frac{s}{-9.13}+1)}{\frac{s^2}{(4.72)^2}+\frac{2(0.0069)s}{4.72}+1}$

TABLE E.1 Comparison of Uncoupled Yaw Channel Transfer Functions

Airframe	Branch	Gain (dB)	Margin (rad/sec)	Phase (deg)	Margin (rad/sec)
Circular	Actuator Command	-10.4	5.19	50.8	16.6
Elliptical		-19.	5.67	49.	16.5
Circular	Acceleration Feedback	10.4	10.2	57.7	3.03
Elliptical		7.8	10.86	54.3	3.0

TABLE E.2 Comparison of Uncoupled Yaw Channel Stability Margins
($\alpha_e = 0$)

Airframe	Branch	Gain (dB)	Margin (rad/sec)	Phase (dB)	Margin (rad/sec)
Circular	Actuator Command	-13.0	6.14	55.1	20.5
Elliptical		-15.5	6.72	48.4	16.93
Circular	Acceleration Feedback	10.1	11.97	52.4	3.87
Elliptical		6.3	11.36	44.9	16.93

TABLE E.3 Comparison of Uncoupled Yaw Channel Stability Margins
(α_e = 20 deg)

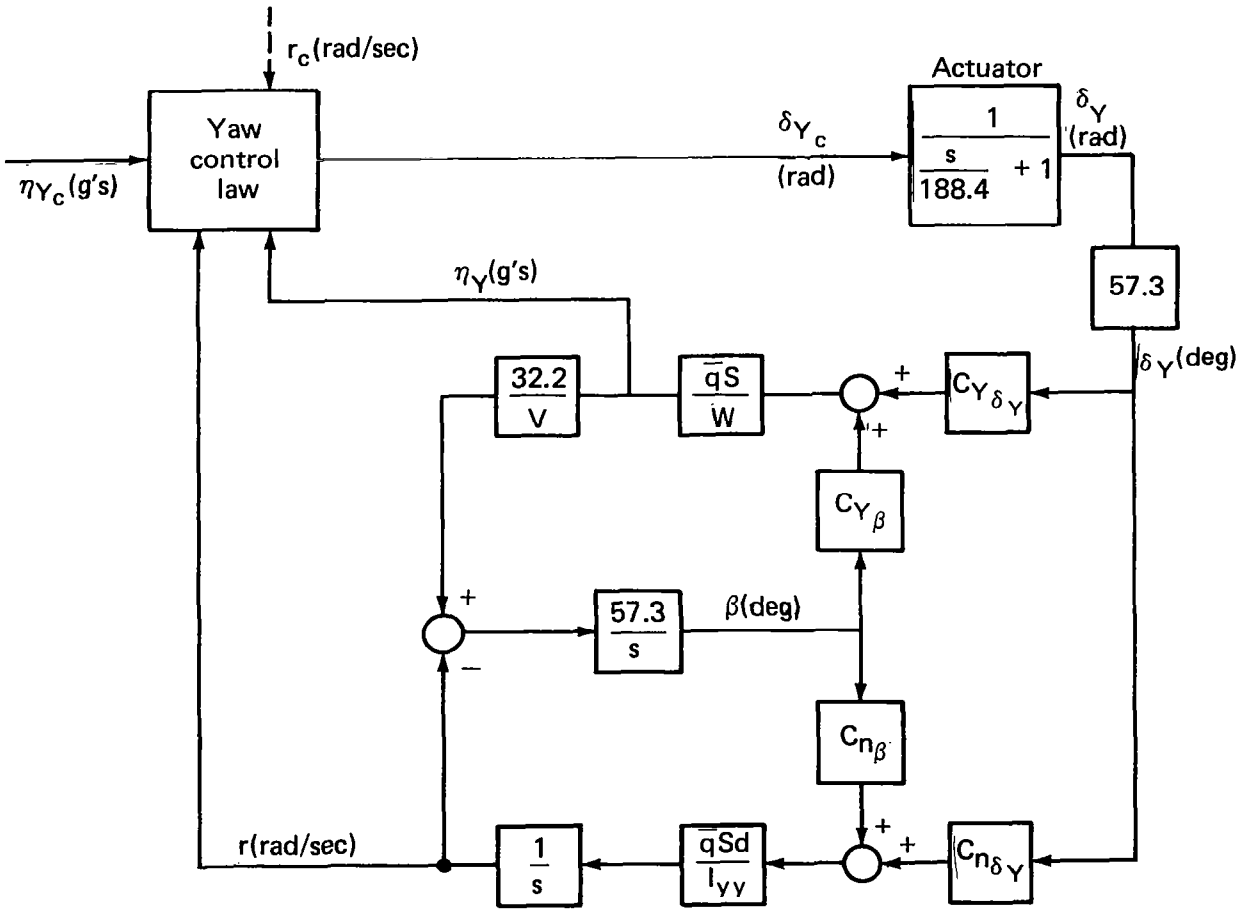

Fig. E.1 Uncoupled yaw channel.

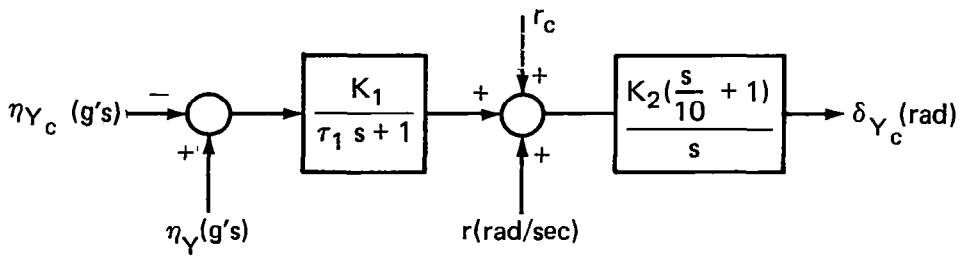

Airframe	K_1	τ_1	K_2
Circular	0.31946	0.2	4.85
Elliptical	0.83935	0.25	6.08

Fig. E.2 Yaw control laws.

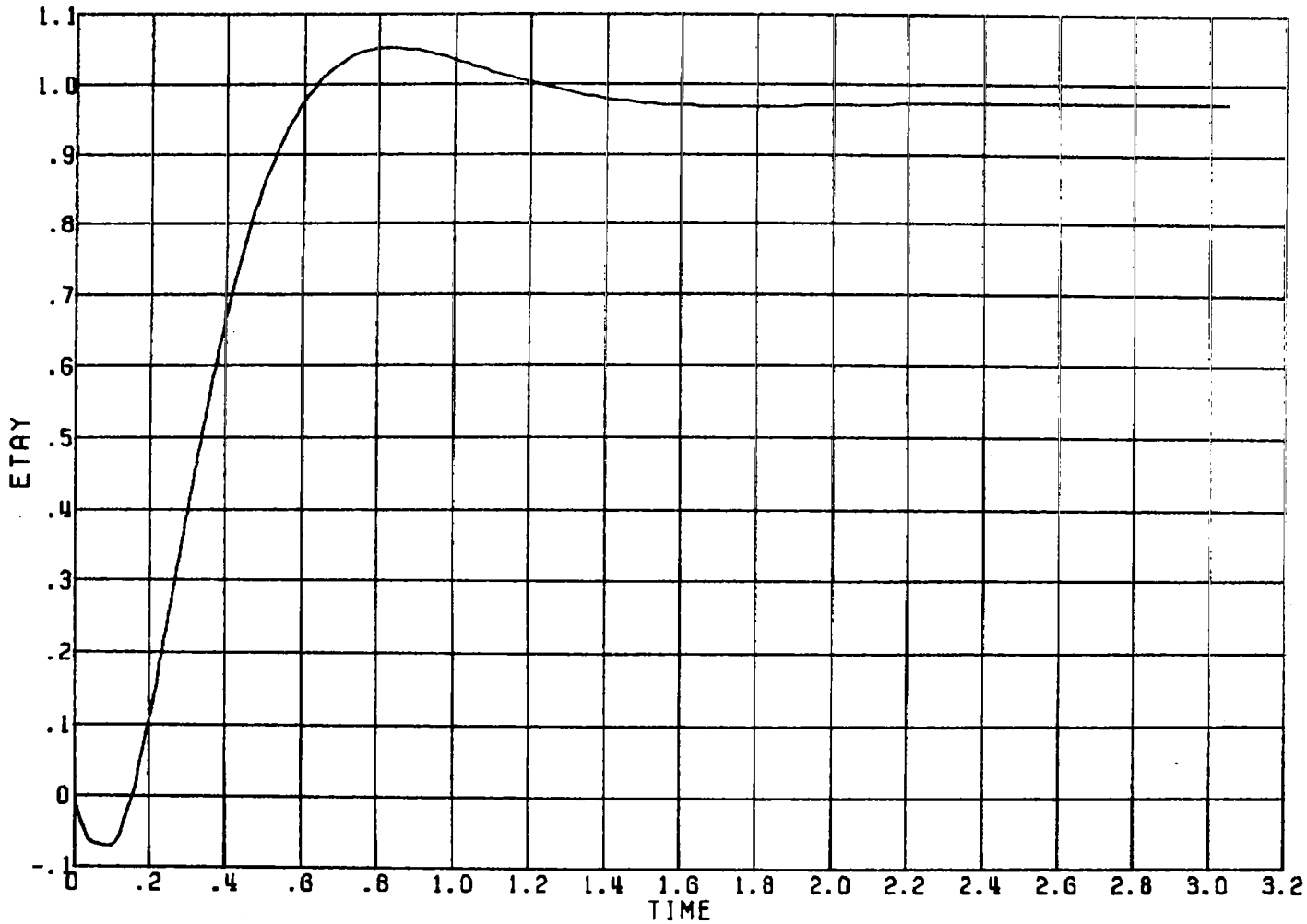

Figure E.3 YAW NORMAL ACCELERATION (GEES) VS. TIME (SEC);
UNCOUPLED YAW CHANNEL;
CIRCULAR AIRFRAME (α_e = 0, 1 GEE COMMAND)

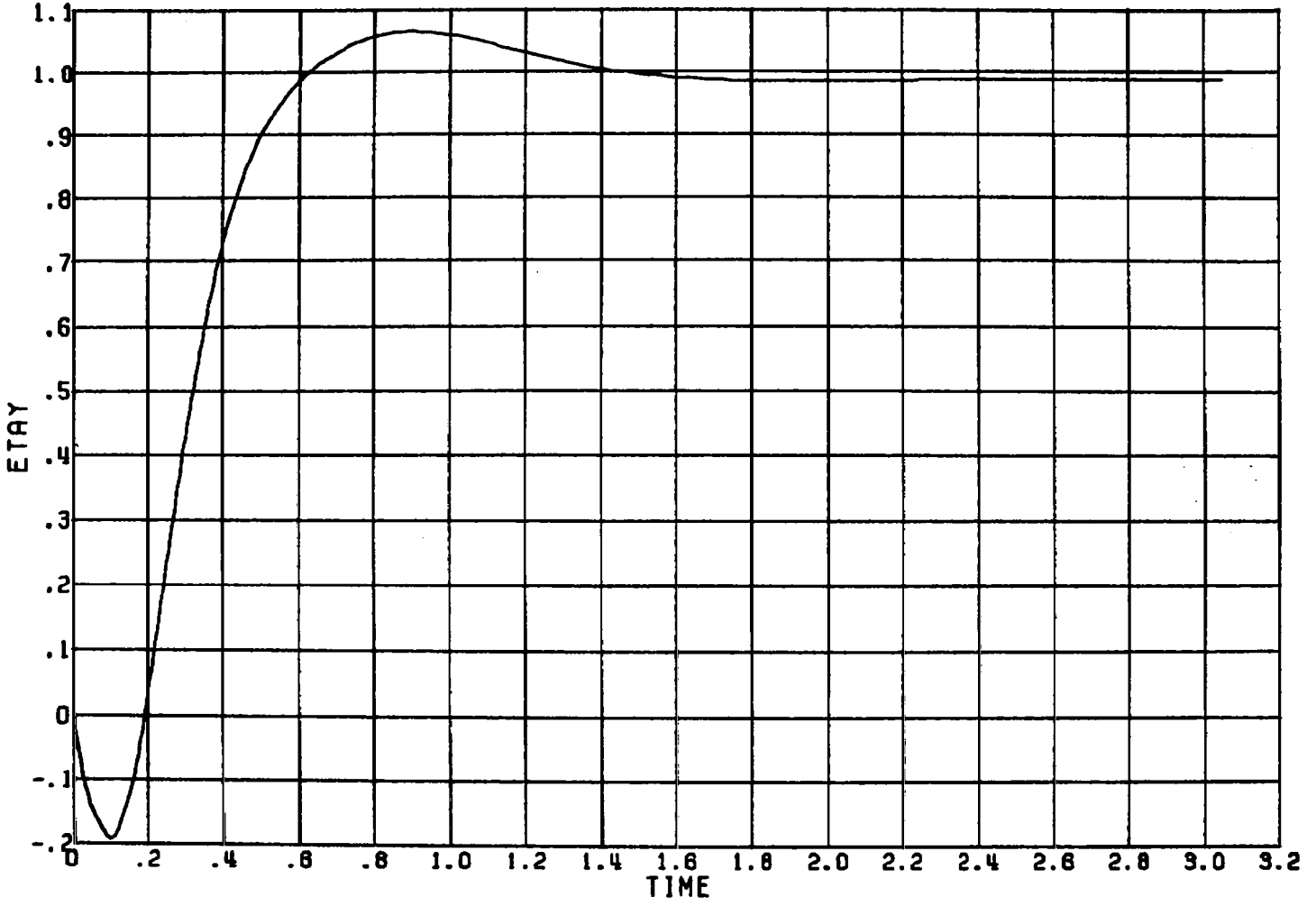

Figure E.4 YAW NORMAL ACCELERATION (GEES) VS. TIME (SEC);
UNCOUPLED YAW CHANNEL;
ELLIPTICAL AIRFRAME (α_e = 0, 1 GEE COMMAND)

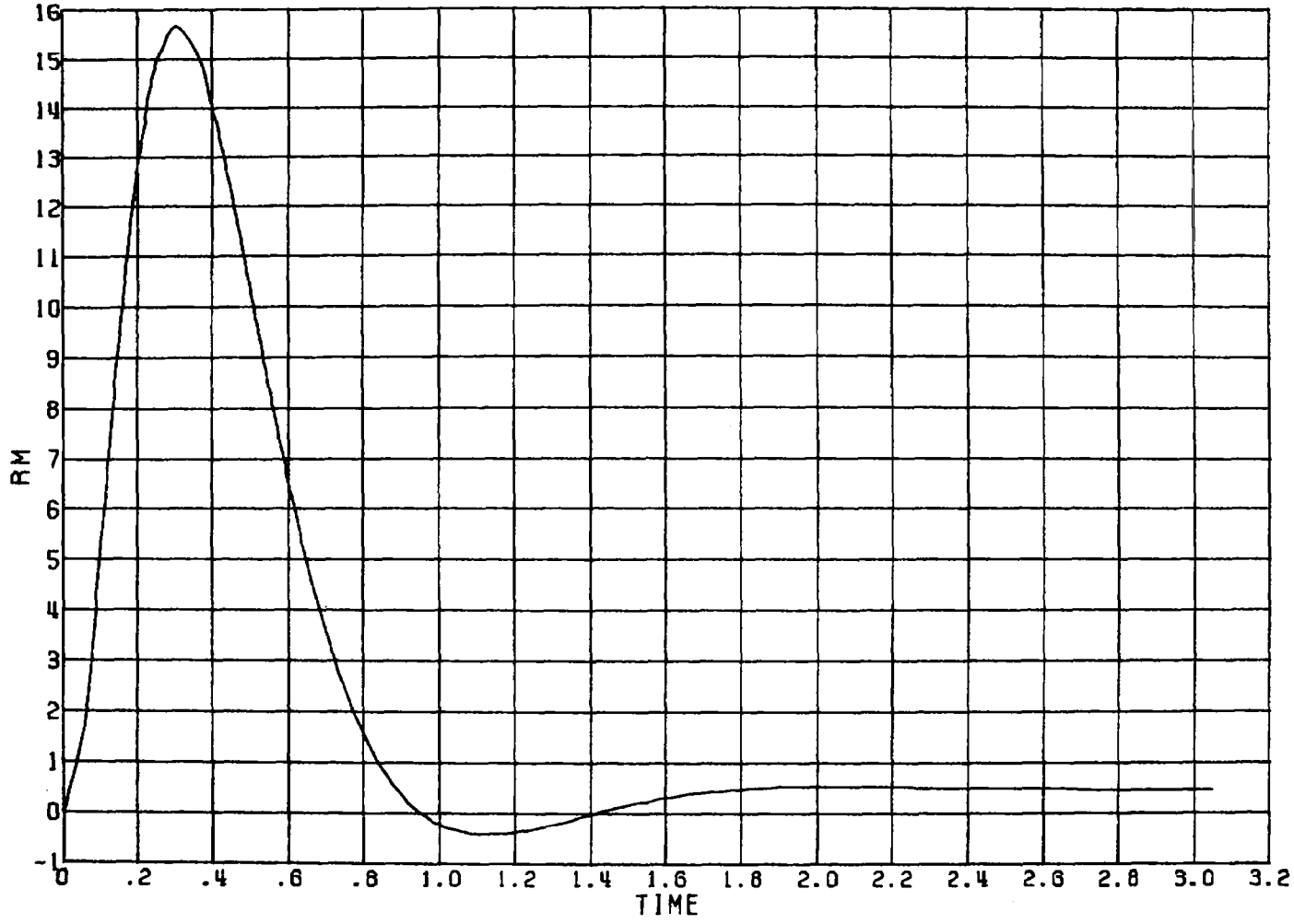

Figure E.5 YAW ANGULAR RATE (DEG/SEC) VS. TIME (SEC);
UNCOUPLED YAW CHANNEL;
CIRCULAR AIRFRAME (α_e = 0, 1 GEE COMMAND)

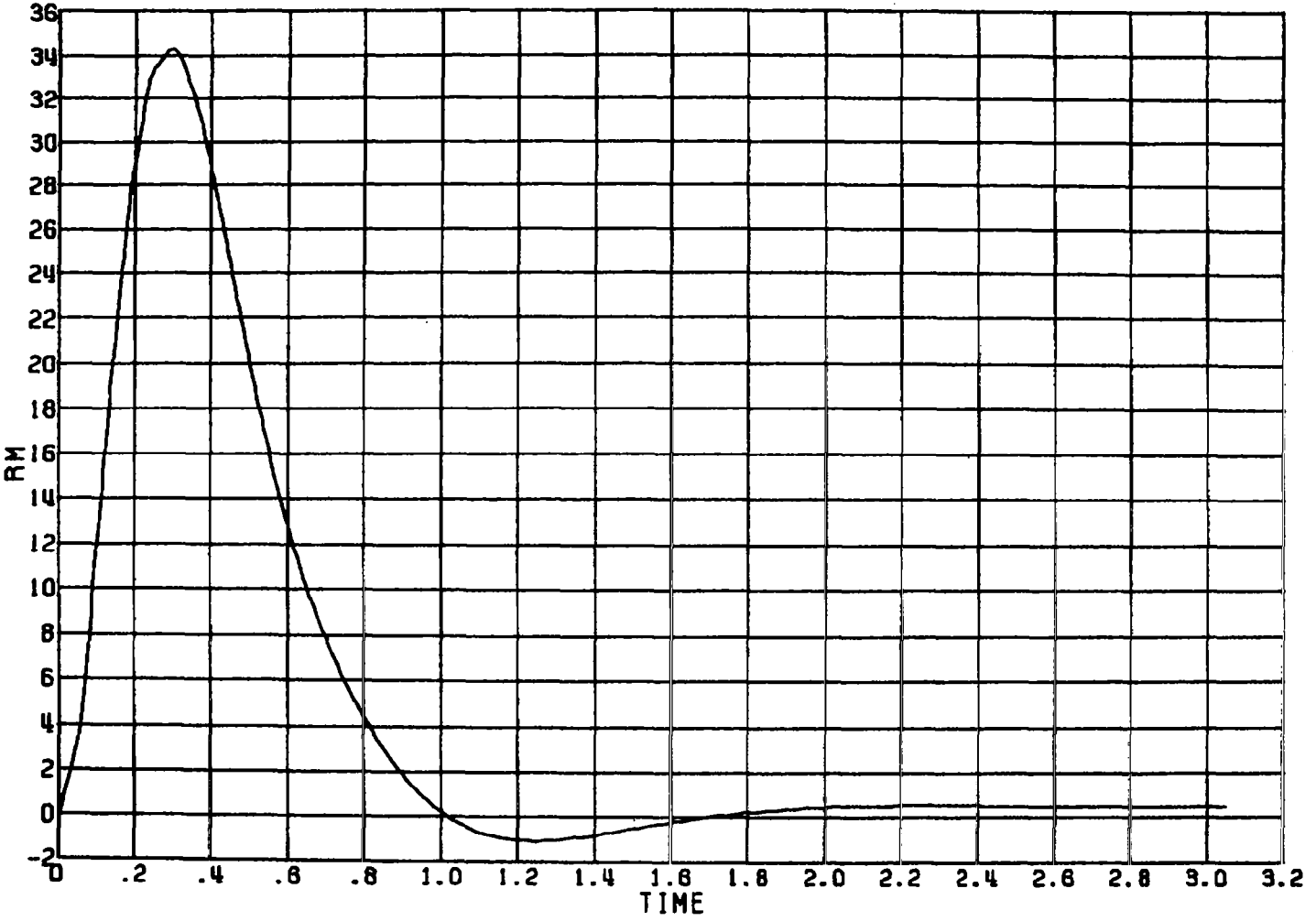

Figure E.6 YAW ANGULAR RATE (DEG/SEC) VS. TIME (SEC);
UNCOUPLED YAW CHANNEL;
ELLIPTICAL AIRFRAME (α_e = 0, 1 GEE COMMAND)

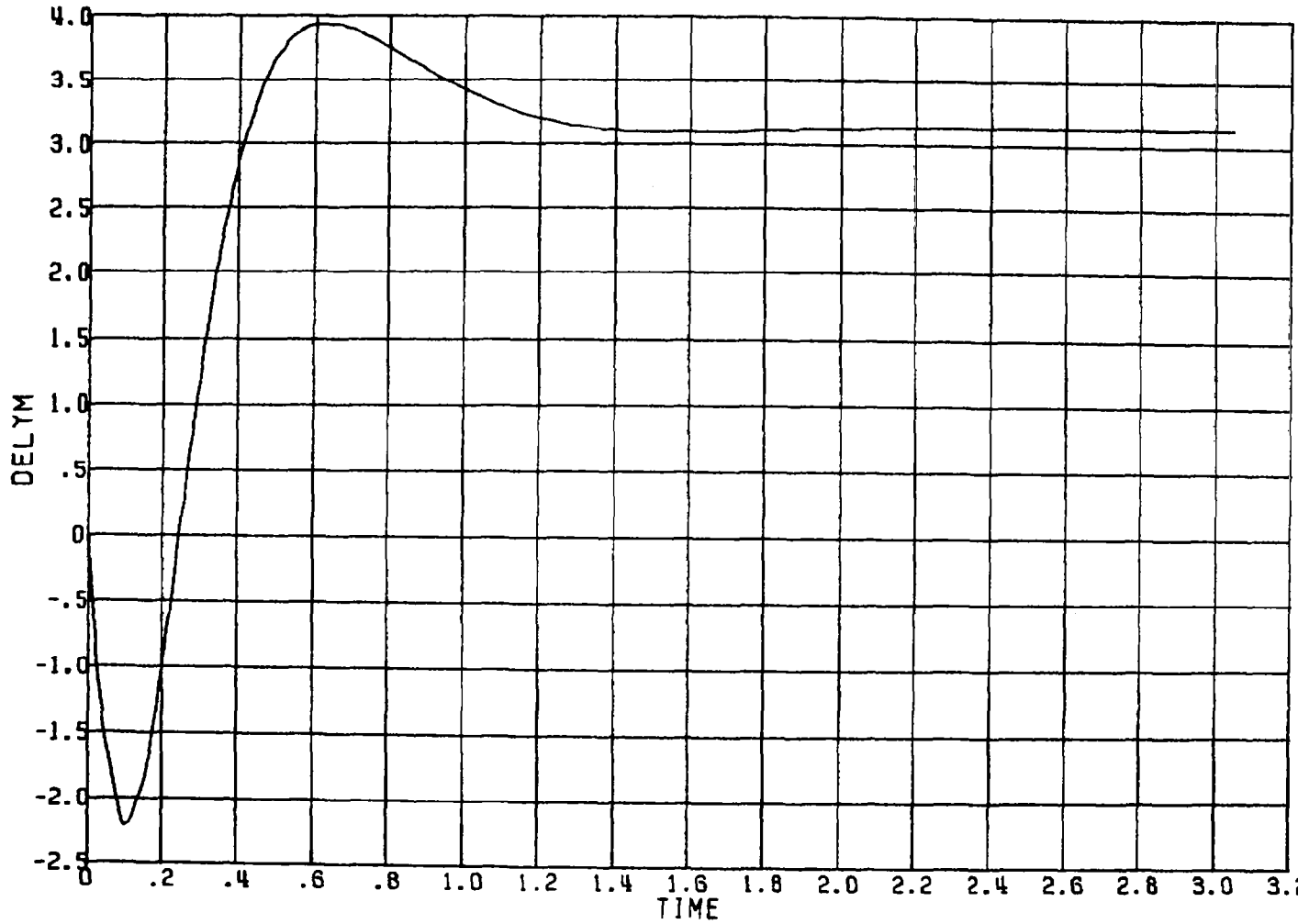

Figure E.7 YAW TAIL INCIDENCE (DEG) VS. TIME (SEC);
UNCOUPLED YAW CHANNEL;
CIRCULAR AIRFRAME (α_e = 0, 1 GEE COMMAND)

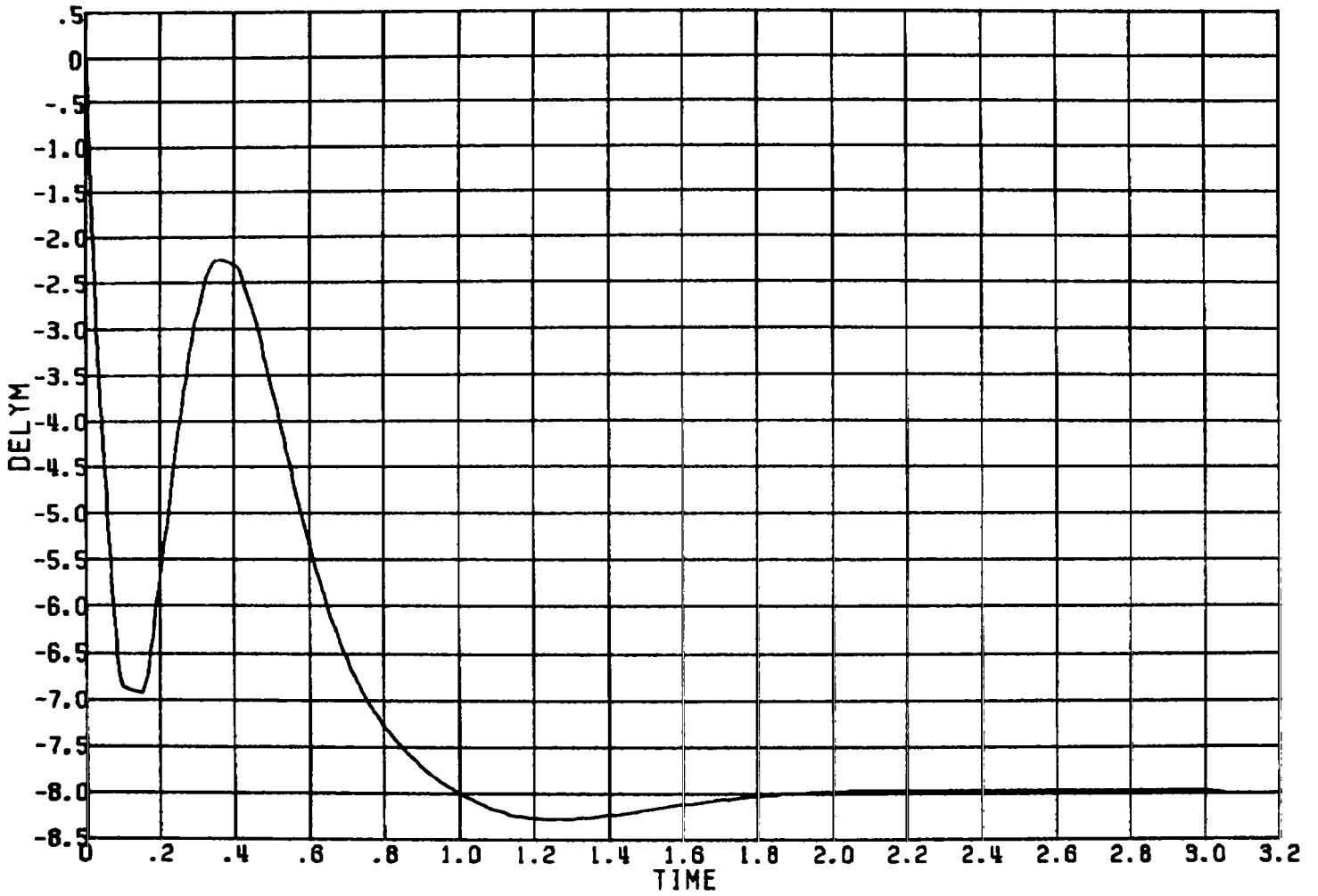

Figure E.8 YAW TAIL INCIDENCE (DEG) VS. TIME (SEC);
UNCOUPLED YAW CHANNEL;
ELLIPTICAL AIRFRAME (α_e = 0, 1 GEE COMMAND)

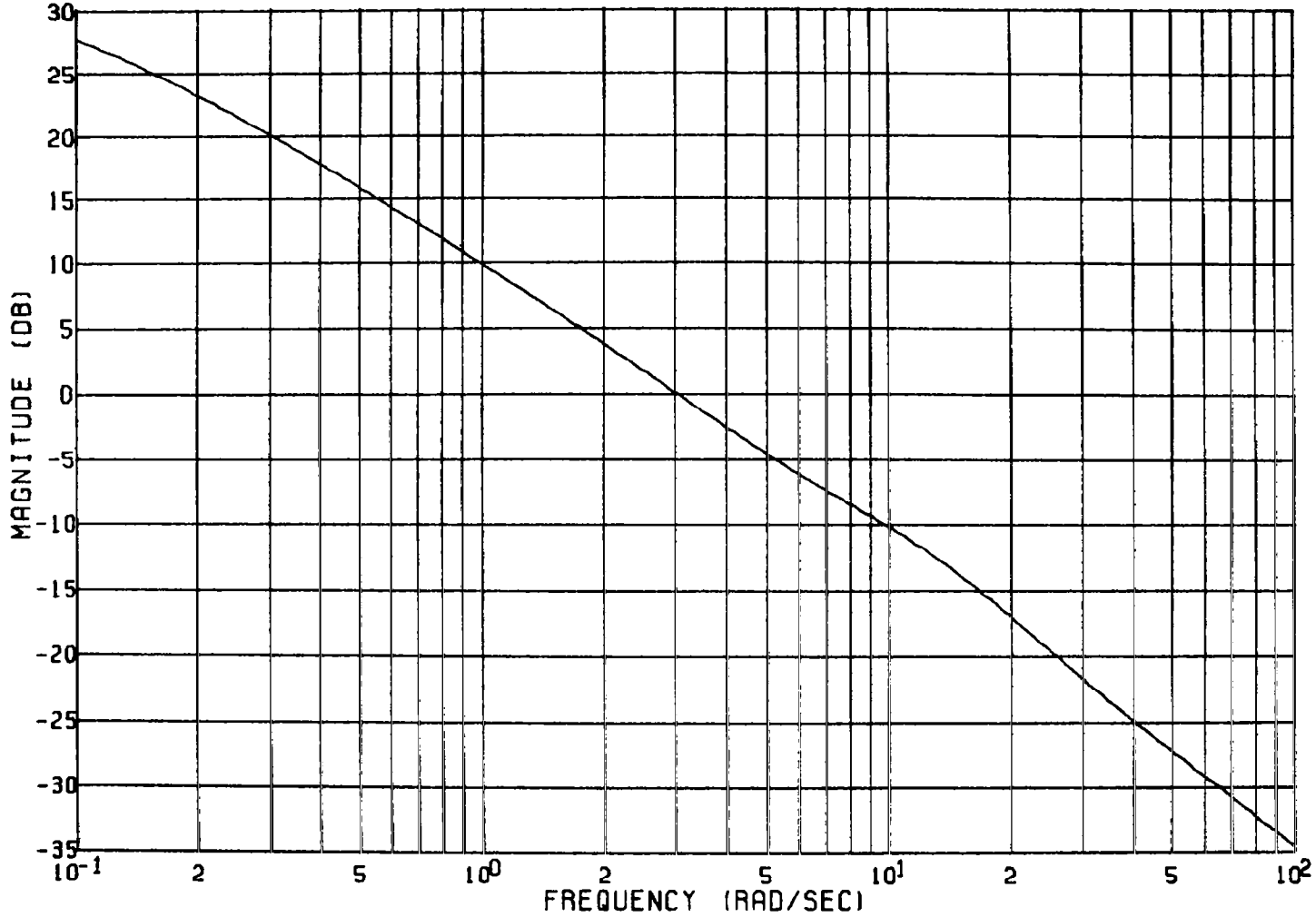

Figure E.9(a) YAW ACCELERATION FEEDBACK; UNCOUPLED YAW CHANNEL;
CIRCULAR AIRFRAME ($\alpha_e = 0$)
GAIN VS. FREQUENCY

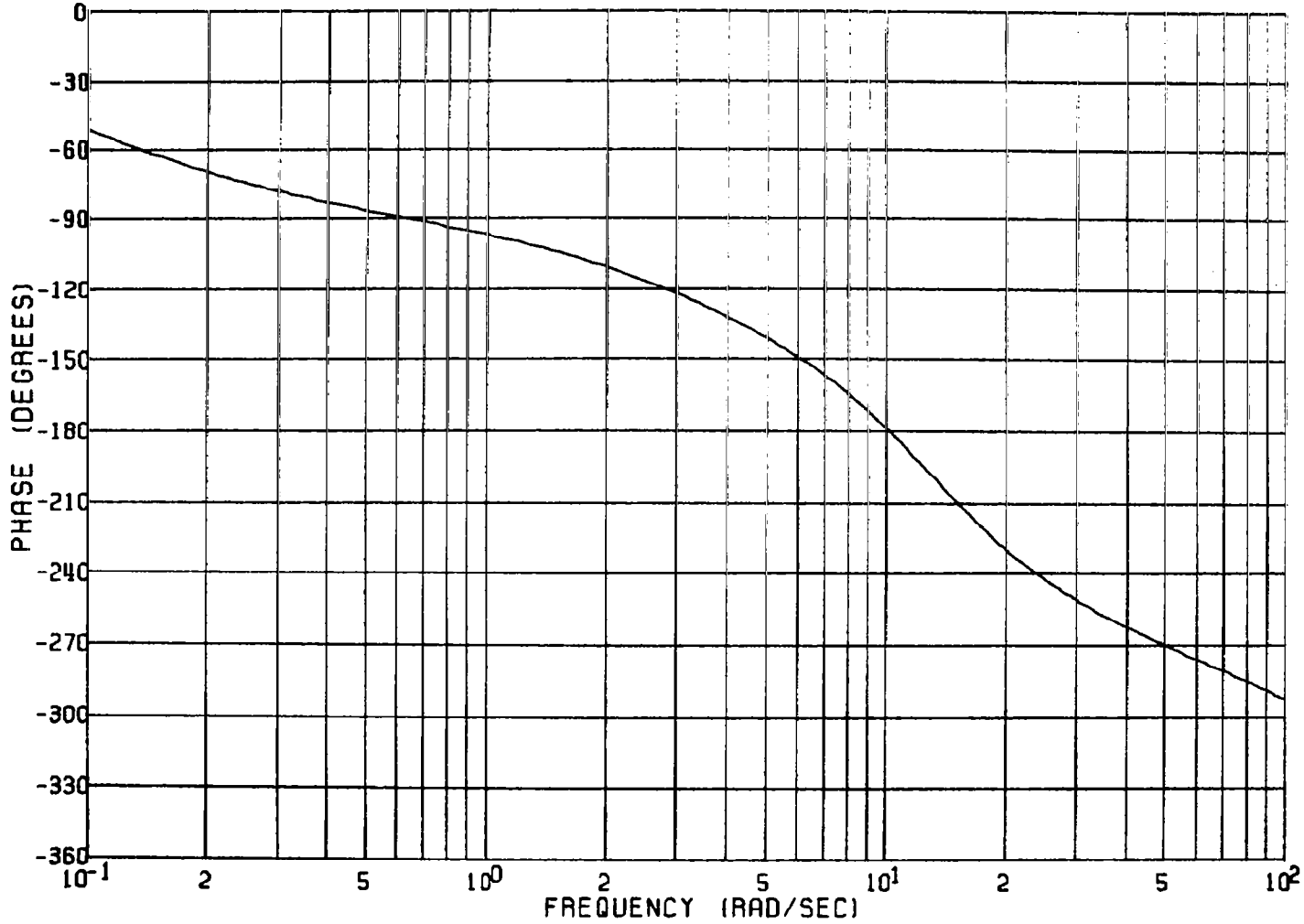

Figure E.9(b) YAW ACCELERATION FEEDBACK; UNCOUPLED YAW CHANNEL; CIRCULAR AIRFRAME ($\alpha_e = 0$) PHASE VS. FREQUENCY

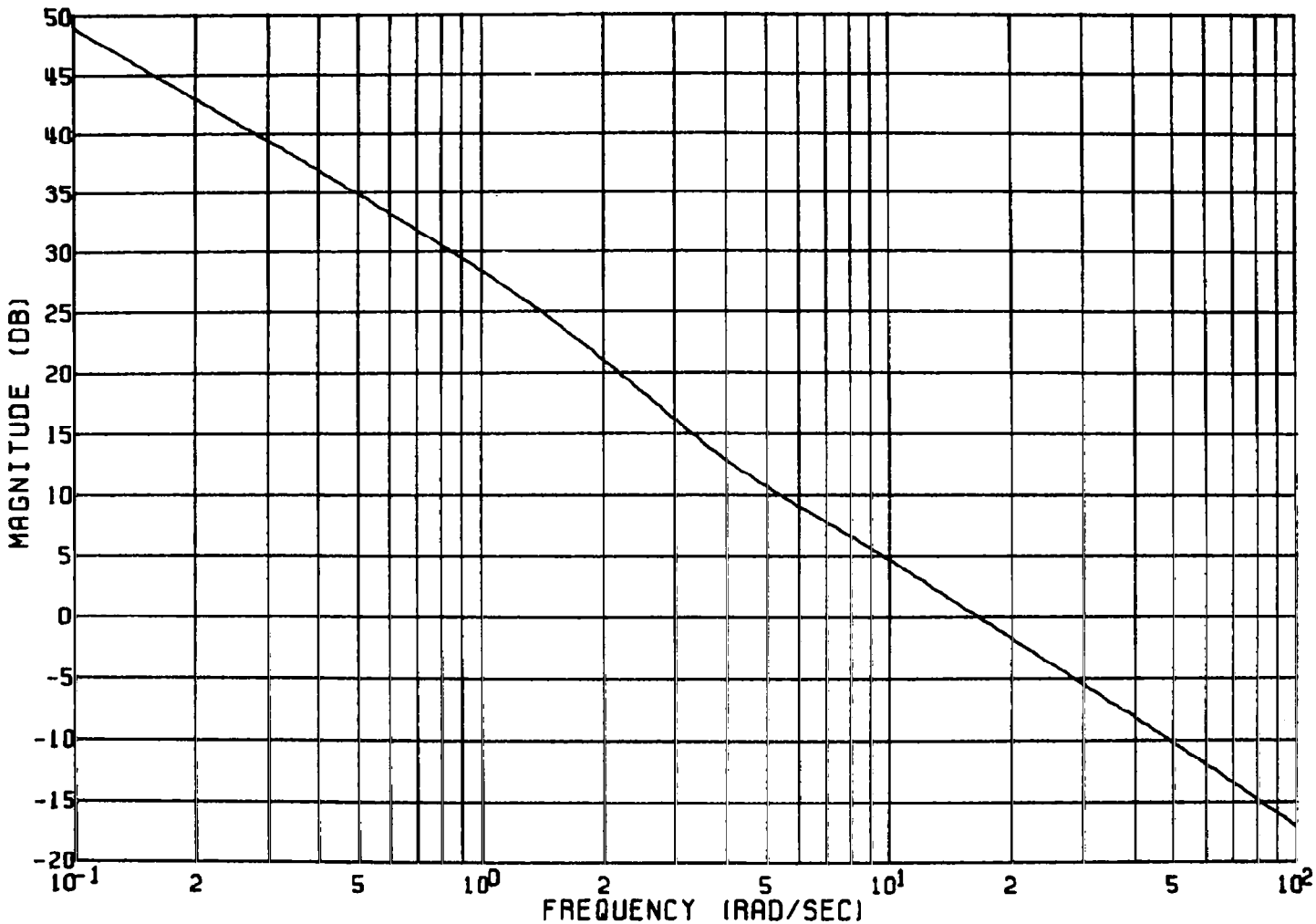

Figure E.10(a) YAW ACTUATOR COMMAND; UNCOUPLED YAW CHANNEL;
CIRCULAR AIRFRAME ($\alpha_e = 0$)
GAIN VS. FREQUENCY

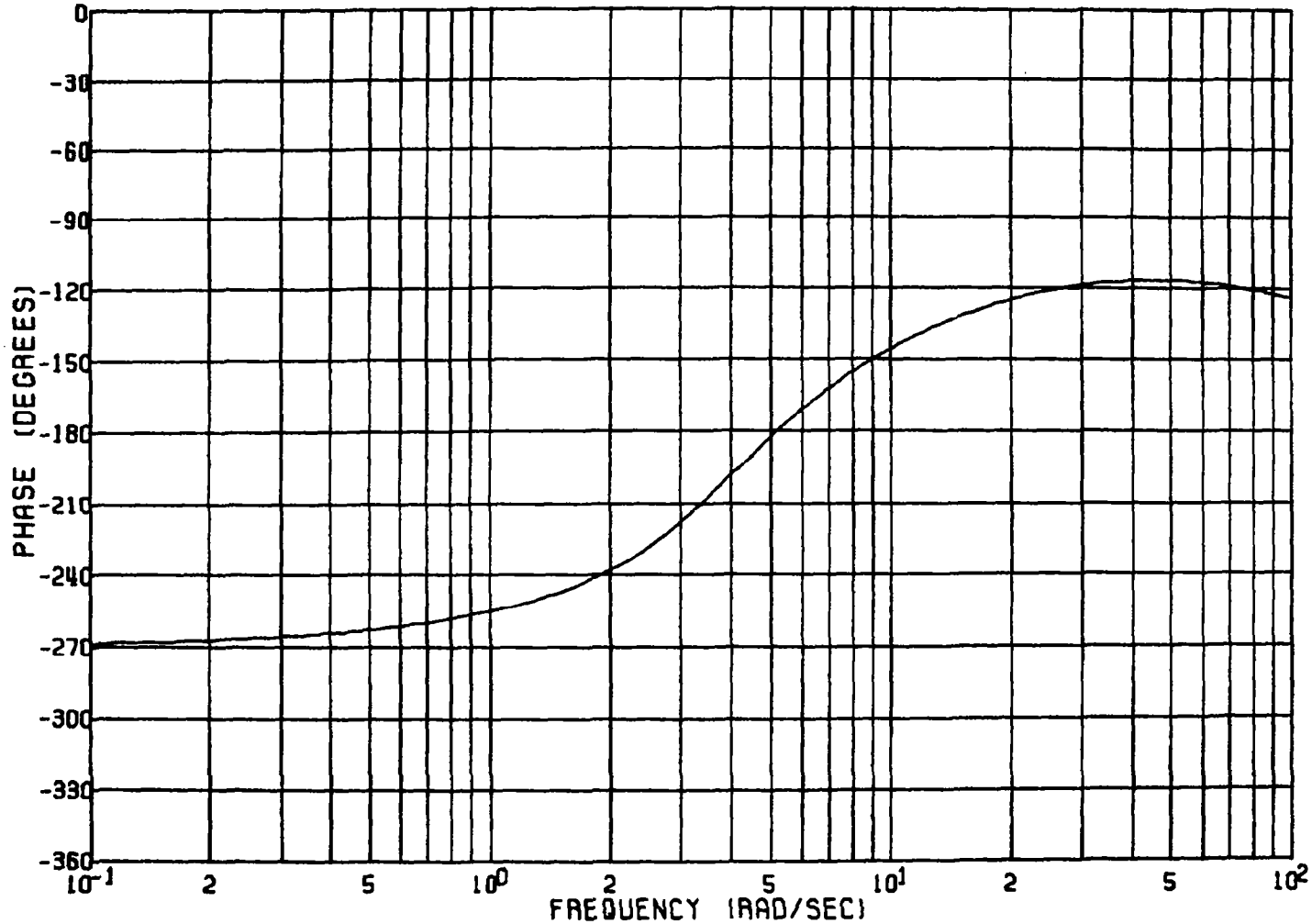

Figure E.10(b) YAW ACTUATOR COMMAND; UNCOUPLED YAW CHANNEL; CIRCULAR AIRFRAME ($\alpha_e = 0$) PHASE VS. FREQUENCY

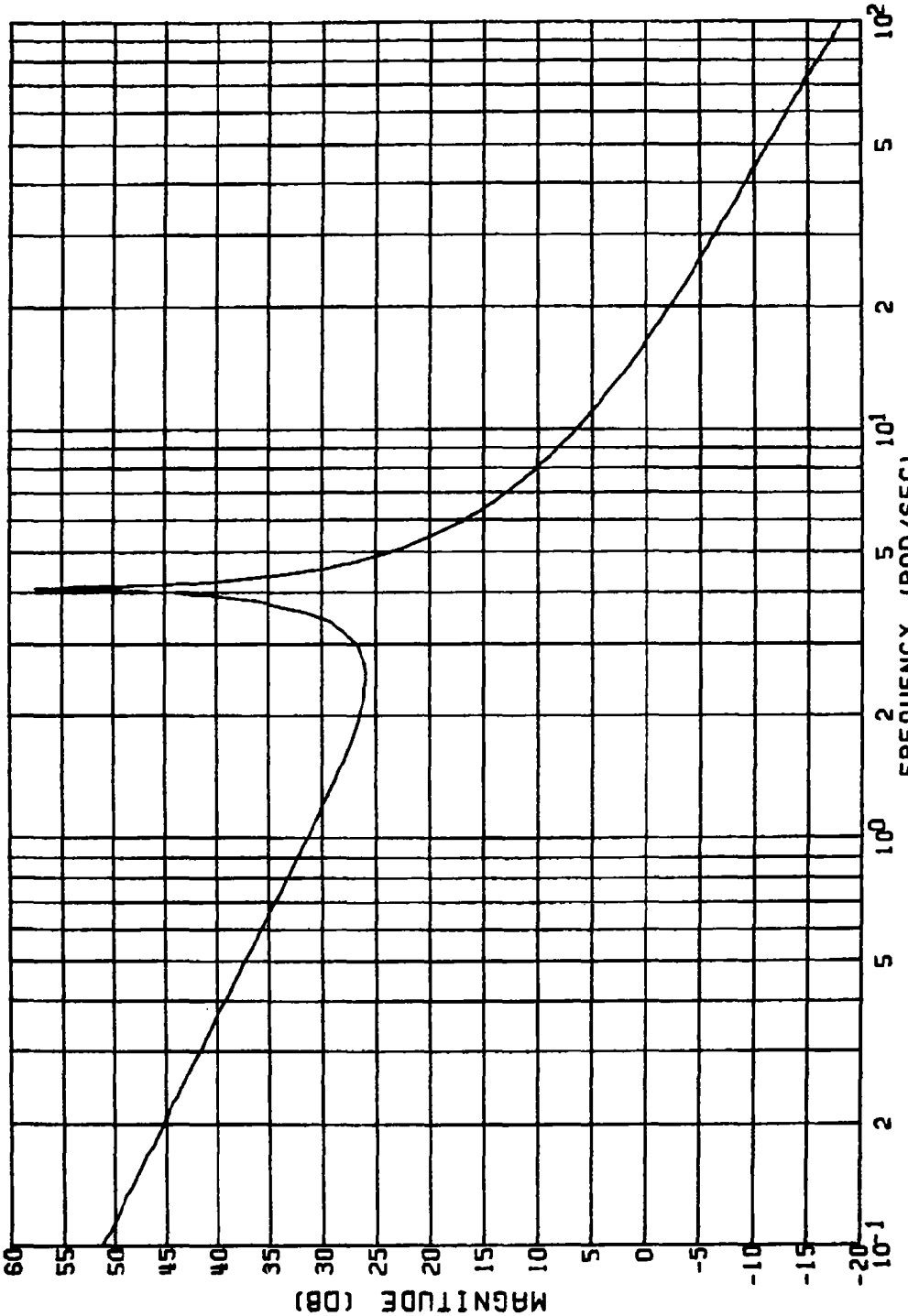

Figure E.11(a) YAW ACCELERATION FEEDBACK; UNCOUPLED YAW CHANNEL; ELLIPTICAL AIRFRAME ($\alpha_e = 0$) GAIN VS. FREQUENCY

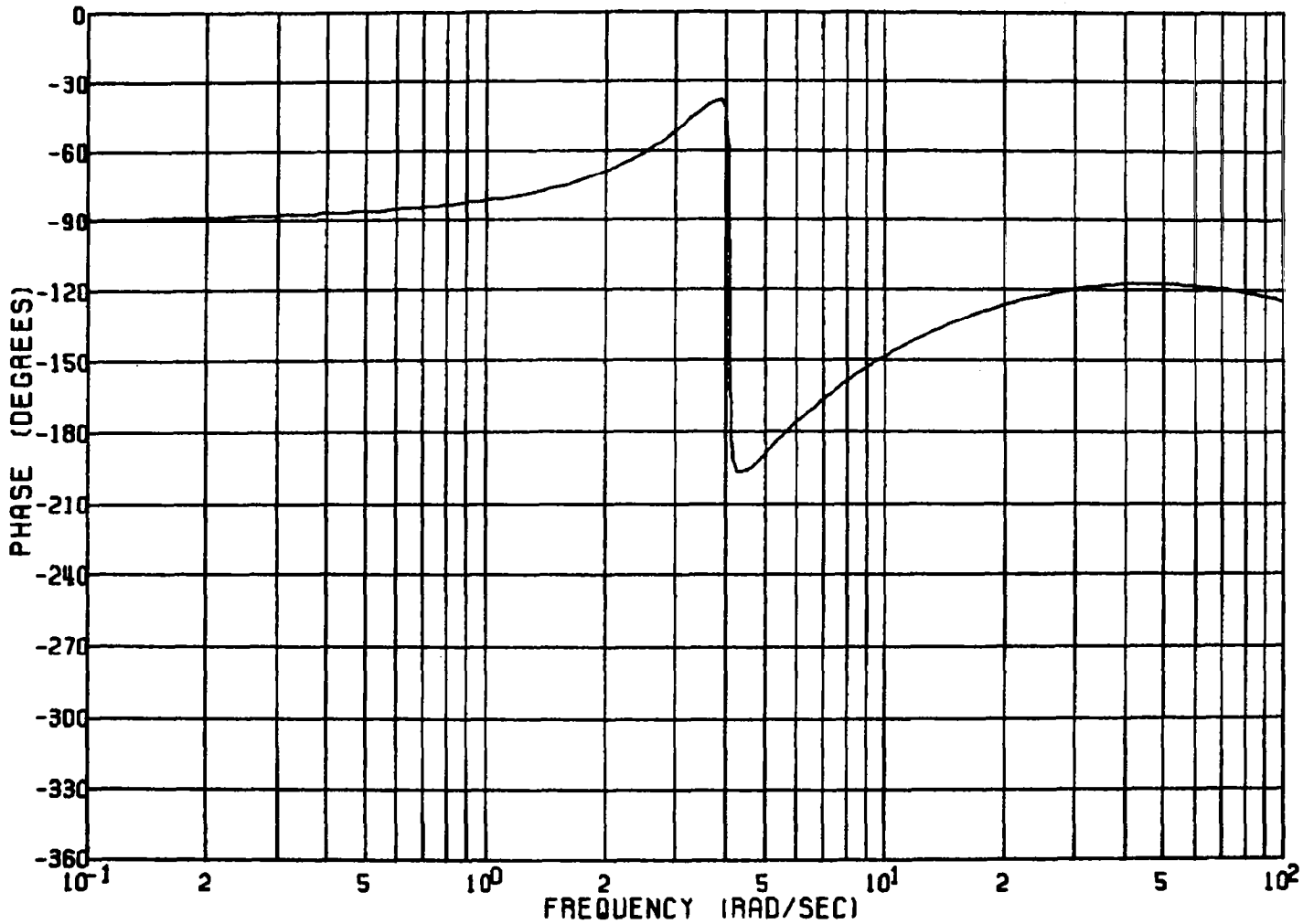

Figure E.11(b) YAW ACCELERATION FEEDBACK; UNCOUPLED YAW CHANNEL;
ELLIPTICAL AIRFRAME ($\alpha_e = 0$)
PHASE VS. FREQUENCY

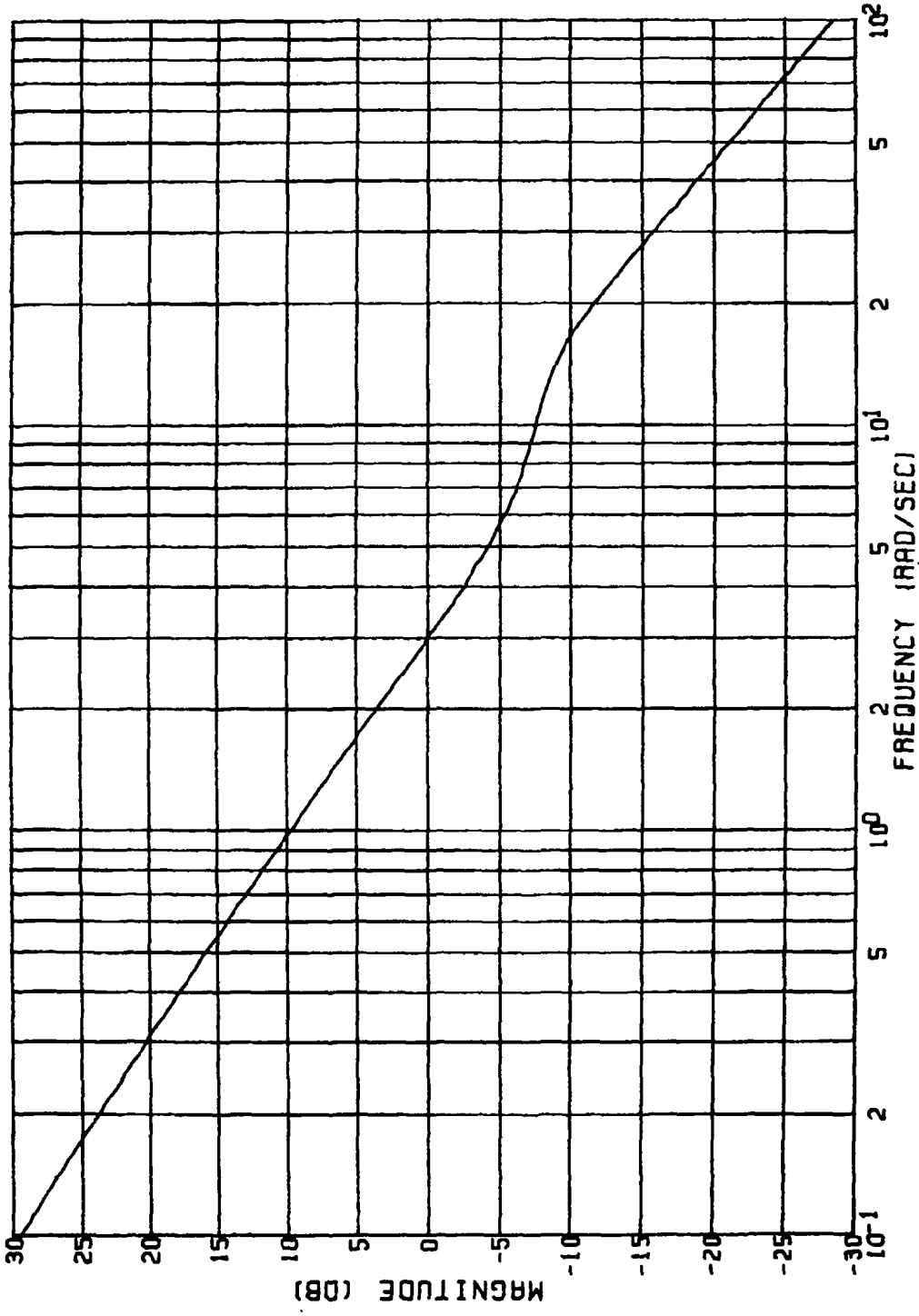

Figure E.12(a) YAW ACTUATOR COMMAND; UNCOUPLED YAW CHANNEL; ELLIPTICAL AIRFRAME ($\alpha_e = 0$) GAIN VS. FREQUENCY

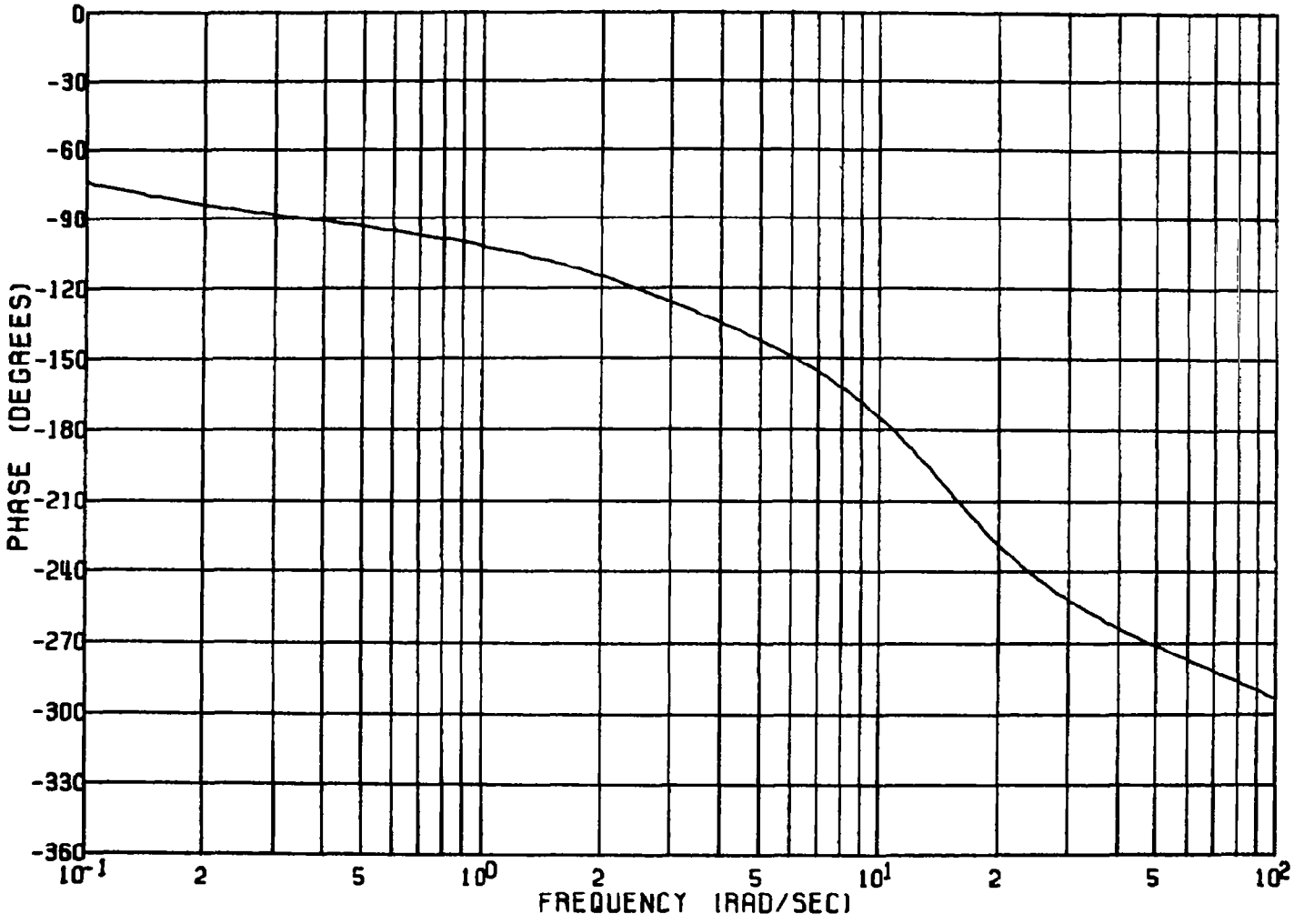

Figure E.12(b) YAW ACTUATOR COMMAND; UNCOUPLED YAW CHANNEL;
ELLIPTICAL AIRFRAME ($\alpha_e = 0$)
PHASE VS. FREQUENCY

APPENDIX F

LINEAR DESIGN AND ANALYSIS OF UNCOUPLED ROLL AUTOPILOTS

The roll channel of a coordinated bank-to-turn (CBTT) autopilot is commanded to roll the missile so as to put the preferred maneuver direction of the missile in the direction of the guidance acceleration command while the pitch channel acceleration is commanded to produce the total magnitude of the guidance acceleration command. The desired maneuver plane acceleration should be attained as rapidly as the achieved body-fixed pitch acceleration. To accomplish this, the uncoupled roll channel autopilot (i.e., pitch and yaw dynamic effects neglected) was designed to have the roll angle time constant equal to the time constant of the normal acceleration achieved by the uncoupled pitch channel autopilot.

A block diagram of the uncoupled roll channel is shown in Figure F.1. The roll control law is commanded by roll angle (ϕ_c) and is governed by roll angular rate (p) and roll angle (ϕ). The aerodynamics, linearized about a trim angle-of-attack is described in Section 5.

The first section of this appendix contains the aerodynamic transfer functions used to design the control law. The second section discusses what type of roll dynamics is desired and compares the circular and elliptical airframes. Section F.2 covers design requirements and technique and presents the control laws. Section F.3 presents a time and frequency domain analysis of the uncoupled roll channel autopilots.

F.1 Aerodynamics Transfer Functions

The aerodynamic roll gain is as follows:

$$\frac{\dot{p}}{\delta_R} = \frac{\bar{q}Sd}{I_{xx}}(57.3)\, C_{\ell_{\delta_R}}, \qquad \text{rad/sec}^2/\text{rad} \qquad \text{F1}$$

It is desirable for the aerodynamic roll gain to be as large as possible to minimize control surface motion. It is also desirable to have as large $C_{\ell_{\delta_R}}$ as possible to minimize the effects of aerodynamic control cross coupling which will be discussed further in Section 7. Table F.1 shows that the circular airframe has a considerally larger aerodynamic roll gain due to a much smaller roll inertia and a larger control derivative $C_{\ell_{\delta_R}}$.

F.2 Requirements and Control Laws

Requirements for the classical design approach are:

1. High Frequency Attenuation in Actuator Command Branch

$\geq$ 15 dB at 100 rad/sec and zero angle-of-attack. This requirement will provide sufficient high frequency attenuation for $\geq$ 30 Hz actuator and for elastic modes when high frequency filters are added, but this requirement limits the speed of roll angle response.

2. Relative Stability

Gain margins $\geq$ 6 dB, phase margins $\geq$ 30 deg with a goal of 12 dB and 50 deg.

3. Time Response of Roll Angle

a) 63 percent time constant of 0.5 seconds for a step command of roll angle at the flight condition of interest and zero angle-of-attack.

b) Overshoot $\leq$ 10 percent. Maneuver plane acceleration response for CBTT will depend on roll angle and body-fixed acceleration responses. This requirement is conservative and may be relaxed depending upon guidance results.

c) Zero steady state roll angle error. This requirement will influence the error in maneuver plane acceleration for CBTT which, if not zero, will effect guidance.

The resulting roll control laws for the circular and elliptical airframes at the flight condition of interest (i.e., Mach 3.95, 60 Kft or 18.3 Km altitude) are shown in Figure F.2. Roll angular acceleration feedback is commonly used by roll stabilized missile autopilots to minimize the effects of aerodynamic cross-coupling at high angles-of-attack. Since roll angular acceleration may be needed it was obtained from roll angular rate via an imperfect differentiator. Lag-leads were used to prevent guidance noise saturation problems. High frequency attenuation is determined by the roll angular acceleration feedback and actuator compensations. These filters and the roll angular rate error compensation were selected so that the closed loop roll angular rate dynamics have minimum effect on roll angle response. Roll angle response is determined by the roll angle error compensation. The dc gain K of the actuator command filter compensates for the change in aerodynamic roll gain of the circular and elliptical airframes. Therefore, the roll angle and roll rate responses will be the same for both airframes. However, the gain K will result in a roll angular deflection for the elliptical airframe which is K times that of the circular airframe.

F.3 Analysis

Figures F.3 and F.4 show the roll angle response of both elliptical and circular airframes. Only the roll tail angular deflection (Figure F.5) is

different for the airframes due to the method for compensating for a reduction in the elliptical aerodynamic roll gain. The time constant of the roll angle response is 0.55 seconds. No attempt was made to adjust it closer to the uncoupled pitch channel time constant of 0.5 seconds.

The relative stability of the uncoupled roll autopilot is shown in Tables F.2 and F.3. Frequency responses given in Table F.2 are shown in Figures F.6 through F.8. The frequency response was calculated up to 100 rad/sec. Therefore, the shape of the response and the attenuation at 100 rad/sec will determine the gain margin if the phase cross-over exceeds 100 rad/sec. All margins are satisfactory. Although the phase margin in the actuator branch is at the required minimum, it may be improved if necessary by decreasing the lead of the actuator command compensation. There was a slight increase in the gains for the actuator command and rate error frequency response curves for 20 degrees angle-of-attack.

$\dot{p}/\delta_r$

Angle-of-Attack (α, deg)	Circular Airframe	Elliptical Airframe
0	460.4	124.2
10	519.8	124.2
20	653.4	156.6

TABLE F.1 Comparison of Uncoupled Roll Channel Aerodynamic Gains

Branch	Gain Margin (dB)	Gain Margin (rad/sec)	Phase Margin (deg)	Phase Margin (rad/sec)
Actuator Command	>19.6	>100	33.4	28.09
Rate Error	>27.2	>100	92.9	10.31
Angle Error	20.6	10.19	63.4	2.083

TABLE F.2 Uncoupled Roll Channel Stability Margins, Elliptical and Circular Airframes, $\alpha_e = 0$

Branch	Gain Margin (dB)	(rad/sec)	Phase Margin (deg)	(rad/sec)
Actuator Command	>16.6	>100	30.2	34.41
Rate Error	>21.55	>100	100.6	11.19
Angle Error	22.5	11.26	64.	2.08

TABLE F.3 Uncoupled Roll Channel Stability Margins, Elliptical and Circular Airframes, α_e = 20 deg.

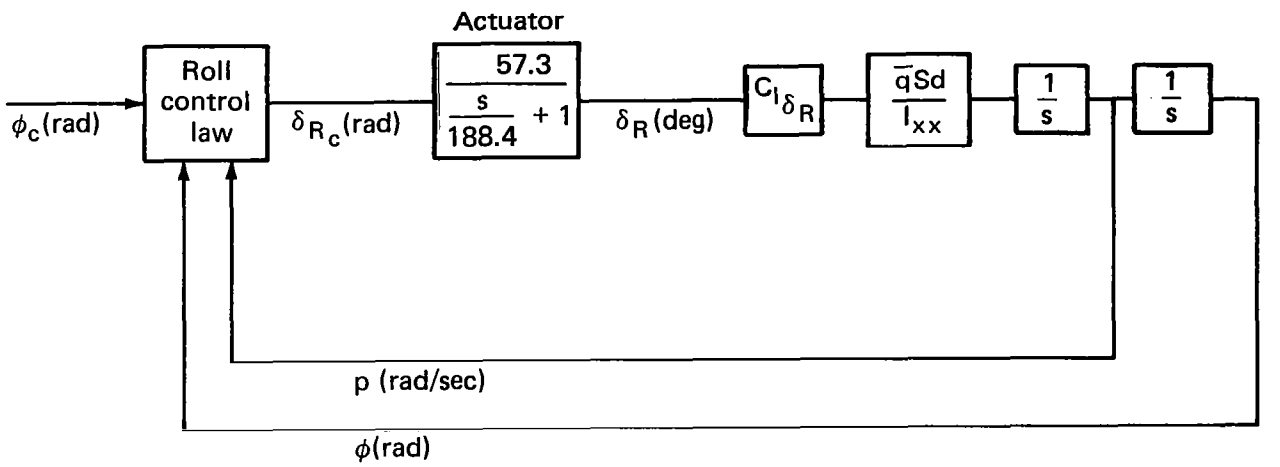

Fig. F.1 Uncoupled roll channel.

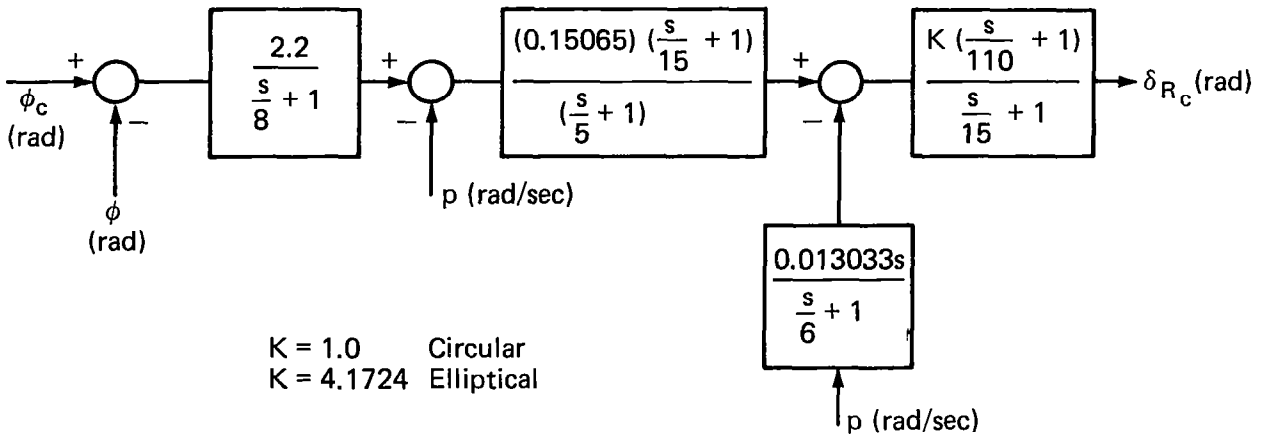

Fig. F.2 Roll control laws.

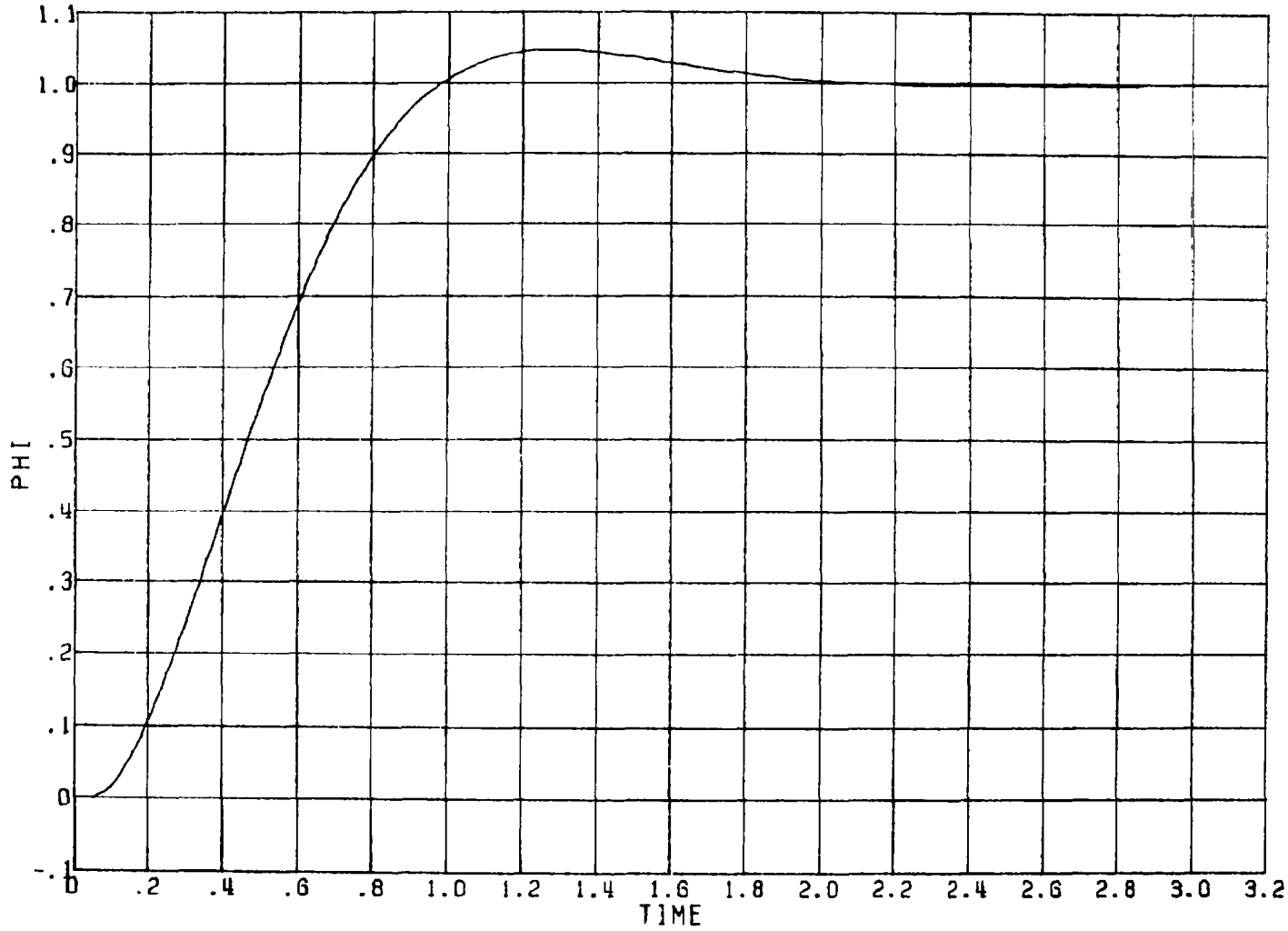

Figure F.3 ROLL ANGLE (DEG) VS. TIME (SEC);
UNCOUPLED ROLL CHANNEL;
CIRCULAR OR ELLIPTICAL AIRFRAMES (1 RADIAN COMMAND, $\alpha_e = 0$)

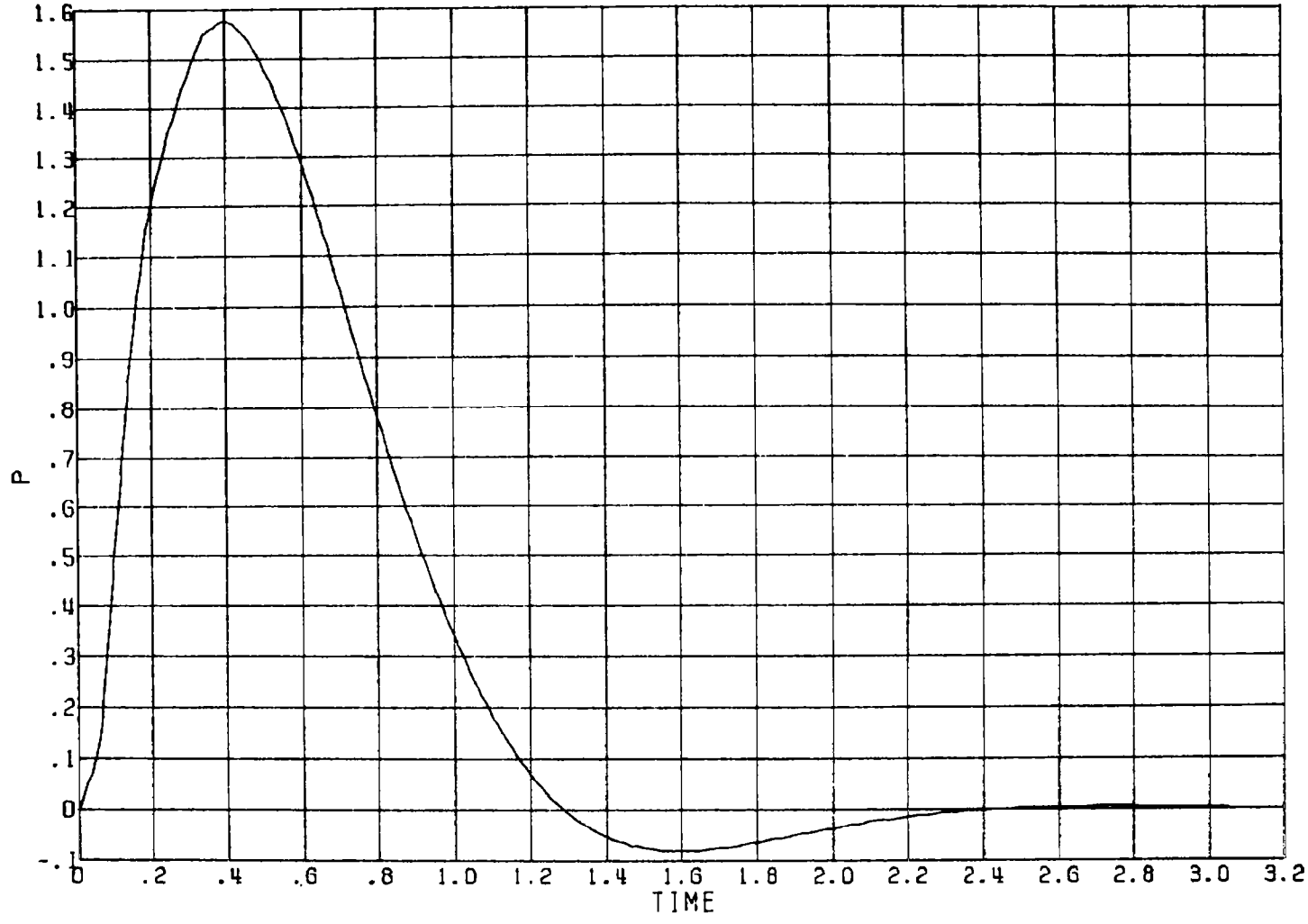

Figure F.4 ROLL ANGULAR RATE (DEG/SEC) VS. TIME (SEC);
UNCOUPLED ROLL CHANNEL;
CIRCULAR OR ELLIPTICAL AIRFRAMES (1 RADIAN COMMAND, $\alpha_e = 0$)

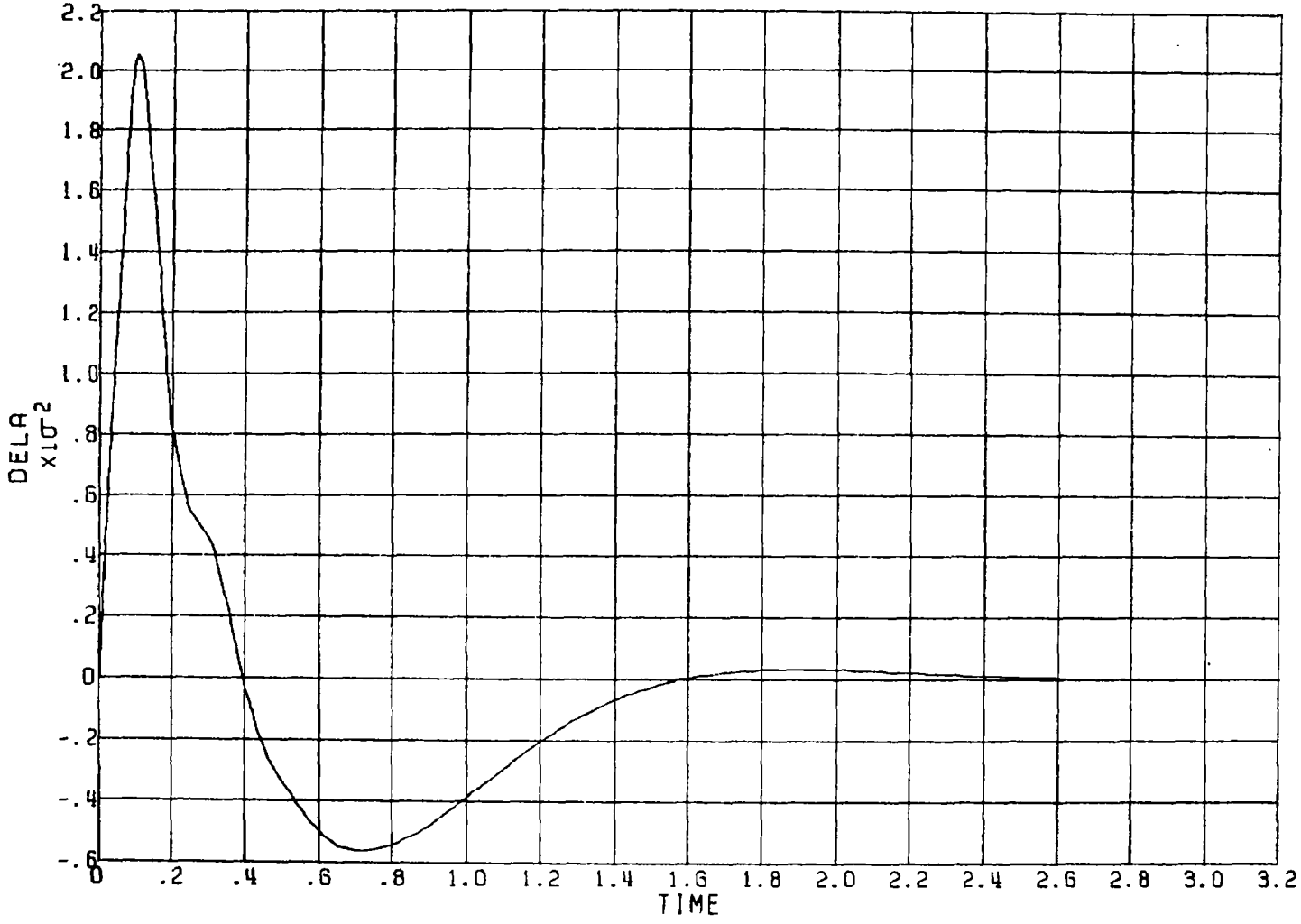

Figure F.5 ROLL TAIL INCIDENCE (DEG) VS. TIME (SEC);
UNCOUPLED ROLL CHANNEL;
CIRCULAR AIRFRAME (1 RADIAN COMMAND, $\alpha_e = 0$)

NOTE: Maximum δ_R for elliptical airframe is factor of 4.2 larger.

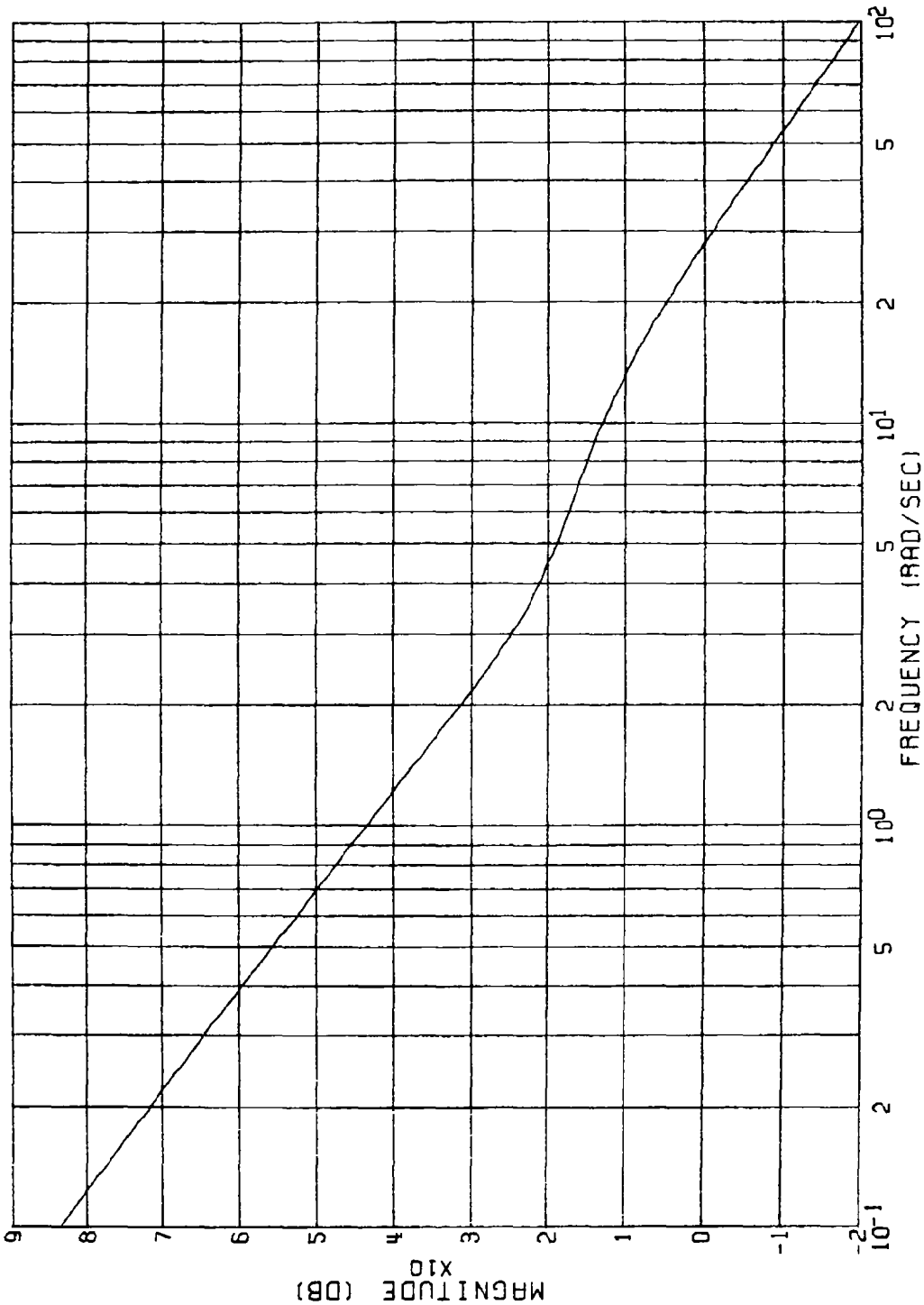

Figure F.6(a) ROLL ACTUATOR COMMAND; UNCOUPLED ROLL CHANNEL; CIRCULAR OR ELLIPTICAL AIRFRAME ($\alpha_e = 0$) GAIN VS. FREQUENCY

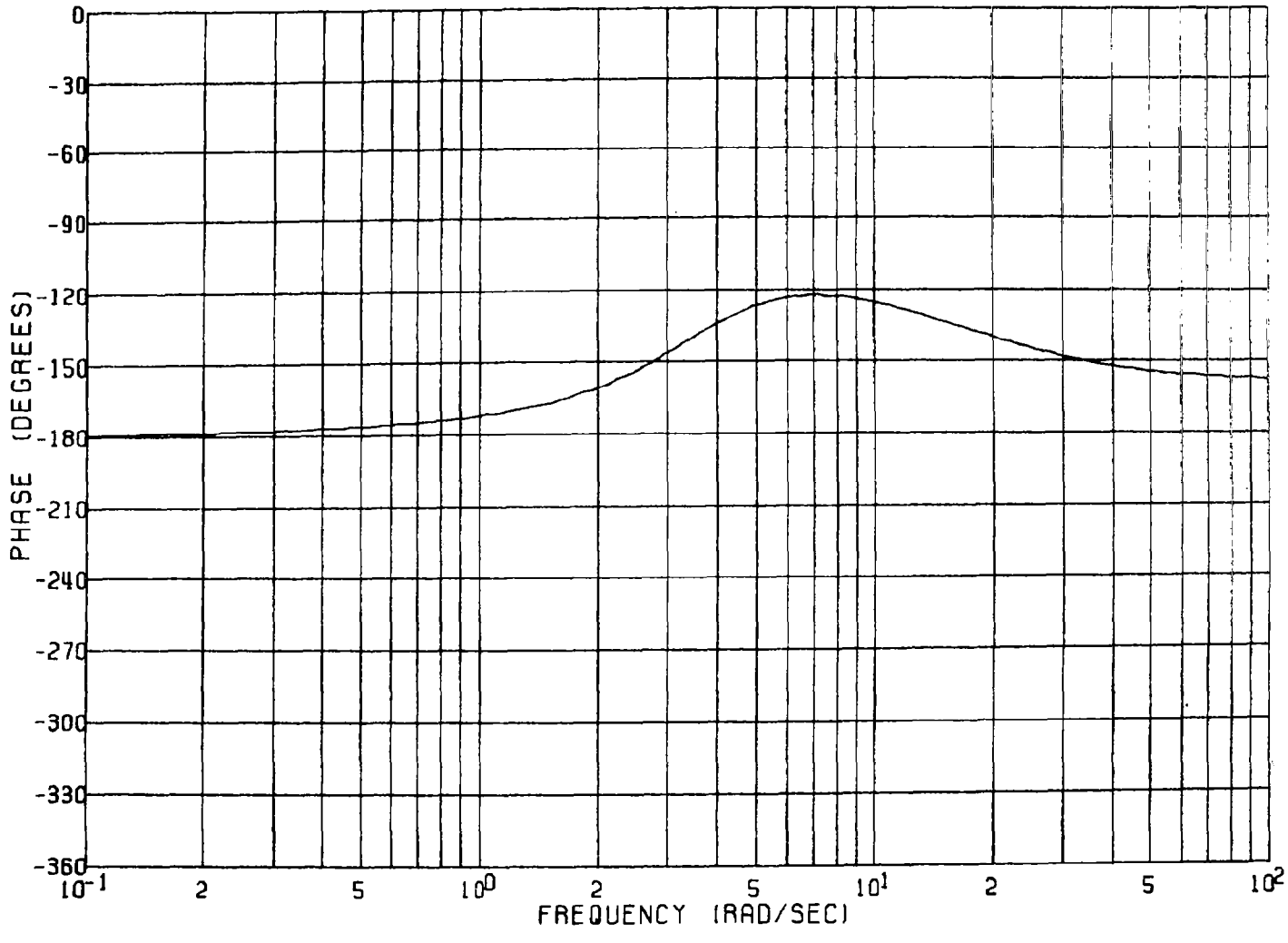

Figure F.6(b) ROLL ACTUATOR COMMAND; UNCOUPLED ROLL CHANNEL; CIRCULAR OR ELLIPTICAL AIRFRAME ($\alpha_e = 0$) PHASE VS. FREQUENCY

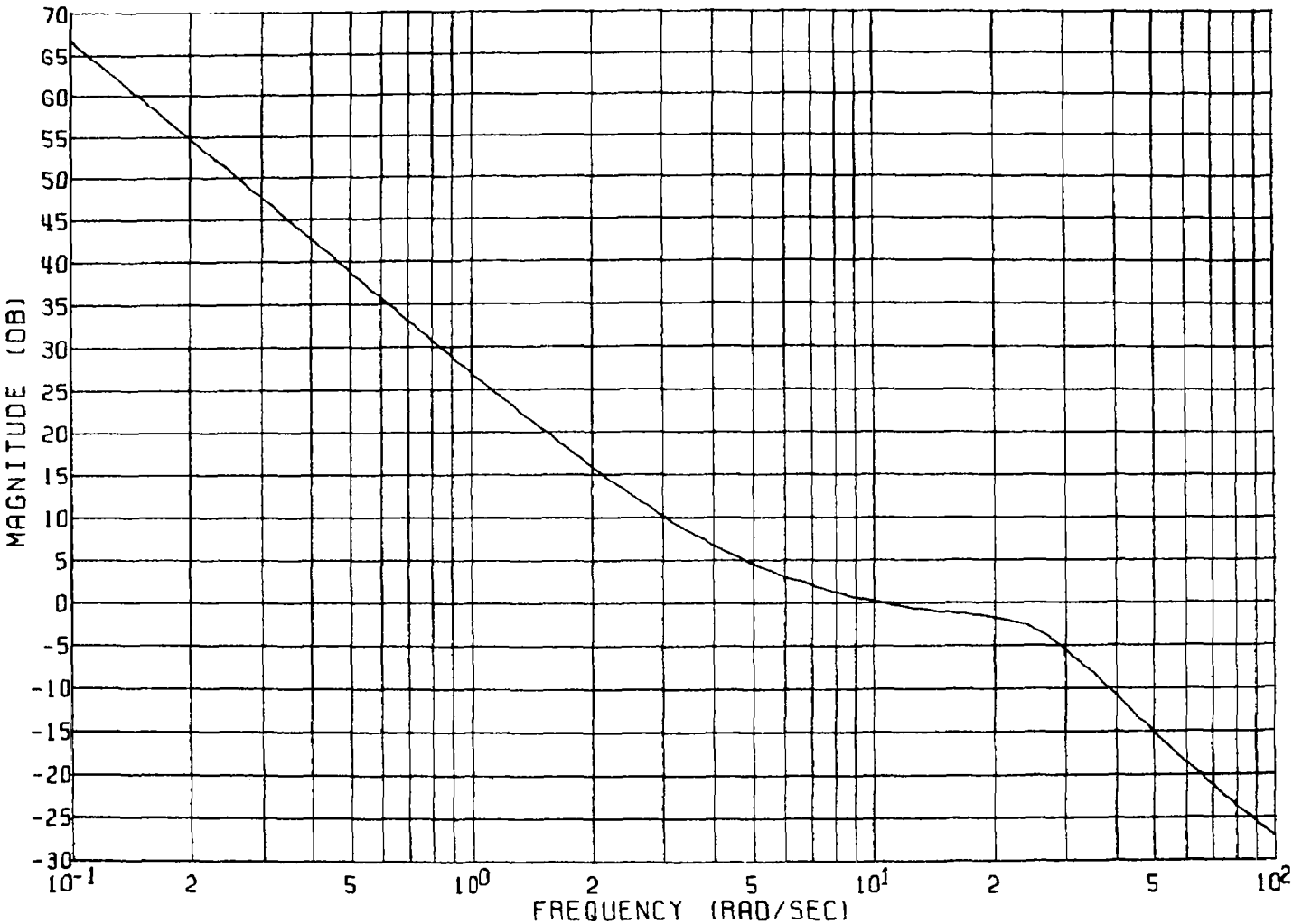

Figure F.7(a) ROLL RATE ERROR; UNCOUPLED ROLL CHANNEL; CIRCULAR OR ELLIPTICAL AIRFRAMES ($\alpha_e = 0$) GAIN VS. FREQUENCY

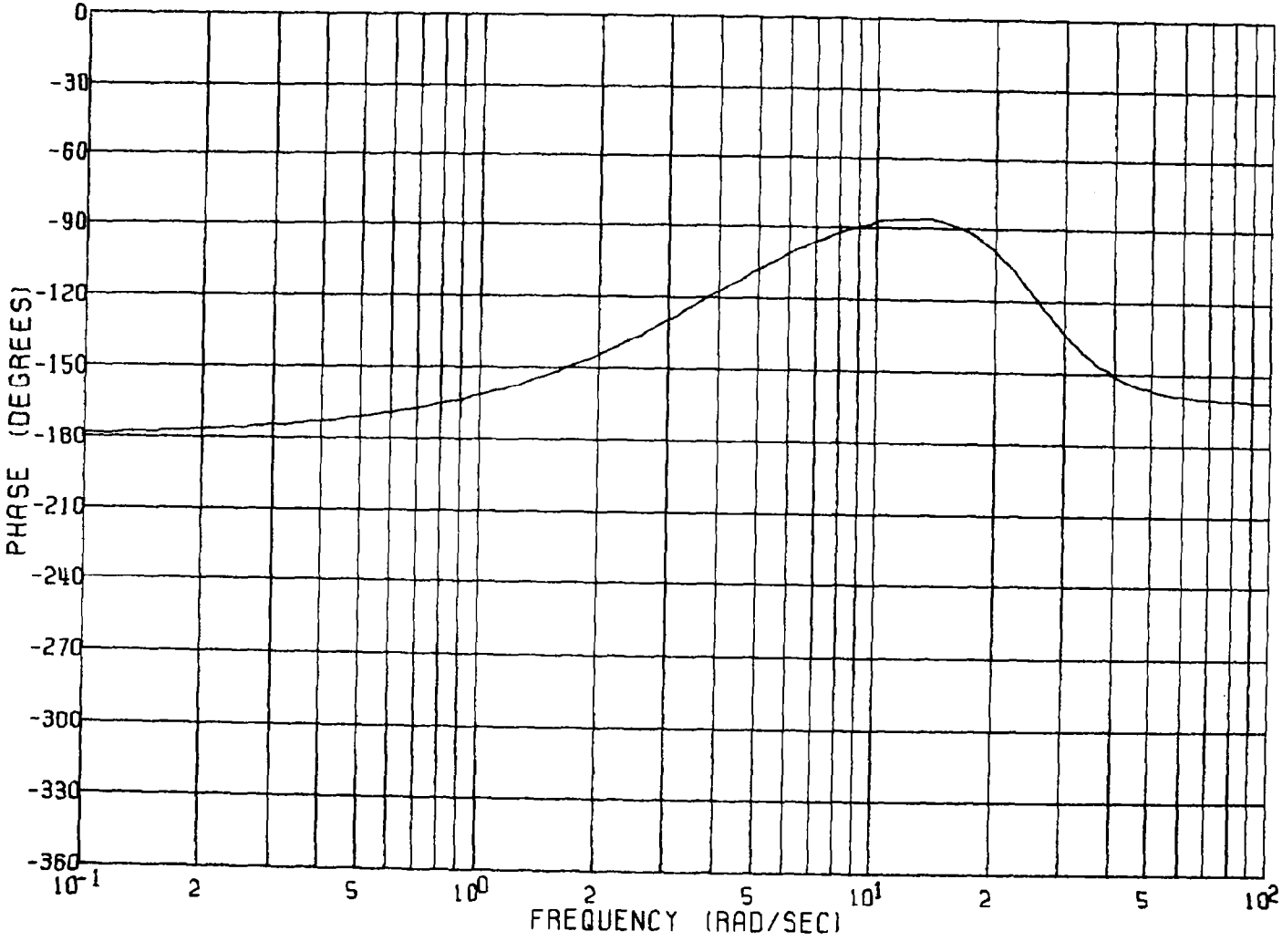

Figure F.7(b) ROLL RATE ERROR; UNCOUPLED ROLL CHANNEL; CIRCULAR OR ELLIPTICAL AIRFRAMES ($\alpha_e = 0$) PHASE VS. FREQUENCY

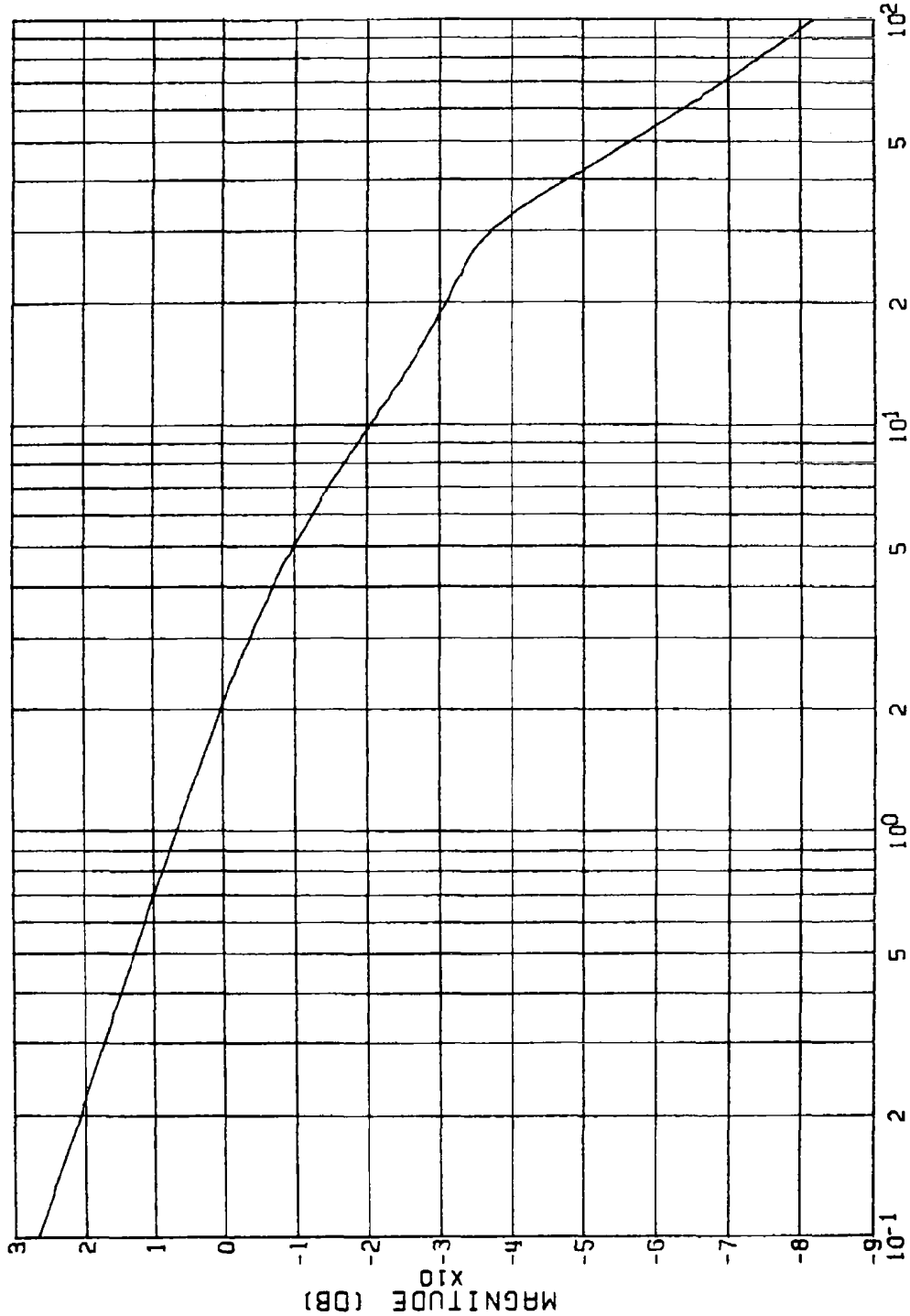

Figure F.8(a) ROLL ANGLE ERROR; UNCOUPLED ROLL CHANNEL; CIRCULAR OR ELLIPTICAL AIRFRAMES ($\alpha_e = 0$) GAIN VS. FREQUENCY

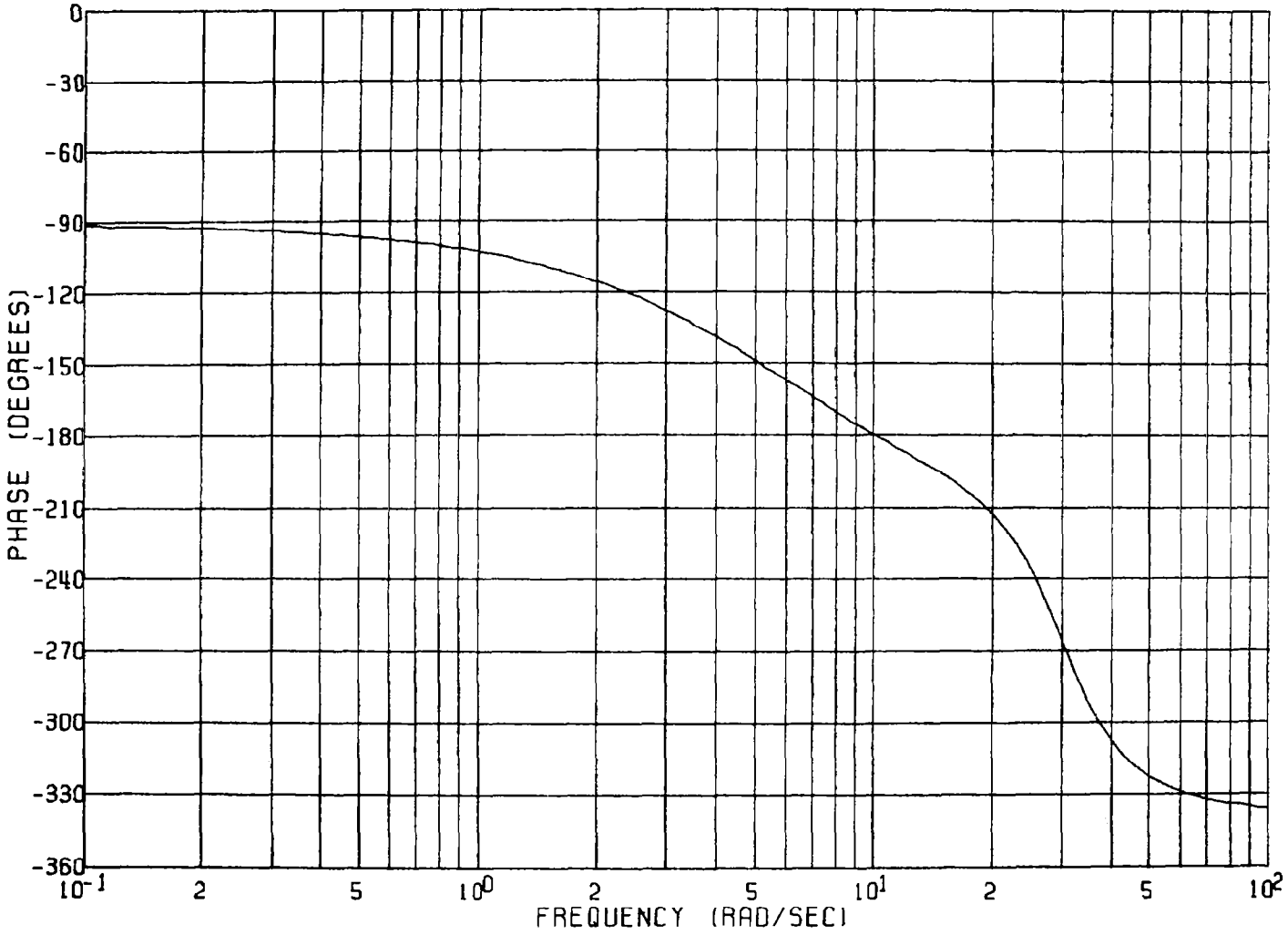

Figure F.8(b) ROLL ANGLE ERROR; UNCOUPLED ROLL CHANNEL; CIRCULAR OR ELLIPTICAL AIRFRAMES ($\alpha_e = 0$) PHASE VS. FREQUENCY

REFERENCES

1. D. Best, "Some Problems of Polar Missile Control," Journal of the Royal Acoustical Society, August 1960.

2. A. N. Thomas, Jr., "New Generation Ramjets - A Promising Future," Astronautics and Aeronautics, June 1980.

3. F. W. Riedel, "Bank-to-Turn Control Technology Survey for Homing Missiles," NASA CR-3325, September 1980.

4. R. T. Reichert, "Homing Performance Comparison of Selected Airframe Configurations Using Skid-to-Turn and Bank-to-Turn Steering Policies," NASA CR-3420, May 1981.

5. E. B. Graves, "Aerodynamic Characteristics of a Monoplanar Misile Concept with Bodies of Circular and Elliptical Cross Sections," NASA TM 74079, December 1977.

1. Report No.	2. Government Accession No.	3. Recipient's Catalog No.
NASA CR-3644		

4. Title and Subtitle	5. Report Date
AN ANALYSIS OF AERODYNAMIC REQUIREMENTS FOR COORDINATED BANK-TO-TURN AUTOPILOTS	November 1982
	6. Performing Organization Code
7. Author(s)	8. Performing Organization Report No.
A. Arrow	
9. Performing Organization Name and Address	10. Work Unit No.
The Johns Hopkins University Applied Physics Laboratory Johns Hopkins Road Laurel, MD 29810	11. Contract or Grant No.
	13. Type of Report and Period Covered
12. Sponsoring Agency Name and Address	Contractor Report
National Aeronautics and Space Administration Washington, DC 20546	14. Sponsoring Agency Code 505-43-23-03 (L-75242A)

15. Supplementary Notes

Langley Technical Monitors: Wallace C. Sawyer and Charlie M. Jackson, Jr.
Appendix A, B, and C by L. L. Cronvich

16. Abstract

Two planar missile airframes were compared having the potential for improved bank-to-turn (BTT) control but having different aerodynamic properties. The comparison was made with advanced level autopilots using both linear and nonlinear 3-D aerodynamic models to obtain realistic missile body angular rates and control surface incidence. Cortical cross-coupling effects are identified and desirable aerodynamics are recommended for improved coordinated BTT (CBTT) performance. In addition, recommendations are made for autopilot control law analyses and design techniques for improving CBTT performance.

17. Key Words (Suggested by Author(s))	18. Distribution Statement
Skid-to-turn Coordinated turn Bank-to-turn missile autopilot	Unclassified - Unlimited Subject Category 02

19. Security Classif. (of this report)	20. Security Classif. (of this page)	21. No. of Pages	22. Price
Unclassified	Unclassified	306	A14

For sale by the National Technical Information Service, Springfield, Virginia 22161

NASA-Langley, 1982